Developing Microfluidic Devices for the Optimization of Nanodiscs to Measure Membrane Protein Structure and Function

by

Colleen Mairead Riordan

A dissertation submitted in partial fulfillment
of the requirements for the degree of
Doctor of Philosophy
(Chemistry)
in The University of Michigan
2021

Doctoral Committee:

Professor Ryan Bailey, Chair
Professor Neil Marsh
Professor Brandon Ruotolo
Professor Anna Schwendeman

Colleen M. Riordan

criorda@umich.edu

ORCID iD: 0000-0001-9260-6875

Dedication

This dissertation is dedicated to everyone that helped and supported me, especially all of my teachers that encouraged my interest in science and my family who always believed in me.

Acknowledgements

First, I would like to thank Professor Ryan Bailey for all of his help and support over the past five years. I really appreciate the understanding and flexibility you provided when I needed to attended multiple doctor and physical therapy appointments. You have been a fantastic advisor and I always appreciated our discussions about new project ideas. I would also like to thank my committee members, Professor Brandon Ruotolo, Professor Neil Marsh and Professor Anna Schwendeman for their support and guidance throughout my time in graduate school. I appreciate the feedback and advice you have provided me. I am also very grateful for the financial support from the National Science Foundation Graduate Research Fellowship Program.

I would also like to thank all of my collaborators for each of their contributions to a number of projects. First, Professor Mukesh Nyati and members of his lab, Ranjit Mehta and Sanjima Pal, for both conversations and advice on working with EGFR and providing the Ba/F3 cell lines for the project. I am also grateful for Professor Brandon Ruotolo and Kristine Parson, as well as Professor Philip Andrews and Lolita Perisimoni, for their efforts on the mass spectrometry collaboration. Finally, Professor Neil Marsh and members of his lab, Dr. Timothy Grunkemeyer and Ayesha Patel, for our collaboration on the viperin project, which has really expanded my knowledge in membrane-associated proteins.

I also want to acknowledge the help from the various Bailey lab members that I have had the pleasure to overlap with throughout graduate school. Each of the previous Bailey lab members have provided support in their own ways over the past five years and I want to thank all

of them: Dr. Alex Stanton. Dr. Richard Graybill, Dr. James Wade, Dr. Heather Robinson, Dr. Yi Xu, Dr. Steve Doonan, Dr. Maria de la Cruz Cardenosa Rubio, Jamy Lee and Robert Moeller. I would particularly like to thank the other five members of my class year, Dr. Emily Mordan, Dr. Cole Chapman, Dr. Sara Medfish, Dr. Shannon Wetzler and Dr. John Orlet, we have had a lot of good times and a lot of bad times but we all survived! I would also like to thank the current graduate students: Nico Mesyngier, Gloria Diaz, Marina Sarcinella, Nick Glenn, Claire Cook and Krista Meserve.

There are a number of lab members that have provided additional support that I would like to individually thank. Particularly James, who initiated the microfluidic Nanodisc project in the Bailey lab and introduced me to all of the new aspects of this research as a first year graduate student. I really appreciated my undergraduate students Jenny Choi and Briana Bowen who helped move my projects forward and taught me to be a better mentor. I would also like to thank Marina, who has really pushed the Nanodisc project in interesting new directions and I look forward to seeing how far she can go. Nico has been an amazing support for microfluidic and clean room questions, discussing various scientific problems, and for driving me to lab in a pandemic. I would also like to thank Cole for driving me all over Ann Arbor for the past five years, including multiple doctor and hospital visits, I might have literally fallen apart without you, instead of just figuratively. Finally, Shannon for always being there as a sounding board for both science and life, and always being willing to get ice cream, chocolate or pizza on a good day or a bad day.

I would also like to thank all of the friends that helped me remove myself from my research in various ways. Being a member of the Women+ Excelling More in Math, Engineering and the Sciences was a big part of my time in graduate school, and I will miss all of the board

members and students. I would like to thank those that I worked closely with, especially Megan, Alex, Sophie, and Harini. The Notre Dame Young Alumni club also helped me take a break from science, and I will really miss the monthly trivia nights and Christmas mass in an Irish pub.

Finally, I want to thank my family for their unending support, even when they did not understand a single word that I was saying while explaining the problems I had had that day with my project. To my brothers, Shane and Conor, thank you for all the laughs over the family group message, I loved the pictures of Notre Dame or every zoo in South Carolina. Special thanks to Shane for helping me format the page numbers of this thesis and providing sour watermelon candies for motivation. Nana, thank you for your supportive phone calls and keeping me updated on the extended family while I am far from home. Mom and Dad, thank you for always being willing to try to understand my Western Blot problems and for our almost-daily phone calls, you do not know how much I looked forward to that time each day.

Table of Contents

Dedication ii

Acknowledgements iii

List of Tables ix

List of Figures x

List of Abbreviations xviii

Abstract xxiii

Chapter 1: An Introduction to Nanodiscs 1

References 7

Chapter 2: The Development of Microfluidic Devices to Study Membrane Protein Structure and Function in Model Membrane Systems: A Review 10

Introduction 10

Forming Membrane Mimetics on Microfluidic Chips 15

Planar Lipid Bilayers 15

Supported Lipid Bilayers 15

Tethered Lipid Bilayers 16

Suspended Lipid Bilayers 18

Droplet Interface Lipid Bilayers 25

3D Lipid Structure Arrays 29

Liposomes 30

Electroformation 30

Jet Flow 32

Transient Membrane Ejection 36

Herringbone mixer 37

Droplet-stabilized 40

Conclusions 42
Nanodiscs 43
Important Considerations 44
Microfluidics for Downstream Analysis of Membrane Proteins 45
Membrane Protein Purification 45
Purification Before Incorporation 45
Purification After Incorporation 46
Membrane Protein Structure 49
Crystallization 49
Membrane Protein Function and Activity 52
Membrane Protein Function 52
Membrane Protein-Ligand Interactions 53
Membrane Protein-Protein Interactions 56
Conclusions and Future Work 57
References 62
Chapter 3: Microfluidic Platform for Efficient Nanodisc Assembly, Membrane Protein Incorporation, and Purification 73
Introduction 73
Experimental Methods 76
Results and Discussion 86
References 104
Chapter 4: Microfluidic Platform for Library Nanodisc Assembly from Whole Cell Lysate to Measure Activity of the Epidermal Growth Factor Receptor 108
Introduction 108
Experimental Methods 111
Results and Discussion 117
Conclusions and Future Work 124
References 135
Chapter 5: Incorporation of Viperin into Library Nanodiscs 138

Introduction 138
Experimental Methods 139
Results and Discussion 142
Conclusions and Future Work 148
References 150
Chapter 6: Mass Spectrometry to Study Membrane Proteins in Nanodiscs 152
Introduction 152
Experimental Methods 155
Results and Discussion 159
Cytochrome P450 Microfluidic Nanodisc Formation and Purification 159
Ion-Mobility Mass Spectrometry Lipid Comparisons 161
Mitochondrial Library Nanodisc Formation and Purification 163
Conclusions and Future Work 167
References 171
Chapter 7: Conclusions and Future Work 174
Conclusions 174
Future Work 176
Microfluidic Device Improvements for Nanodisc Formation 176
New Microfluidic Devices for Downstream Analysis 184
Lipid Identity 188
Other Membrane Proteins of Interest 190
References 191

List of Tables

Table 3.1: Sample Nanodisc Preparation Sheet for Single Port Device. **80**

Table 3.2: Sample Nanodisc Preparation Protocol for a Three-Port Mixing Device. **81**

Table 4.1: Nanodisc Component Preparation Calculations. **115**

Table 6.1: Example of the tables used to prepare the components for the Nanodisc formation. Information such as the concentrations and ratios can be modified and the necessary volumes needed to be combined will update. **159**

Table 6.2: Lipid Mixture to Emulate Endoplasmic Reticulum in Nanodiscs. **168**

List of Figures

Figure 1.1: Image of an Empty Nanodisc. In blue are the two Membrane Scaffold Proteins and the red circles are the lipid heads. The difference in potential diameter references the range of commercially available lengths of MSP. **2**

Figure 1.2: The Nanodisc formation process. Nanodiscs are formed through the removal of detergent from a solubilized solution containing a membrane scaffold protein (MSP), lipids and membrane protein. **3**

Figure 2.1: Representative cartoon of the tethered bilayer lipid membrane array. The surface coating begins with physical absorption of the biotinylated bovine serum albumin (biot-BSA) to the gold surface. Then the lipid bilayer is formed by flowing first Avidin, and then liposomes with ~1% biotinylated PE which will bind to the Avidin and be subjected to PEG-triggered fusion to form the bilayer. Finally, the membrane protein of interest (CT in the figure) is introduced and binds to specific lipids. Reprinted from Taylor *et. al.* **18**

Figure 2.2: Visualization of the lipid-bilayer formation by microfluidic solvent extraction. (A) The organic phase containing lipids is formed surrounded by two aqueous phases. The lipids spontaneously assemble at the hydrophobic-hydrophilic interface, as seen in the inset figure. (B) The organic solvent partitions into the PDMS, causing the two layers of lipids to move closer. (C) Finally, the lipids touch, forming a lipid bilayer, as seen in the inset. Reprinted from Malmstadt *et. al*. **24**

Figure 2.3: Micrograph of the four-droplet network microfluidic chips. Each droplet is numbered 1-4 from left to right. The lipid bilayers at the droplet interfaces are lettered A-C from left to right. The scale bar is 1 mm. Reprinted from Casekalska *et. al*. **28**

Figure 2.4: Formation of liposomes via jet flow in a microfluidic device. (a) Schematic demonstrating the vesicle formation from a planar lipid membrane via the pulsed jet flow, causing the lipids to pitch off into a vesicle with the jetted material encapsulated within. (b) Images of the vesicle formation via high-speed CCD camera. The vesicles formed within 10 ms. Reprinted from Funakochi *et. al.* **33**

Figure 2.5: Schematic images of the automatic liposome generation system using jet flow. The green circular section is the rotational piece, while the grey is stationary. (a) Top-down view of the device, showing the six rotating wells and one fixed well, each with a single lipid layer on the outside of the wells. When the wells line up, a lipid bilayer forms and jet flow liposome formation can occur. (b) Side-on view of the device, showing the motor and pressure controller needed for function, as well as a view of where in the well the liposome formation occurs. Reprinted from Gotanda *et. al.* **35**

Figure 2.6: Schematic of the herringbone mixer device. The organic stream containing the lipids and the aqueous buffer stream are introduced through the two inlets using a syringe pump and then mixing is induced by using the herringbone structures seen in the inset figure. The structures cause rapid mixing of the two phases which increases the polarity experienced by the lipids, causing lipid nanoparticle (LNP) formation. Reprinted from Zhigaltsev *et. al.* **38**

Figure 2.7: Schematic of the microfluidic assembly of droplet-stabilized cell-like compartments. Using standard droplet microfluidic technologies, like the picoinjector seen here, transmembrane proteins were incorporated into the giant liposomes. Scale bar is 50 μm. Reprinted from Weiss *et. al.* **41**

Figure 2.8: The microfluidic device and the overall operating system for the separation and detection of membrane proteins. (A) Schematic of the microfluidic device. (B) Picture of the microfluidic device with a US penny for size comparison. (C) Schematic of the overall set up, including the syringe pumps, the sample tubes, and the imaging equipment used. Reprinted from Hu *et. al*. **46**

Figure 2.9: Pictures and schematic of the membrane protein array. The left figure demonstrates the microfluidic chip, composed of two PDMS layers, a 64 x 64 unit cell array and a control layer with the valves. The middle figure demonstrates 6 of these separate units, with colors representing the different PDMS layers. The right figure is a schematic of each individual cell, and the steps that occur within the chip. Reprinted from Glick *et. al* **56**

Figure 3.1. **Platform Device Designs**. (**A**) A single-port device consists of reagent and detergent removal bead inlets, a bead bed with integrated posts for structural support, and an outlet for Nanodisc elution. The device has a bead bed volume of 60 μL and yields 0.1-2 nmol of Nanodiscs. (**B**) The purification devices feature multi-directional flow for loading of Nanodiscs formed using devices from A. (**C**) Interfacing Nanodisc self-assembly and purification can be achieved as a single, integrated platform. **85**

Figure 3.2: Additional Device Designs for Microfluidic Nanodisc assembly. (**A**) A 3-port inlet device for on-chip reagent mixing with the same bed volume as the standard single port device is suitable for applications where exposure to lipid-solubilizing detergents may damage to membrane protein to be incorporated. The bed volume of both assembly and purification can be tuned to the desired application. (**B**) The smallest device designed was 10 μL, and this bed volume can be interfaced with either a single or multiport inlet. (**C**) This alternative design consists of a larger total bed volume of 120 μL with four beds. Each bed is packed individually and can be filled with either detergent removal resin or affinity purification resin.(**D**) Another large volume device (120 μL) consists of two packed beds interfaced with a multiport inlet for on-chip reagent mixing. **88**

Figure 3.3. Flow Visualization of 3 Port Mixing Device. The multiport device design used on-chip reagent mixing prior to Nanodiscs assembly upon detergent removal. The mixing channel featured alternating juts to encourage efficient mixing. Three different colors of food dye are fed into the device and complete mixing is clearly apparent. **89**

Figure 3.4. Detergent Removal Device Capacity. Elution fractions collected from single port and multiport devices flowing 1% CHAPS (black and blue dots), 20 mM sodium cholate (red and green dots), and treated with concentrated sulfuric acid show increased absorbance once the detergent removal capacity is reached. This plot shows the detergent removal capacity for a device bed volume of 60 μL. The detergent removal capacity for both detergents is >90 μL, which corresponds to 1.5 μmol (0.9 mg) CHAPS and 1.8 μmol (0.78 mg) sodium cholate. The region shaded in grey represents the Nanodisc collection region. No Nanodiscs were collected from an assembly device above 90 μL of elution volume to ensure adequate detergent removal for samples fractions. **90**

Figure 3.5. **Microfluidic Self-Assembly with Empty Nanodiscs**. SEC analysis of Nanodiscs formed from a single-port device with DMPC and a DMPC:MSP ratio of 80:1 (**A**) and POPC and a POPC:MSP ratio of 60:1 (**B**) with MSP1D1. Approximate Nanodisc concentrations for each are 25 μM. (**C**) Atomic force microscopy (AFM) of DMPC Nanodiscs formed with the Nanodisc assembly module without prior purification show Nanodiscs of appropriate dimension with no evidence of large lipid aggregates. (**D**) Dynamic light scattering (DLS) analysis of DMPC Nanodiscs indicating a single, monodisperse peak corresponding to Nanodiscs. **92**

Figure 3.6. Assembly of Nanodisc at Various Device Flow Rates. Size exclusion chromatograms (SEC) monitored at 280 nm for DMPC Nanodiscs with MSP1D1formed at variable flow rates indicate minimal to no effect on overall Nanodisc assembly. **93**

Figure 3.7. Comparison of Mixing versus No Mixing. Nanodiscs formed with either multiport (3-port) or single port devices using MSP1D1 and sodium cholate as detergent both result in monodisperse Nanodiscs that co-elute when analyzed with SEC monitored at 280 nm. There was no observed impact on Nanodisc formation when prepared at RT using DMPC lipids (**A**) or at 4°C using POPC lipids (**B**). **94**

Figure 3.8. Microfluidic Gradient with Fluorescent Lipids. (**A**) The flow rate for lipid-containing syringe was increased continuously at a rate of 0.1 μL/s ^{2} for the syringe containing DMPC with 0.05% Liss Rhod PE (Syringe 3) and -0.1 μL/s ^{2} for DMPC only syringe (Syringe 1). The syringe with MSP was held at a constant flow rate of 10 μL/min (Syringe 2). (**B**) The fluorescence with a maximum at 590 nm shows an increase in intensity as a function of flow rate. This corresponds to an increasing fluorescent lipid content and, thus lipid bilayer composition, over the course of the microfluidic gradient. (C)This increase in fluorescence over time measured at 590 nm is also seen in the SEC Nanodisc peak, showing incorporation of fluorescent lipids into Nanodiscs following the gradient. **96**

Figure 3.9. **Incorporation of CYP3A4 into Nanodiscs**. Size exclusion chromatograms recorded at 280 nm and 417 nm (**A**) demonstrate the successful incorporation of CYP3A4 into Nanodiscs using the microfluidic assembly module. Equivalently sized Nanodiscs were formed either with (red) or without (black) CYP3A4 in combination with DMPC lipids, MSP1D1, and CHAPS detergent. The filled Nanodiscs, which had a MSP:CYP3A4 ratio of 20:1, were confirmed by the strong absorbance at 417 nm with minimal signal for the empty Nanodiscs. (**B**) Purification with His-tag with POPC, MSP1E3D1, and CYP3A4 (both CYP3A4 and MSP have His-tag) at a ratio of 10:1 MSP:CYP3A4 **(C**) Purification of CYP3A4 Nanodiscs made with DMPC MSP1D1(-) (that indicates His-tag is removed) at a ratio of 20:1 MSP:CYP3A4. **97**

Figure 3.10. Incorporation of CYP3A4 into Nanodiscs with a 3-Port Assembly Device. CYP3A4 incorporation into DMPC and MSP1D1 Nanodiscs using a 3 port assembly device measured at both 280 nm and 417 nm with SEC show incorporation of CYP3A4 into the Nanodiscs as indicated by the co-elution of the 417 nm and 280 nm peaks. No Nanodisc purification was performed prior to SEC analysis. **98**

Figure 3.11: Microfluidic purification of Nanodiscs by affinity chromatography. 100

Figure 3.12. Polyacrylamide Gel Electrophoresis of Nanodiscs with incorporated CYP3A4. SDS-PAGE gel of DMPC and MSP1D1 Nanodiscs filled with CYP3A4 throughout the assembly and purification process stained with Coomassie Blue. Bands corresponding to CYP3A4 (57 kDA) and MSP1D1 (24.6 kDa) are present in all filled Nanodiscs and in Nanodisc components. Empty Nanodiscs only show the MSP band. **101**

Figure 3.13. **Spin Shift Assays for Nanodiscs Filled with CYP3A4**. (**A**) UV/Vis absorption difference spectrum demonstrates the low to high spin shift for CYP3A4 in Nanodiscs (black) and free CYP3A4 (red) induced by the binding of bromocriptine (BCT), a type I CYP3A4 binder. Binding of BCT results in a decrease in the absorbance maximum of 417 nm and an increase at 390 nm. (**B**) Imidazole, a type II CYP3A4 binder, induces a shift in the absorbance maximum for CYP3A4 from 417 nm to 422 nm. **102**

Figure 4.1: Microfluidic device designed for rapid and efficient formation of Nanodiscs with integrated membrane proteins. The fluidic bed packed with detergent removal resin enables rapid Nanodisc assembly in 5 minutes, as compared to overnight in bulk preparation, and requires less input material. **117**

Figure 4.2: Formation of Library Nanodiscs using microfluidic device compared to bulk preparations as detected by SEC. A). Both microfluidic and conventional bulk Nanodiscs are well-formed. B). Bulk Nanodiscs using microfluidic reagent and time scales show no Nanodisc formation as compared to components before detergent removal. **118**

Figure 4.3: SDS-PAGE and Western Blot of Purified Nanodiscs to confirm EGFR incorporation. *Lane 1:* L858R Lysate; *Lane 2*: L858R Nanodiscs after purification; *Lane 3*: L858R/T790M/C797S (LTC) lysate; *Lane 4*: LTC Nanodiscs after purification; *Lane 5*: WT lysate; *Lane 6*: WT Nanodiscs after purification. A) SDS-PAGE to visualize all proteins in the samples. MSP1E3D1 is the band present ~32 kDa in all the Nanodisc lanes (even numbered lanes). B) Western Blot for EGFR shows that EGFR is successfully incorporated into the L858R and LTC Nanodiscs. The WT lysate does not contain EGFR, as expected. Since the membrane protein bands are present after Ni-NTA purification, the membrane proteins must be incorporating into Nanodiscs, as any free membrane protein will be eluted during the purification process. **120**

Figure 4.4: The Universal Kinase Activity Assay schematic. ATP, an EGFR specific substrate, and the sample of interest (in this case Library Nanodiscs) are incubated together. If the sample contains active EGFR, the protein will phosphorylate the substrate using the tertiary phosphate of the ATP, leaving ADP. Then, coupling phosphatase is added to convert ADP to AMP and a free phosphate. Malachite Green reagents are added to colorimetrically measure the concentration of free phosphate, which corresponds to the activity of the EGFR in the sample. Modified from the Universal Kinase Assay Directions. **121**

Figure 4.5: EGFR Activity Assay. The samples were each incubated with either 200 nM Osimertinib or DMSO as a control, with three wells for each condition. The average of the sample with inhibitor was subtracted from the average of the control sample, resulting in the relative change in activity. The assay was repeated three times with three separate Nanodisc preparations and the relative changes in activity were averaged. **123**

Figure 4.6: Absorbances of the various samples in the Universal Kinase Assay. (+) indicates that 200 nM Osimertinib inhibitor was added to the sample. The samples without the (+) have DMSO added as the control. The absorbances are n=3 replicates of different Nanodisc samples, each with n=3 wells averaged. **126**

Figure 4.7: Absorbance values for the samples and controls for both Ba/F3 lysate (A) and Library Nanodiscs (B). The samples with the full activity assay are blue, the controls without the EGFR specific substrate are orange, the controls without ATP are green, and the controls without both EGFR substrate and ATP are purple. Note the differences in the absorbance axis for the lysate (0-1.6 absorbance units) and the Nanodiscs (0-0.3 absorbance units). **127**

Figure 4.8: Western Blot for EGFR of the EGFR-specific purification of L858R lysate and Nanodiscs using Protein A beads. *Lane 1*: L858R Lysate; *Lane 2*: Pure Lysate Fraction 1; *Lane 3*: Pure Lysate Fraction 2; *Lane 4*: L858R Nanodiscs; *Lane 5*: Pure Nanodiscs Fraction 1; *Lane 6*: Pure Nanodiscs Fraction 2; *Lane 7*: Lysate Wash Step; *Lane 8*: Nanodisc Wash Step. **128**

Figure 4.9: Western Blot for EGFR of the EGFR-specific purification of L858R lysate using Avidin beads and desthiobiotinylated antibodies. *Lane 1*: L858R lysate; *Lane 2*: Loading lysate to beads (material that does not bind to beads); *Lane 3*: Wash step 1; *Lane 4:* Wash step 5; *Lane 5*: Biotin Elution 1; *Lane 6*: Biotin Elution 2; *Lane 7*: Biotin Elution 3; *Lane 8*: Combined & Concentrated Biotin Elutions; *Lane 9*: Laemelli Buffer Elution. The Laemelli buffer is used to completely denature the beads and release any EGFR not released by the biotin. The EGFR band is just above the 200 kDa band in the ladder, and the unknown band in Lanes 8-9 is approximately 250 kDa. **130**

Figure 4.10: Western Blot for EGFR of the EGFR-specific purification of L858R and WT EGFR lysate using Sepharose beads pre-conjugated with anti-EGFR. *Lane 1*: L858R lysate; *Lane 2*: WT EGFR Lysate; *Lane 3*: Loading L858R lysate to beads (material that does not bind to beads); *Lane 4:* Loading WT EGFR lysate to beads; *Lane 5*: Wash L858R-loaded beads; *Lane 6*: Wash WT EGFR-loaded beads; *Lane 7*: Laemelli Buffer Elution of L858R; *Lane 8*: Laemelli Buffer Elution of WT EGFR. The Laemelli buffer is used to completely denature the beads and release all EGFR. The EGFR band is just above the 200 kDa band in the ladder. **131**

Figure 5.1: The microfluidic device used to form Library Nanodiscs. The components mixture containing MSP, lipids and cell lysate is introduced through the inlet and flows though the packed bead bed filled with detergent removal resin. As the detergent is removed, the Nanodiscs spontaneously self-assemble, incorporating membrane proteins, which can be collected through the outlet. **142**

Figure 5.2: Size-Exclusion Chromatograph of the Nanodiscs containing viperin. The first peak around 12 minutes is the aggregate peak, composed of lipids, MSP and cell lysate components that have not incorporated into the Nanodisc. The second peak at ~18 minutes is the Nanodisc peak. There is another smaller peak around 28 minutes of any buffer and lysate components that are exceptionally small. **143**

Figure 5.3: Western blot for anti-viperin of the Nanodiscs using different percentages of POPE, with the remaining lipid composition POPC. The lanes are labeled as follows: **B**: Before purification Nanodiscs; **A**: SEC Aggregate Peak; **N**: SEC Nanodisc peak; **L**: HEK cell lysate. The viperin band is noted by the red box across all lanes. Based on relative intensities of the viperin band in the SEC Nanodisc peaks, the 20% POPE 80% POPC Nanodisc lipid composition was determined to be optimal. **145**

Figure 5.4: The structures and charges of the four lipids used throughout this chapter. Each lipid has the same tails but distinct lipid head groups. Top left: POPC; Top right: POPE. Both of these lipids are zwitterionic, with a net neutral charge. Bottom left: POPA, which has a negative charge. Bottom right: POPS, which contains 2 negative and 1 positive charge, leading to a net negative charge. **146**

Figure 5.5: Western Blot using anti-viperin of the Nanodiscs formed with POPA (left) and POPS (right). The key labeling the lanes is as follows: B: Before purification Nanodiscs; A: SEC Aggregate Peak; N: SEC Nanodisc peak; L: HEK cell lysate. The viperin band is noted by the red VIP for both blots. The red numbers indicate the percent incorporation, calculated by dividing the viperin band intensity in that lane by that of the lysate lane. **147**

Figure 5.6: Western Blot (left) and SDS-PAGE (right) after the two-step viperin Nanodisc purification process. On the left, the blot probed with anti-viperin. The viperin band is present at approximately 42 kDa. On the right, the SDS-PAGE gel stained with silver stain, in which both the 42 kDa viperin band and the ~32 kDa MSP1E3D1 bands are visible. Lower-concentration Empty Nanodiscs were also run, and the MSP band is present while the viperin band is not. There is a band slightly higher than 50 kDa that appears to be a contaminant in the MSP, as it is seen in both the Empty and Viperin Nanodiscs. **148**

Figure 6.1: Size-exclusion chromatogram of the Filled Nanodiscs using MSP1D1, POPC and CYP3A4. The Nanodiscs elute around 1.8 mL and there is a clear aggregate peak that elutes just after 1 mL. Fractions were collected every minute to separate the aggregate from the Nanodiscs. The highest concentration fractions from the main Nanodisc peak were used for IM-MS. **160**

Figure 6.2: Ion-Mobility Mass Spectrometry of POPC and DMPC Nanodiscs. Top: Collision-Induced Unfolding (CIU) Fingerprints for the 15+ CYP3A4 liberated from POPC ND (left) and DMPC NDs (right) Bottom: Feature detection analysis performed using CIUSuite2 illustrates discrete features, unfolding, resulting from various lipid composition the CYP3A4 is liberated from POPC (left) and DMPC (right). Bar graph: Intensity values extracted from the CIU fingerprints (indicated by white boxes) for the third feature and fourth feature to visualize differences in the 55-65V region. POPC NDs yellow bars, DMPC NDs blue bars. **162**

Figure 6.3: The Root Mean Square Deviation plot. This indicates structural dissimilarities between the CYP liberated from its lipid environment (RMSD baseline values Holo DMPC: 10.3 and Holo POPC: 6.9. **163**

Figure 6.4: Venn diagram indicating the number of identified peptide sequences for each of the three lipid compositions. The smaller number is the total number of unique sequences identified while the larger number indicates the percentage of the total that falls within that section. The lipid identities at 40% POPC, 40% POPE and 20% cardiolipin (CL) on the top left; 50% POPC and 50% POPE on the top right; and 100% POPC on the bottom. **165**

Figure 6.5: Graph showing the classification of the identified proteins in each of the Nanodisc lipid compositions. The 100% POPC Nanodiscs are in yellow, the 50% POPC and 50% POPE Nanodiscs are in blue, and the 40% POPC, 40% POPE and 20% CL Nanodiscs are in green. **166**

Figure 7.1: Photograph of a Nanodisc formation device fabricated using hot embossing in cyclic olefin copolymer. A C_{18} acrylate monolith was then directly photopolymerized within the device. **179**

Figure 7.2: An illustration of the types of modules that could be used to develop droplet microfluidic Nanodisc formation devices. These images were modified from Doonan *et. al.*[19] and Xu *et. al.*[11] and are not to scale. (A) A T-junction demonstrates one method of droplet formation, with the oil phase in white and the aqueous phase in blue. The arrows indicate the direction of flow. (B) A K-channel which can be used to add material to droplets (in orange). The solution is added to the blue droplet, as shown by the diagonal orange lines in the droplet to the right. The gray lines underneath the channel are an electrode channel which might be necessary to destabilize the droplet to add solution. (C) Delay channels used to add time on device to allow for the detergent removal reaction to take place. The number and size of these delay channels can be optimized as necessary. (D) Using a K-channel design to split droplets by flowing oil through the K-channel (white). (E) The beads remain in the main channel while the solution-only droplets are pulled up into another channel, which can then be collected for downstream analysis. **183**

Figure 7.3: The CAR-Wash Technique. This device involves electrocoalescence of input droplets using an electric field applied across the washing buffer stream (in blue) and a nearby ground electrode. Next, a channel-adjacent permanent magnet attracts sample-enriched magnetic beads (brown circles) across the buffer stream while flow forces confine waste material (in yellow) to the original streamline. An oil co-flow (in grey) prevents bead trapping at the bottom channel walls and, at the end of the module, resegments droplets in washing buffer for further manipulations. Arrows indicate flow directions. Reprinted from Doonan *et. al*. **186**

List of Abbreviations

α-HL:	α-hemolysin
ACN:	Acetonitrile
ADP:	Adenosine diphosphate
Adx:	Adrenodoxin
AFM:	Atomic Force Microscopy
ALK:	Anaplastic Lymphoma Kinase
AMP:	Adenosine monophosphate
ApoA1:	Apolipoprotein A1
ATP:	Adenosine Triphosphate
BACE:	β-secretase
BCA:	Bicinchoninic Acid
BSA:	Bovine Serum Albumin
C797S:	EGFR mutation: Cystine to Serine at amino acid 797
CAR:	Coalesce-Attract-Resegment
CHAPS:	3-[(3-Cholamidopropyl)dimethylammonio]-1- propanesulfonate
CID:	Collision-induced dissociation
CIU:	Collision-induced unfolding
CL:	Cardiolipin
CLIC1:	Chloride Intracellular Ion Channel 1
COC:	Cyclic Olefin Copolymer
CRP:	Cytochrome P450 reductase
CV:	Coefficients of Variation
Cx43:	Connexin43
CXL:	Chemical cross linking

ddhCTP: 3’-deoxy-3’,4’-didehydro-cytidine triphosphate

DIB: Droplet Interface Bilayer

DLS: Dynamic Light Scattering

DMEM: Dulbecco's Modification of Eagel's media

DMPC: 1,2-dimyristoyl-*sn*-glycero-3-phosphocholine

DMSO: Dimethyl sulfoxide

DNA: Deoxyribonucleic acid

DSC: Differential scanning calorimetry

DTB: Desthiobiotin

DTT: Dithiothreitol

E. coli: Escherichia coli

EDTA: ethylenediaminetetraacetic acid

EGFR: Epidermal Growth Factor Receptor

EM: Electron Microscopy

ER: Endoplasmic Reticulum

ESI: Electrospray Ionization

ETC: Electron transport chain

FBS: Fetal Bovine Serum

GBM: Glioblastoma

GFP: Green Fluorescent Protein

GPCR: G-protein coupled receptors

GUV: Giant Unilamellar Vesicle

HCMV: Human Cytomegalovirus

HDL: High-Density Lipoproteins

HEK: Human Embryonic Kidney

hERG: Human ether-a-go-go related gene

His: Histidine

HVC: Hepatitis C

IAA:	Iodacetamide
IB:	Isolation Buffer
IC_{50}:	Concentration of an inhibitor where the response (or binding) is reduced by half
IFN:	Interferon
IL-3:	Interleukin 3
IM:	Ion Mobility
L858R:	EGFR mutation: Leucine to Arginine at amino acid 858
LAMB:	Large-Area Model Biomembranes
LC:	Liquid Chromatography
LCP:	Lipid Cubic Phase
LFA-1:	Lymphocyte function-associated antigen 1
LPN:	Lipid Nanoparticle
LR-PE:	1,2-dimyristoyl-sn-glycero-3-phosphoethanolamine- N-(lissamine rhodamine B sulfonyl)
LTC:	L858R-T790M-C797S triple mutant EGFR
mAb:	Monoclonal Antibody
McsL:	Mechanosensitive channel of large-conductance
mPES:	Modified Polyethersulfone
MS:	Mass Spectrometry
MSP:	Membrane Scaffold Protein
MTSET:	2-(trimethylammonium)ethyl methanethiosulfonate
MWCO:	Molecular Weight Cut-Off
Na_vSp:	Voltage-gated sodium channel pore
ND:	Nanodisc
NMDA:	N-Methyl-D-aspartic acid
NMR:	Nuclear Magnetic Resonance
NS4B:	Nonstructural protein 4B
NSCLC:	Non-Small Cell Lung Cancer
NTA:	Nitrilotriacetic Acid

OptiDIB:	Optically Assembled Droplet Interface Bilayer
PAGE:	Polyacrylamide Gel Electrophoresis
PBS:	Phosphate-Buffered Saline
PDMS:	Poly(dimethylsiloxane)
PDX:	Patient-derived Xenograft
PEG:	Poly(ethylene glycol)
PMSF:	Phenylmethylsulfonyl fluoride
POPA:	1-palmitoyl-2-oleoyl-sn-glycero-3-phosphate
POPC:	1-palmitoyl-2-oleoyl- *sn*-glycero-3-phosphocholine
POPE:	1-palmitoyl-2-oleoyl-sn-glycero-3-phosphoethanolamine
POPS:	1-palmitoyl-2-oleoyl-sn-glycero-3-phospho-L-serine
PTB:	Protein Data Bank
RMSD:	Root Mean Square Deviation
RNA:	Ribonucleic acid
RTK:	Receptor Tyrosine Kinase
SDB:	Standard Disk Buffer
SDS:	Sodium Dodecyl Sulfate
SEC:	Size-Exclusion Chromatography
SMA:	Styrene-Maleic Acid
SPR:	Surface Plasmon Resonance
ssMP:	Single-Span Membrane Protein
SUV:	Small Unilamellar Vesicle
SV40:	Simian vacuolating virus 40
Syb:	Synaptobrevin
T790M:	EGFR mutation: Threonine to Methionine at amino acid 790
TBST:	Tris-buffered Saline with Tween
TKI:	Tyrosine Kinase Inhibitor
TRAIL:	TNF-related apoptosis-inducing ligand

TRPML1: Transient receptor potential mucolipin 1

TRPV1: Transient receptor potential cation channel subfamily V member 1

t-SNARE: Target-soluble *N*-ethylmaleimide-sensitive factor attachment protein receptor

UV: Ultra-Violet

v-SNARE Vesicle-soluble *N*-ethylmaleimide-sensitive factor attachment protein receptor

XRD: X-Ray Diffraction

Abstract

Membrane proteins are essential to cellular functions, including cell-cell communication and signal transduction. However, the study of membrane proteins has lagged behind that of soluble proteins as once removed from the native cell lipid bilayer membrane proteins tend to misfold and aggregate, leading to loss of structure and function. To enable the study of stable and active membrane proteins, a variety of membrane mimetics have been developed.

The membrane protein mimetic used throughout this dissertation will be Nanodiscs, which are introduced in chapter one. The second chapter is a review of microfluidic devices that have been developed to study membrane proteins. The third chapter describes the microfluidic device we developed to form Nanodiscs containing membrane proteins on a faster timescale (5 minutes) and utilizing less material (90 μL). We formed both empty Nanodiscs and Nanodiscs containing the membrane protein cytochrome P450 CYP3A4 using our device and confirmed that the CYP3A4 remained functional after microfluidic incorporation, as measured with ligand binding assays.

The fourth chapter discusses using the microfluidic device to form Library Nanodiscs, a type of Nanodisc that is formed with cell lysate or isolated cell membranes instead of with a recombinantly expressed and purified membrane protein. I was able to confirm the incorporation of full-length Epidermal Growth Factor Receptor (EGFR) into Nanodiscs and had some success in measuring EGFR activity changes in response to tyrosine kinase inhibitors. These results that indicated EGFR in Nanodiscs had activity responses that are not noticed in lysate, potentially suggesting that Nanodisc incorporation allows for improved activity. However, high background

in the activity measurements from other membrane proteins present in the Nanodisc sample has led to the necessity to purify for only EGFR-containing Nanodiscs, which is still a work in progress to obtain high concentrations of these pure samples for activity measurements.

The fifth chapter describes a collaboration with the lab of Professor Neil Marsh, University of Michigan, focused on incorporating viperin into Nanodiscs. Viperin is a membrane-associated protein that interacts with different membranes within the cell, and we were interested in probing how this interaction impacts viperin's structure and function. We have determined the lipid composition that allows for optimal viperin incorporation which is important for our downstream activity assay and structural measurements.

The sixth chapter was performed in collaboration with the labs of Professor Brandon Ruotolo and Professor Philip Andrews, University of Michigan, in which we applied mass spectrometry to Nanodiscs with a focus on the impact of lipid composition on membrane proteins. With the Ruotolo lab, we incorporated cytochrome P450s into Nanodiscs and determined structural information about CYP3A4 in different lipid compositions using ion mobility-mass spectrometry. We found that changing the lipid environment caused changes in the protein gas-phase unfolding which indicates differences in the CYP3A4 structure in each lipid environment. With the Andrews lab, we formed Library Nanodiscs of different lipid compositions using mitochondrial lysate and used peptide-fingerprinting mass spectrometry to test which membrane proteins incorporate into Nanodiscs of each lipid composition. Though replicates still need to be performed, some proteins seem to incorporate into Nanodiscs of any lipid composition while others only incorporate into one Nanodisc.

Finally, I end with conclusions and future work in chapter 7. There are a variety of other areas in which this project will continue within the Bailey lab, including microfluidic and biological improvements.

Chapter 1: An Introduction to Nanodiscs

Membrane proteins are important for many cellular processes, but their study has lagged significantly behind that of soluble proteins. Cell-cell communication, energy production and signal transduction are all dependent on membrane proteins, and approximately 2/3 of pharmaceuticals target membrane proteins.[1,2] However, there is a lack of knowledge about the structure and function a majority membrane proteins, as seen by the low percentage (~3%) of membrane protein structures in the protein data bank.[3,4] Once removed from the native cell lipid bilayer, membrane proteins tend to misfold and aggregate, causing loss of native structure and function complicating accurate charachterization.[2,5,6] Studying membrane proteins within the cell bilayer is difficult because of the complex background caused by the variable lipids and other proteins also embedded in the bilayer.[7,8] To enable the study of structurally and functionally sound membrane proteins, a variety of membrane mimetics have been developed to stabilize the proteins outside the native cell membrane.[9]

One membrane protein mimetic that has recently gained traction are Nanodiscs, developed by the Sligar lab **(Figure 1.1).**[10,11] This mimetic is a soluble lipid bilayer that is stabilized by two membrane scaffold proteins (MSP). MSP was derived from Apolipoprotein A1 (ApoA1), the main protein component of high-density lipoproteins (HDL) in the human body.[12] Utilizing this scaffold protein allows for remarkably homogenous size distributions of the Nanodiscs.[13] Nanodiscs also allow access to both sides of the lipid bilayer and allow for precise control of the lipid composition and stoichiometry. Another advantage of using MSP is that a

number of MSP modifications have been engineered to enable better membrane protein incorporation and downstream processing.[11] The addition of up to three α- helices to the MSP, the sequence of which are repeats of an α- helix within the original ApoA1 sequence, allows for an increase in the Nanodisc diameter, from 9 nm to just less than 13 nm. This larger diameter allows for the incorporation of larger membrane proteins or protein complexes. Purification tags, such as a 6-histadine tag for Ni-NTA purification, allow for downstream purification to clean up the Nanodisc samples, such as extra lipids and unincorporated membrane proteins.

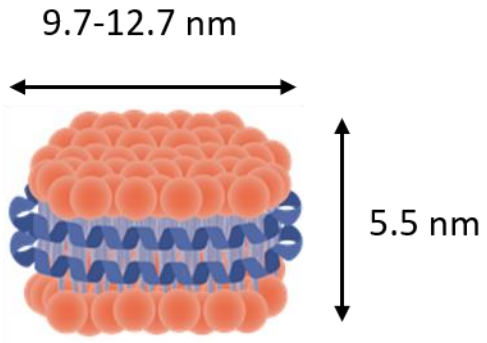

Figure 1.1: Image of an Empty Nanodisc. In blue are the two Membrane Scaffold Proteins and the red circles are the lipid heads. The difference in potential diameter references the range of commercially available lengths of MSP.

Nanodiscs have been used to stabilize many different classes of membrane proteins for downstream analysis. Structural studies in Nanodiscs have been performed using X-ray crystallography for bacteriorhodopsin[14]; electron microscopy for the ryanodine receptor[15] and TRPV1 ion channel[16]; and nuclear magnetic resonance (NMR) for the neurotrophin receptor p75NTRc.[17] The size homogeneity of Nanodiscs is one advantage, and the MSP prevents aggregation and preserves membrane protein structure during the processing required for each method. Nanodiscs have also been used as for testing membrane-associated proteins, especially for determining the impact of specific lipid compositions on proteins binding to a membrane surface, as it is possible to specifically control the Nanodisc lipid composition.[18] There have also

been membrane protein activity studies performed in Nanodiscs, including binding of small molecules to α-synuclein[19] and the GPCR neurotensin[20] and binding of other proteins to the P-gp transporter[21] and the sensor histidine kinase CpxA.[22]

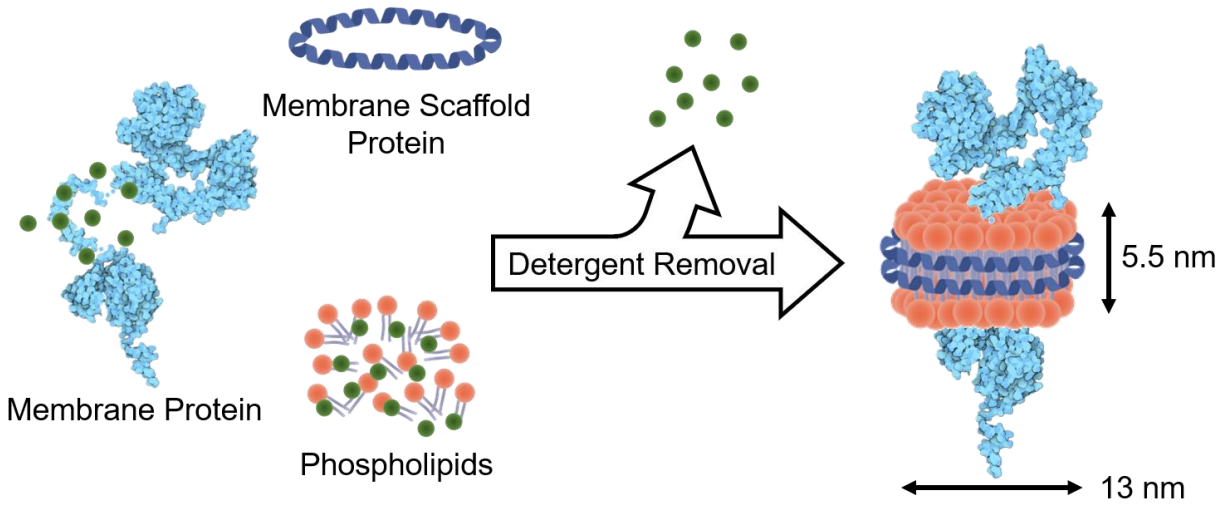

Figure 1.2: The Nanodisc formation process. Nanodiscs are formed through the removal of detergent from a solubilized solution containing a membrane scaffold protein (MSP), lipids and membrane protein.

Nanodiscs are formed by mixing the components (lipids, MSP, and potentially the membrane protein of interest), all solubilized in detergent, and then slowly removing the detergent, which causes spontaneous Nanodisc assembly **(Figure 1.2).**[23] The detergent is usually removed using oligosaccharide-based detergent removal beads but can also be removed by dialysis. The standard bead-based process can take between 2 and 18 hours, dependent on the lipid, detergent, and membrane protein identity.[10,24] The temperature that Nanodiscs are formed at is lipid dependent, based on the phase transition of the lipid used. This means that for certain lipid compositions, the Nanodiscs, and more importantly the membrane protein, might be at a suboptimal temperature for up to 18 hours, which could cause unknown alterations to the protein

structure and function. A method of forming Nanodiscs that will cut down on formation time would be advantageous both for improved high throughput analysis and protein functionality.

There has recently been significant research into expanding the diameter of the Nanodiscs from the ~13 nm maximum commercially available MSP to closer to 100 nm.[25] These larger diameters allow the study of large membrane protein complexes and processes that occur on the membrane surface, such as viral interactions and vesicle fusion.[26] One method that has been used to expand the Nanodisc diameter up to 50 nm is the formation of covalently circularized Nanodiscs, in which the termini of the scaffold proteins are covalently linked using a sortase.[27] This covalent linkage creates homogeneity in size, which tends to be more difficult as the diameters increase, however, these larger proteins tend to aggregate and are difficult to express in *E. coli* at high yields. Another method to stabilize larger diameter Nanodiscs of up to 70 nm uses DNA origami barrel scaffolds. The DNA scaffolds recruit small, non-circularized Nanodiscs which, upon the addition of detergent and excess lipids, merge together, forming a large lipid bilayer encircled by the MSP stabilized by the DNA scaffold.[28]

Other types of Nanodiscs have also recently gained traction, using scaffolds other than MSP to stabilize the lipid bilayer. These scaffolds include styrene-maleic acid (SMA) and peptide-based belts.[29, 30] One of the advantages of the SMA scaffold is that using these to form Nanodiscs does not require any detergent, which is a concern with MSP Nanodisc formation as detergent is known to destabilize membrane proteins.[29] However, forming SMA Nanodiscs, especially with more complicated lipid compositions, often requires multiple freeze-thaw cycles, which can also destabilize membrane proteins. These SMA Nanodiscs are also very sensitive to certain pH ranges or divalent ion concentrations which can be a concern for downstream processes such as activity assays that often require different buffers than the initial formation

conditions.[31] Both SMA and peptide Nanodiscs also tend to have a less controlled size and stoichiometry, as it is often unclear exactly how many of the scaffolds are present per Nanodiscs, as compared always having two MSP per Nanodisc.

There are disadvantages to using standard MSP-based Nanodiscs in certain conditions, such as for very large protein complexes or when particularly concerned about the impact of detergent at any point in the formation process. Other disadvantages as compared to commonly used membrane mimetics, including micelles, liposomes and planar bilayers, will be further covered in chapter two. However, there are also many advantages to these Nanodiscs. The ability to access both sides of the lipid bilayer, stability in a wide range of buffers and ionic conditions, and control of the size, lipid identity and composition and stoichiometry are all positives that have allowed MSP Nanodiscs to be applied to a wide range of membrane proteins to increase knowledge of these proteins' structures and activities.

One negative of Nanodiscs mentioned above is the long timeframe needed for formation, especially when using complex lipid mixtures or incorporating membrane proteins. To expedite the Nanodisc formation process we have developed a microfluidic device which I will discuss in chapter three. Microfluidics is defined as the manipulation of fluids on the sub-microliter scale and there have been a wide range of biological and chemical processes that have been converted to the microfluidic scale to decrease both the time and reagents used.[32-34] Developing a microfluidic device for Nanodisc formation with membrane proteins incorporated allows for faster formation, which could be important in preventing membrane protein instability, and lower membrane protein concentration, which is important because of the difficulty of obtaining high protein concentrations.

In the next chapter, I will present a review of the ways that microfluidics has already been applied to the study of membrane proteins and discuss further optimizations that I believe can be made. In chapter three I describe the microfluidic device we have developed in the Bailey lab for Nanodisc formation and purification, including demonstrating successful incorporation of the membrane protein cytochrome P450 CYP3A4. In chapter four I discuss how we have used this microfluidic device to form Nanodiscs from whole cell lysate, allowing for the incorporation of membrane proteins directly from the lysate into Nanodiscs without the need for purification. We have incorporated the Epidermal Growth Factor Receptor, EGFR, into Nanodiscs using our device and measured activity inhibition in the presence of tyrosine kinase inhibitors.

Chapters five and six are collaborative projects with labs of Professor Neil Marsh, Professor Brandon Ruotolo and Professor Philip Andrews, all of the University of Michigan, in which we applied microfluidic Nanodisc formation to a range of different membrane proteins and downstream applications. With Prof. Marsh, we have studied the membrane-associated protein viperin incorporated into Nanodiscs of various lipid compositions to determine the impact of a lipid bilayer on viperin activity and structure. We have used ion mobility-mass spectrometry with Prof. Ruotolo to study the impact of lipids and ligands on CYP3A4 structure. With Prof. Andrews, we determined which membrane proteins from lysed mitochondria incorporate into Nanodiscs of various lipid compositions using mass spectrometry. Finally, in chapter seven I summarize the research I have completed and expand into areas in which the Bailey lab plans to continue this project.

References:

1. Overington, J. P., Al-Lazikani, B. & Hopkins, A. L. How many drug targets are there? *Nat. Rev. Drug Discov.* **5**, 993–996 (2006).

2. Cross, T. A., Sharma, M., Yi, M. & Zhou, H. X. Influence of solubilizing environments on membrane protein structures. *Trends Biochem. Sci.* **36**, 117–125 (2011).

3. Hendrickson, W. A. Atomic-level analysis of membrane-protein structure. *Nat. Struct. Mol. Biol.* **23**, 464–467 (2016).

4. Konijnenberg, A., Van Dyck, J. F., Kailing, L. L. & Sobott, F. Extending native mass spectrometry approaches to integral membrane proteins. *Biol. Chem.* **396**, 991–1002 (2015).

5. Garavito, R. M. & Ferguson-Miller, S. Detergents as Tools in Membrane Biochemistry. *J. Biol. Chem.* **276**, 32403–32406 (2001).

6. Engelman, D. M. Membranes are more mosaic than fluid. *Nature* **438**, 578–580 (2005).

7. Van Meer, G., Voelker, D. R. & Feigenson, G. W. Membrane lipids: Where they are and how they behave. *Nat. Rev. Mol. Cell Biol.* **9**, 112–124 (2008).

8. Seddon, A. M., Curnow, P. & Booth, P. J. Membrane proteins, lipids and detergents: Not just a soap opera. *Biochim. Biophys. Acta - Biomembr.* **1666**, 105–117 (2004).

9. Arslan, A. & Fatih, Y. Biomimetic Lipid Membranes: Fundamentals, Applications, and Commercialization. *Springer International Publishing.* (2019).

10. Denisov, I. G., Grinkova, Y. V., Lazarides, A. A. & Sligar, S. G. Directed Self-Assembly of Monodisperse Phospholipid Bilayer Nanodiscs with Controlled Size. *J. Am. Chem. Soc.* **126**, 3477–3487 (2004).

11. Denisov, I. G. & Sligar, S. G. Nanodiscs in Membrane Biochemistry and Biophysics. *Chem. Rev.* **117**, 4669–4713 (2017).

12. Brouillette, C. G. *et al*. Structural models of human apolipoprotein A-I: a critical analysis and review. *Bilchimica et Biophysica Acta.* **1531**, 4-46 (2001).

13. Bayburt, T. H. & Sligar, S. G. Membrane protein assembly into Nanodiscs. *FEBS Lett.* **584**, 1721–1727 (2010).

14. Rasmussen, S. G. F. *et al.* Structure of a nanobody-stabilized active state of the β2 adrenoceptor. *Nature* **469**, 175–181 (2011).

15. Efremov, R. G., Leitner, A., Aebersold, R. & Raunser, S. Architecture and conformational switch mechanism of the ryanodine receptor. *Nature* **517**, 39–43 (2015).

16. Gao, Y., Cao, E., Julius, D. & Cheng, Y. TRPV1 structures in nanodiscs reveal

mechanisms of ligand and lipid action. *Nature* **534**, 347–351 (2016).

17. Mineev, K. S., Goncharuk, S. A., Kuzmichev, P. K., Vilar, M. & Arseniev, A. S. NMR Dynamics of Transmembrane and Intracellular Domains of p75NTR in Lipid-Protein Nanodiscs. *Biophys. J.* **109**, 772–782 (2015).

18. Muehl, E. M. *et al.* Multiplexed silicon photonic sensor arrays enable facile characterization of coagulation protein binding to Nanodiscs with variable lipid content. *J. Biol. Chem.* **39**, *16249-16256*, (2017).

19. Zhang, Z. *et al.* Ca2 + modulating α-synuclein membrane transient interactions revealed by solution NMR spectroscopy. *Biochim. Biophys. Acta - Biomembr.* **1838**, 853–858 (2014).

20. Inagaki, S. *et al.* Modulation of the interaction between neurotensin receptor NTS1 and Gq protein by lipid. *J. Mol. Biol.* **417**, 95–111 (2012).

21. Trahey, M. *et al.* Applications of lipid nanodiscs for the study of membrane proteins by surface plasmon resonance. *Curr. Protoc. Protein Sci.* **2015**, 29.13.1-29.13.16 (2015).

22. Hörnschemeyer, P., Liss, V., Heermann, R., Jung, K. & Hunke, S. Interaction analysis of a two-component system using nanodiscs. *PLoS One* **11**, 1–19 (2016).

23. Bayburt, T. H., Grinkova, Y. V. & Sligar, S. G. Self-Assembly of Discoidal Phospholipid Bilayer Nanoparticles with Membrane Scaffold Proteins. *Nano Lett.* **2**, 853–856 (2002).

24. Marty, M. T., Wilcox, K. C., Klein, W. L. & Sligar, S. G. Nanodisc-solubilized membrane protein library reflects the membrane proteome. *Anal. Bioanal. Chem.* **405**, 4009–4016 (2013).

25. Padmanabha Das, K.M. *et al.* Large Nanodiscs: A Potential Game Changer in Structural Biology of Membrane Protein Complexes and Virus Entry. *Front. Bioeng. biotech.* **8**, 1–7 (2020).

26. Bao, H. *et al.* Dynamics and number of trans-SNARE complexes determine nascent fusion pore properties. *Nature.* **554**, 260–263 (2018).

27. Nasr, M.L. *et al.* Covalently circulized nanodiscs for studying membrane proteins and viral entry. *Nat. Methods.* **14**, 49-52 (2017).

28. Zhao, Z. *et al*. DNA-corralled nanodiscs for the structural and functional characterization of membrane proteins and viral entry. *J. Am. Chem. Soc.* **140**, 10639–10643 (2018).

29. Dörr, J. M. *et al.* Detergent-free isolation, characterization, and functional reconstitution of a tetrameric K+ channel: the power of native nanodiscs. *Proc. Natl. Acad. Sci. U. S. A.* **111**, 18607–12 (2014).

30. Dominguez Pardo, J. J. *et al.* Solubilization of lipids and lipid phases by the styrene–

maleic acid copolymer. *Eur. Biophys. J.* **46**, 91–101 (2017).

31. Chen, A., Majdinasab, E. J., Fiori, M. C., Liang, H. & Altenberg, G. A. Polymer-Encased Nanodiscs and Polymer Nanodiscs: New Platforms for Membrane Protein Research and Applications. *Front. Bioeng. Biotechnol.* **8**, 1–8 (2020).

32. Du, G., Fang, Q. & den Toonder, J. M. J. Microfluidics for cell-based high throughput screening platforms-A review. *Anal. Chim. Acta* **903**, 36–50 (2016).

33. Lee, J., Soper, S. A. & Murray, K. K. Microfluidics with MALDI analysis for proteomics-A review. *Anal. Chim. Acta* **649**, 180–190 (2009).

34. Zhu, Y. & Fang, Q. Analytical detection techniques for droplet microfluidics-A review. *Anal. Chim. Acta* **787**, 24–35 (2013).

Chapter 2: The Development of Microfluidic Devices to Study Membrane Protein Structure and Function in Model Membrane Systems: A Review

Introduction:

Membrane proteins play a variety of essential roles in many cell processes, including cell-cell communication, signal transduction and energy production.[1] Though learning more about membrane proteins is crucial, their study has lagged behind that of soluble proteins.[1] Studying membrane proteins is more challenging as once membrane proteins are removed from the native cell membrane lipid bilayer, the proteins tend to aggregate and misfold, leading to differences in the protein structure and function.[2] The presence of a stable lipid bilayer plays an important role in the ability to study properly folded and active membrane proteins, especially as certain membrane proteins have demonstrated necessary interactions with specific lipids to be active.[3,4] To enable the study of membrane proteins there have been a number of model membrane systems, called membrane mimetics, that have been developed to stabilize membrane proteins.[5–7]

The first class of membrane mimetics can be classified as mimetics formed using stabilizing agents. The most basic of these is the detergent micelle, which can use many classes of detergents, including both ionic and nonionic detergents, to stabilize membrane proteins in solution.[8] Detergents are important in many membrane protein studies as detergents are often

used to remove membrane proteins from the native cell membrane before downstream analysis. Detergent micelles can be formed by adding detergents to a cell membrane, but detergents often cause loss of membrane protein structure and function, limiting their applicability in membrane protein research.[9] A related method uses amphipols, a more recently developed class of surfactants, as the basis for micelle formation.[10–12] These amphipols are composed of a hydrophilic backbone with hydrophobic chains, the structures of which were designed to be similar to detergents, though potentially with a more mild effect on the functionality of membrane proteins. The main issue with both detergent micelles and amphipols is that neither use lipids, so these model systems are not ideal for native membrane protein structure stabilization.[7] The other issue is that these micelles are small, with diameters on the single nanometer range, leading to strong membrane curvature which can cause membrane proteins to adapt non-native structures.[7] These problems with stabilizing agents indicate that to study stable membrane proteins, lipid bilayers should be used as the membrane mimetic.

Bicelles are a soluble lipid-based membrane mimetic that has been derived from the detergent micelle.[13,14] Bicelles are composed of lipid aggregates of short chain phospholipids stabilized with detergents. Less detergent is needed to stabilize the membrane proteins than in detergent micelles, which along with the presence of lipids, can allow a membrane protein to retain more of its native structure.[14] There are restrictions in the identities of the lipids and detergents that can be combined to successfully form bicelles and only a lipid monolayer is formed, both of which could negatively impact certain membrane proteins, especially those with large inner and outer domains.[15]

One commonly used membrane mimetic is a soluble lipid bilayer method called the liposome.[16,17] Liposomes are composed of two concentric spheres of lipids, with the lipid heads

in the central compartment and outside sphere exposed to aqueous solution. There are numerous methods to form liposomes using both mechanical and chemical means as has been discussed in recent reviews, many of which have been transferred to microfluidic methods.[18] Usually lipids are solubilized in an organic phase or detergent and then added to an aqueous solution, after which the organic phase or detergent is removed, leaving behind the stable liposome in the aqueous solution. Depending on the method of formation, liposomes can be polydisperse, leading to the necessity of purification to obtain a monodisperse sample. Liposomes are often used to study membrane proteins, especially transmembrane proteins that are involved in transport, as the compartmentalization in liposomes allows for the measurements of molecular flux, to determine membrane protein activity. There can be issues with the directionality of the membrane protein insertion in liposomes, as there is no access to the section of the protein that ends up within the inner compartment, though there have been recent developments to improve the control of membrane protein insertion.[19]

Another important soluble mimetic that has recently gained traction is the Nanodisc, which is a lipid bilayer held together by a scaffold wrapped around the hydrophobic tails of the lipids. There are multiple forms of Nanodiscs, depending on the scaffold composition, including peptides,[20,21] proteins,[22–24] and polymers.[25,26] These scaffolds allow for better control of the size of the mimetic, as the size of the scaffold will determine the bilayer diameter, allowing for more homogenous formation. Another benefit of Nanodiscs is the access to both sides of the lipid bilayer, allowing for the study of membrane structures on both domains of a transmembrane protein.[27] Depending on the scaffold used, each form of Nanodiscs does have some drawbacks, including the necessity to use freeze-thaw cycles or detergents to incorporate membrane proteins,

both of which could destabilize the protein.[22,25] Nanodiscs also have no inner compartment to enable simple ion channel studies often employed using liposomes.

The last major class of membrane mimetics can be classified as planar lipid bilayers.[28,29] These bilayers are easy to assemble on a surface and can allow the characterization of lipids or membrane proteins using surface-sensitive analytical techniques, such as surface plasmon resonance. However, the surfaces that support the bilayer can sterically hinder the insertion of membrane proteins with large inner and outer domains. There have been various techniques developed to overcome this limitation, including tethering between the lipids and the underlying surface[30] or small apertures across which a suspended lipid bilayer can be formed.[31]

Each of these membrane mimetics has advantages and disadvantages, many of which are complimentary. This means that careful selection of the mimetic to match the membrane protein of interest and the planned study is very important.

One of the major difficulties of studying membrane proteins is the low concentration of membrane proteins in each cell as compared to soluble proteins.[32] Membrane protein experiments often require recombinant expression to accrue high enough concentrations of these proteins. It can be exceptionally difficult to obtain full length membrane proteins containing all native post-translational modifications using recombinant systems, requiring careful selection of the host cell used as the expression system.[33] To avoid the need for using host cells, it is possible to use cell-free protein synthesis, in which DNA or mRNA, nucleotides, amino acids and cell lysate are combined to create a more controlled setting in which to synthesize membrane proteins.[34] However, it would be ideal to have technologies which could use lower membrane protein concentrations in their analysis.

To enable the study of membrane proteins on a smaller scale, microfluidic devices can be implemented.[35–37] Microfluidics is defined as fluidic channels with features smaller than 1 micron in diameter. This allows for the miniaturization of a variety of processes to enable the use of less material on faster time scales, typically only requiring microliters of sample.[38–43] A wide range of biological assays have been performed on the microfluidic scale to expand research on previously hard-to-study areas as has been discussed in prior reviews. Using microfluidics could potentially lower the concentrations of membrane proteins needed for membrane mimetic development and downstream membrane protein assays.

To create membrane mimetics using microfluidic devices, several steps would need to be performed. Ideally, a microfluidic device would be able to separate out membrane proteins of interest from whole cell lysate or be able to perform cell-free synthesis on chip. The membrane proteins would then be incorporated into a stable lipid bilayer and finally, downstream structural or functional analysis would occur. Though there are currently a variety of microfluidic methods able to perform unique steps of these processes, there are very few devices able to perform all steps of interest on one device.

Over the course of this review, we will discuss the variety of microfluidic devices that have already been developed to form membrane mimetics and whether it has or could be successfully used to incorporate membrane proteins. We will also discuss devices that have been used for membrane protein studies that do not include membrane mimetic formation on device. Finally, we will theorize on ways that microfluidics devices can be further developed to combine all necessary steps to study membrane protein structure and function while stabilized in a lipid bilayer on a single device.

Section 1: Forming Membrane Mimetics on Microfluidic Chips

1.1: Planar Lipid Bilayers

There are two main methods through which supported lipid bilayers are typically formed.[28,29] The first involves forming unilaminar lipid vesicles in an aqueous solution and then adding these vesicles to a surface, where the vesicles absorb and fuse to form a lipid bilayer. Membrane proteins can be incorporated into bilayers using this method, but it requires a great amount of optimization of factors that affect the ability of the vesicles to absorb to the solid support and fuse together. The second method involves forming a lipid monolayer on an aqueous-air surface and then pulling a hydrophilic solid support vertically through the lipids. This forms a lipid monolayer on the solid surface, which can then be pushed horizontally through a second aqueous-air lipid monolayer, forming a lipid bilayer on the solid surface. This method often cannot be used for membrane protein incorporation because the air exposure during the formation causes damage to the proteins that cannot be reversed even after the stable lipid bilayer is formed.[44]

1.1a: Supported Lipid Bilayers

The first microfluidic method to form supported lipid bilayers was described in 2001.[45] The microfluidic device was composed of poly(dimethylsiloxane) (PDMS) on a glass substrate and comprised a linear array of eight individually addressable 50 μm wide channels. The lipid bilayers were formed in the channels using the unilamellar vesicle technique by flowing lipid vesicles through each channel followed by a buffer wash step. This microfluidic device was not initially used to study membrane proteins but has been used in multiple other publications to study soluble protein-ligand[46] and protein-lipid[47,48] interactions. There have been no publications using this device to study integral membrane proteins, potentially because of the lack of room for membrane protein insertion between the lipids and glass surface.

There have been similar microfluidic devices that use the unilaminar lipid vesicle method, with differences in channel sizes, lipid compositions and other variables to allow for membrane protein studies.[49] The benefit of using the lipid vesicle method is that instead of lipid-only vesicles, proteolipid vesicles can be used, in which the membrane proteins are pre-loaded into the lipid vesicles so that the lipid bilayer and membrane protein insertion can be performed in one step. This does require proteolipid vesicle formation first off-chip, adding steps that could cause loss of membrane protein sample or destabilization of the protein. The ion channel, gramicidin A, was incorporated into a microfluidic biosensor to measure the flux of hydrogen ions through the channel. After the proteolipid vesicles were fused into a lipid bilayer on the surface, the change in pH caused by the ion channel's transport was measured, allowing for the label-free study of the behavior of this transmembrane protein.[50]

Solid supported lipid bilayers are simple to form in microfluidic channels by flowing pre-formed lipid vesicles through the device. The issue is that it is difficult to study full-length transmembrane proteins because there is often not sufficient room for the inner domain between the solid support and the lipids. While some studies have gotten around this by using only sections of the membrane protein,[49] any studies that use a partial protein instead of the full-length protein could potentially cause misleading results, as it is difficult to prove that the domains removed do not have an effect on the structure or activity of the remaining protein. This suggests that alternative microfluidic methods should be explored to form planar lipid bilayers to incorporate membrane proteins.

1.1b: Tethered Lipid Bilayers

To create more room for integral membrane proteins, a tethering unit, often a polymer or peptide, can be used to connect the solid support to the bottom layer of the lipid bilayer.[51] The

first tethered bilayer in a microfluidic device used biotin-avidin chemistry as the tether. A PDMS-glass microchip was coated with biotinylated bovine serum albumin, which was used to pull down avidin. To form the membrane, biotinylated small unilamellar lipid vesicles (SUVs) were flown through the channels and immobilized on the avidin surface, and were fused into a lipid membrane by injected concentrated poly(ethylene glycol) (PEG)-8000. [52] **(Figure 2.1)** This tethered bilayer formation method was later used by the same lab to study multiplexed analysis of lipid-protein interactions using surface plasmon resonance (SPR), though only soluble membrane-associated proteins were studied.[53] This microfluidic device can form a tethered lipid bilayer, but the necessity of biotinylated lipids increases necessary experimental steps and potentially limits the lipids that could be used.

There have been other successful microfluidic experiments in which tethered bilayers have been used to study membrane proteins. In one such case, proteolipid SUVs were used to incorporate target-soluble *N*-ethylmaleimide-sensitive factor attachment protein receptor (t-SNARE), a membrane protein involved in almost all known intracellular fusion, into the lipid membrane during bilayer formation tethered to a PEG polymer brush on a glass slide. Then fusion rates of vesicle-associated vesicle-SNAREs (v-SNARE) with the membrane incorporated t-SNAREs could be studied, leading to the conclusion that there is a minimum number of v-SNAREs per vesicle and t-SNAREs in the membrane needed for fusion to occur.[54,55] This SNARE complex formation information is important to understand how fusion occurs *in-vivo* between vesicles and cell membranes.

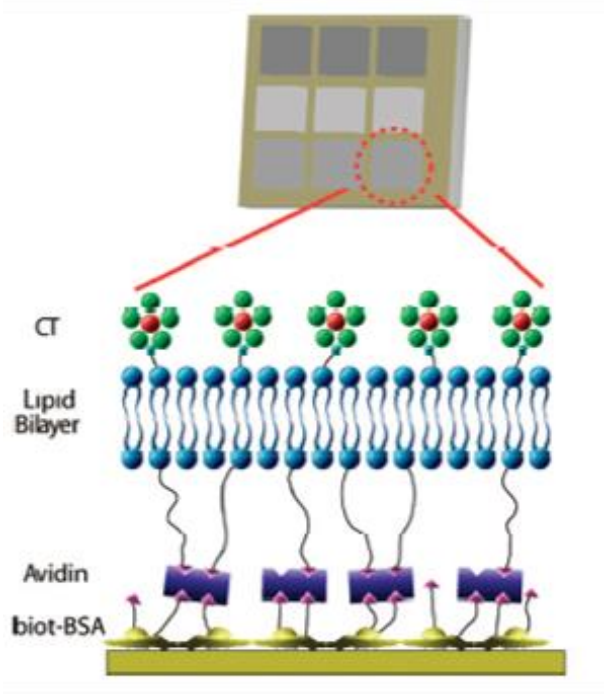

Figure 2.1: Representative cartoon of the tethered bilayer lipid membrane array. The surface coating begins with physical absorption of the biotinylated bovine serum albumin (biot-BSA) to the gold surface. Then the lipid bilayer is formed by flowing first Avidin, and then liposomes with ~1% biotinylated PE which will bind to the Avidin and be subjected to PEG-triggered fusion to form the bilayer. Finally, the membrane protein of interest (CT in the figure) is introduced and binds to specific lipids. Reprinted from Taylor *et. al.*[53]

Using a tethered lipid bilayer allows for the study of membrane proteins on a solid surface, which can be advantageous for certain surface-based analytical methods, such as SPR or electrochemical detection. However, there can be concerns when using a tethered lipid bilayer, including the need to insert the membrane protein in the correct orientation. Additionally, the membrane proteins must be first inserted into SUVs off-chip before forming the lipid bilayer on-chip, which is not ideal when trying to streamline the MP characterization process.

1.1c: Suspended Lipid Bilayers

One of the more common methods that has been applied to probe a variety of membrane proteins microfluidically is the formation of suspended lipid bilayers within small apertures, usually with a diameter around 100-200 μm.[31,56] This allows for the study of a single ion

channel of interest as measurement of the electrophysiology of the protein is possible by inserting electrodes into the aqueous solutions on either side of the aperture. There are multiple ways to form these bilayers. The Mueller-Rudin method, also known as the painting method, "paints" a lipid-oil mixture across the aperture and then allows the oil to thin, leading to the formation of the lipid bilayer in the aperture. A potential drawback is that a small amount of oil remains between the lipid layers, especially near the walls of the aperture, which could have a negative impact on membrane proteins. Another common method is the Montal-Mueller, or folding, method, in which a lipid monolayer formed on an air-water interface is brought into contact with both sides of the aperture to form the lipid bilayer.[54] It is also possible to insert the cell membrane from a live cell into the aperture and then remove the remainder of the cell to allow for studies of the native cell membrane.[29]

One issue with using these larger apertures is that the bigger the aperture, the more unstable the lipid bilayer is, which decreases the length of time the ion channel can be studied. There are a number of ways that these bulk apertures have been optimized to allow for more stable bilayers, including changing the material of the aperture and tapering the aperture shape.[31] However, transitioning to microfluidics allows for even smaller diameters of the aperture, a major advantage, both for extending the time stable bilayers last and to decrease the amount of materials used.

The first microfluidic device in this area used a chemically engraved glass aperture that was then silanized and incorporated into a simple glass microfluidic device composed of a linear fluidic channel with the aperture in the middle of the device, with a well over the aperture to allow for fluid on each side of the membrane. The lipid bilayer was formed by injecting the lipids in *n*-decane into the base of the well and then adding aqueous buffer into the upper well. A

majority of the time, the lipid bilayer did not spontaneously form, and thus the buffer had to be agitated or removed and re-injected, indicating that forming bilayers using this method took significant effort on the part of the user.[57] Further development to make this technique more reproducible led to the formation of a similar design but using a polymer microfluidic device that used a brief air-exposure method to form the lipid bilayer, with successful bilayer formation ~90% of the time.[58] This process still required some manual effort on the part of the user, to pipette in the lipid solution and then reinject buffer on top of the membrane after ensuring that the air-exposure step led to membrane formation.

As discussed in a previous section, the necessity of the air-exposure step does lead to concerns about the ability to incorporate membrane proteins, as there is not much known about how air-exposure could impact the structure or activity of membrane proteins. However, membrane proteins were successfully inserted into the suspended lipid bilayers in these air-exposure based polymer microfluidic devices by first incorporating the proteins into liposomes and then injecting these proteoliposomes into the upper well of the microfluidic device. The potassium channel KcsA was inserted into the lipid bilayers about 80% of the time as monitored by electrical activity across the membrane. These KcsA membrane proteins in the suspended lipid bilayer were stable for about 1 hour after formation and the incorporation process took 20-30 minutes.[59] The plexity of these microfluidic devices was increased by forming arrays of 12 apertures to form individually addressable lipid bilayers with a formation rate of 80% after two air-exposure steps, though the authors note that improved control of the fluid dispensing in terms of both timing and volume would be necessary to fully take advantage of increasing the plexity of this method.[60]

One means of improving the fluidic control of the microfluidic devices is to use the passive flow of microliter sized droplets and the lipid bilayer painting method instead of air exposure. Though the plexity of this new platform was decreased to six bilayers per chip, the applicability to multiplexed ion channel membrane protein studies was successfully demonstrated. Both α-hemolysin and KcsA were successfully inserted and dose-dependent blocking and IC_{50} curves were developed with β-cyclodextrin and polyethylene glycol (for α-hemolysin) or tetraethylammonium (for KcsA).[61] The wider applicability of this system to important biological questions such as membrane protein-drug interactions was shown as well by incorporating the prokaryotic voltage-gated sodium channel pore (Na_vSp), testing the dose-dependent response to the channel blocking drug nifedipine and successfully determining the IC_{50}.[62] If this system could be better fluidically-controlled and the lipid bilayer formation method automated, it could be an excellent way to study a variety of channel-based membrane proteins interactions with a variety of water-soluble ligands and drugs.

Another class of devices were fabricated on silicon-on-insulator substrates, with each compartment having a circular shape with a picoliter volume sealed well on top, with a thin silicon membrane between them containing a pore between 220 nm and 2 μm diameter. To form the lipid bilayers, giant unilamellar vesicles were formed off-chip and then added to the chip where vesicle fusion was induced with a high ionic concentration buffer. The advantage of this method over the previously described aperture-based devices is that no organic solvent or air-exposure is needed for the bilayer formation, potentially improving membrane protein stability, and the smaller sizes of the compartments and pores allowd for high plexity on a smaller scale.[63]

Successful membrane protein incorporation on a 2025 nanopore array was performed using the often-used model membrane protein α-hemolysin and was confirmed by measuring the

transport of two fluorescent dye molecules. The transport of a red dye that was small enough to travel through the channel formed by the α-hemolysin versus a green dye conjugated to dextran, which made the dye too large to transport, allowed for the distinction between successful α-hemolysin incorporation (only red dye) and lipid membrane rupture (green and red dye).[64] The wider applicability of this method was shown using the mechanosensitive channel of large-conductance (McsL) modified to only open when adding a specific reagent 2-(trimethylammonium)ethyl methanethiosulfonate (MTSET). The ligand-triggered opening of McsL was measured by Oy647 efflux, and hundreds of these opening events were measured on a single chip.[65] The microfluidic chip has recently been optimized by incorporating inverted-pyramidal cavities instead of circular cavities, increasing the efficiency and stability of lipid bilayer formation while maintaining the ability to incorporate membrane proteins.[66] Though these devices have many advantages, including the highest plexity and the ability to measure channel flux for more than just ion channels, there are also a few disadvantages. The necessity for a fluorescent dye to be transported for the measurement does still limit the types of channels that can be studied, as channels that transport only specific molecules will not be able to transport the dye. The success rates of measurements were also low, with only a 8% success rate at measuring the efflux of the dye, suggesting the majority of the membrane proteins are not being measured successfully, which could be problematic with rare samples.[65]

There are multiple other interesting aperture-based microfluidic devices that have been used to study membrane proteins in lipid bilayers. A recently published a paper describes a 16-plex device that successfully incorporated hERG, TRPV1 and NMDA channels from crude cell membranes directly into the microfluidic device without detergents and were able to measure the open/close activity of all the channels. They were also able to use organelle membranes,

including the TRPML1 membrane protein from the lysosomal membrane and the RyR channels from SR membranes.[67] This ability to incorporate membrane proteins into these bilayers directly from the cells without the need to isolate the proteins or use detergent for solubilization is essential for saving time, reducing protein loss and preventing detergent denaturation of the membrane proteins. Increasing the plexity further would really increase the applicability of this device.

Though most of the suspended-bilayer methods use small apertures, it is also important to consider the impact that the larger cell membrane could have on the structure or function of membrane proteins. The formation of more realistic mimetics has been demonstrated by forming millimeter-area bilayers, termed large-area model biomembranes (LAMBs).[68] Both α-hemolysin and alamethicin ion channels have been successfully incorporated into LAMBs,[69] suggesting that these larger lipid bilayers can be used to study membrane proteins, while potentially allowing for more interesting membrane protein interaction studies between multiple large proteins.

One final suspended lipid bilayer-based approach uses 3D printed devices to form asymmetric lipid bilayers. Cell membranes physiologically have different lipid membrane compositions on either side of the bilayer, so mimetic systems that can successfully form these asymmetric bilayers are often considered more biologically significant. These devices have a 100 μm aperture where the bilayer forms and connects two open crossed-channels, meaning that different lipid compositions can be introduced into each channel to form this asymmetry.[70] A variety of membrane proteins have been successfully incorporated into these bilayers including t-SNARE, α-hemolysin, and α-synuclein, resulting in the discovery of three different methods of action on the membrane for α-synuclein.[70,71] 3D-printed microfluidic devices also improved accessibility, as no cleanroom would be needed as is required for PDMS or glass microfluidic

device formation. However, as the device currently stands, there is only one aperture, so though one single membrane protein can be intensely studied, as in the case of α-synuclein,[71] there is no clear way to increase plexity for larger studies.

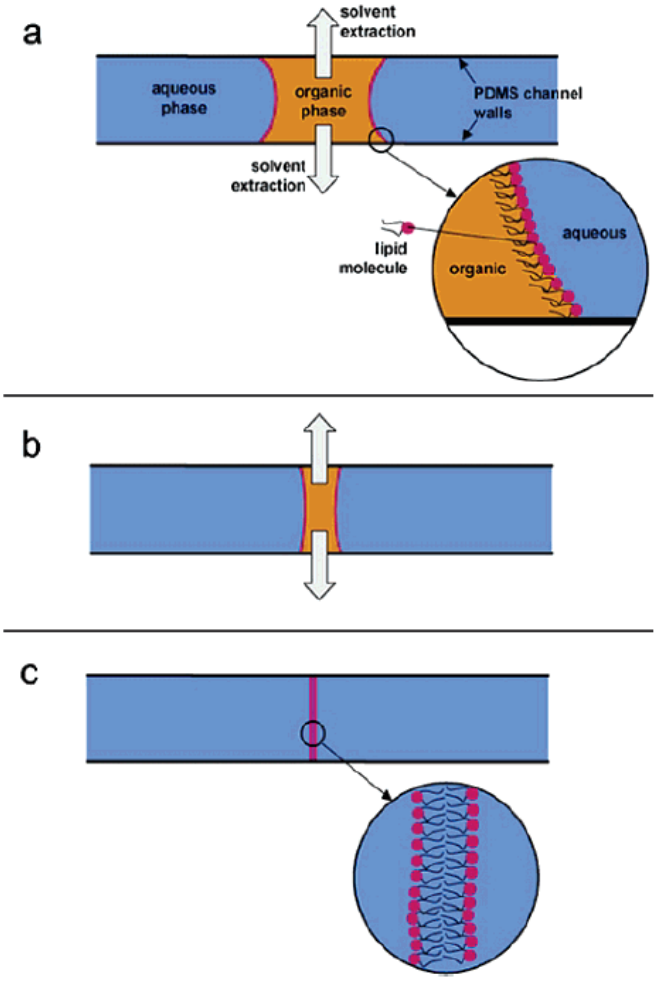

Figure 2.2: Visualization of the lipid-bilayer formation by microfluidic solvent extraction. (A) The organic phase containing lipids is formed surrounded by two aqueous phases. The lipids spontaneously assemble at the hydrophobic-hydrophilic interface, as seen in the inset figure. (B) The organic solvent partitions into the PDMS, causing the two layers of lipids to move closer. (C) Finally, the lipids touch, forming a lipid bilayer, as seen in the inset. Reprinted from Malmstadt *et. al.*[72]

One interesting approach based on the theory of the bulk Montal-Mueller method that does not use an aperture is the formation of free-standing lipid bilayers in small microfluidic devices using a solvent extraction method.[72] A small amount of lipids in an organic solvent is flowed through the device, surrounded by an aqueous buffer on either side. Since one of the properties of PDMS is that organic solvents will partition into the PDMS, the solvent will be extracted, leaving behind a vertical lipid bilayer across the microfluidic channel surrounded by aqueous solvent on both sides **(Figure 2.2).** α-hemolysin, a water-soluble bacterial protein that can form heptameric pores in lipid membranes, was successfully inserted into the lipid bilayer simply by including the α-hemolysin in the aqueous buffer. This incorporation suggests the potential to study membrane proteins using this microfluidic method. However, this method has not been further applied to the study of membrane proteins because of a number of limitations, including low plexity and limited control of membrane formation and protein insertion because of the placement of the bilayer in the channel.

There have been a number of different microfluidic devices developed that can form suspended lipid bilayers, and overall these have been relatively successful for incorporating membrane proteins. However, all of the membrane proteins that have been studied so far are channel proteins, as these are easier to measure activity via transport of ions or fluorescent molecules. There are also issues with formation, automation and control of the bilayer formation process that need to be addressed.

1.1d: Droplet Interface Lipid Bilayers

This primarily microfluidic method was first described in 2006, using two different but very simple devices to form and interface two lipid monolayers. One device had two circular wells containing organic solvent into which a water droplet could be injected to form a

water/organic interface. The second device consisted of two channels (one containing lipids in organic solvent and one containing the aqueous solvent) in a cross-shaped device with syringe pumps to control the bilayer formation.[73] Both devices could successfully incorporate α-hemolysin at the lipid bilayer interface. The initial two-well device design was improved to allow for solution exchange within the water droplet by introducing fluidic channels within each droplet, as without solution exchange the ions inside the droplet will be depleted rapidly, limiting the length of a activity study.[74] α-hemolysin was once again introduced into the lipid bilayer and the solution exchange channels could be used to introduce hepta-6-sulfato-β-cyclodextrin, a blocker of α-hemolysin, into the droplet, suggesting a potential use for ligand and drug studies as well.

A second way to form these droplet interface bilayers is droplet dielectrophoresis. Instead of manually manipulating the droplets into contact to form the bilayer, droplets can be moved based on changing an electric current. The microfluidic device developed contained six pairs of individually addressable platinum electrodes on a glass substrate with a plastic reservoir bonded to the surface of the device to contain the organic solution.[75] It was shown that two aqueous droplets could be brought in and out of contact, forming and breaking a lipid bilayer at the interface of the droplets. There might be issues with the effect of this electrical current on a membrane protein's structure or function, if successfully inserted, which was not demonstrated.

One of the interesting uses of droplet interface bilayers is that long networks of droplets can be formed, to make extended structures that could be compared to a number of interacting cells or a tissue. Microfluidic methods allow large numbers of these droplets to be formed and controlled, such as a microfluidic device to form droplet networks containing lipid bilayers of controllable size and composition by developing a droplet-on-rails method. The 'rails' are

grooves on the channel surface that lower the energy state of the droplet, encouraging the droplets to enter the groove and follow the rail to help control droplet proximity.[76] The same lab developed a more advanced way to control the bilayer network assembly and even form 3D droplet-based networks using optical tweezers.[77] Termed the optically assembled droplet interface bilayer (OptiDIB) network, the ability to form 3D networks expands the biological relevance to the way cells interact in real space instead of just on a flat surface. The only studies done on these networks involved passive diffusion between the droplets, with no membrane protein incorporation. However, it would be interesting to see this expanded to a membrane protein incorporation platform, especially for modeling the passage of substrates from extracellular spaces to within organelles, passing though multiple membrane proteins.

A microfluidic device that demonstrated membrane protein incorporation allows for the manipulation of two unique droplets with fluid flow to interact to form a bilayer, into which electrodes can be inserted to make electrical measurements of the membrane proteins inserted. Then, one or both of the droplets can be ejected and new droplet(s) can be moved to the electrode position to form a new lipid bilayer.[78] α-hemolysin was inserted into the lipid bilayer by adding soluble α-hemolysin to one droplet while the second droplet containd only buffer. Successful membrane protein incorporation was measured by changes in the electrical current. The buffer droplet was then removed and a new buffer containing γ-cyclodextrin, a reversible α-hemolysin blocker, was moved into place. Decreases in current were seen, which were restored by once again replacing the blocker-containing droplet with a buffer droplet, indicating that the α-hemolysin was both present and functional in the lipid bilayer.[78]

The device was slightly upgraded using the same basic principle to allow for a network of four droplets instead of two.[79] **(Figure 2.3)** Inhibitors were screened across the three bilayers by

adding α-hemolysin to three droplets and the γ-cyclodextrin to the fourth. A decrease in current was noted across all three bilayers, suggesting successful membrane protein formation and inhibitor transport. The most recent version of this device can rapidly form droplet interface bilayer pairs of controlled composition using hydrodynamic traps to allow for splitting, merging, and storing droplets in side-wells. This allows for on-chip preparations of dilutions of inhibitors to study a whole range of membrane protein inhibition on-chip. The system can form arrays of 12 controllably different droplet lipid bilayers in 5 minutes. This device also demonstrated using dyes to monitor ion channel transport through α-hemolysin instead of the electrical measurements,[80] showing greater potential for wider applicability beyond ion transport.

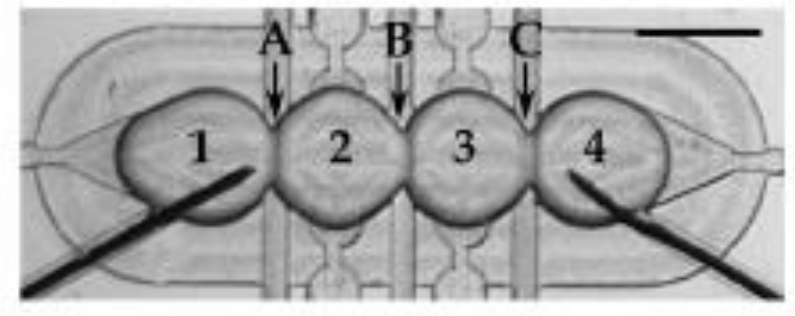

Figure 2.3: Micrograph of the four-droplet network microfluidic chips. Each droplet is numbered 1-4 from left to right. The lipid bilayers at the droplet interfaces are lettered A-C from left to right. The scale bar is 1 mm. Reprinted from Casekalska *et. al*.[79]

A different device that used a droplet interface bilayer microfluidic device to study membrane proteins focused on the human chloride intracellular ion channel 1 (CLIC1).[81] The microfluidic device can form arrays of droplet interface bilayers in parallel, incorporate a human chloride channel and then use fluorescence to measure chloride ion flux through the protein. The flux through the chloride channel was directly compared to the general movement of the chloride through α-hemolysin pores, because of the ability to form different droplet arrays, resulting in a

more well-controlled system for CL1C1 analysis. This microfluidic method could be used to measure and compare ion flux through different membrane proteins, potentially in the presence or absence of different concentrations of various inhibitors if higher array numbers and good fluidic control could be developed.

Overall, forming droplet interface bilayers on-chip has been a frequently and successfully used method to study membrane proteins, especially transport channels. The ability to perform functional screening using either electrical or fluorescent-based methods increases applicability over just ion-based channels, and we expect to see more membrane proteins that transport uncharged molecules being characterized in the future. Though some low-level plexity has been shown, high plexity (on the order of 20+) has yet to be developed.

1.1e: 3D Lipid Structure Arrays

While model lipid bilayers are traditionally formed planarly, there has been some recent interest in developing 3D lipid structures, to better mimic the surface of a cell. Using an array of microwells in SU-8, three-dimensional freestanding lipid bilayer were formed that are more comparable to a full cell membrane than a flat lipid bilayer. Small unilamellar vesicles in aqueous solution were filled to the top of the microwell and then dried to form multilayered-lipid films inside the wells. When aqueous buffer was added and an electric field was applied, the vesicles fused and eventually formed 3D bilayers attached to the top of the microwell.[82] α-hemolysin was inserted into the bilayers using simple flow in aqueous solution and allowed for measurable transport in and out of the well through the 3D bilayer. A direct comparison of α-hemolysin transport in a suspended 2D lipid bilayer to the transport in these 3D bilayers would be really interesting, to determine the impact of the dimensionality of the model on membrane proteins. The same basic microfluidic device can be used to incorporate human 5-HT_{3A}

receptor,[83] and the transport of 5-HT though the receptor was measured using fluorescence. Though not widely applied so far, this 3D method is a recent development that allows for a more native-like lipid bilayer that has already been able to incorporate membrane proteins for transport measurements. It would be interesting to see direct comparisons between 2D and 3D bilayers to determine if this more native-like lipid bilayer does impact membrane protein incorporation, structure or function, and if this impact is the same for different classes of membrane proteins.

1.2: Liposomes

There are a number of ways that liposomes are commonly formed traditionally and using microfluidics, both of which have been previously reviewed.[17,18] As these reviews do an excellent job focusing on liposome formation, we will focus on only the methods that have successfully been translated into microfluidic devices and have shown successful membrane protein incorporation on-device.

1.2a: Electroformation

Electroformation is a common method used to form liposomes in many settings. Lipids in an organic solvent are spread over the surface of a planar electrode and the solvent is evaporated, creating a dry lipid film on the electrode. The electrode is then placed in an aqueous solution and an electric field is applied, leading to the lipids peeling off the electrode and forming vesicles in the aqueous solution.[84] The vesicle formation tends to be polydisperse and can lead to multilamellar vesicles, as the formation process relies on how the lipids peel off the electrode and interact with each other during this process. As the lipid film has to be dried before the vesicle formation can begin, there cannot be any direct incorporation of membrane proteins into the vesicles. Membrane protein incorporation must take place after liposome formation in a separate process. Another issue is that low ionic strength buffers are required for forming larger

liposomes (<1 μm), unless using modified lipids, as the ions interfere with the lipid bilayer formation after the electric field is applied. This can limit some biological applications, as physiological buffers are at much higher ionic strengths.[85]

There have been a number of microfluidic devices that allow for electroformation of liposomes on a smaller scale. The first formed giant unilamellar vesicles (GUVs, 10-100 μm diameter) in a PDMS-based flow chamber with ITO electrodes. The use of the flow chamber allowed the researchers to form surface-attached liposomes in a low ionic strength buffer, and then replace that buffer with a high ionic strength buffer to perform physiologically relevant interaction studies. The microfluidically formed GUVs were then used for the study of the membrane-associated protein annexin V binding to the phospholipid phosphatidylserine (PS). The GUVs demonstrated that annexin V binding was dependent on PS concentration and that this binding decreases as ionic strength increases. The group further developed this microfluidic device to allow for the study of more than 100 giant liposomes in parallel, to study membrane fusion.[86] Other early work in electroformation in microfluidic channels found that the liposomes formed were mostly unilamellar (90%) but there were significant size variations – though the goal was to form only giant liposomes, only 54% of liposomes formed were greater than 10 μm in diameter.[87] This inconsistency in size could lead to issues with downstream analysis.

One of the more complicated microfluidic devices developed allowed for integration of liposome generation using electroformation, followed by the analysis of the liposomes all on the same device.[88] The focus was not on analyzing a membrane protein but using melittin, a pore-forming antimicrobial peptide, to study the interactions between the different lipid compositions in the liposomes and the peptide. Examples of microfluidic devices, such as this one, that combine bilayer formation and analysis, are ideal, as they prevent loss of sample or deformation

of the liposomes between formation and analysis, though a membrane protein has not been studied using this device.

Though to a certain extent microfluidics can improve the electroformation process by allowing for the use of high ionic strength buffers and improved unilamellar formation, there are still a number of difficulties. The most important is that because the formation depends on a dried lipid film, there is a limited number of liposomes that can be formed before the lipids run out and the device is no longer functional, preventing continuous formation. There are also concerns about membrane protein incorporation occurring after liposome formation, as membrane proteins cannot be inserted before the lipid film drying step.

1.2b: Jet Flow

A microfluidic liposome formation method without a bulk comparison is the use of jet flow. A lipid membrane was formed within an aqueous solution by interfacing two lipid-stabilized water droplets. Then a glass capillary nozzle was used to shoot jets of aqueous solution across the membrane. This jetted solution pushes the lipid membrane out until it pinched off at the base, forming a lipid vesicle.[89] **(Figure 2.4)** These liposomes tend to be large and relatively monodisperse, with the first reported formation in the 300-600 μm range.[89] Further development by this lab allowed for the formation of cell-sized asymmetric membranes, by first forming an asymmetric lipid tube and then applying the jet flow.[90] The membrane protein connexin43 (Cx43) fused with green fluorescent protein (GFP) was inserted into the liposomes and the fluorescence was compared between different symmetric and asymmetric lipid compositions. It was found that the presence of a negatively charged lipid (DOPS) in the outer leaflet significantly influenced the amount of Cx43 inserted into the liposomes, indicating the importance of lipid composition on membrane protein incorporation.

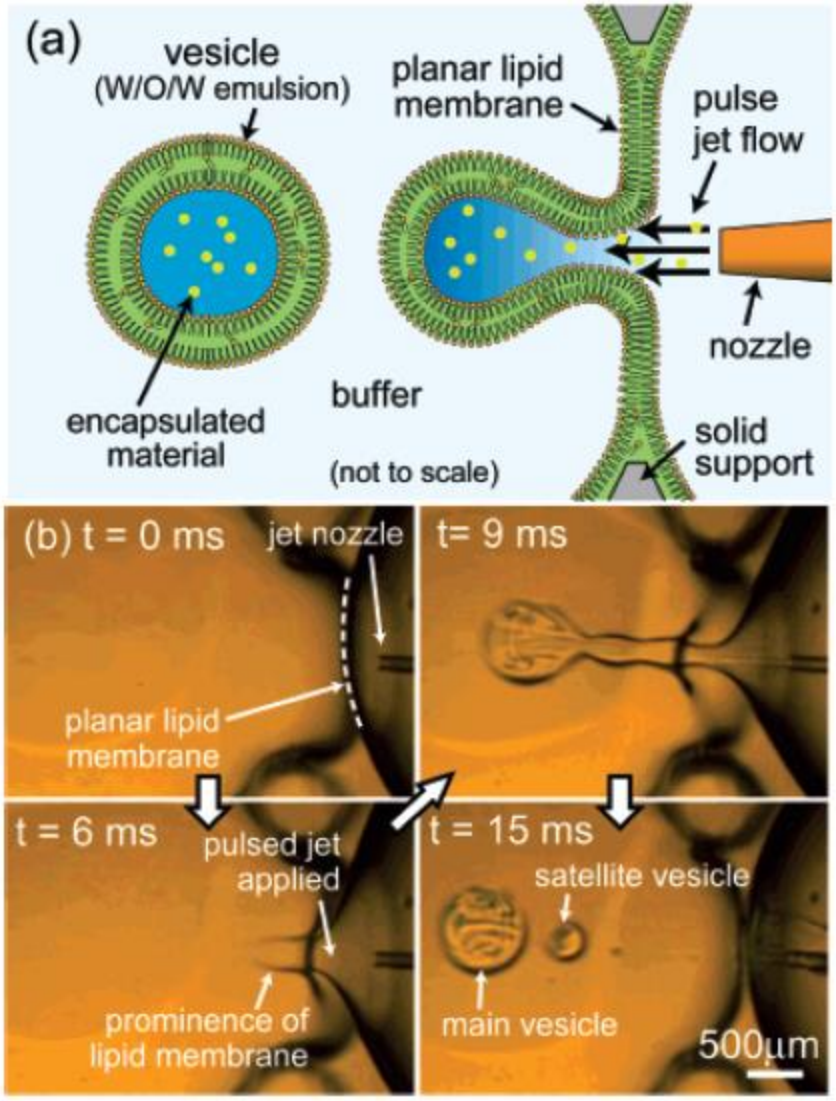

Figure 2.4: Formation of liposomes via jet flow in a microfluidic device. (a) Schematic demonstrating the vesicle formation from a planar lipid membrane via the pulsed jet flow, causing the lipids to pitch off into a vesicle with the jetted material encapsulated within. (b) Images of the vesicle formation via high-speed CCD camera. The vesicles formed within 10 ms. Reprinted from Funakochi *et. al.* [89]

One of the disadvantages of the jet-flow method is that it is difficult to set up the lipid bilayers inside the microfluidic devices, and thus is limited in the number of liposomes that can be generated. A recent paper overcame these limitations by developing an automated jet flow generation system for liposomes.[91] The new device has six wells, each with a lipid monolayer on

the outside. The wells rotate so as to interface with a seventh fixed well, which contains a lipid monolayer as well as the glass capillary for jetting. **(Figure 2.5)** At optimized rotation speeds, lipid bilayers were successfully formed between the fixed well and rotating wells, allowing for the jetting of liposomes. To test lipid bilayer formation, the membrane pore protein α-hemolysin (α-HL) was introduced into the buffer. If a lipid bilayer formed, the α-HL would incorporate, as tracked by an increase in current through the bilayer. Liposome formation was found to occur within 30 seconds of rotation. This is an interesting example of using a membrane protein to actually test the new microfluidic device, instead of to study a new membrane protein, but also suggests future promise for using this jet-flow based device for membrane protein studies.

A separate lab also has developed devices to form liposomes using jet flow. The initial device determined that stable vesicles of around 200 μm were monodisperse, varying in size by 2-3% on the same lipid membrane and up to 7% when the lipid membranes were reformed.[92] They also demonstrated that it was possible to control the encapsulation of a material of interest, such as α-HL, within the jetted flow without significant incorporation of the buffer surrounding the lipid membrane.[92] Further work demonstrated an ability to control the lipid composition to form asymmetric membranes and correctly orient transmembrane proteins of interest.[93] Planar lipid bilayers were formed with the SNARE protein synaptobrevin (Syb) with a GFP fusion (GFP-Syb) incorporated, so that when the jetting occurred the membrane proteins were successfully incorporated into the liposomes, confirmed by GFP fluorescence. To correctly orient the membrane protein, the protein must be initially incorporated into the correct lipid droplet from which the jetting will occur – either the inner droplet where the jet is inserted or the outer droplet. This method was used to correctly orient and incorporate claudin-4, a transmembrane protein involved in forming interfaces between cells. The impact of claudin-4 on

protein and lipid segregation between liposome interfaces was then studied on-device, an example of developing an on-chip method to learn more about a specific membrane protein of interest.[94]

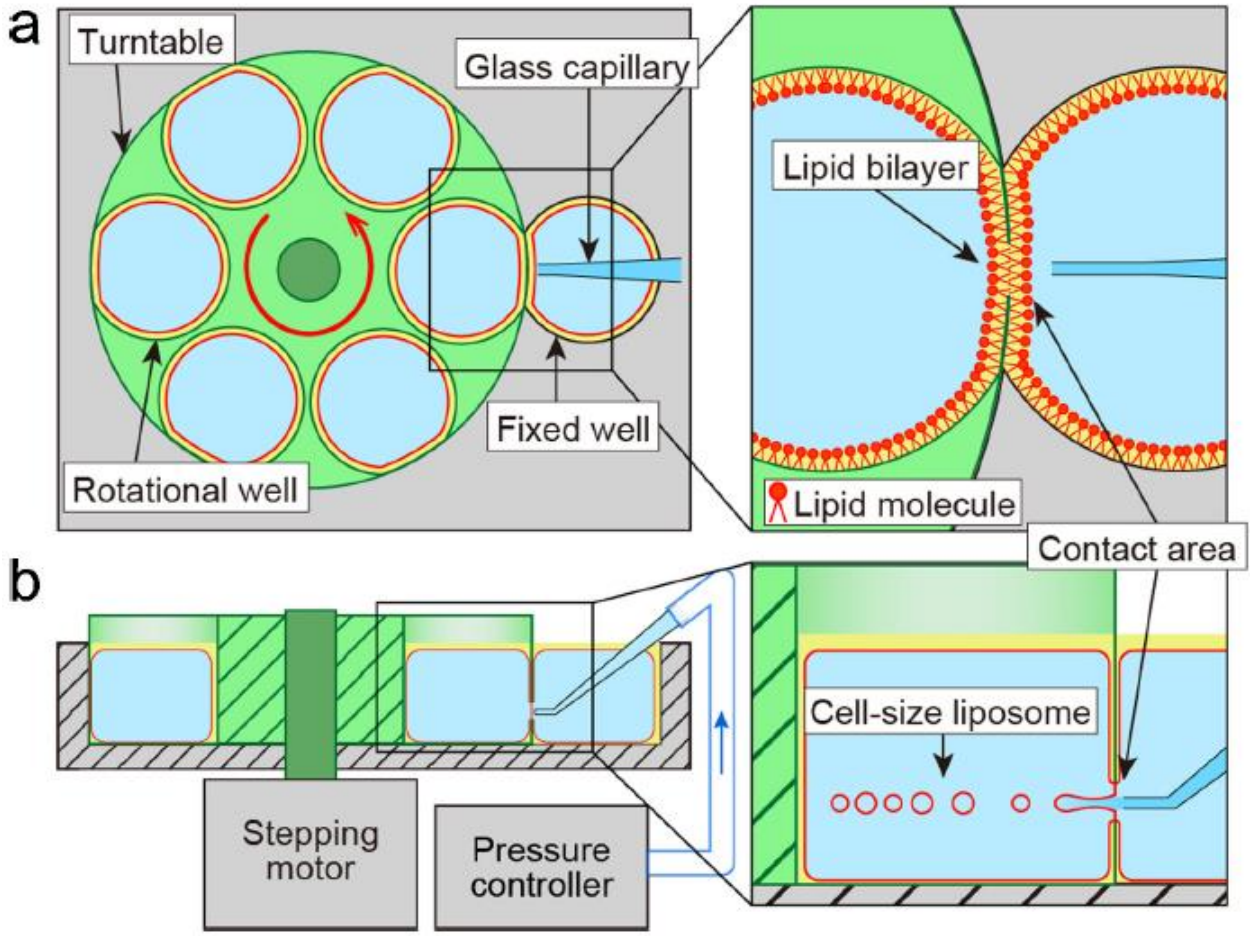

Figure 2.5: Schematic images of the automatic liposome generation system using jet flow. The green circular section is the rotational piece, while the grey is stationary. (a) Top-down view of the device, showing the six rotating wells and one fixed well, each with a single lipid layer on the outside of the wells. When the wells line up, a lipid bilayer forms and jet flow liposome formation can occur. (b) Side-on view of the device, showing the motor and pressure controller needed for function, as well as a view of where in the well the liposome formation occurs. Reprinted from Gotanda *et. al.* [91]

Though there are interesting examples of using the jet flow technique to study membrane proteins of interest, there are some concerns over the effect the high shear stress from the jet flow

would have on the membrane proteins, as it could potentially cause damage that would change the protein structure or activity. There is also a potential problem with oil remaining within the lipid bilayers after jetting, as this could affect the membrane protein stability. However, jet flow does form monodisperse liposomes, the sizes of which can be slightly tuned by the volume and length of the jetting. And though the initial methods had issues with the nontrivial setup of the lipid bilayer needed, there have been significant improvements in this area recently that allow this method to be more replicable and automated, and thus applicable to larger studies. The successful formation of liposomes containing membrane proteins and then performing protein studies on the same chip shows great potential for this method.

1.2c: Transient Membrane Ejection

Similar to jet flow, transient membrane ejection involves forming a lipid bilayer at a junction on the microfluidic device and then deforming it to form a liposome. In this case, however, a laser is used to heat aluminum in the device, forming a microbubble. This deforms the lipid bilayer upwards into a steady stream of aqueous solution, which causes the deformed lipid film to pinch off into a liposome.[95] By utilizing multiple small chambers on the device, each functioning as a small junction, multiple monodisperse vesicles can be formed simultaneously. These liposomes were able to incorporate α-HL, which was added to the solution outside the liposomes after formation, into the lipid bilayer. The successful α-H incorporation was seen as formation of a pore that allowed the release of previously encapsulated calcein fluorescent molecules from within in liposome.[95]

A slightly different ejection method uses a pneumatic valve to create an air bubble that causes the liposome formation, instead of the laser method described above.[96] This method can also successfully generate giant lipid vesicles, though instead of incorporating a membrane

protein, the authors focused on the ability of the liposomes to encapsulate material from the aqueous phase within the liposome, tested using calcein.

A limitation with both methods, as mentioned before with the jet flow method, is the possibility for incorporation of some oil residue between the lipid layers, which could cause concern for membrane protein incorporation and activity. This method has only used α-HL so far but does show some potential for membrane protein incorporation. It would be really interesting if the devices that have multiple chambers could each have a different lipid composition, forming liposomes with different lipid compositions on the same device, which could allow for really interesting studies of how membrane proteins react to specific lipids.

1.2d: Herringbone Mixer

Another interesting microfluidic liposome formation approach uses a herringbone mixer, a type of microfluidic channel which is often employed to achieve mixing on microfluidic devices. **(Figure 2.6)** To form the liposomes, a stream of lipids dissolved in ethanol and a stream of aqueous solution meet directly before the herringbone mixer and are mixed within this structure, leading to spontaneous liposome assembly.[97] These liposomes were on the smaller side as compared to some of the methods described above, with diameters less than 80 nm, and could be tuned by changing the lipid identities and relative ratios dissolved in the ethanol. This device was not used to incorporate membrane proteins but rather to encapsulate macromolecules of interest in clinical drug delivery, including small interfering RNA (siRNA) therapeutics.[98,99]

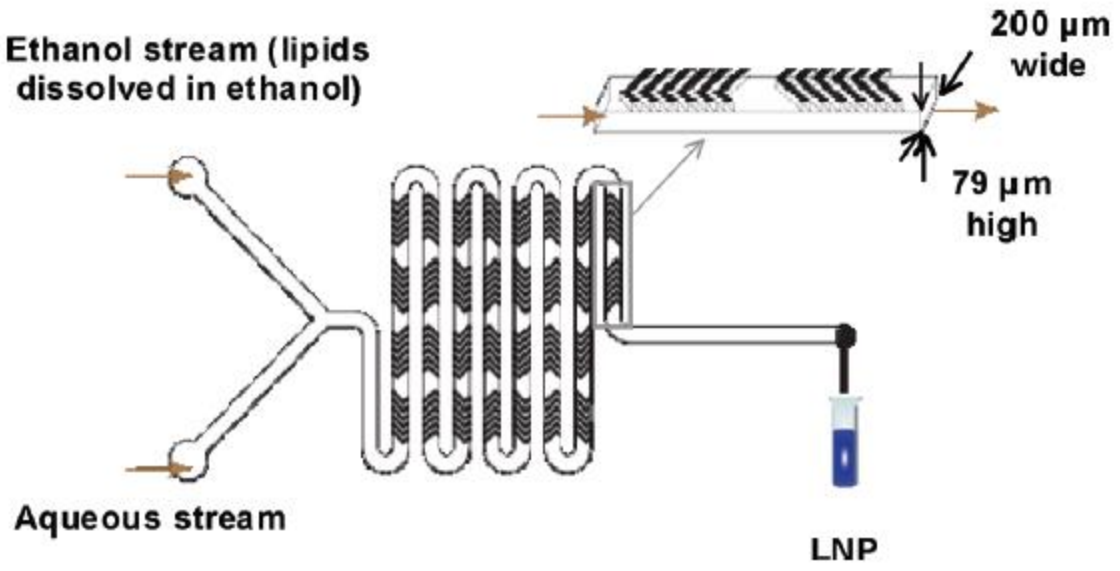

Figure 2.6: Schematic of the herringbone mixer device. The organic stream containing the lipids and the aqueous buffer stream are introduced through the two inlets using a syringe pump and then mixing is induced by using the herringbone structures seen in the inset figure. The structures cause rapid mixing of the two phases which increases the polarity experienced by the lipids, causing lipid nanoparticle (LNP) formation. Reprinted from Zhigaltsev *et. al.* [97]

The optimization of this method of liposome formation has been extensively performed. The effects of both the total flow rate through the device and the flow ratio between the solvent/lipid mixture and the aqueous buffer were characterized for their effects on liposome size and polydispersity.[100] By optimizing the lipid/buffer flow rate ratio, they were able to form highly monodisperse liposomes of ~50 nm diameter. More recently, they have further expanded the basic microfluidic device to include purification of the liposomes using tangential flow filtration via a modified polyethersulfone (mPES) column followed by in-line size monitoring by dynamic light scattering (DLS), to ensure a truly monodisperse sample.[101] Finally, the tunability of the sizes of the liposomes formed was demonstrated, going from 50 nm up to 750 nm in diameter, simply by changing the concentration of the aqueous buffer that mixes with the solvent/lipids on the device.[102] This is important as this lab was again interested in using these

liposomes for clinical drug delivery, as the final paper included cellular uptake studies across a range of liposomes. No work was done incorporating membrane proteins within these liposomes, but the ability to tune the size of the liposomes to allow space for incorporating larger membrane proteins of membrane protein complexes could be useful.

There is one example we have found in which the herringbone mixer formation was used to successfully incorporate membrane proteins into liposomes. Using a commercially available form of the microfluidic device called the NanoAssemblr,[103] membrane proteins derived from leukocytes were incorporated into the liposomes.[104] They reoptimized the flow rate ratio, total flow rate and temperature to determine the conditions necessary to use the NanoAssemblr platform for membrane protein incorporation at the same time as liposome formation. Membrane proteins were introduced in the aqueous phase. It was noted that incorporating membrane proteins did increase the polydispersity of the sample, but that can be expected as there are likely a range of incorporation into liposomes, containing zero, one, or multiple membrane proteins, changing the overall sizes. The membrane proteins LFA-1 and CD47 were confirmed to be present in the liposomes using flow cytometry, though the proteins' structure and functions were not tested. There was no discussion of the potential impact of the ethanol or the potentially harsh mixing conditions on the structure or function of the membrane protein of interest, all of which might be concerning.

Moving forward, ensuring that the membrane proteins incorporated using this method are not just incorporated, but actually retain their native structure and function is an important test. That the herringbone mixer was able to incorporate membrane proteins directly from leukocyte membranes into the liposomes is very encouraging, as this removes any necessity for membrane protein recombinant expression and/or purification. Confirming the identities of more of the

incorporated membrane proteins and performing downstream structural or functional assays are necessary next steps. The fact that this herringbone mixer method has already been developed into a commercially available system is especially encouraging, as often times microfluidic devices are limited only to those that have access to a cleanroom and significant training. Moving more microfluidic devices into commercially available or easily-formed devices is key to widening their applications.

1.2e: Droplet-Stabilized

The Weiss lab has developed microfluidic devices that use droplet-stabilized giant unilamellar vesicles to form synthetic cells.[105] These water-in-oil droplets are stabilized by a perfluorinated polyether and polyethylene glycol doped into the oil phase, with the lipid bilayer formed between the polymers and the aqueous phase. The most impressive part of using droplet-stabilized liposome synthesis is that previously-developed high-throughput microfluidic technologies, such as the picoinjector, can be used to inject materials into the center of the liposome after formation for downstream studies. **(Figure 2.7)** It is even possible to incorporate proteoliposomes into the droplet liposomes to make larger droplet-stabilized liposomes which include a membrane protein, as has been down with F_0F_1-ATP synthase.[105] The activity of these membrane proteins were confirmed by creating a pH gradient that led to ATP synthesis within the liposomes, as measured by the concentration of ATP within the liposome after a set period of time. Further development of this microfluidic system to allow for the study of smaller liposomes, or model organelles, within these larger droplet-stabilized GUVs, has also been described.[106,107]

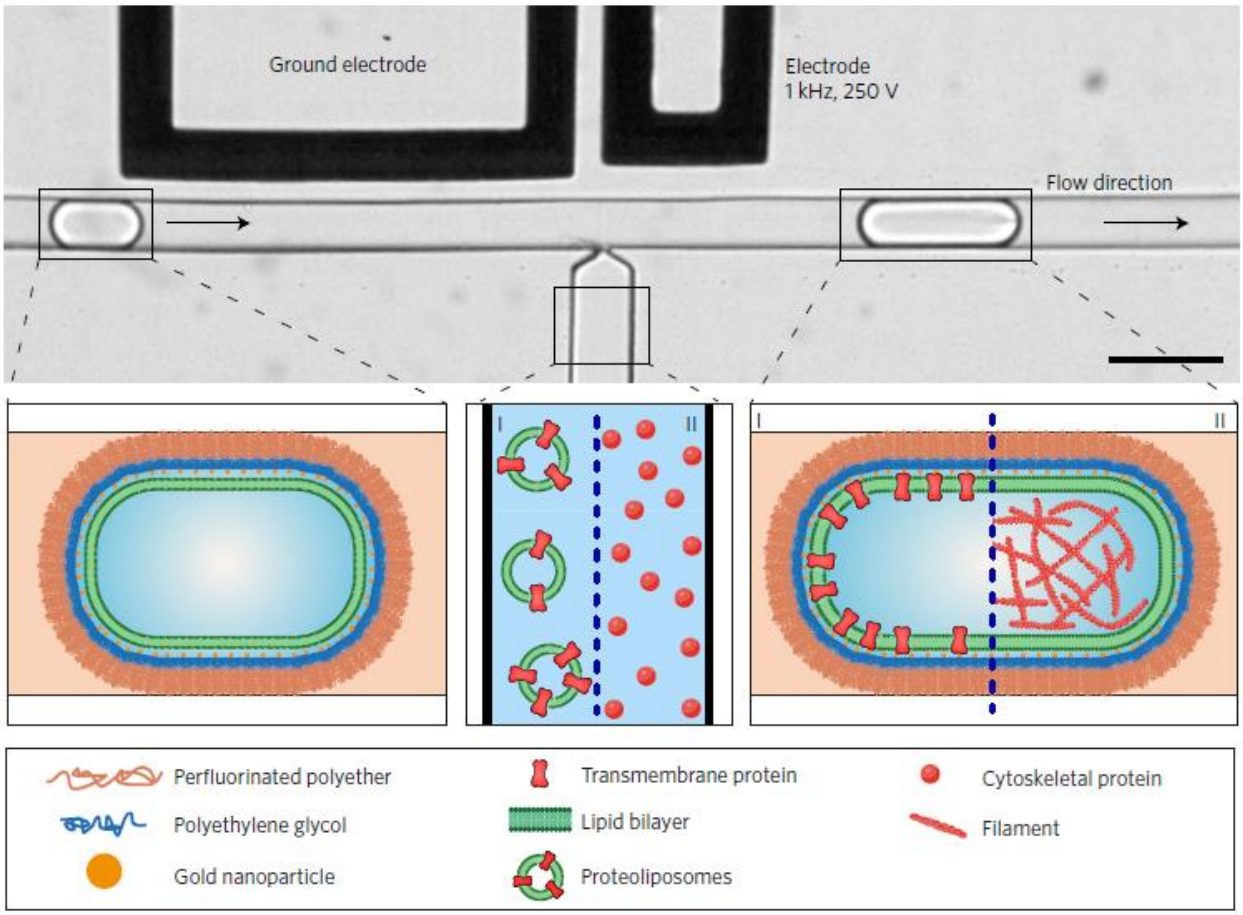

Figure 2.7: Schematic of the microfluidic assembly of droplet-stabilized cell-like compartments. Using standard droplet microfluidic technologies, like the picoinjector seen here, transmembrane proteins were incorporated into the giant liposomes. Scale bar is 50 μm. Reprinted from Weiss *et. al.* [105]

This droplet-stabilization method is clearly an interesting method that has already been implemented to study membrane proteins on a microfluidic device. The Weiss lab has focused on utilizing these GUVs for model-cell studies, which does involve membrane protein incorporation, but the incorporated membrane proteins were previously incorporated in proteoliposomes off-chip rather than directly from a cell membrane or lysis solution. The ability to use previously developed droplet microfluidic methods to manipulate the droplets, including adding materials to the liposomes, could lead to interesting studies of membrane protein structure

and function. As there are already established methods for adding materials, mixing, and even washing materials in droplets, activity assays within these liposomes should be possible.[108–110]

1.2f: Conclusions

There are a number of microfluidic methods that have been successfully developed to form liposomes, both those adopted from standard bulk methods and those only possible because of the advantages of microfluidic development. Though we have covered only a handful of these methods, those that have been used for membrane protein incorporation, there have been a number of other important applications that are not covered in this review, especially concerning encapsulation and drug delivery.[111]

One issue described for many liposome formation techniques is large size distributions of the formed liposomes. To end up with monodisperse liposomes, a microfluidic device was developed that could separate and trap liposomes based on size.[112] The separation module uses deterministic lateral displacement, a previously described hydrodynamic separation that uses posts carefully spaced apart to change the direction different sized liposomes travel. The liposomes then move into the trapping region, composed of posts that are shaped to hold liposomes, with narrow gaps that allows for continued fluid flow without the liposomes escaping. The device was able to trap liposomes of a specified size with coefficients of variation (CVs) from 5-12%, depending on the target diameter – lower variation was seen for smaller diameters (12 μm target, 5% CV) than larger diameters (20 μm target, 12% CV). This separation device be incorporated into the devices discussed in this section, to streamline the production of monodisperse liposomes for downstream analysis.

Another major issue mentioned in many of these methods is the incorporation of non-aqueous solvents, either oil or alcohol (depending on the method), within the layers of the lipid bilayers. It is a major concern that any successfully incorporated membrane proteins will have potentially problematic interactions with the solvent, causing a change in the membrane protein native structure or function. There has been significant focus on methods to either remove the necessity to have strong solvents or to remove any incorporated oil or alcohol from the liposomes after formation, which has allowed the study of functionality of robust membrane proteins. However, to ensure these systems are generalizable to more sensitive MPs, solvent extraction and purification should be a major area of focus for these microfluidic device moving forwards.

1.3: Nanodiscs

So far, our lab has been the only one to report formation of Nanodiscs using a microfluidic device, with a focus on creating membrane scaffold protein-belt (MSP) Nanodiscs. Nanodiscs are most often formed in bulk by removing the detergent solubilizing the membrane scaffold protein, lipids and membrane protein of interest by mixing these components with detergent removal resin over a time of 4 hours to overnight.[113] Our Nanodisc-forming microfluidic device is composed of a bead bed packed with detergent removal resin. Upon flow through of the Nanodisc components mixture, Nanodiscs are formed within five minutes.[114] This microfluidic device can form Nanodiscs with similar dispersity and concentration to the bulk process, but significantly faster with a lower input of materials. Our initial paper demonstrated the incorporation of functional cytochrome P450 CYP3A4 into Nanodiscs using this device, by introducing the CYP3A4 protein, solubilized in detergent, as part of the components mixture.

Unpublished work has also demonstrated the ability to incorporate other membrane proteins, including Epidermal Growth Factor Receptor (EGFR) and viperin, into Nanodiscs directly from whole cell lysate using the microfluidic device, while maintaining the protein functionality. Being able to use whole cell lysate rather than purified protein expands the range of proteins that can be studied, as the proteins do not need to be recombinantly expressed or purified. This is particularly important for proteins like EGFR, which have only been recombinantly expressed in their truncated form and thus may not have accurate structure or activity.

Our microfluidic device can successfully produce Nanodiscs containing membrane proteins but so far, the downstream activity and functional assays have occurred off-chip. Further development of devices that allow for both Nanodisc formation and purification and these downstream assays are among our goals in the near future.

1.4: Important Considerations

There have been a number of examples of different types of model membrane lipid bilayers that have been produced in microfluidic devices, some of which are derivations of traditional bulk methods while others are newly developed because of the benefits specific to microfluidics. While some of these methods have been able to successfully incorporate membrane proteins and even allow for the measurement of activity of membrane proteins on chip, the vast majority of the membrane proteins incorporated have been ion channels, especially the relatively simple pore protein α-hemolysin. This is an encouraging start, but more work needs to be done in this area to ensure that more classes of important membrane proteins, such as kinases and G-protein coupled receptors (GPCRs), can be studied.

Section 2: Microfluidics for Downstream Analysis of Membrane Proteins

2.1: Membrane Protein Purification

It is essential to be able to purify the membrane proteins of interest from the other lysate components, when using either native membrane proteins or recombinantly expressed proteins. All the other proteins and small molecules from the cell lysis could interfere with downstream analyses. Often times, recombinantly expressed proteins can have purification tags added to a terminus of the protein to make purification easier, theoretically without significantly changing the protein structure and function, but this is not always possible. Other purification methods must be developed, either for before incorporation into a membrane mimetic, or for after incorporation, which can also be necessary to remove any non-incorporated materials.

2.1a: Purification Before Incorporation

Purification of membrane proteins from cell lysate can be difficult because of the necessity to use detergent to solubilize the proteins. One method often used for membrane protein purification uses an aqueous two-phase system composed of polymer and detergent, as the membrane proteins will remain in the detergent phase while soluble proteins end up in the polymer phase.[115] A microfluidic method of separation has been developed using a relatively simple device, composed of a serpentine channel with three inlets and three outlets.[116] The middle inlet was connected to a syringe pump containing the crude cell extract in detergent while the two outer inlets contained a PEG polymer. The purified membrane proteins were collected from the middle outlet while the two outer outlets went to waste. **(Figure 2.8)** The use of a microfluidic device allowed for a rapid separation, taking only 5-7 seconds with about 90% of the collected fraction composed of membrane proteins, though the structure and function of these proteins were not confirmed. This device could be a fantastic initial module for removing

unwanted soluble proteins before the isolated membrane proteins are sent on for downstream analysis, as long as this process does not negatively impact the membrane proteins.

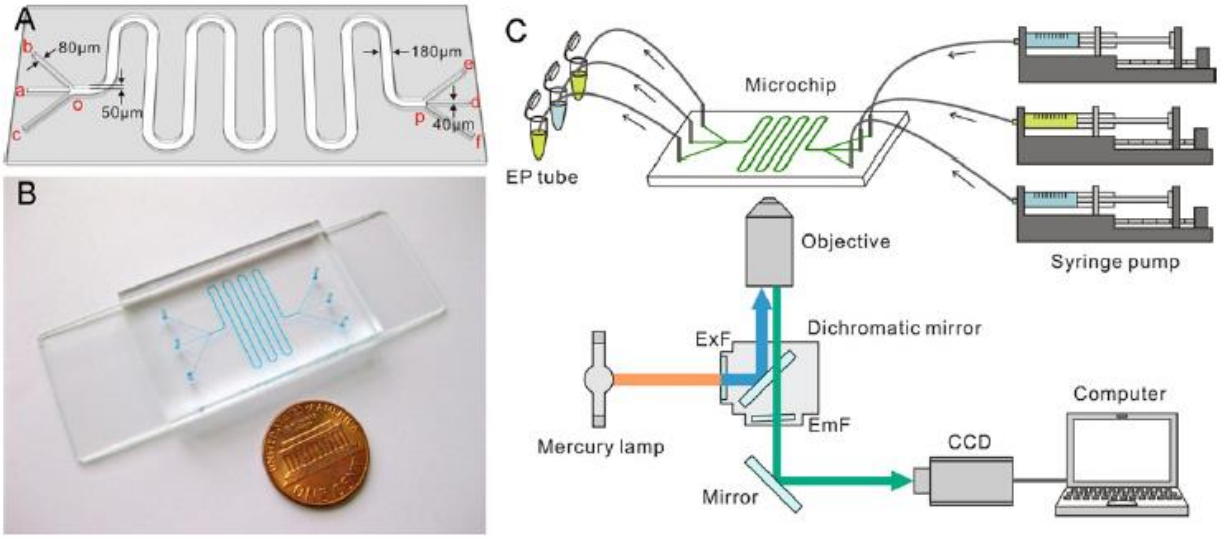

Figure 2.8: The microfluidic device and the overall operating system for the separation and detection of membrane proteins. (A) Schematic of the microfluidic device. (B) Picture of the microfluidic device with a US penny for size comparison. (C) Schematic of the overall set up, including the syringe pumps, the sample tubes, and the imaging equipment used. Reprinted from Hu *et. al*.[117]

2.1b: Purification After Incorporation

One interesting way to either accumulate or separate proteolipid layers (membrane proteins incorporated into a lipid layer or bilayer) used hydrodynamic forces in a microfluidic device. The supported lipid bilayer was tethered to the bottom of the microfluidic device and a bulk flow of liquid was applied through the device, the force of which caused the lipids in the upper leaflet of the bilayer to move in the direction of the flow. Any membrane proteins incorporated into the upper layer of the bilayer moved in that direction as well, leading to accumulation of the lipid-layer which contained proteins towards the outlet of the channel. To separate proteins from one

another, the bulk liquid was flowed in the opposite direction (towards the inlet) causing the membrane proteins to separate based on the size and conformation of the protein as well as the interactions between the protein and the lipid bilayer.[118] Two proteins, both about 60 kDa in molecular weight, streptavidin and cholera toxin, were able to be concentrated and then separated on the microfluidic device, suggesting high resolution for protein separation.

There could be some interesting potential applications of this device. The authors suggest that a membrane protein of interest could be accumulated in a section of the device to allow for the study of a variety of activity measurements, such as ligand binding, at a higher local surface concentration. This would be ideal as a current problem with membrane protein functionality assays is the low concentration of these proteins, as discussed later in this chapter. This device could also allow for the testing of various mutations to a membrane protein on the same chip, especially if the mutant proteins have different sizes or interactions with the lipid bilayer.

However, there are some potential limitations in using this separation mechanism for all membrane proteins incorporated in lipids. First, this method only works for membrane proteins that integrate into one layer of the lipid bilayer, not full transmembrane proteins. It also is not clear what impact the high sheath flow rate might have on the integrity of the membrane protein structure, as this has yet to be tested.

A more specific method for membrane protein enrichment for a membrane protein of interest in a lipid bilayer, also used hydrodynamic flow in a microfluidic device. This device utilized a Ni-NTA capture area to specifically enrich the membrane protein of interest, which was engineered to contain a histidine tag to bind to the NTA.[119] The device was able to concentrate a His_6-tagged β-secretase (BACE) membrane protein by 3-fold to study ligand binding. The biggest issue with this device is that it requires the membrane protein of interest to be engineered

with the His-tag, which is not always possible. Some membrane proteins cannot be recombinantly expressed at full length or tend to crash out of solution when tagged.

The device was updated to no longer require the His-tag, and thus removed the need for recombinant expression, by relying on the specificity of antibody interactions.[120] Membrane proteins were incorporated into a supported lipid bilayer directly from cell-derived membrane vesicles, removing the need to recombinantly express and then solubilize the membrane proteins. Using cell-derived vesicles should help preserve the native membrane protein structure, allowing more accurate studies. However, using cell-derived vesicles will incorporate all membrane proteins into the lipid bilayer, rather than just the protein of interest. To purify, antibody-bound nanoparticles specific to the membrane protein of interest were bound to the membrane protein and then hydrodynamic flow was applied. Because the nanoparticles were significantly larger than the other membrane proteins in the lipid bilayer, the membrane protein of interest bound to the nanoparticle moved the fastest through the membrane, allowing for that protein to be segregated into one area of the bilayer without other proteins around. Once again using BACE1 as the model protein, the updated device was able to enrich the membrane protein concentration a thousand-fold. This improved device removes the biggest disadvantages of the original device though there are still a few potential problems, including the need for a specific antibody for the membrane protein of interest, the antibody not interfering with the membrane protein of interest's functionality for downstream analysis, and the potential impact of the high flow rate sheath flow.

The Bailey lab has also described methods that can be used to purify membrane proteins incorporated into Nanodiscs to allow for downstream analysis. The basic device developed for Nanodisc formation can be filled with Ni-NTA beads, in place of detergent removal resin, to

capture and purify any Nanodiscs, as the membrane scaffold protein was engineered with a His-tag.[114] We have also developed a method to purify Nanodiscs containing a specific membrane protein of interest out of a mixture of Library Nanodiscs containing other membrane proteins from cell lysate utilizing antibody-based beads for purification in the same basic device to allow downstream activity assay analysis without significant background (Chapter 4). As with the previous study, this does require an antibody specific for the membrane protein of interest conjugated to the beads.

Purification is very important for downstream structural or functional assays of membrane proteins, especially when starting with a complex biological sample. There have been microfluidic methods developed for membrane protein purification, both in solution and in lipid membranes. However, more work needs to be done to confirm these purifications do not negatively impact the membrane protein structure, which would also change the protein activity.

2.2: Membrane Protein Structure

Knowledge about membrane protein structures has lagged significantly behind that of soluble membrane proteins, as less than 3% of protein structures in the protein data bank (PDB) represent membrane proteins.[121] Having information about membrane protein structures can lead to understanding about the protein function, especially in regards to drug binding sites.

2.2a: Crystallization

To determine membrane protein structure, protein crystallization is performed and typically followed by x-ray diffraction (XRD) analysis. However, it is very difficult to grow crystals of sufficient quality to accurately determine protein structure, a problem that becomes even more significant for membrane proteins, because of the low concentrations and aggregation issues in solution. There has previously been a review focusing on using microfluidics for

protein crystallization, mostly focused on soluble protein screening,[122] so we will briefly describe the initial microfluidic development to focus on the application of microfluidic x-ray crystallography to membrane proteins.

The first microfluidic devices for soluble protein crystal growth were developed by the Quake lab in 2002, using 480 valves to perform 144 reactions in parallel, each requiring only 10 nL of protein.[123] This significant decrease in the volume of protein solution needed for each separate reaction allows for screening of numerous crystallizations conditions simultaneously to determine the optimal conditions needed to form the best protein crystals. Further developments of this device allowed for this optimization along with *in situ* structure determination, preventing potential damage to the crystals by having to remove the crystals from the device.[124]

A different microfluidic method uses droplet microfluidics, in which each droplet represents a separate nanoliter-sized crystallization reaction.[125] Hundreds of individual droplets can be formed at a rate of a few droplets per second, once again allowing for rapid and small-scale crystallization optimization which can be followed by XRD measurements on-chip.[126] Initial membrane protein crystallization experiments were performed in similar droplets to those used for the soluble proteins, though there were some issues rising from the high concentrations of detergents needed to solubilize the membrane proteins in the droplets.[127] To improve this process, the lipidic cubic phase (LCP) method was applied to the droplet microfluidic system. Nanoliter-sized droplets of the LCP materials (traditionally 2 parts protein with 3 parts lipid mixed at 20 °C leads to spontaneous self-assembly of LCP)[128] were formed and merged with aqueous droplets containing the membrane protein and a precipitant. Bacterial photosynthetic reaction centers were successfully crystalized from three different bacterial strains, showing the success of this LCP droplet method to screen and optimize the crystal formation of multiple

membrane proteins.[129] As the authors stipulate, more tests of previously unoptimized membrane proteins do need to be performed to confirm that this optimization method can be widely applied.

Lipid mesophases, a term that has been used interchangeably with LCP but refers to the same combination of lipids and proteins in an aqueous solution,[130] have also been described in microfluidic devices. Instead of using droplets, their initial device had a single crystallization chamber on the millimeter scale with multiple channels and valves allowing for the formation of the lipid mesophase and introduction of the membrane protein and precipitant solutions to allow for crystal formation.[131] Bacteriorhodopsin was successfully crystalized in the lipidic mesophase at about a 1000-fold decrease in reagent use compared to traditional crystallization methods. Further improvements to the device increased the plexity and developed the chip in x-ray transparent materials to allow for XRD measurements on chip.[132] The latest device is capable of simultaneously testing 192 crystallization conditions using as little as 8 nL of the membrane protein solution, though at concentrations of 13 mg/mL. A number of membrane proteins have been successfully crystallized using this method, including a photosynthetic reaction center L223SW mutant at a resolution of 3.5 Å.[119] The same lab has also shown the ability to transfer sub-microscopic membrane protein crystals from initial off-chip screens into the device to grow the crystals to a large enough size for the x-ray crystallography analysis.[120] The sequential development of this microfluidic device to the point of being able to screen hundreds of optimization conditions to form successful membrane protein crystals and take x-ray diffraction methods on-chip is an excellent demonstration of what is needed to increase our knowledge of membrane proteins' structure.

2.3: Membrane Protein Function and Activity

One of the biggest problems with studying membrane protein activity and function is the necessity for large quantities of membrane protein to perform these studies, often on the order of milligrams of protein. There have been a variety of microfluidic devices developed with the purpose of discovering new details about membrane proteins' activity while requiring less membrane protein input. Many of the papers discussed above that focused on incorporating membrane proteins into model membrane systems also measured the protein activity to ensure continued functionality. However, many of the membrane proteins studied to date in model membrane systems have been channel proteins, as their function can be measured relatively easily using electrochemical and/or fluorescent methods. Other classes of membrane proteins often add more difficulty to these activity or functional measurements, leading to the need to develop more complicated microfluidic methods to elucidate this information.

2.3a: Membrane Protein Function

To study the impact of different extracellular sections of a membrane protein on the overall membrane protein function, proteoliposomes were trapped on the channel walls of a microfluidic device, followed by a partial trypsin digestion to excise peptides and identify these sequences using mass spectrometry (MS). This method had been previously used to identify a large number of membrane-associated proteins from proteoliposomes isolated from red blood cells.[133] The same basic microfluidic device was used to bind proteoliposomes formed with a membrane protein of interest, in this case the ion channel TRPV1.[134] After peptides were cleaved off with trypsin and identified via MS, patch-clamp recordings were used to measure the function of the remaining parts of TRPV1, in order to probe the structure-function relationship of each peptide sequence. This approach could be applied to a variety of ion channels but is limited

by the trypsin digest, which will not be able to excise peptides from the 'intracellular' domain within the liposome or the intramembrane domain spanning the lipid bilayer.

To measure small molecule kinetics through ion channels, a microfluidic device was developed that incorporated the ion channels into GUVs and then trapped these GUVs in specific places throughout the device.[135] The use of microfluidics makes it easier to manipulate GUVs into the 60 separate traps without breaking the vesicles. It is then feasible to measure the movements of fluorescent small molecules such as calcein through α-hemolysin in a single GUV using confocal microscopy, without interference from the other GUVs. This could allow for kinetic measurement through any ion channel in a multiplexed fashion. However, the use of confocal microscopy limits this methodology to membrane proteins whose activity can be measured by visual changes, such as transport of dye molecules.

2.3b: Membrane Protein-Ligand Interactions

One aspect of learning more about membrane proteins is identifying what ligands each protein interacts with, to better understand the role that these membrane proteins play in the cell as well as help develop potential ways to either block or increase the membrane protein activity as needed for treatment.

To identify potential inhibitors of the transmembrane protein nonstructural protein 4B (NS4B) involved in hepatitis C (HVC) RNA replication, the Quake lab used a microfluidic affinity assay that had in the past been used to study interactions of soluble proteins.[136] The assay used mechanical trapping of molecular interactions to detect even low-affinity interactions. As previously only soluble proteins had been used for this assay, one major change was that the NS4B was expressed off-chip in the presence of canine microsomal membranes to allow for proper protein folding and stability within those membranes and then the membrane proteins

were added to the device. The assay can successfully measure the binding constants of interactions between NS4B and RNA, and as such was used to perform high-throughput screening of small molecules to identify which molecules could potentially be used as NS4B inhibitors to treat HVC.[137] This is an interesting way to study membrane protein inhibition, the impressiveness of which could be increased by the expanded capability of the microfluidic platform to perform 14,792 on-chip experiments[138], though this has not been used yet for membrane proteins.

Another method for drug-inhibition experiments used immobilized proteoliposomes within the microfluidic device to study ATP-binding cassette transporters, which are involved in the export of drugs from cells. To immobilize the proteoliposomes, DNA duplexes were used, in which one strand of DNA was on the outside of the liposome and the matching strand was located in a specific place in the microfluidic channel.[139] To measure membrane protein transport, a fluorescent molecule, Rh123, was used, and the proteins were inserted inside-out into the liposomes. When ATP was present, Rh123 was pumped into the lumen of the liposome, causing fluorescence within the liposome to increase. Inhibitors of the transporter could be tested to see if these molecules impacted the amount of fluorescence within the liposome. The biggest issue with this method is that it can only be used for transporters that are able to move a fluorescent molecule into or out of the liposome. It also requires precise incorporation of the transporter into the liposome to ensure that all the transporters are in the same orientation, so that no transporters are pumping in the opposite direction. Using DNA as a scaffold to immobilize a lipid bilayer has some advantages, as potentially different DNA tags could be used to multiplex specifically tagged unique liposomes, to study different membrane proteins or a single membrane protein in distinct lipid environments. The impact of the DNA tag on the membrane

proteins would need to be tested though, as any interactions between the protein and tag could change the protein structure or function.

To identify interactions between a specific membrane protein, G-Protein-Coupled Receptor (GPCR) Ste2, and a set of developed ligands, a previously developed microfluidic device, the LPI^{TM} FlowCell, was coupled with mass spectrometry.[140] Proteoliposomes were formed from cell membranes expressing Ste2 and were immobilized to the surfaces of the device. Then a variety of pheromone analogs of the natural pheromone peptide α-factor were flowed across the device. The device output went through the MS in a time-dependent manner. The strength of the interactions between the ligands and the membrane proteins determined the amount of time the ligand, in this case the pheromone, spent on the device, similar to the idea of affinity chromatography, leading to new information about which ligands interact with Ste2.

A different approach was focused not on screening inhibitors of membrane proteins but screening a large array of 2,100 membrane proteins with pathogens to discover which membrane proteins each pathogen used to enter a cell.[141] **(Figure 2.9)** To form this membrane protein array, the proteins were fully synthesized on-chip, as discussed more fully later in this chapter, which is one of the ideal solutions to membrane protein expression, as it limits the necessary input and potential loss of sample in transferring proteins to the microfluidic device. The proteins were coexpressed with microsomal membranes for protein stability. Once expressed, the membrane proteins in the membranes were immobilized on the array using antibodies. The paper did mention that they attempted to express ~2,700 proteins but only successfully expressed 2,100, which is about 80%, on-chip, which suggests that this method will not work for all membrane proteins of interest. There was no further information on the classification of the 20% of proteins which were not expressed which would be interesting to know to see if the expression was

limited to certain membrane protein classes or sizes. The authors also did not check every membrane protein to ensure that each was successfully folded and active, they found that out of 13 tested, 10 were active, or about 75% of those expressed. Testing the activity of more of the 2,100 is needed to draw full conclusions about the success of this assay at characterizing all pathogen-membrane protein interactions. The assay was able to identify membrane proteins that interacted with fluorescently labeled viruses SV40 and L-HDAg. Further work with this microfluidic membrane protein array was used to screen for interactions with the hepatitis C virus non-structural protein 3/4a protease, leading to Neurogulin 1 being discovered as a cleavage target.[142]

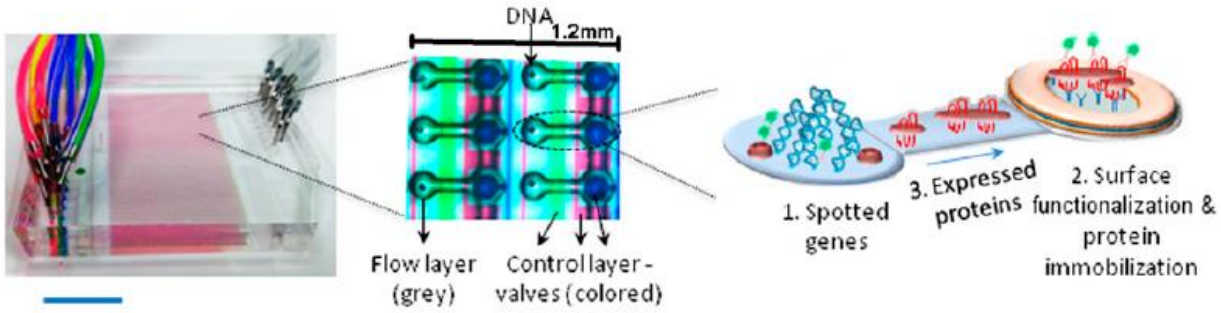

Figure 2.9: Pictures and schematic of the membrane protein array. The left figure demonstrates the microfluidic chip, composed of two PDMS layers, a 64 x 64 unit cell array and a control layer with the valves. The middle figure demonstrates 6 of these separate units, with colors representing the different PDMS layers. The right figure is a schematic of each individual cell, and the steps that occur within the chip. Reprinted from Glick *et. al.*[141]

2.3c: Membrane Protein-Protein Interactions

Beyond membrane protein-ligand interactions, membrane protein interactions with other proteins, both other membrane proteins and soluble proteins, are essential to fully understand membrane protein function in the cell. These protein-protein interactions play a variety of

essential roles, including activating protein function and leading to downstream signaling cascades.[143]

There have been a number of different microfluidic devices that have been used to screen protein-protein interactions between soluble proteins through a variety of interesting methods, including chromatography, electrical detection, and droplet-based methods.[144–146] We have found only one example of a microfluidic device developed to study membrane protein-protein interactions. The interactions were measured by tracking differences in the time it took to move a specific distance within the microfluidic device. The membrane protein used was claudin-2, a tight junction protein, in a polymer vesicle used as the model membrane for protein stability. Both weak interactions between claudin-2 molecules and strong interactions with anti-claudin-2 antibodies on the microfluidic device walls were measured by comparing the travel times of the vesicles.[147]

The difficulty is increased for studying membrane protein-protein interactions over ligand interactions for a few reasons, including difficulty obtaining as high concentrations of proteins and fewer proteins that are already labeled for fluorescence or colorimetric assays when compared to ligands. However, it should be possible to continue to modify the microfluidic devices discussed above to allow for studying protein interactions as well, even if this requires tagging the proteins of interest, which leads to potential concerns about changing the protein native structure.

Section 3: Conclusions and Future Work

There have been some significant advances in the ability to use microfluidics to study membrane proteins but there is still a long way to go, especially for certain classes of membrane proteins. Most of the membrane proteins that have been successfully studied are channel

proteins, especially ion channels, as measurements of channel activity using apertures or liposomes are comparatively easy. Ion transport can be monitored using changes in conductance and transport though some channels can be tracked using fluorescently labeled ligands. There is a need to continue to develop the capability of microfluidics to study the activity of other classes of membrane proteins, especially larger, more complicated proteins with multiple transmembrane domains such as GPCRs.

One area that could potentially allow for an increased range of membrane proteins to be studied is to develop improved microfluidic devices to isolate or synthesize membrane proteins on the microfluidic device. As membrane proteins are often expressed at much lower concentrations than soluble proteins, acquiring sufficient concentrations of membrane proteins for downstream structural and activity assays can be very difficult. Because of this, most research is performed on recombinantly expressed membrane proteins. However, recombinant expression often synthesizes proteins that are missing post-translational modifications and might be truncated or misfolded, leading to inaccurate studies.[33,148]

A more recent approach to synthesizing proteins is cell-free synthesis, in which all the various building blocks needed for the protein (nucleotides, DNA or mRNA, amino acids, etc.) are combined, usually in crude cell extract or lysate.[149] There are a wide variety of cell types that can be used as the basis of the synthesis, and the choice of lysate used is mainly based on the protein of interest. There have been a number of cell-free systems that have been used to express membrane proteins, all of which use some level of membrane mimetic to ensure proper folding of the membrane protein. The initial experiments were focused on expressing pore proteins to allow for sustained protein expression in an artificial cell over a longer period of time as the pore would allow for the essential expression components and nutrients to continue to be provided. α-

hemolysin was expressed within a phospholipid vesicle using an *E. coli* expression system to increase the length of expression from approximately 5 hours to up to 4 days.[150]

Recently there have been multiple examples of using cell-free expression systems to express membrane proteins to allow for downstream studies of these membrane proteins without having to go through the time-consuming process of expression, purification and reconstitution in a lipid model membrane. To study single-channel electrophysiology, the potassium channels KcsA and hERG were expressed using a commercial *E. coli* cell-free expression system and incorporated into a lipid monolayer by placing a droplet of the cell-free mixture in an oil-lipid mixture.[151] The droplet was then brought into contact with a lipid-surrounded droplet containing buffer, forming a lipid bilayer with the ion channel of interest connecting the two droplets, into both of which an electrode was inserted to allow for current measurements to occur in an example of the droplet interface bilayer (DIB) formation method for liposomes. This type of system can be used for cell-free synthesis of more complicated membrane proteins as well, such as the *E.coli* multi-drug transporter EmrE.[152]

Droplet interface bilayer systems are often used for ion channels, but there have also been successful DIB methods developed for other classes of membrane proteins. A simple cell-free expression method was developed that could theoretically be able to express any single-span membrane protein (ssMP), which represents about 50% of all membrane proteins.[153] This one-pot approach combined a cell-extract-based cell-free protein synthesis with oil droplets, and was able to synthesize and insert two active apoptosis-inducing human ssMPs, FasL and TRAIL into the DIB. The oil droplets have a hydrophobic interior for the transmembrane helix, but there are no lipids, which can play an essential role in the activity of many membrane proteins.[154] Also, this method only has aqueous phase on the outside of the oil droplet, so there is no place for a

second hydrophilic domain of the membrane protein, and often both the inner and outer hydrophilic domains play a role in the activity of the protein.

There have been a number of cell-free protein synthesis approaches developed using microfluidics which have been previously reviewed.[34] The advantage of these systems tend to be the ability to continuously form membrane proteins by supplying more of the essential formation materials over time. The initial devices were very simple, two inlets and an outlet,[155] but over time devices have become more complex, allowing multiplexing for parallel protein synthesis[156] or developing methods for longer reactions and high yields.[157] Though there have been a large number of devices developed that can allow for the cell-free synthesis of soluble membrane proteins, there are very few examples of membrane protein expression in a microfluidic device.

One such example of a membrane protein expression microfluidically is the bacterial cytoskeleton membrane-associated protein MreB, which was expressed in a microfluidic device to understand how MreB influences the shape of rod-like bacteria.[158] Microfluidic single emulsion droplets were formed with the cell-free synthesis aqueous solution segmented into droplets by oil. The protein synthesis then occurred within each droplet in a serpentine storage chamber. MreB aggregates could be seen at the droplet water/oil interface by 24 hours after droplet formation. Though MreB is a membrane associated protein, it is not a transmembrane protein, interacting with the lipid bilayer through a N-terminal amphipathic helix. This microfluidic droplet method might be able to be used more generally for membrane protein synthesis, but it would require a way to incorporate a lipid bilayer into the droplets, possibly by using a double-emulsion of W/O/W, with lipids added to the oil phase.

Previously in this review we discussed the development of an array of 2,100 membrane proteins that were expressed on a microfluidic device using cell-free synthesis.[141] Though this is

technically an example of successful membrane protein synthesis on device, rather than focusing on expressing an important membrane protein of interest, these are actually all proteins derived from synthetic genes. Though ~80% of these genes were able to be expressed on the microfluidic device, there is no guarantee that known membrane proteins of interest would be successfully expressed using this method.

The optimal microfluidic device for membrane protein analysis would be able to synthesize the membrane protein of interest directly into a lipid bilayer-based membrane mimetic or isolate the full-length proteins from cell lysate directly into a membrane mimetic. Then these mimetics, with the membrane protein inserted, would likely need to be purified on-chip to remove background materials or increase size homogeneity. The purified proteolipic mimetic would then undergo downstream measurements, whether they be structural or activity-based analysis, perhaps even both. An ideal system would be able to provide all steps of interest on one device, but for initial designs, multiple microfluidic devices that could be used in parallel would be a step in the right direction. It is often difficult to combine multiple steps on a single microfluidic device as these steps might require different flow rates, buffers, or incompatible reaction times. The more complexity added to a single device also can lead to increased pressure, which can cause device failure.

The field of microfluidics to study membrane proteins has expanded significantly and many successful devices have been used to increase our knowledge about membrane protein structure and function. The increases in overall microfluidic devices and automation can be further modified and combined to continue to push these advances forwards. The ability to efficiently study membrane proteins of interest in lower concentrations than ever before will be advantageous in improving our membrane protein knowledge in the future.

References:

1. Overington, J. P., Al-Lazikani, B. & Hopkins, A. L. How many drug targets are there? *Nat. Rev. Drug Discov.* **5**, 993–996 (2006).

2. Cross, T. A., Sharma, M., Yi, M. & Zhou, H. X. Influence of solubilizing environments on membrane protein structures. *Trends Biochem. Sci.* **36**, 117–125 (2011).

3. van Meer, G. & de Kroon, A. I. P. M. Lipid map of the mammalian cell. *J. Cell Sci.* **124**, 5–8 (2011).

4. Van Meer, G., Voelker, D. R. & Feigenson, G. W. Membrane lipids: Where they are and how they behave. *Nat. Rev. Mol. Cell Biol.* **9**, 112–124 (2008).

5. Engelman, D. M. Membranes are more mosaic than fluid. *Nature* **438**, 578–580 (2005).

6. Arslan, A. & Fatih, Y. Biomimetic Lipid Membranes: Fundamentals, Applications, and Commercialization. *Springer International Publishing.* (2019).

7. Seddon, A. M., Curnow, P. & Booth, P. J. Membrane proteins, lipids and detergents: Not just a soap opera. *Biochim. Biophys. Acta - Biomembr.* **1666**, 105–117 (2004).

8. Garavito, R. M. & Ferguson-Miller, S. Detergents as Tools in Membrane Biochemistry. *J. Biol. Chem.* **276**, 32403–32406 (2001).

9. Brotherus, J. R., Jost, P. C., Griffith, O. H. & Hokin, L. E. Detergent Inactivation of Sodium- and Potassium-Activated Adenosinetriphosphatase of the Electric Eel. *Biochemistry* **18**, 5043–5050 (1979).

10. Zoonens, M. & Popot, J. L. Amphipols for Each Season. *J. Membr. Biol.* **247**, 759–796 (2014).

11. Le Bon, C., Marconnet, A., Masscheleyn, S., Popot, J. L. & Zoonens, M. Folding and stabilizing membrane proteins in amphipol A8-35. *Methods* **147**, 95–105 (2018).

12. Tao, H. *et al.* Engineered nanostructured β-sheet peptides protect membrane proteins. *Nat. Methods* **10**, 759–761 (2013).

13. Whiles, J. A., Deems, R., Vold, R. R. & Dennis, E. A. Bicelles in structure-function studies of membrane-associated proteins. *Bioorg. Chem.* **30**, 431–442 (2002).

14. Dürr, U. H. N., Gildenberg, M. & Ramamoorthy, A. The magic of bicelles lights up membrane protein structure. *Chem. Rev.* **112**, 6054–6074 (2012).

15. Czerski, L. & Sanders, C. R. Functionality of a membrane protein in bicelles. *Anal. Biochem.* **284**, 327–333 (2000).

16. Akbarzadeh, A., Rezaei-sadabady, R., Davaran, S., Joo, S. W. & Zarghami, N. Liposome :

classification , preparation , and applications. *Nanoscale Research Letters.* **8**, 1–9 (2013).

17. Patil, Y. P. & Jadhav, S. Novel methods for liposome preparation. *Chem. Phys. Lipids* **177**, 8–18 (2014).

18. Van Swaay, D. & Demello, A. Microfluidic methods for forming liposomes. *Lab Chip* **13**, 752–767 (2013).

19. Tunuguntla, R. *et al.* Lipid bilayer composition can influence the orientation of proteorhodopsin in artificial membranes. *Biophys. J.* **105**, 1388–1396 (2013).

20. Anantharamaiah, G. M. *et al.* Structural requirements for antioxidative and anti-inflammatory properties of apolipoprotein A-I mimetic peptides. *J. Lipid Res.* **48**, 1915–1923 (2007).

21. Kanellis, P. *et al.* Studies of Syntheric Peptide Analogs of the Amphipathic Helix. *The Journal of Biological Chemistry.* **255**, 11464–11472 (1980).

22. Denisov, I. G. & Sligar, S. G. Nanodiscs in Membrane Biochemistry and Biophysics. *Chem. Rev.* **117**, 4669–4713 (2017).

23. Denisov, I. G. & Sligar, S. G. Nanodiscs for structural and functional studies of membrane proteins. *Nat. Struct. Mol. Biol.* **23**, 481–486 (2016).

24. McLean, M. A., Gregory, M. C. & Sligar, S. G. Nanodiscs: A Controlled Bilayer Surface for the Study of Membrane Proteins. *Annu. Rev. Biophys.* **47**, 107–124 (2018).

25. Dörr, J. M. *et al.* Detergent-free isolation, characterization, and functional reconstitution of a tetrameric K+ channel: the power of native nanodiscs. *Proc. Natl. Acad. Sci. U. S. A.* **111**, 18607–12 (2014).

26. Dominguez Pardo, J. J. *et al.* Solubilization of lipids and lipid phases by the styrene–maleic acid copolymer. *Eur. Biophys. J.* **46**, 91–101 (2017).

27. Orwick-Rydmark, M. *et al.* Detergent-free incorporation of a seven-transmembrane receptor protein into nanosized bilayer lipodisq particles for functional and biophysical studies. *Nano Lett.* **12**, 4687–4692 (2012).

28. Castellana, E. T. & Cremer, P. S. Solid supported lipid bilayers: From biophysical studies to sensor design. *Surf. Sci. Rep.* **61**, 429–444 (2006).

29. Loose, M. & Schwille, P. Biomimetic membrane systems to study cellular organization. *J. Struct. Biol.* **168**, 143–151 (2009).

30. Rossi, C., Briand, E., Parot, P., Odorico, M. & Chopineau, J. Surface response methodology for the study of supported membrane formation. *J. Phys. Chem. B* **111**, 7567–7576 (2007).

31. Fertig, N. *et al.* Stable integration of isolated cell membrane patches in a nanomachined aperture. *Appl. Phys. Lett.* **77**, 1218–1220 (2000).

32. Von Heijne, G. The membrane protein universe: What's out there and why bother? *J. Intern. Med.* **261**, 543–557 (2007).

33. Grisshammer, R. Understanding recombinant expression of membrane proteins. *Curr. Opin. Biotechnol.* **17**, 337–340 (2006).

34. Damiati, S., Mhanna, R., Kodzius, R. & Ehmoser, E. K. Cell-free approaches in synthetic biology utilizing microfluidics. *Genes (Basel).* **9**, (2018).

35. Battle, K. N., Uba, F. I. & Soper, S. A. Microfluidics for the analysis of membrane proteins: How do we get there? *Electrophoresis* **35**, 2253–2266 (2014).

36. Hirano-Iwata, A., Ishinari, Y., Yamamoto, H. & Niwano, M. Micro- and nano-technologies for lipid bilayer-based ion-channel functional assays. *Chem. - An Asian J.* **10**, 1266–1274 (2015).

37. Péterfi, Z., Kustos, I., Kilár, F. & Kocsis, B. Microfluidic chip analysis of outer membrane proteins responsible for serological cross-reaction between three Gram-negative bacteria: Proteus morganii O34, Escherichia coli O111 and Salmonella Adelaide O35. *J. Chromatogr. A* **1155**, 214–217 (2007).

38. Hansen, C. & Quake, S. R. Microfluidics in structural biology: Smaller, faster... better. *Curr. Opin. Struct. Biol.* **13**, 538–544 (2003).

39. Whitesides, G. M. The origins and the future of microfluidics. *Nature* **442**, 368–73 (2006).

40. Duncombe, T. A., Tentori, A. M. & Herr, A. E. Microfluidics: Reframing biological enquiry. *Nat. Rev. Mol. Cell Biol.* **16**, 554–567 (2015).

41. Capretto, L., Carugo, D., Mazzitelli, S., Nastruzzi, C. & Zhang, X. Microfluidic and lab-on-a-chip preparation routes for organic nanoparticles and vesicular systems for nanomedicine applications. *Adv. Drug Deliv. Rev.* **65**, 1496–1532 (2013).

42. Chen, X., Shen, J., Hu, Z. & Huo, X. Manufacturing methods and applications of membranes in microfluidics. *Biomed. Microdevices* **18**, (2016).

43. Fan, B. *et al.* Development of microfluidic systems enabling high-throughput single-cell protein characterization. *Sensors (Switzerland)* **16**, 1–12 (2016).

44. D'Imprima, E. *et al.* Protein denaturation at the air-water interface and how to prevent it. *Elife* **8**, 1–18 (2019).

45. Yang, T., Jung, S. Y., Mao, H. & Cremer, P. S. Fabrication of phospholipid bilayer-coated microchannels for on-chip immunoassays. *Anal. Chem.* **73**, 165–169 (2001).

46. Jung, H., Robison, A. D. & Cremer, P. S. Detecting protein-ligand binding on supported bilayers by local pH modulation. *J. Am. Chem. Soc.* **131**, 1006–1014 (2009).

47. Shengjuler, D., Sun, S., Cremer, P. S. & Cameron, C. E. PIP-on-a-chip: A Label-free Study of Protein-phosphoinositide Interactions. *J. Vis. Exp.* **2**, 1–15 (2017).

48. Shengjuler, D. *et al.* The RNA-Binding Site of Poliovirus 3C Protein Doubles as a Phosphoinositide-Binding Domain. *Structure* **25**, 1875-1886.e7 (2017).

49. Dong, Y., Phillips, K. S. & Cheng, Q. Immunosensing of Staphylococcus enterotoxin B (SEB) in milk with PDMS microfluidic systems using reinforced supported bilayer membranes (r-SBMs). *Lab Chip* **6**, 675–681 (2006).

50. Li, Z., Tang, Y., Zhang, L. & Wu, J. Label-free study of the function of ion channel protein on a microfluidic optical sensor integrated with artificial cell membrane. *Lab Chip* **14**, 333–341 (2014).

51. Jackman, J. A., Knoll, W. & Cho, N. J. Biotechnology applications of tethered lipid bilayer membranes. *Materials (Basel).* **5**, 2637–2657 (2012).

52. Taylor, J. D., Phillips, K. S. & Cheng, Q. Microfluidic fabrication of addressable tethered lipid bilayer arrays and optimization using SPR with silane-derivatized nanoglassy substrates. *Lab Chip* **7**, 927–930 (2007).

53. Taylor, J. D., Linman, M. J., Wilkop, T. & Cheng, Q. Regenerable tethered bilayer lipid membrane arrays for multiplexed label-free analysis of lipid-protein interactions on poly(dimethylsiloxane) microchips using SPR imaging. *Anal. Chem.* **81**, 1146–1153 (2009).

54. Karatekin, E. *et al.* A fast, single-vesicle fusion assay mimics physiological SNARE requirements. *Proc. Natl. Acad. Sci. U. S. A.* **107**, 3517–3521 (2010).

55. Karatekin, E. & Rothman, J. E. Fusion of single proteoliposomes with planar, cushioned bilayers in microfluidic flow cells. *Nat. Protoc.* **7**, 903–920 (2012).

56. Hirano-Iwata, A. *et al.* Free-standing lipid bilayers in silicon chips-membrane stabilization based on microfabricated apertures with a nanometer-scale smoothness. *Langmuir* **26**, 1949–1952 (2010).

57. Sandison, M. E., Zagnoni, M., Abu-Hantash, M. & Morgan, H. Micromachined glass apertures for artificial lipid bilayer formation in a microfluidic system. *J. Micromechanics Microengineering* **17**, (2007).

58. Sandison, M. E., Zagnoni, M. & Morgan, H. Air-exposure technique for the formation of artificial lipid bilayers in microsystems. *Langmuir* **23**, 8277–8284 (2007).

59. Zagnoni, M., Sandison, M. E., Marius, P., Lee, A. G. & Morgan, H. Controlled delivery of proteins into bilayer lipid membranes on chip. *Lab Chip* **7**, 1176–1183 (2007).

60. Zagnoni, M., Sandison, M. E. & Morgan, H. Microfluidic array platform for simultaneous lipid bilayer membrane formation. *Biosens. Bioelectron.* **24**, 1235–1240 (2009).

61. Saha, S. C., Powl, A. M., Wallace, B. A., de Planque, M. R. R. & Morgan, H. Screening ion-channel ligand interactions with passive pumping in a microfluidic bilayer lipid membrane chip. *Biomicrofluidics* **9**, (2015).

62. Saha, S. C. *et al.* Characterization of the prokaryotic sodium channel NavSp pore with a microfluidic bilayer platform. *PLoS One* **10**, 1–10 (2015).

63. Buchholz, K. *et al.* Silicon-on-insulator based nanopore cavity arrays for lipid membrane investigation. *Nanotechnology* **19**, (2008).

64. Kleefen, A. *et al.* Multiplexed parallel single transport recordings on nanopore arrays. *Nano Lett.* **10**, 5080–5087 (2010).

65. Urban, M. *et al.* Highly parallel transport recordings on a membrane-on-nanopore chip at single molecule resolution. *Nano Lett.* **14**, 1674–1680 (2014).

66. Diederichs, T., Nguyen, Q. H., Urban, M., Tampé, R. & Tornow, M. Transparent Nanopore Cavity Arrays Enable Highly Parallelized Optical Studies of Single Membrane Proteins on Chip. *Nano Lett.* **18**, 3901–3910 (2018).

67. Kamiya, K. *et al.* Electrophysiological measurement of ion channels on plasma/organelle membranes using an on-chip lipid bilayer system. *Sci. Rep.* **8**, 2–10 (2018).

68. Beltramo, P. J., Van Hooghten, R. & Vermant, J. Millimeter-area, free standing, phospholipid bilayers. *Soft Matter* **12**, 4324–4331 (2016).

69. Beltramo, P. J., Scheidegger, L. & Vermant, J. Toward Realistic Large-Area Cell Membrane Mimics: Excluding Oil, Controlling Composition, and Including Ion Channels. *Langmuir* **34**, 5880–5888 (2018).

70. Heo, P. *et al.* Highly Reproducible Physiological Asymmetric Membrane with Freely Diffusing Embedded Proteins in a 3D-Printed Microfluidic Setup. *Small* **15**, 1–13 (2019).

71. Heo, P. & Pincet, F. Freezing and piercing of in vitro asymmetric plasma membrane by α-synuclein. *Commun. Biol.* **3**, 1–8 (2020).

72. Malmstadt, N., Nash, M. A., Purnell, R. F. & Schmidt, J. J. Automated formation of lipid-bilayer membranes in a microfluidic device. *Nano Lett.* **6**, 1961–1965 (2006).

73. Funakoshi, K., Suzuki, H. & Takeuchi, S. Lipid bilayer formation by contacting monolayers in a microfluidic device for membrane protein analysis. *Anal. Chem.* **78**, 8169–8174 (2006).

74. Tsuji, Y. *et al.* Droplet-based lipid bilayer system integrated with microfluidic channels for solution exchange. *Lab Chip* **13**, 1476–1481 (2013).

75. Aghdaei, S., Sandison, M. E., Zagnoni, M., Green, N. G. & Morgan, H. Formation of artificial lipid bilayers using droplet dielectrophoresis. *Lab Chip* **8**, 1617–1620 (2008).

76. Carreras, P. *et al.* A microfluidic platform for size-dependent generation of droplet interface bilayer networks on rails. *Biomicrofluidics* **9**, (2015).

77. Friddin, M. S. *et al.* Optically assembled droplet interface bilayer (OptiDIB) networks from cell-sized microdroplets. *Soft Matter* **12**, 7731–7734 (2016).

78. Czekalska, M. A. *et al.* A droplet microfluidic system for sequential generation of lipid bilayers and transmembrane electrical recordings. *Lab Chip* **15**, 541–548 (2015).

79. Czekalska, M. A., Kaminski, T. S., Horka, M., Jakiela, S. & Garstecki, P. An automated microfluidic system for the generation of droplet interface bilayer networks. *Micromachines* **8**, (2017).

80. Czekalska, M. A., Kaminski, T. S., Makuch, K. & Garstecki, P. Passive and parallel microfluidic formation of droplet interface bilayers (DIBs) for measurement of leakage of small molecules through artificial phospholipid membranes. *Sensors Actuators, B Chem.* **286**, 258–265 (2019).

81. Zhang, Y., Bracken, H., Woolhead, C. & Zagnoni, M. Functionalisation of human chloride intracellular ion channels in microfluidic droplet-interface-bilayers. *Biosens. Bioelectron.* **150**, 111920 (2020).

82. Kang, D. H., Han, W. B., Choi, N., Kim, Y. J. & Kim, T. S. Tightly Sealed 3D Lipid Structure Monolithically Generated on Transparent SU-8 Microwell Arrays for Biosensor Applications. *ACS Appl. Mater. Interfaces* **10**, 40401–40410 (2018).

83. Han, W. B., Kang, D. H., Na, J. H., Yu, Y. G. & Kim, T. S. Enhancement of membrane protein reconstitution on 3D free-standing lipid bilayer array in a microfluidic channel. *Biosens. Bioelectron.* **141**, 111404 (2019).

84. Angelova, M. I. & Dimitrov, D. S. Liposome Electro formation. 303–311 (1986).

85. Bucher, D. J. *et al.* Incorporation of influenza virus M-protein into liposomes. *J. Virol.* **36**, 586–590 (1980).

86. Estes, D. J., Lopez, S. R., Fuller, A. O. & Mayer, M. Triggering and visualizing the aggregation and fusion of lipid membranes in microfluidic chambers. *Biophys. J.* **91**, 233–243 (2006).

87. Kuribayashi, K., Tresset, G., Coquet, P., Fujita, H. & Takeuchi, S. Electroformation of giant liposomes in microfluidic channels. *Meas. Sci. Technol.* **17**, 3121–3126 (2006).

88. Paterson, D. J., Reboud, J., Wilson, R., Tassieri, M. & Cooper, J. M. Integrating microfluidic generation, handling and analysis of biomimetic giant unilamellar vesicles. *Lab Chip* **14**, 1806–1810 (2014).

89. Funakoshi, K., Suzuki, H. & Takeuchi, S. Formation of giant lipid vesiclelike compartments from a planar lipid membrane by a pulsed jet flow. *J. Am. Chem. Soc.* **129**, 12608–12609 (2007).

90. Kamiya, K., Kawano, R., Osaki, T., Akiyoshi, K. & Takeuchi, S. Cell-sized asymmetric lipid vesicles facilitate the investigation of asymmetric membranes. *Nat. Chem.* **8**, 881–889 (2016).

91. Gotanda, M., Kamiya, K., Osaki, T., Miki, N. & Takeuchi, S. Automatic generation system of cell-sized liposomes. *Sensors Actuators, B Chem.* **292**, 57–63 (2019).

92. Stachowiak, J. C. *et al.* Unilamellar vesicle formation and encapsulation by microfluidic jetting. *Proc. Natl. Acad. Sci. U. S. A.* **105**, 4697–4702 (2008).

93. Richmond, D. L. *et al.* Forming giant vesicles with controlled membrane composition, asymmetry, and contents. *Proc. Natl. Acad. Sci. U. S. A.* **108**, 9431–9436 (2011).

94. Belardi, B. *et al.* Claudin-4 reconstituted in unilamellar vesicles is sufficient to form tight interfaces that partition membrane proteins. *J. Cell Sci.* **132**, (2019).

95. Ota, S., Yoshizawa, S. & Takeuchi, S. Microfluidic formation of monodisperse, cell-sized, and unilamellar vesicles. *Angew. Chemie - Int. Ed.* **48**, 6533–6537 (2009).

96. Kurakazu, T. & Takeuchi, S. Generation of lipid vesicles using microfluidic T-junctions with pneumatic valves. *Proc. IEEE Int. Conf. Micro Electro Mech. Syst.* 1115–1118 (2010).

97. Zhigaltsev, I. V. *et al.* Bottom-up design and synthesis of limit size lipid nanoparticle systems with aqueous and triglyceride cores using millisecond microfluidic mixing. *Langmuir* **28**, 3633–3640 (2012).

98. Leung, A. K. K., Tam, Y. Y. C., Chen, S., Hafez, I. M. & Cullis, P. R. Microfluidic Mixing: A General Method for Encapsulating Macromolecules in Lipid Nanoparticle Systems. *J. Phys. Chem. B* **119**, 8698–8706 (2015).

99. Kulkarni, J. A., Witzigmann, D., Chen, S., Cullis, P. R. & Van Der Meel, R. Lipid Nanoparticle Technology for Clinical Translation of siRNA Therapeutics. *Acc. Chem. Res.* **52**, 2435–2444 (2019).

100. Kastner, E. *et al.* High-throughput manufacturing of size-tuned liposomes by a new microfluidics method using enhanced statistical tools for characterization. *Int. J. Pharm.* **477**, 361–368 (2014).

101. Forbes, N. *et al.* Rapid and scale-independent microfluidic manufacture of liposomes entrapping protein incorporating in-line purification and at-line size monitoring. *Int. J. Pharm.* **556**, 68–81 (2019).

102. Lou, G., Anderluzzi, G., Woods, S., Roberts, C. W. & Perrie, Y. A novel microfluidic-

based approach to formulate size-tuneable large unilamellar cationic liposomes: Formulation, cellular uptake and biodistribution investigations. *Eur. J. Pharm. Biopharm.* **143**, 51–60 (2019).

103. Nanomedicines, D. F. NanoAssemblr ™ Benchtop Instrument Demo. 888

104. Molinaro, R. *et al.* Design and Development of Biomimetic Nanovesicles Using a Microfluidic Approach. *Adv. Mater.* **30**, 1–9 (2018).

105. Weiss, M. *et al.* Sequential bottom-up assembly of mechanically stabilized synthetic cells by microfluidics. *Nat. Mater.* **17**, 89–95 (2018).

106. Haller, B. *et al.* Charge-controlled microfluidic formation of lipid-based single- and multicompartment systems. *Lab Chip* **18**, 2665–2674 (2018).

107. Staufer, O., Schröter, M., Platzman, I. & Spatz, J. P. Bottom-Up Assembly of Functional Intracellular Synthetic Organelles by Droplet-Based Microfluidics. *Small.* **1906426**, 1-9, (2020).

108. Doonan, S. R. & Bailey, R. C. K-Channel: A Multifunctional Architecture for Dynamically Reconfigurable Sample Processing in Droplet Microfluidics. *Anal. Chem.* **89**, 4091–4099 (2017).

109. Xu, Y. *et al.* A droplet microfluidic platform for efficient enzymatic chromatin digestion enables robust determination of nucleosome positioning. *Lab Chip* **18**, 2583–2592 (2018).

110. Doonan, S. R., Lin, M. & Bailey, R. C. Droplet CAR-Wash: Continuous picoliter-scale immunocapture and washing. *Lab Chip* **19**, 1589–1598 (2019).

111. Sercombe, L. *et al.* Advances and challenges of liposome assisted drug delivery. *Front. Pharmacol.* **6**, 1–13 (2015).

112. Kazayama, Y., Teshima, T., Osaki, T., Takeuchi, S. & Toyota, T. Integrated Microfluidic System for Size-Based Selection and Trapping of Giant Vesicles. *Anal. Chem.* **88**, 1111–1116 (2016).

113. Denisov, I. G. & Sligar, S. G. Nanodiscs in Membrane Biochemistry and Biophysics. *Chem. Rev.* **117**, 4669–4713 (2017).

114. Wade, J. H. *et al.* Microfluidic platform for efficient Nanodisc assembly, membrane protein incorporation, and purification. *Lab Chip* **17**, 2951–2959 (2017).

115. Iqbal, M. *et al.* Aqueous two-phase system (ATPS): an overview and advances in its applications. *Biol. Proced. Online* **18**, 1–18 (2016).

116. Hu, R. *et al.* Rapid, highly efficient extraction and purification of membrane proteins using a microfluidic continuous-flow based aqueous two-phase system. *J. Chromatogr. A* **1218**, 171–177 (2011).

117. Hu, R. *et al.* Rapid, highly efficient extraction and purification of membrane proteins using a microfluidic continuous-flow based aqueous two-phase system. *J. Chromatogr. A* **1218**, 171–177 (2011).

118. Jönsson, P., Gunnarsson, A. & Höök, F. Accumulation and separation of membrane-bound proteins using hydrodynamic forces. *Anal. Chem.* **83**, 604–611 (2011).

119. Gunnarsson, A. *et al.* Affinity Capturing and Surface Enrichment of a Membrane Protein Embedded in a Continuous Supported Lipid Bilayer. *ChemistryOpen* **5**, 445–449 (2016).

120. Lundgren, A. *et al.* Affinity Purification and Single-Molecule Analysis of Integral Membrane Proteins from Crude Cell-Membrane Preparations. *Nano Lett.* **18**, 381–385 (2018).

121. Hendrickson, W. A. Atomic-level analysis of membrane-protein structure. *Nat. Struct. Mol. Biol.* **23**, 464–467 (2016).

122. Echelmeier, A., Sonker, M. & Ros, A. Microfluidic sample delivery for serial crystallography using XFELs. *Anal. Bioanal. Chem.* **411**, 6535–6547 (2019).

123. Hansen, C. L., Skordalakest, E., Berger, J. M. & Quake, S. R. A robust and scalable microfluidic metering method that allows protein crystal growth by free interface diffusion. *Proc. Natl. Acad. Sci. U. S. A.* **99**, 16531–16536 (2002).

124. Hansen, C. L., Classen, S., Berger, J. M. & Quake, S. R. A microfluidic device for kinetic optimization of protein crystallization and in situ structure determination. *J. Am. Chem. Soc.* **128**, 3142–3143 (2006).

125. Zheng, B., Roach, L. S. & Ismagilov, R. F. Screening of protein crystallization conditions on a microfluidic chip using nanoliter-size droplets. *J. Am. Chem. Soc.* **125**, 11170–11171 (2003).

126. Zheng, B., Tice, J. D., Roach, L. S. & Ismagilov, R. F. A droplet-based, composite PDMS/glass capillary microfluidic system for evaluating protein crystallization conditions by microbatch and vapor-diffusion methods with on-chip X-ray diffraction. *Angew. Chemie - Int. Ed.* **43**, 2508–2511 (2004).

127. Li, X., Klemic, K. G., Reed, M. A. & Sigworth, F. J. Microfluidic system for planar patch clamp electrode arrays. *Nano Lett.* **6**, 815–819 (2006).

128. Caffrey, M. A comprehensive review of the lipid cubic phase or in meso method for crystallizing membrane and soluble proteins and complexes. *Acta Crystallogr. Sect. FStructural Biol. Commun.* **71**, 3–18 (2015).

129. Li, L. *et al.* A plug-based microfluidic system for dispensing lipidic cubic phase (LCP) material validated by crystallizing membrane proteins in lipidic mesophases. *Microfluid. Nanofluidics* **8**, 789–798 (2010).

130. Caffrey, M. & Cherezov, V. Crystallizing Membrane Proteins Using Lipidic Mesophases Martin Caffrey1 and Vadim Cherezov2 1. *Nat. Protoc.* **4**, 706–731 (2010).

131. Perry, S. L., Roberts, G. W., Tice, J. D., Gennis, R. B. & Kenis, P. J. A. Microfluidic generation of lipidic mesophases for membrane protein crystallization. *Cryst. Growth Des.* **9**, 2566–2569 (2009).

132. Khvostichenko, D. S., Schieferstein, J. M., Pawate, A. S., Laible, P. D. & Kenis, P. J. A. X-ray transparent microfluidic chip for mesophase-based crystallization of membrane proteins and on-chip structure determination. *Cryst. Growth Des.* **14**, 4886–4890 (2014).

133. Jansson, E. T. *et al.* Microfluidic flow cell for sequential digestion of immobilized proteoliposomes. *Anal. Chem.* **84**, 5582–5588 (2012).

134. Trkulja, C. L., Jansson, E. T., Jardemark, K. & Orwar, O. Probing structure and function of ion channels using limited proteolysis and microfluidics. *J. Am. Chem. Soc.* **136**, 14875–14882 (2014).

135. Robinson, T., Kuhn, P., Eyer, K. & Dittrich, P. S. Microfluidic trapping of giant unilamellar vesicles to study transport through a membrane pore. *Biomicrofluidics* **7**, (2013).

136. Maerkl, S.J. & Quake, S.R. A Systems Approach to Measuring the Binding Energy Landscapes of Transcription Factors. *Science.* **315**, 233–237 (2007).

137. Einav, S. *et al.* Discovery of a hepatitis C target and its pharmacological inhibitors by microfluidic affinity analysis. *Nat. Biotechnol.* **26**, 1019–1027 (2008).

138. Gerber, D., Maerkl, S. J. & Quake, S. R. An in vitro microfluidic approach to generating protein-interaction networks. *Nat. Methods* **6**, 71–74 (2009).

139. Sasaki, H *et al*. Single-vesicle estimation of ATP-binding cassette transporters in microfluidic channels. *Lab Chip*, **12**, 702-704 (2012).

140. Olesen, K. *et al.* Detection of ligand-receptor binding using microfluidic frontal affinity chromatography on proteoliposomes derived directly from native cell membranes. *J. Chromatogr. B Anal. Technol. Biomed. Life Sci.* **931**, 84–89 (2013).

141. Glick, Y. *et al.* Pathogen receptor discovery with a microfluidic human membrane protein array. *Proc. Natl. Acad. Sci. U. S. A.* **113**, 4344–4349 (2016).

142. Schwartz, N. *et al.* Neuregulin 1 discovered as a cleavage target for the HCV NS3/4A protease by a microfluidic membrane protein array. *N. Biotechnol.* **45**, 113–122 (2018).

143. Cho, W. & Stahelin, R. V. Membrane-protein interactions in cell signaling and membrane trafficking. *Annu. Rev. Biophys. Biomol. Struct.* **34**, 119–151 (2005).

144. García, C. D., Hadley, D. G. J., Wilson, W. W. & Henry, C. S. Measuring protein

interactions by microchip self-interaction chromatography. *Biotechnol. Prog.* **19**, 1006–1010 (2003).

145. Javanmard, M. *et al.* A microfluidic platform for characterization of proteinprotein interactions. *IEEE Sens. J.* **9**, 883–891 (2009).

146. Srisa-Art, M. *et al.* Analysis of protein-protein interactions by using droplet-based microfluidics. *ChemBioChem* **10**, 1605–1611 (2009).

147. Tan, D. C. W. *et al.* A novel microfluidics-based method for probing weak protein-protein interactions. *Lab Chip* **12**, 2726–2735 (2012).

148. Goehring, A. *et al.* Screening and large-scale expression of membrane proteins in mammalian cells for structural studies. *Nat. Protoc.* **9**, 2574–2585 (2014).

149. Chong, S. Overview of Cell-Free Protein Synthesis: Historic Landmarks, Commercial Systems, and Expanding Applications. *Curr Protoc Mol Biol.* **108**, 1–11 (2015).

150. Noireaux, V. & Libchaber, A. A vesicle bioreactor as a step toward an artificial cell assembly. *Proc. Natl. Acad. Sci. U. S. A.* **101**, 17669–17674 (2004).

151. Friddin, M. S. *et al.* Single-channel electrophysiology of cell-free expressed ion channels by direct incorporation in lipid bilayers. *Analyst* **138**, 7294–7298 (2013).

152. Elfaramawy, M. A. *et al.* Quantitative analysis of cell-free synthesized membrane proteins at the stabilized droplet interface bilayer. *Chem. Commun.* **54**, 12226–12229 (2018).

153. Yunker, P. J. *et al.* One-pot system for synthesis, assembly, and display of functional single-span membrane proteins on oil-water interfaces. *Proc. Natl. Acad. Sci. U. S. A.* **113**, 608–613 (2016).

154. Cournia, Z. *et al.* Membrane Protein Structure, Function, and Dynamics: a Perspective from Experiments and Theory. *J. Membr. Biol.* **248**, 611–640 (2015).

155. Nojima, T. *et al.* Cell-free protein synthesis in a microfabricated reactor. *Bioprocess Eng.* **22**, 13–17 (2000).

156. Hahn, G. H., Asthana, A., Kim, D. M. & Kim, D. P. A continuous-exchange cell-free protein synthesis system fabricated on a chip. *Anal. Biochem.* **365**, 280–282 (2007).

157. Mei, Q., Khnouf, R., Simon, A. & Fan, Z. H. Protein synthesis in a device with nanoporous membranes and microchannels. *Lab Chip* **10**, 2541–2545 (2010).

158. Chanasakulniyom, M. *et al.* Expression of membrane-associated proteins within single emulsion cell facsimiles. *Analyst* **137**, 2939–2943 (2012).

Chapter 3: Microfluidic Platform for Efficient Nanodisc Assembly, Membrane Protein Incorporation, and Purification

I would like to thank all of my co-authors on this published chapter: James Wade and Joshua Jones (both of Ryan Bailey's lab) and Ivan. Lenov, a member of Stephen Sligar's lab at the University of Illinois at Urbana-Champaign. I also acknowledge support from the National Institutes of Health (NIH) for funding under awards GM110432 and CA177462.

This chapter is modified from a published paper: Wade, J.H.; Jones, J.D.; Lenov, I.L.; Riordan, C.M.; Sligar, S.G.; Bailey, R.C. Microfluidic platform for efficient Nanodisc assembly, membrane protein incorporation, and purification. *Lab Chip.* **17**, *2951-2959* (2017).

Introduction

Membrane proteins play pivotal roles in cellular processes as the primary units of biomolecular transport and cellular communication. Because of their importance, membrane proteins are the most common targets for pharmaceutical agents.[1,2] Key to the study of membrane proteins is maintaining protein function in vitro. Purified membrane proteins exhibit substantially reduced activity outside of a native lipid bilayer environment, primarily because of protein misfolding in aqueous solutions.[3–7] Soluble lipid bilayer systems, such as protein-lipid micelles and liposomes, act as water-soluble and semi-native environments that have facilitated the characterization of many membrane proteins.[4,8,9] However, limitations of these systems have inspired exploration into alternative lipid bilayer mimetics for structural and functional studies of

membrane proteins. For example, liposome preparations often have high viscosities and/or turbidity that present major challenges for cell-free expression systems and many biophysical methods to interrogate functional protein activity.[10,11] Proteins solubilized in detergent micelles often demonstrate structural changes caused by the non-native environment.[5]

Nanodiscs are soluble, protein stabilized discoidal lipid bilayers that offer enabling advantages over liposomes and micelles for membrane protein studies.[12] In comparison to liposomes, micelles, and other soluble lipid bilayer systems, such as those made with styrene-maleic acid copolymers,[13–15] Nanodiscs are remarkably homogenous and stable in aqueous solutions. Beyond bilayer and protein stability, Nanodiscs have added advantages of access to both sides of the bilayer and precise control of bilayer composition, stoichiometry, and size.[16–18] The variable sizes of Nanodiscs allow for the incorporation of mono- or dimeric membrane proteins and can even support incorporation of multiprotein complexes essential for maintaining protein function.[19–21] The enhanced functionalities of Nanodiscs have resulted in their wide adoption as the preferred lipid bilayer mimetic system across diverse facets of membrane protein biology.[12,22]

For balance, it is worth noting that micellar and liposomal systems do have advantages in certain applications--particularly those that require compartmentalization or asymmetry across the bilayer. Furthermore, though commercially available, Nanodiscs do require a membrane scaffold protein (MSP), which adds a potential level of complexity, and the spectroscopic overlap between the MSP and incorporated membranes might complicate some assays, such as protein content determination via simple UV absorbance. Nevertheless, Nanodiscs have emerged as a powerful technology that continues to enable many studies that require model membrane interfaces.

Conventional Nanodisc assembly is achieved by solubilizing phospholipids and membrane proteins with detergents in the presence of a MSP. Upon removal of detergent, Nanodiscs self-assemble with MSP wrapping around a discoidal phospholipid bilayer with an integrated membrane protein.[16,23] A variety of membrane proteins have been incorporated into Nanodiscs, demonstrating the generality of the platform.[12,22,24] Despite this versatility, the incorporation of new membrane proteins within Nanodiscs does require empirical optimization, which typically involves serial screening of different detergents and phospholipids, as well as determining ideal ratios of reagents (e.g., phospholipid to MSP ratio). This laborious task can consume unacceptably large amounts of starting material—an impediment that is particularly limiting for many membrane proteins, which are natively expressed at low levels and are notoriously challenging to recombinantly express.[7,25,26]

Microfluidic technologies have emerged as robust alternatives to many bulk-scale molecular biology protocols featuring intrinsic miniaturization and low reagent consumption..[27–29] The ability to precisely manipulate small fluid volumes facilitates precise timing of fluid handling steps, and the short distances involved in microfluidics leads to efficient diffusion and expedient reaction processing. The additional benefits of parallelization and modular device design have further positioned microfluidics as powerful tools for improved protein processing and characterization.[30–34]

This study describes an integrated platform for Nanodisc assembly and purification using a microfluidic device that supports rapid Nanodisc assembly and reduced membrane protein consumption. Moreover, we demonstrate that these membrane proteins retain functional activity, which is indicative of incorporation into a fully reconstituted model membrane system. In series with Nanodisc assembly, a purification module can be incorporated into the device and tuned to

specific sample processing applications, adding additional functional capabilities to the platform. Importantly, the device architecture incorporates multiple inlets for on-chip reagent mixing at user-defined ratios and times. This multi-port design allows for avoidance of conditions where prolonged reagent mixing results in deleterious effects, such as reduced protein activity after exposure to detergents. This design also allows for the generation of temporal reagent gradients (e.g. lipids or surfactants), facilitating screening of variable membrane protein incorporation conditions within a single experiment. The capabilities of this new platform are demonstrated by the formation and characterization of Nanodiscs without incorporated protein (termed empty Nanodiscs) having variable lipid composition, and through the on-chip incorporation of Cytochrome P450 into Nanodiscs and subsequent confirmation of functional enzyme activity.[11,12] Though the focus in this study is on well-characterized proteins that have been previously shown to incorporate into Nanodiscs, we anticipate that this platform will offer broad utility for determining incorporation conditions for new proteins in which minimal reagent consumption and high throughput, gradient-based screening approaches are advantageous.

Experimental Methods

Materials. Amerlite XAD-2 hydrophobic beads, ethylenediaminetetraacetic acid (EDTA), dimethyl sulfoxide, 3-[(3-Cholamidopropyl)dimethylammonio]-1- propanesulfonate (CHAPS), sodium cholate, and other chemicals were purchased from Sigma Aldrich (St. Louis, MO, USA) unless otherwise indicated. Pierce Detergent Removal Resin was purchased from ThermoFisher Scientific (Waltham, MA, USA). The phospholipids 1,2-dimyristoyl-*sn*-glycero-3-phosphocholine (DMPC), 1-palmitoyl-2-oleoyl- *sn*-glycero-3-phosphocholine (POPC), and 1,2-dimyristoyl-sn-glycero-3-phosphoethanolamine- N-(lissamine rhodamine B sulfonyl) (LR-PE) were purchased from Avanti Polar Lipids (Alabaster, AL, USA). The membrane scaffold

proteins (MSP) used were MSP1D1 and MSP1E3D1, which were expressed and purified as previously described.[16,17] Both MSPs have an N-terminal His-tag that can be used for affinity purification. The His-tag can be removed using a Tobacco Etch Virus protease to completely and specifically cleave the tag. Cytochrome P450 3A4 (CYP3A4) was expressed from the NF-14 construct in the pCWOri+ vector with a histidine affinity tag. CYP3A4 was purified and incorporated into Nanodiscs as previously described.[35–38] All buffers were prepared with deionized water and filtered prior to use.

Microfluidic Design & Fabrication. Microfluidic device masters were designed using AutoCad (Autodesk Inc., San Rafael, CA), and photomasks were printed by CAD/Art Services,Inc. (Bandon, OR, USA). SU-8 2100, an epoxy-based negative photoresist, was purchased from Microchem (Westborough, MA, USA) and used to fabricate masters according to standard photolithography methods.[39] Device features were designed to be 200 μm in height and confirmed using profilometry. Polydimethylsiloxane (PDMS) was purchased from Momentive (Waterford, NY, USA) under the name RTV615 silicone rubber kit. The two-part mixture was combined 10:1 monomer:initiator, thoroughly mixed, and degassed under vacuum prior to pouring onto the negative master mold. PDMS was cured at 70°C for a minimum of 1 h. Device stamps were cut out of the PDMS mold, and access ports were added using Integra Miltex biopsy punches. Stamps were cleaned with Scotch Magic Tape to remove dust and other particulates prior to bonding to glass slides.

Silastic tubing with an inner diameter of 0.040" (Dow Corning, Midland, MI, USA) was used for the bead filling port, and 0.022" inner diameter Teflon tubing (Cole-Parmer, Vernon Hills, IL, USA) was used for all other ports. Filling of the bead bed was performed using either a custom built pressure system or manually with a disposable syringe attached to the Silastic

tubing. For manual filling, a density-balanced bead slurry was prepared from Pierce Detergent Removal Resin, Optiprep density gradient medium, and water. To prevent the loss of beads, the bead inlet tubing was clamped with a hemostat. The detergent removal capacity for this resin was previously demonstrated to be 1-10 mg of detergent per 1 mL of detergent removal resin across a wide variety of detergents, including sodium cholate and CHAPS.[40]

Microfluidic Nanodisc Assembly. Prior to Nanodisc assembly, all devices were washed with methanol for at least 20 min at 30 μL/min followed by a water rinse for at least 10 min at the same flow rate. Detergent bead beds could be regenerated by first rinsing device with water for 10 min and then following the same washing procedure for new devices. The lower limits of rinsing times were not determined, but could likely be shortened. Phospholipids used for Nanodisc assembly were stored in chloroform at -20°C. Prior to use, the phospholipids were dried to a lipid film and stored under vacuum for a minimum of 4 h. Nanodisc reagents were prepared in Standard Disc Buffer (SDB; 20 mM Tris HCl pH 7.4, 0.1 M NaCl, 0.5 mM EDTA, and 0.01% NaN_3). In cases where temperature control was needed, the microfluidic device was placed directly into a temperature controlled environment. For example, Nanodisc assembly with POPC lipids, which is optimum at 4°C, was performed with the devices on ice.

Nanodisc Assembly with Single Port Devices. Reagents for Nanodisc assembly were prepared according to desired ratios for lipid:MSP and MSP:CYP3A4. **Table 3.1** provides an example reagent sheet for Nanodisc assembly with a single port device. Reagents were mixed immediately prior to Nanodisc assembly, loaded into a syringe, and flowed through the device. The typical flow rate used for single port devices was 30 μL/min controlled by a Pump 11 Pico Plus Elite Dual Syringe Pump from Harvard Apparatus (Holliston, MA, USA). The eluent was collected in fractions from 5-100 μL and analyzed with SEC and/or AFM. Nanodisc self-

assembly is initiated upon removal of detergent via adsorption onto the detergent removal resin beads. Some sample loss is like to occur caused by adsorption on the resin beads and onto the walls of the PDMS device. The resin has been previously shown to preserve more than 90% of protein samples.[40] Because the surface area of the detergent removal resin is much higher than that of the PDMS device, adsorption onto the PDMS walls is likely a minor contributor to sample loss as opposed to the much larger surface area of the resin beads in the packed bed.

Nanodisc Assembly with Multi-Port Devices. Multi-port devices were prepared following the same sample protocol as single port devices. The reagents were divided into three syringes: (1) lipid with detergent, (2) MSP with detergent, (3) either buffer or membrane protein of interest. An example reagent sheet for a multi-port device is provided in **Table 3.2**. Reagent concentrations were determined such that optimal reagent ratios were achieved when all syringes flowed at the same rate, usually 10 μL/min for each syringe. Gradient experiments were performed by changing the flow rate of one of the syringes. The Pico Plus Elite pumps can be programmed with linear gradients for automated gradient experiments. See Figure **3.10** for additional details on the microfluidic gradients.

Table 3.1: Sample Nanodisc Preparation Sheet for Single Port Device.

User Inputs	
Total Sample Volume (µL)	400
[MSP1D1] (µM)	175.0
DMPC:MSP1D1 Ratio	80
[DMPC] stock (mM)	36.9
Dried DMPC (µL)	200.0
Desired [DMPC] (mM)	50.0
Desired final cholate concentration	20.0
Desired final MSP concentration	50.0
MSP1D1 Preparation Calculations	
nmol of MSP1D1	20
Final [MSP1D1] (µM)	50
Lipid Preparation Calculations	
nmol of DMPC	1600
Final [DMPC] (µM)	4000
Instructions	**Volume (µL)**
0: 100 mM Cholate Stock into Lipid Film	147.6
1: MSP1D1 stock into Tube #1	114.3
1: SDB(-) Buffer into Tube #1	19.0
2: 50 mM DMPC Lipid Stock into Tube #2	32.0
2: 100 mM Cholate Stock into Tube #2	48.0
2: SDB(-) Buffer into Tube #2	53.3
3: SDB(-) Buffer Tube #3	133.3
Syringe ID	**Flow Rate (µL/min)**
Total device flow rate	30.0
MSP1D1 Syringe (1)	10.0
DMPC Lipid Syringe (2)	10.0
Buffer Syringe (3)	10.0

Table 3.2: Sample Nanodisc Preparation Protocol for a Three-Port Mixing Device.

User Inputs	
Total Sample Volume (µL)	100
[MSP1E3D1] (µM)	125
CYP3A4 Stock Concentration (µM)	26.4
MSP1E3D1:CYP3A4 Ratio	10
POPC:MSP1E3D1 Ratio	120
[POPC] stock (mM)	35.4
Dried POPC (µL)	200
[POPC] after addition of detergent (mM)	50.0
Desired final [Cholate] (mM)	20
Desired [CYP3A4] (µM)	3.4
CYP3A4 Preparation Calculations	
nmol of CYP 3A4	0.3
Final [CYP3A4] (µM)	3.4
MSP1E3D1 Preparation Calculations	
nmol of MSP1E3D1	3.4
Final [MSP1E3D1] (µM)	34.0
Lipid Preparation Calculations	
nmol of POPC	408
Final [POPC] (µM)	4080
Reagents	**Volume (µL)**
100 mM Cholate into Lipid Film	141.6
SDB Buffer with 0.1% Emulgen 913	38.6
CYP3A4 Stock	12.9
MSP1E3D1 stock	27.2
50 mM POPC Stock	8.2
SDB Buffer	1.3
100 mM Cholate Stock	11.8

Colorimetric Quantitation of Detergent Removal. The amount of either sodium cholate or CHAPS in a solution can be determined colorimetrically by oxidation of the detergents with

concentrated sulfuric acid. To quantitate the detergent removal capacity of the devices, detergent-containing solutions were flowed across the packed beds of the devices and fractions were collected from the eluent. The concentration of detergent in each fraction was quantified according to a previously described method (**Figure 3.4**).[41]

Nanodisc Characterization by Size Exclusion Chromatography. Eluent fractions collected from the microfluidic devices were characterized by size exclusion chromatography (SEC) to assess the quality of Nanodisc assembly. Fractions were injected onto a Superdex 200 Increase 3.2/300 or 10/300 column (GE Healthcare, Pittsburgh, PA, USA). The 10/300 column was operated at a flow rate of 0.75 mL/min, and the 3.2/300 column was operated at a flow rate of 50 μL/min. Absorbances were measured at 280 nm to monitor Nanodisc formation and 417 nm to follow CYP3A4 incorporation into Nanodiscs. The following proteins (with known hydrodynamic radii) were used as chromatographic standards: Thyroglobulin (17 nm), Ferritin (12.2 nm), Bovine Liver Catalase (10.4 nm), and Bovine Serum Albumine (7.1 nm).

Nanodisc Characterization by AFM. Characterization of Nanodiscs with atomic force microscopy (AFM) was performed with a Cypher ES Environmental AFM (Asylum Research, Santa Barbara, CA, USA) equipped with a fluid cell. To prepare the surface for Nanodisc analysis, mica was glued to a stainless steel disc and cleaned with cellophane tape. Nanodiscs were diluted between 10 and 100 fold, and 10 μL of diluted sample was applied to the mica surface. The surface was then rinsed with 10-20 μL of imaging buffer (10 mM Tris-HCL pH 7.4, 0.15 M NaCl, 10 mM $MgCl_2$). A PAP pen (Ted Pella Inc,. Redding, CA, USA) was used to circumscribe an area of mica with a hydrophobic border, which was used to prevent flow of solution off of the mica. After 10 min, 5-10 mL of imaging buffer was passed through the cell to remove any unadsorbed material. The sample was then mounted onto the imaging stage. Contact

imaging was performed under imaging buffer with a thin-legged 310 μm cantilever with a nominal spring constant of 0.01 N/m.

Nanodisc Characterization by Dynamic Light Scattering. Characterization of Nanodiscs with dynamic light scattering (DLS) was performed using the Litesizer 500 Particle Analyzer (Anton Parr, Ashland, VA, USA). DLS was performed on Nanodiscs with DMPC phospholipids and MSP1D1 with Nanodiscs eluted from the assembly device. No sample purification was performed prior to analysis, and samples were analyzed at a concentration of 25 μM following the manufacturer's recommended protocol.

SDS-PAGE Analysis of Nanodiscs. Nanodisc assembly and purification was assessed using sodium dodecyl sulfate polyacrylamide gel electrophoresis (SDS-PAGE) on a 4-12% gradient gel (Bio-Rad, Hercules, CA, USA) under reducing conditions. The gel was stained with Coomassie Blue (Bio-Rad) after rinsing with deionized water. Both electrophoresis and staining followed the manufacturer's recommended protocol. SDS-PAGE gels were imaged with a ChemiDoc MP Imaging System (Bio-Rad), and further analysis was performed using Fiji.[42]

Nanodisc Purification with Affinity Chromatography. A slurry of Ni-NTA agarose resin was prepared in water. Using a syringe, methanol and water of sufficient volume to completely fill the device (approximately 100 μL each) were pushed through the device by hand. A syringe was then filled with Ni-NTA slurry and an 18 gauge needle was attached to the syringe with silastic tubing securely nested over needle. The silastic tubing was inserted into the filling port, and the resin bed was filled by applying steady pressure to the syringe plunger. Once the device was filled, the silastic tubing was clamped immediately above the filling port with either a hemostat or cable tie. To prepare the filled device for purification, the device was washed with 4 bed volumes of water

followed by 8 bed volumes of Purification Buffer (250 mM NaH_2PO_4, pH 8.0 50 mM NaCl) at a flow rate of 30 μL/min. The Nanodisc solution was then flowed across the packed bed at a flow rate of 10 μL/min. Then, the device was washed with the Wash Buffer (250 mM NaH_2PO_4, pH 8.0 50 mM NaCl, and 10 mM imidazole) at 30 μL/min for 6 bed volumes. After washing, 5 bed volumes of Elution Buffer (250 mM NaH_2PO_4, pH 8.0 50 mM NaCl, and 250 mM imidazole) were flowed through the device at 10 μL/min. Elution fractions were collected typically at volumes between 5 and 60 μL. The protein content of each fraction was determined using a Qubit 3.0 Fluorometer (ThermoFisher) following the manufacturer's recommended protocol. The purification modules could be reused after washing with 0.5M NaOH flowing at 30 μL/min for 30 min.

According to the manufacturer (Sigma), Ni-NTA resin can bind 5-10 mg of protein per mL of resin.The standard device design has 60 μL of resin. At a Nanodisc concentration of 30 μM (60 μM MSP), there is ~0.135 mg of MSP per 90 μL fraction collected from a single device. This equates to more than 3 fractions (90 μL fraction from a standard Nanodisc assembly device) per 60 μL Ni-NTA device. Fractions containing 0.5 mg/mL total protein content or greater were combined into a single fraction. For subsequent spectroscopic analysis, imidazole was removed from the fractions using 3.5 kDa MWCO filters (ThermoFisher) according to manufacturer-recommended protocols. SDB was used as dialysis buffer.

Spin-Shift Assays with CYP3A4 in Nanodiscs. Prior to performing the spin shift assay, Nanodiscs were formed using the microfluidic assembly and purification modules according to the specified protocol. Purified Nanodiscs containing CYP3A4 were added to a quartz cuvette. Absorption spectra were acquired using a StellarNet Black Comet UV-visible spectrometer optically connected to a StellarNet cuvette holder and Halogen lamp light source using two 400 μm fiber-optic cables with 0.22 numerical aperture (Thorlabs). A baseline spectrum was collected for

the CYP3A4 Nanodisc solution. Bromocriptine was dissolved in DMSO at 5 mg/mL and stored at -20°C for short term storage. Prior to use for the spin-shift assay, the solution was allowed to equilibrate to ambient temperature and diluted to 0.1 mg/mL in a 1:9 DMSO:SDB solution. The bromocriptine solution was then added to the cuvette with pipette mixing before collecting absorption spectra. For the imidazole spin-shift assay, the absorption spectrum was collected after purification but prior to dialysis to remove imidazole. This spectrum was then compared to the baseline absorption spectrum for the bromocriptine spin shift assay.

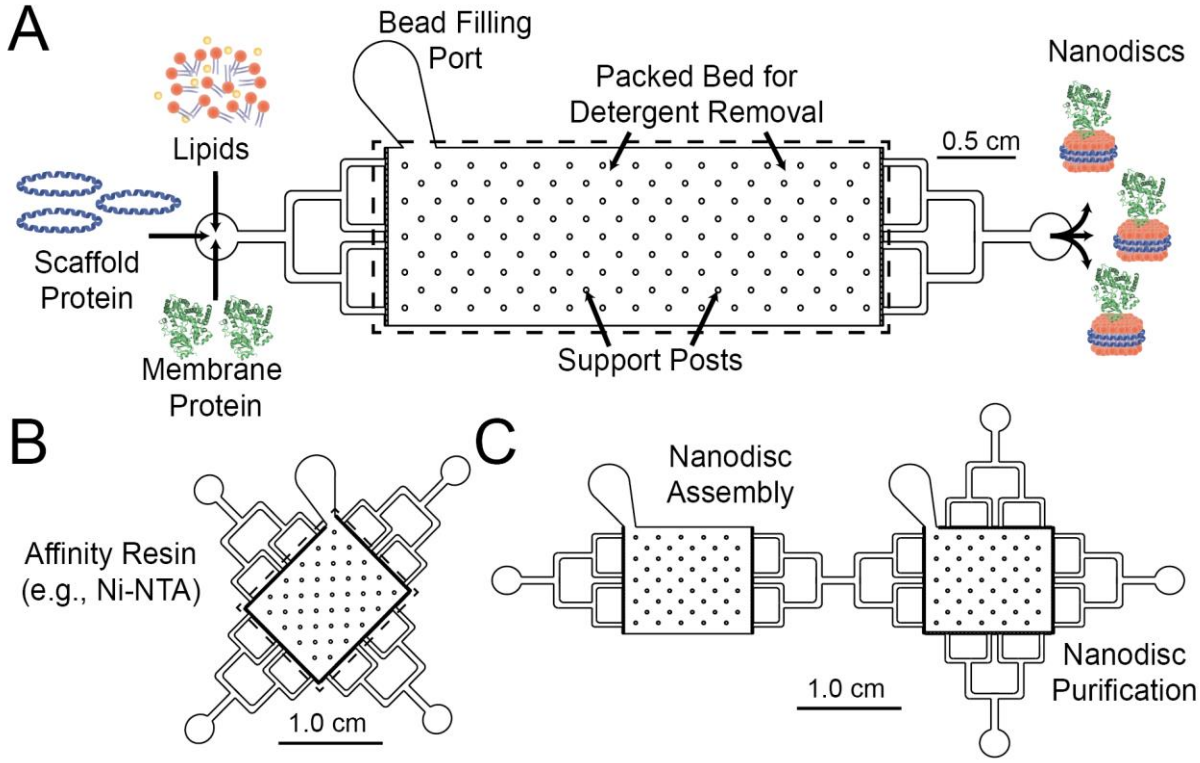

Figure 3.1. **Platform Device Designs**. (**A**) A single-port device consists of reagent and detergent removal bead inlets, a bead bed with integrated posts for structural support, and an outlet for Nanodisc elution. The device has a bead bed volume of 60 µL and yields 0.1-2 nmol of Nanodiscs. (**B**) The purification devices feature multi-directional flow for loading of Nanodiscs formed using devices from A. (**C**) Interfacing Nanodisc self-assembly and purification can be achieved as a single, integrated platform.

Results and Discussion

This microfluidic platform is modular and can be divided into two primary functions: (1) Nanodisc assembly and (2) purification of assembled Nanodiscs. The Nanodisc assembly consists of reagent inlets, a larger inlet for loading resin material, a packed bed of detergent removal resin, and an outlet for the collection of Nanodiscs **(Figure 3.1a).** Mixing of Nanodisc reagents can be performed either on- or off-chip. For on-chip mixing, the devices include multiple reagent inlets and a serpentine mixing chamber with alternative jutting structures to ensure efficient mixing **(Figure 3.1b).** The bead bed consists of capture structures at the inlet and outlet of the bed along with posts for structural support throughout the bed. The design uses a three-port reagent inlet for on-chip mixing and a bed volume of either 20 or 60 μL, though the modularity of the platform allows for individual devices to be tailored for specific experiments **(Figure 3.2)**. Flow through the various device designs was visualized with dye, demonstrating rapid and efficient mixing for multiport devices **(Figure 3.3).** Components were flowed through the device and Nanodiscs self-assemble as the detergent was removed by the on-chip packed resin bed.[40] To demonstrate this assembly, Nanodiscs were formed on the device through the removal of two types of bile-salt detergents: sodium cholate and 3-((3-cholamidopropyl) dimethylammonio)-1-propanesulfonate (CHAPS) **(Figure 3.4)**. Detergent choice for Nanodisc assembly is typically dictated by the stability of the membrane protein target,[4,12] and the ability of the resin to remove many types of detergents ensures the generality of this microfluidic device for many model membrane mimetic systems.[40]

The purification module **(Figure 3.1c)** is conceptually similar to the Nanodisc assembly device in that they both rely on microstructures to capture a bead-based bed of resin that achieves the end function. However, the resin used in this module can be tuned to enable affinity-based

purification, and subsequent elution, of Nanodisc-incorporated membrane proteins. For proof-of-principle, Ni-nitrilotriacetic acid (Ni-NTA) agarose resin was used as the affinity resin for purification. For the present study, we only used Ni-NTA as a purification resin, though other bead-based purification systems are compatible with the current design (e.g., immunoaffinity purification). The standalone design consists of a (1) single inlet, (2) a packed bed of affinity purification resin, and (3) an outlet for the collection of purified Nanodisc material. The purification module can also be integrated directly downstream of the Nanodisc assembly module through the simple addition of of inlet and outlet ports with a flow direction perpendicular to the flow from the assembly module **(Figure 3.1c).**

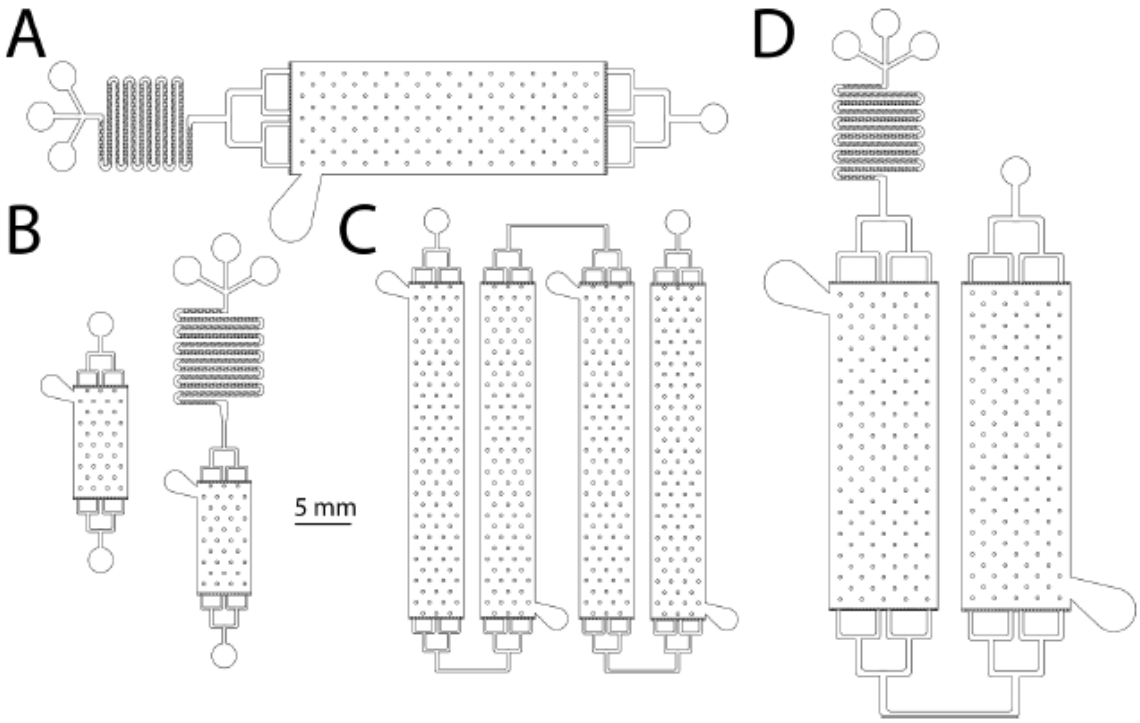

Figure 3.2: Additional Device Designs for Microfluidic Nanodisc assembly. (**A**) A 3-port inlet device for on-chip reagent mixing with the same bed volume as the standard single port device is suitable for applications where exposure to lipid-solubilizing detergents may damage to membrane protein to be incorporated. The bed volume of both assembly and purification can be tuned to the desired application. (**B**) The smallest device designed was 10 μL, and this bed volume can be interfaced with either a single or multiport inlet. (**C**) This alternative design consists of a larger total bed volume of 120 μL with four beds. Each bed is packed individually and can be filled with either detergent removal resin or affinity purification resin.(**D**) Another large volume device (120 μL) consists of two packed beds interfaced with a multiport inlet for on-chip reagent mixing.

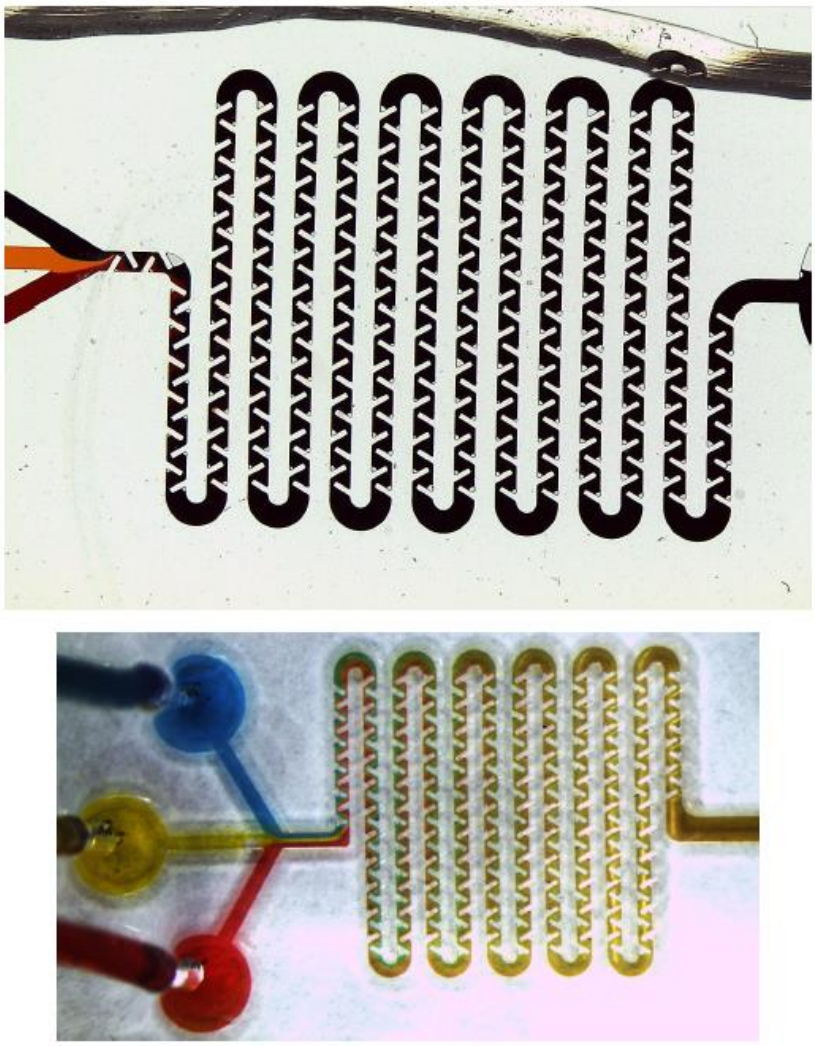

Figure 3.3. Flow Visualization of 3 Port Mixing Device. The multiport device design used on-chip reagent mixing prior to Nanodiscs assembly upon detergent removal. The mixing channel featured alternating juts to encourage efficient mixing. Three different colors of food dye are fed into the device and complete mixing is clearly apparent.

For both modules, microfluidic devices were fabricated from polydimethylsiloxane (PDMS) stamps bonded to glass using standard soft lithography. Briefly, a master mold was fabricated using 2-D photolithography with silicon wafers and an epoxy-based negative photoresist. PDMS stamps were made from the master molds and plasma bonded to glass.

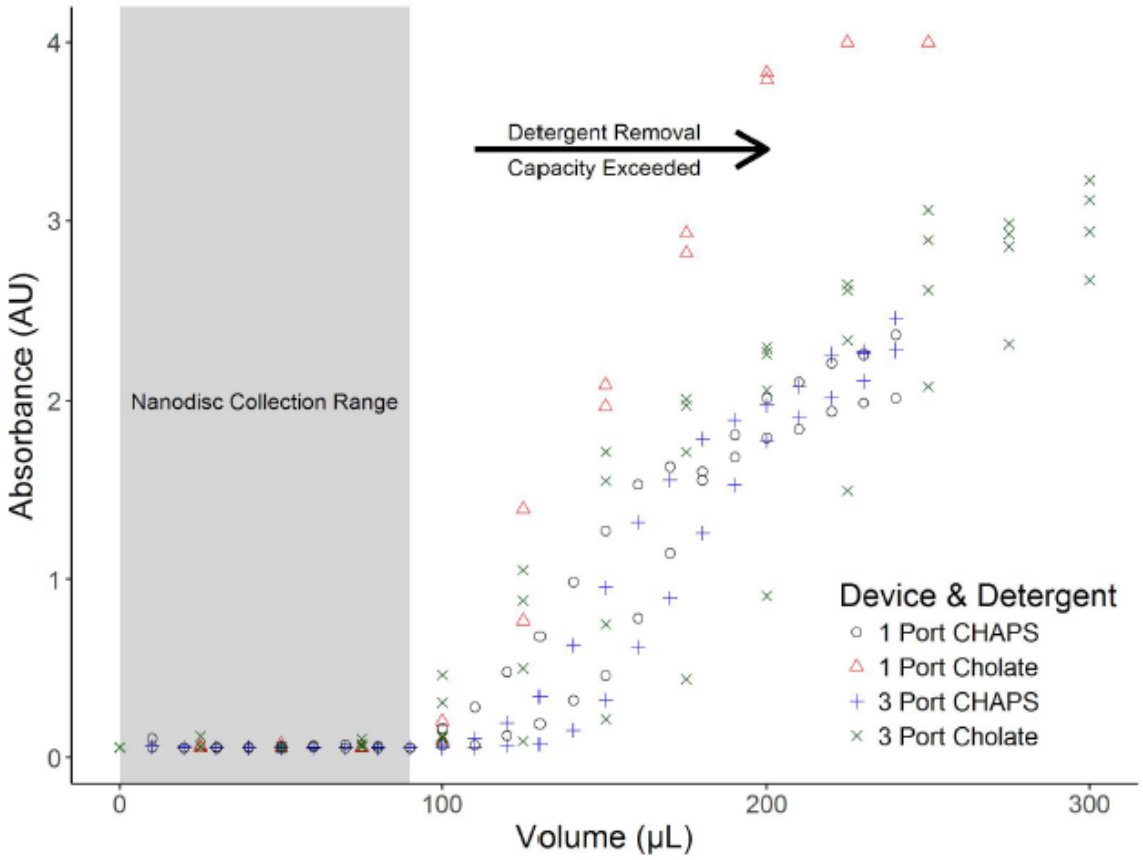

Figure 3.4. Detergent Removal Device Capacity. Elution fractions collected from single port and multiport devices flowing 1% CHAPS (black and blue dots), 20 mM sodium cholate (red and green dots), and treated with concentrated sulfuric acid show increased absorbance once the detergent removal capacity is reached. This plot shows the detergent removal capacity for a device bed volume of 60 µL. The detergent removal capacity for both detergents is >90 µL, which corresponds to 1.5 µmol (0.9 mg) CHAPS and 1.8 µmol (0.78 mg) sodium cholate. The region shaded in grey represents the Nanodisc collection region. No Nanodiscs were collected from an assembly device above 90 µL of elution volume to ensure adequate detergent removal for samples fractions.

To demonstrate this approach for microfluidic Nanodisc assembly, initial experiments focused on the creation of Nanodiscs without incorporation of a membrane protein. Beyond providing a simple system for assessing Nanodisc assembly, “empty” Nanodiscs of precise lipid composition have found broad utility in probing protein-lipid interactions of fundamental

important to a number of biological processes, including the blood coagulation cascade.[43–45] Nanodiscs were formed using either 1,2-dimyristoyl-sn-glycero-3-phosphocholine (DMPC) or 1-palmitoyl-2-oleoyl-sn-glycero-3-phosphocholine (POPC), and two different MSPs (MSP1D1 or MSP1E3D1). MSP1D1 results in Nanodiscs 9.7 nm in diameter with 120 to 160 lipids per Nanodisc and a lipid:MSP ratio of 60:1 to 80:1 (there are two MSPs per Nanodisc), depending on the packing density of the lipids. MSP1E3D1 gives larger 12.7 nm diameter Nanodiscs with lipid:MSP ratios ranging from 120:1 to 150:1.[16]

The Nanodisc reagents were initially mixed off-chip and then flowed through the single-port inlet device design and across the packed bed of detergent removal resin. Nanodisc assembly occurs immediately upon removal of detergent as the solution flows across the packed bed. Size exclusion chromatography (SEC) was used to assess Nanodisc purity, size, and dispersity. Chromatograms showed a single, narrow peak at the appropriate elution times relative to a mixture of protein standards **(Figure 3.5a-b).** Successful microfluidic assembly of Nanodiscs was also orthogonally confirmed by atomic force microscopy **(Figure 3.5c)** and dynamic light scattering **(Figure 3.5d).** Nanodisc assembly was found to be independent of device flow rates after testing from 1 μL/min to 100 μL/min **(Figure 3.6).** Since Nanodisc assembly is entirely based upon detergent removal, the removal capacity of the basic assembly module **(Figure 3.1a)** was experimentally determined to be ~1 mg of detergent, for both sodium cholate and CHAPS **(Figure 3.4).** Once the detergent capacity is reached for a given bed volume, the detergent removal resin can be regenerated by rinsing with methanol. Nanodisc assembly can be performed repeatedly on a single device with no observable degradation in Nanodisc quality.

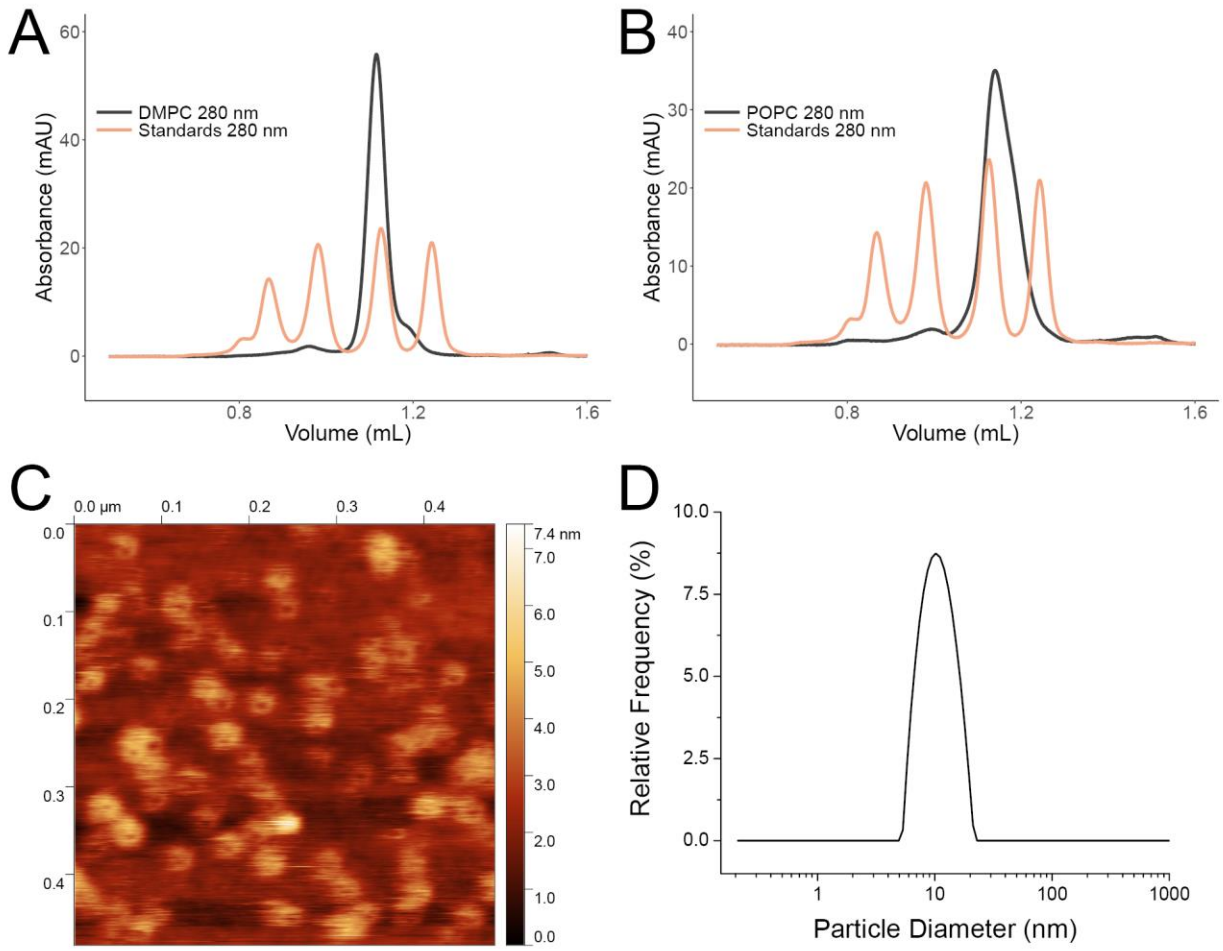

Figure 3.5. **Microfluidic Self-Assembly with Empty Nanodiscs**. SEC analysis of Nanodiscs formed from a single-port device with DMPC and a DMPC:MSP ratio of 80:1 (**A**) and POPC and a POPC:MSP ratio of 60:1 (**B**) with MSP1D1. Approximate Nanodisc concentrations for each are 25 µM. (**C**) Atomic force microscopy (AFM) of DMPC Nanodiscs formed with the Nanodisc assembly module without prior purification show Nanodiscs of appropriate dimension with no evidence of large lipid aggregates. (**D**) Dynamic light scattering (DLS) analysis of DMPC Nanodiscs indicating a single, monodisperse peak corresponding to Nanodiscs.

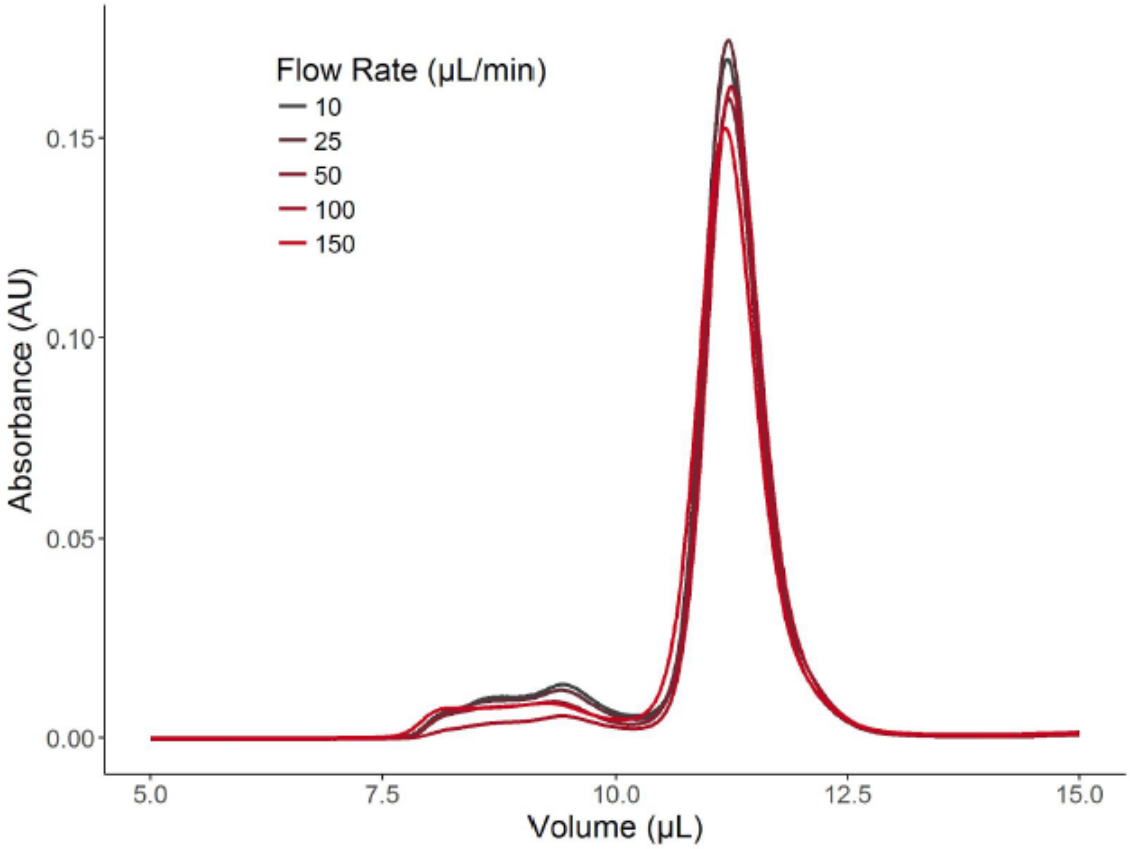

Figure 3.6. Assembly of Nanodisc at Various Device Flow Rates. Size exclusion chromatograms (SEC) monitored at 280 nm for DMPC Nanodiscs with MSP1D1 formed at variable flow rates indicate minimal to no effect on overall Nanodisc assembly.

In contrast to the single port module that requires all reagents to be combined off-chip, the multi-port detergent removal device allows on-chip reagent mixing so that the Nanodisc components are only combined immediately before detergent removal and Nanodisc assembly. A device with three inlet ports **(Figure 3.1b)** was used for Nanodisc assembly with both DMPC and POPC. The three inlets were used to flow: (1) detergent solubilized phospholipids, (2) MSP, and (3) SDB. There were no observed differences in Nanodisc quality as compared to premixing with single port devices **(Figure 3.7).**

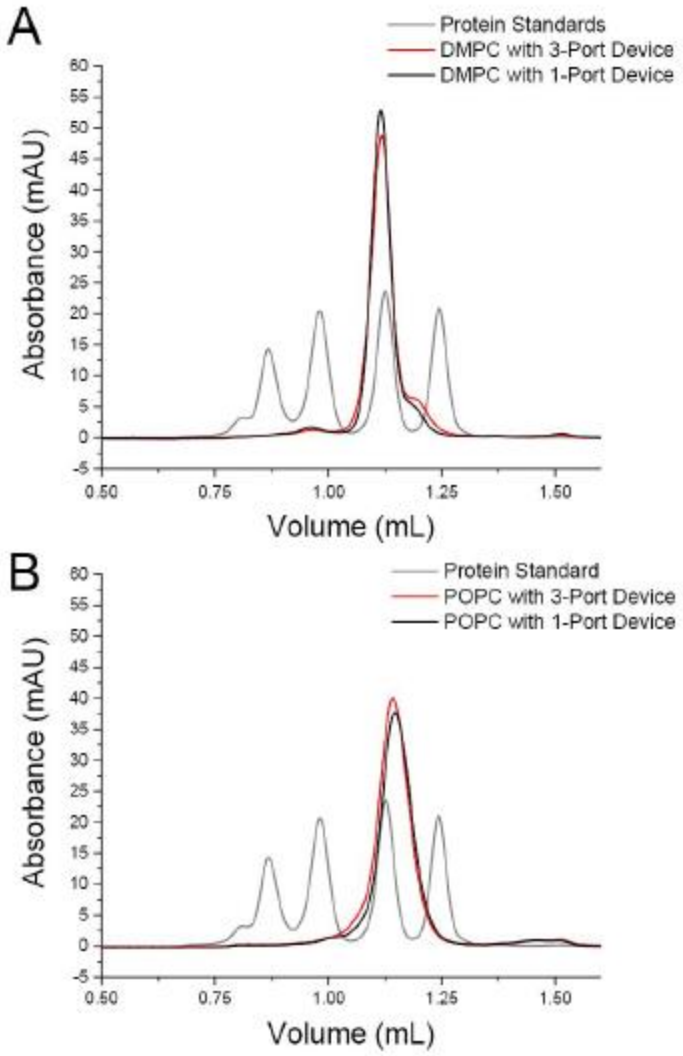

Figure 3.7. Comparison of Mixing versus No Mixing. Nanodiscs formed with either multiport (3-port) or single port devices using MSP1D1 and sodium cholate as detergent both result in monodisperse Nanodiscs that co-elute when analyzed with SEC monitored at 280 nm. There was no observed impact on Nanodisc formation when prepared at RT using DMPC lipids (**A**) or at 4°C using POPC lipids (**B**).

Beyond on-chip mixing, the multi-port design also offers the ability to tune reagent composition as a function of time. For example, flow rates at different inlets can be tuned over time to generate temporal microfluidic gradients that offer dynamically varying conditions over which Nanodisc assembly can be screened. To demonstrate this capability, we used a

programmable syringe pump to dynamically change the the lipid composition of Nanodiscs over time. Nanodisc lipid composition was determined using a fluorescent phospholipid, 1,2-dimyristoyl-sn-glycero-3-phosphoethanolamine-N-(lissamine rhodamine B sulfonyl) (LR-PE), in addition to DMPC **(Figure 3.8).** For the 3-port device, the flow rate for the MSP containing inlet was held constant while the rate of the DMPC inlet was decreased and the rate of the fluorescent lipid was increased over the course of the Nanodisc assembly. The fluorescence intensity associated with the LR-PE lipid steadily increased with elution volume indicating an increase in Nanodisc formed with fluorescent lipid. The composition of the Nanodiscs with the addition of the fluorescent lipid was assessed with SEC **(Figure 3.8c).** It is worth noting that screening Nanodisc assembly conditions will result in poor Nanodisc formation when Nanodisc reagent stoichiometries are suboptimal. Key to gradient analysis, however, is delivery of Nanodisc reagents across the packed bed of detergent removal resin in the proportion to their delivery into the mixing device. Longitudinal mixing would blur the microfluidic gradient, and **Figure 3.8b** suggests that this form of mixing is minimal for the Nanodisc assembly module.

To demonstrate the platform's utility for the incorporation of membrane proteins into Nanodiscs, cytochrome P450 3A4 (CYP3A4) was used as a model system. Cytochromes P450 are ubiquitous membrane proteins that predominantly serve as oxidase enzymes in electron transfer chains.[46] CYP3A4 is the most abundant cytochrome P450 expressed in the human liver and small intestines, and approximately half of small molecule pharmaceuticals are thought to be metabolized by CYP3A4.[47] Alone, CYP3A4 forms aggregates in solution after isolation and purification; however, the incorporation of CYP3A4 into Nanodiscs prevents aggregation and also allows precise control over the protein's oligomeric state.[48] The role of CYP3A4 in drug metabolism has motivated a wide variety of studies incorporating CYP3A4 into

Nanodiscs.[11,38,48–52] As such, CYP3A4 was chosen as an important proof-of-principle membrane protein with which to demonstrate the utility of this microfluidic Nanodisc assembly platform.

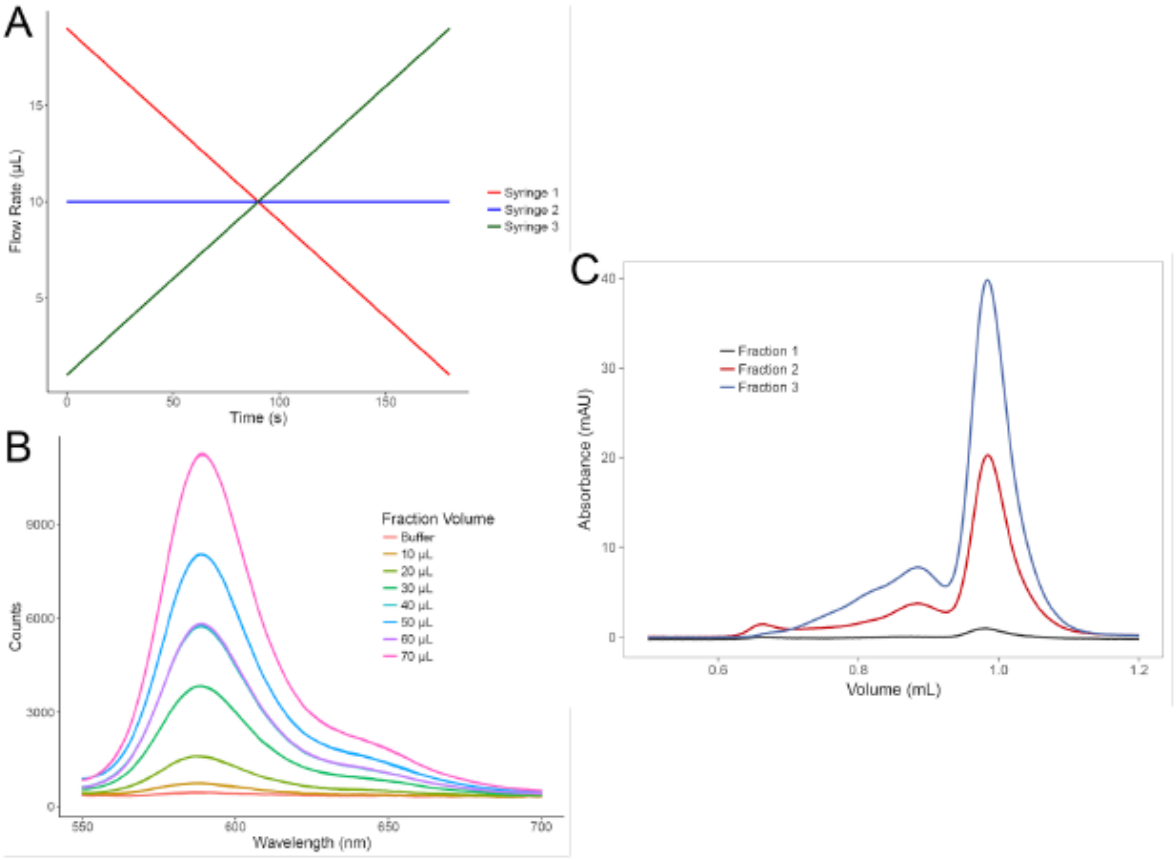

Figure 3.8. Microfluidic Gradient with Fluorescent Lipids. (**A**) The flow rate for lipid-containing syringe was increased continuously at a rate of 0.1 µL/s ₂ for the syringe containing DMPC with 0.05% Liss Rhod PE (Syringe 3) and -0.1 µL/s ₂ for DMPC only syringe (Syringe 1). The syringe with MSP was held at a constant flow rate of 10 µL/min (Syringe 2). (**B**) The fluorescence with a maximum at 590 nm shows an increase in intensity as a function of flow rate. This corresponds to an increasing fluorescent lipid content and, thus lipid bilayer composition, over the course of the microfluidic gradient. (C)This increase in fluorescence over time measured at 590 nm is also seen in the SEC Nanodisc peak, showing incorporation of fluorescent lipids into Nanodiscs following the gradient.

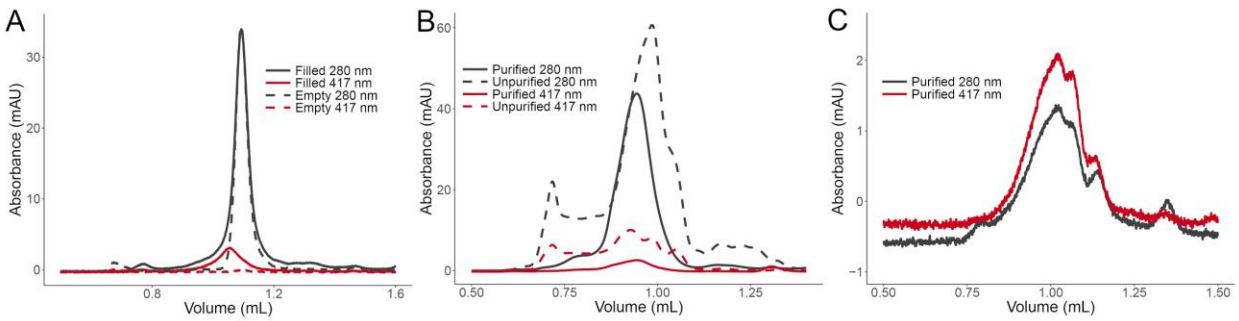

Figure 3.9. **Incorporation of CYP3A4 into Nanodiscs**. Size exclusion chromatograms recorded at 280 nm and 417 nm (**A**) demonstrate the successful incorporation of CYP3A4 into Nanodiscs using the microfluidic assembly module. Equivalently sized Nanodiscs were formed either with (red) or without (black) CYP3A4 in combination with DMPC lipids, MSP1D1, and CHAPS detergent. The filled Nanodiscs, which had a MSP:CYP3A4 ratio of 20:1, were confirmed by the strong absorbance at 417 nm with minimal signal for the empty Nanodiscs. (**B**) Purification with His-tag with POPC, MSP1E3D1, and CYP3A4 (both CYP3A4 and MSP have His-tag) at a ratio of 10:1 MSP:CYP3A4 **(C**) Purification of CYP3A4 Nanodiscs made with DMPC MSP1D1(-) (that indicates His-tag is removed) at a ratio of 20:1 MSP:CYP3A4.

The strong optical absorbance of the CYP3A4 heme cofactor (λ_{max} = 417 nm) provides a useful spectroscopic handle for monitoring protein incorporation into Nanodiscs. Using the single port inlet device with off-chip reagent mixing, the CYP3A4 protein was found to readily incorporate into Nanodiscs composed of DMPC as a model lipid. Nanodisc assembly was characterized by SEC with absorbance detection at both 280 nm, for general protein (including MSP) absorbance, and at 417 nm for the heme cofactor of CYP3A4, and compared against the same SEC analysis for empty Nanodiscs **(Figure 3.9a).** The elution peaks for filled Nanodiscs shows clear absorption at both 280 and 417 nm, which is consistent with well-formed Nanodiscs incorporating CYP3A4. Empty Nanodiscs have only an absorbance at 280 nm. Notably, the 417 nm absorbance for filled Nanodiscs is shifted to a slightly earlier elution compared to 280 nm, which is in agreement with the CYP3A4-containing Nanodiscs having a slightly larger hydrodynamic radius compared with empty Nanodiscs. We also demonstrated that CYP3A4 can

be incorporated into Nanodiscs using on-chip reagent mixing **(Figure 3.10).** The ability to mix on-chip is important given that some classes of membrane proteins can denature or deactivate with prolonged detergent exposure.[4] It is also important to point out that at this CYP3A4:lipid:MSP incorporation stoichiometry filled Nanodiscs are assembled in a large background of empty Nanodiscs, a point that will be discussed later. SDS-PAGE and SEC analysis of Nanodiscs filled with CYP3A4 after purification indicate that 5-20% of Nanodiscs contain incorporated CYP3A4 **(Figure 3.12).**

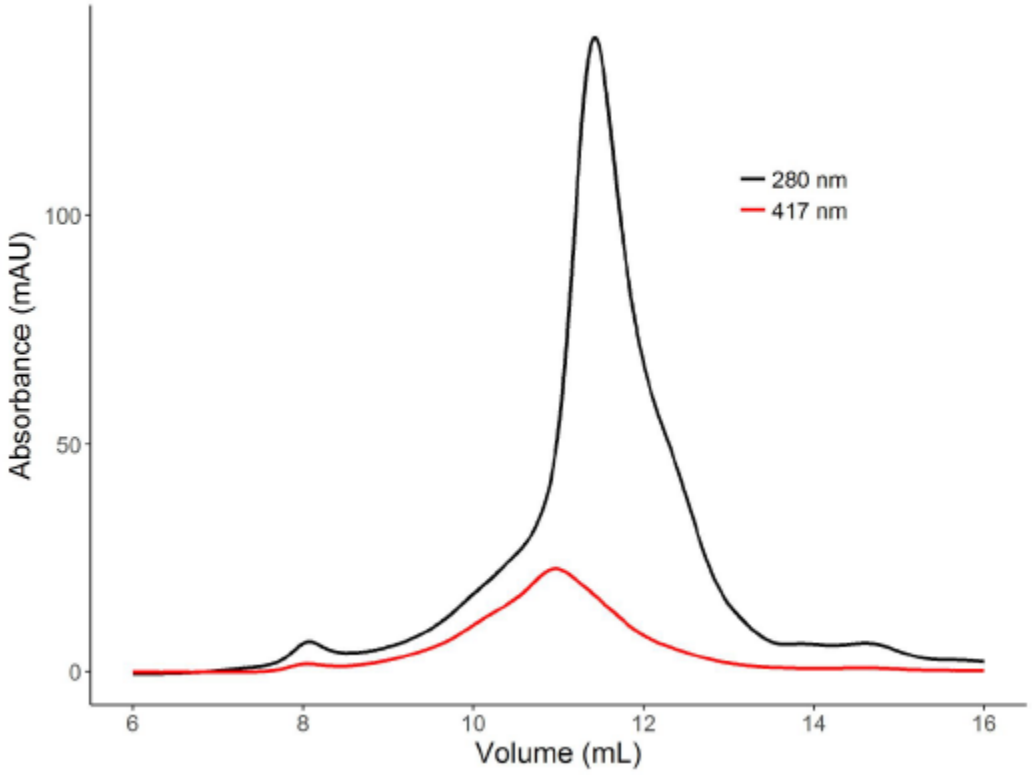

Figure 3.10. Incorporation of CYP3A4 into Nanodiscs with a 3-Port Assembly Device. CYP3A4 incorporation into DMPC and MSP1D1 Nanodiscs using a 3 port assembly device measured at both 280 nm and 417 nm with SEC show incorporation of CYP3A4 into the Nanodiscs as indicated by the co-elution of the 417 nm and 280 nm peaks. No Nanodisc purification was performed prior to SEC analysis.

As demonstrated above, the Nanodisc assembly module produces well-formed Nanodiscs of homogenous distribution. However, the incorporation of membrane proteins into Nanodiscs, as with all other lipid bilayer systems, does not result in the incorporation of all solubilized membrane proteins into Nanodiscs. As such, membrane protein aggregates that can interfere with downstream assays of membrane protein structure of function will remain in the sample after Nanodisc assembly. Often the most time-consuming process when using Nanodiscs for membrane protein studies is purification.[23] Two approaches are typically combined for this process: affinity purification and fractionation with SEC. Each step can result in loss of Nanodisc product or dilution of Nanodiscs, requiring additional re-concentrating processing steps for many applications. To improve the purification process, we designed an affinity purification module for the platform, as described above **(Figure 3.1b-c).** Ni-NTA was used for affinity-based purification. MSP1D1 and MSP1E3D1 scaffold proteins have N-terminal His-tags to allow for efficient Nanodisc purification **(Figure 3.11).**

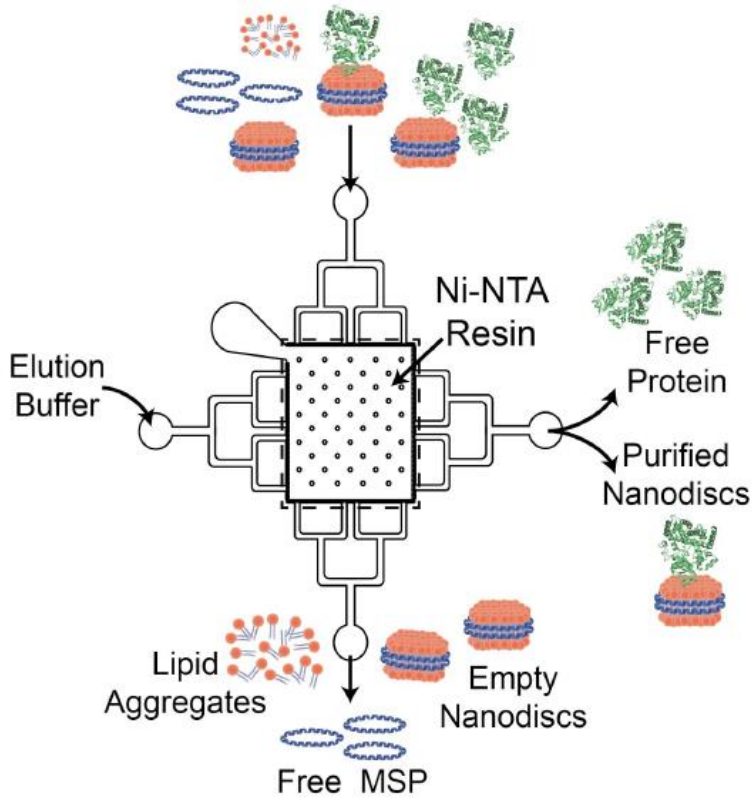

Figure 3.11: Microfluidic purification of Nanodiscs by affinity chromatography.

As demonstration of the utility of the affinity purification module, CYP3A4 was incorporated into Nanodiscs using POPC as the lipid, cholate as the detergent, and the larger MSP1E3D1. POPC has a single point of unsaturation in the lipid tail that, while helping create a more native-like environment for membrane proteins, also forms more loosely packed bilayers and a wider dispersity of resulting Nanodiscs. Chromatograms of CYP3A4-containing Nanodiscs before and after purification with the Ni-NTA module (dotted traces in **Figure 3.9b**) clearly demonstrate the improvement in collected Nanodiscs. Specifically, faster eluting contaminants such as cytochrome and lipid aggregates are removed, as are smaller lipid aggregates at longer elution times.

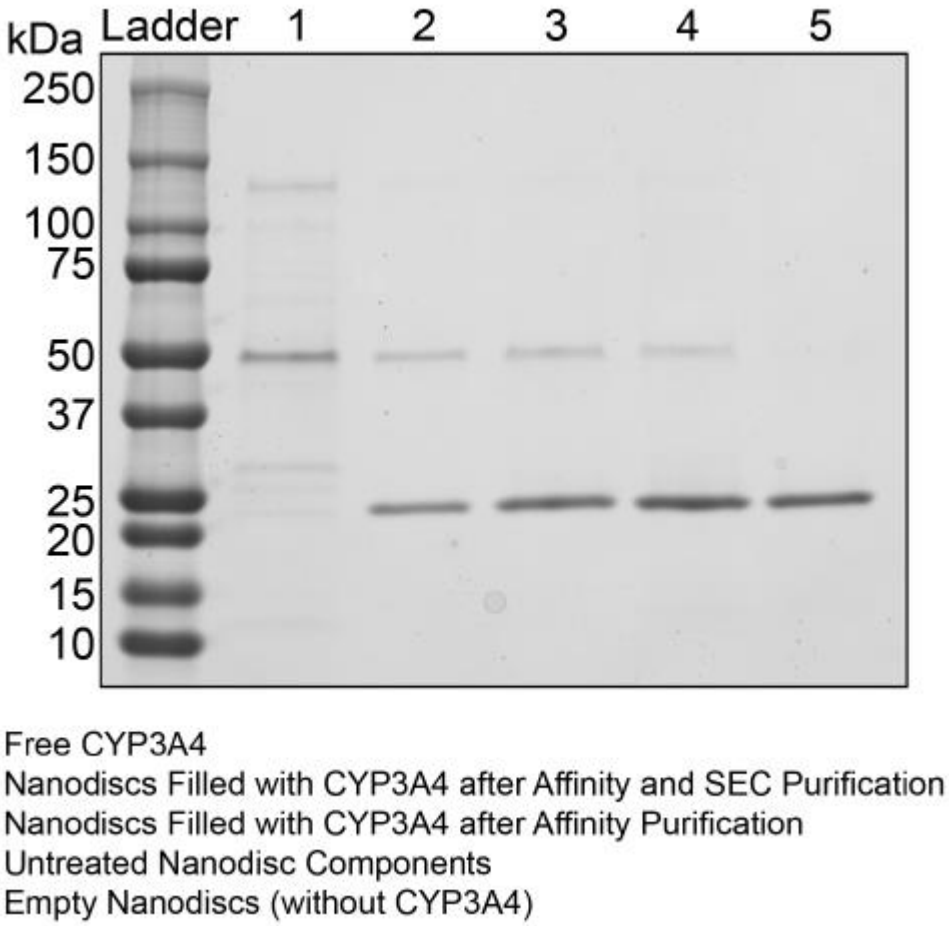

Figure 3.12. Polyacrylamide Gel Electrophoresis of Nanodiscs with incorporated CYP3A4. SDS-PAGE gel of DMPC and MSP1D1 Nanodiscs filled with CYP3A4 throughout the assembly and purification process stained with Coomassie Blue. Bands corresponding to CYP3A4 (57 kDA) and MSP1D1 (24.6 kDa) are present in all filled Nanodiscs and in Nanodisc components. Empty Nanodiscs only show the MSP band.

Purification using engineered affinity tags on MSP offers a generalizable approach for Nanodisc purification, though this results in a mixture of Nanodiscs containing the protein of interest with a background of empty Nanodiscs. For applications requiring only Nanodiscs with incorporated protein, affinity purification using features of the incorporated protein is needed. To demonstrate this capability, Nanodiscs filled with His-tagged CYP3A4 were made using MSP from which the N-terminal His-tag was cleaved prior to Nanodisc assembly. Purification via the

Ni-NTA resin module described above showed only filled Nanodiscs, as evidenced by the overlap of the absorbance signals measured at both 280 nm and 417 nm **(Figure 3.9c).** Importantly, this approach is generalizable to other affinity purification approaches, such as antibody-based affinity chromatography.

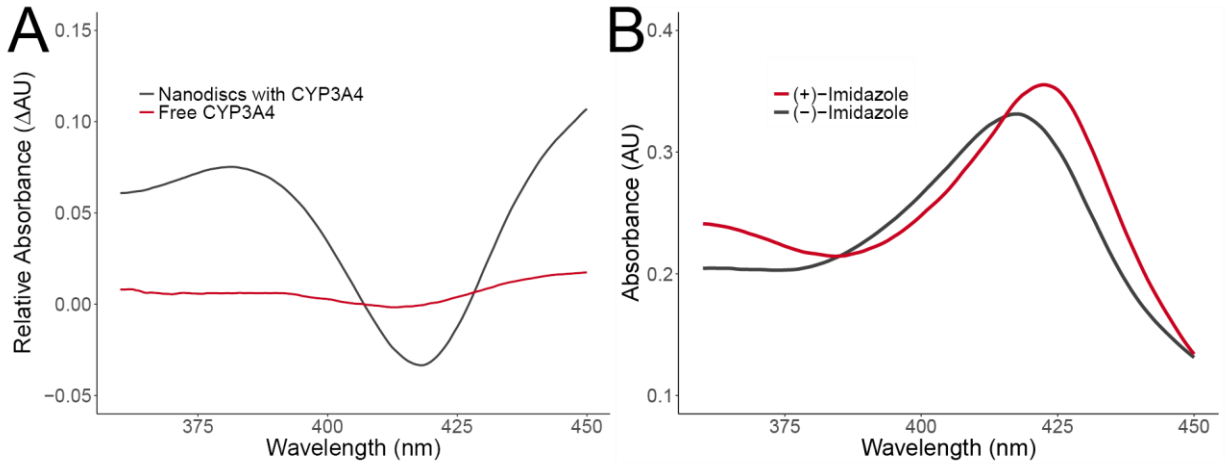

Figure 3.13. **Spin Shift Assays for Nanodiscs Filled with CYP3A4**. (**A**) UV/Vis absorption difference spectrum demonstrates the low to high spin shift for CYP3A4 in Nanodiscs (black) and free CYP3A4 (red) induced by the binding of bromocriptine (BCT), a type I CYP3A4 binder. Binding of BCT results in a decrease in the absorbance maximum of 417 nm and an increase at 390 nm. (**B**) Imidazole, a type II CYP3A4 binder, induces a shift in the absorbance maximum for CYP3A4 from 417 nm to 422 nm.

It is clearly essential that membrane proteins retain their function upon Nanodisc incorporation, and CYP3A4 provides an opportunity to spectroscopically verify substrate binding and protein activity.[11] Specifically, binding induced changes to the spin state of the 3d electrons of the Fe^{3+} in the heme cofactor cause the optical absorption to shift. Type I binders induce a change in the coordination of Fe^{3+} from six- to five-coordinate with a corresponding decrease in the Soret absorption band (417 nm) and increase in absorbance at 390 nm.[53] To demonstrate type I binding with CYP3A4-containing Nanodiscs assembled with the platform,

bromocriptine, a type I binder of CYP3A4, was titrated into the Nanodisc solution resulting in a reduction in the absorbance at 417 nm and an increase at 390 nm (shown as a difference spectra in **Figure 3.13a**). Minimal low to high spin shift is observed for CYP3A4 not incorporated into Nanodiscs, which is only detergent-stabilized. Type II binders of CYP3A4 have an unobstructed nitrogen atom that coordinates with Fe^{3+} resulting in a six-coordinate geometry at the activation site and a shift in maximal absorbance from 417 nm to 422 nm. Imidazole, a type II binder of CYP3A4, is a component of the elution buffer and so the as-eluted Nanodiscs show an absorbance maximum at 422 nm; however, after removal of imidazole via buffer exchange, the absorbance shifts to 417 nm **(Figure 13b).** Taken together, these substrate binding spectroscopic shifts demonstrate the viability of proteins incorporated into Nanodiscs assembled with the microfluidic platform.

In conclusion, Nanodiscs have emerged as a powerful construct that are enabling for numerous biochemical and biophysical studies of model membrane environments; however, the determination of optimal assembly and membrane protein incorporation conditions can require time- and material-consuming iterations. We have developed a microfluidic Nanodisc assembly platform that is capable of rapidly assembling Nanodiscs with generality for different lipid and detergent compositions. We also demonstrated the successful incorporation of a membrane protein and show that its activity towards substrate binding was preserved through microfluidic preparation. This platform will serve as a powerful tool for the facile assembly of Nanodiscs and screening for incorporation conditions while minimizing reagent consumption and time. Furthermore, continued miniaturization and automation of the technology will further increase the accessibility of the Nanodisc platform across the broad biochemical research community.

References:

1. Yildirim, M. A. et al. Drug-target network. *Nat. Biotechnol.* **25**, *1119–1126* (2007).

2. Engelman, D. M. Membranes are more mosaic than fluid. *Nature*. **438**, *578–580* (2005).

3. Silvius, J. R. Solubilization and Functional Reconstitution of Biomembrane Components. *Annu. Rev. Biophys. Biomol. Struct.* **21**, *323–348* (1992).

4. Seddon, A. M.; Curnow, P; Booth, P. J. Membrane Proteins, lipids and detergents: not just a soap opera. *Biochim. Biophys. Acta*, **1666**, *105–117* (2004).

5. Cross, T.A. *et al*. Influence of solubilizing environments on membrane protein structures. *Trends Biochem. Sci.* **36**, *117–125* (2011).

6. Bernaudat, F. *et al.* Heterologous expression of membrane proteins: choosing het appropriate host. *PLoS One*. **6**, e29191, (2011).

7. A. Goehring, A. et al. Screening and large-scale expression of membrane proteins in mammalian cells for structural studies. *Nat. Protoc.* **9**, *2574–2585* (2014).

8. Garavito, R. M. and Ferguson-Miller, S. Detergents as Tools in Membrane Biochemistry. *J. Biol. Chem.* **276**, *32403–32406* (2001).

9. Akbarzadeh, A. *et al*. Liposome: classification, preparation, and applications. *Nanoscale Res. Lett.* **8**, *102-111* (2013).

10. Proverbio, D. Membrane Proteins Production for Structural Analysis. *Mus-Veteau, Springer New York, New York, NY*, **1**, *45–70 (2011).*

11. Denisov, I. G. and Sligar, S. G. Cytochromes P450 in Nanodiscs. *Biochim. Biophys. Acta*. **1814**, *223–229* (2011).

12. Denisov, I. G. and Sligar, S. G. Nanodiscs in Membrane Biochemistry and Biophysics. *Chem. Rev.* **117**, *4669–4713* (2017).

13. Morgan, C.R. *et al*. Confirmational Transitions in the Membrane Scaffold Protein of Phospholipid Bilayer Nanodiscs. *Mol. Cell. Proteomics.* **10**, *M111.010876* (2011).

14. Ravula, T. *et al*. pH Tunable and Divalent Metal Ion Tolerant Polymer Lipid Nanodiscs. *Langmuir*. **33**, *10655-10662* (2017).

15. Jamshad, M. *et al.* Structural analysis of a nanoparticle containing a lipid bilayer used for detergent-free extraction of membrane proteins. *Nano Res.* **8**, *774–789* (2015).

16. Denisov, I. G.; Grinkova, Y. V.; Lazarides, A. A.; Sligar, S. G. Directed Self-Assembly of Monodisperse Phospholipid Bilayer Nanodiscs with Controlled Size. *J. Am. Chem. Soc.* **126**, *3477–3487* (2004).

17. Bayburt, T. H.; Grinkova, Y. V.; Sligar, S. G. Self-Assembly of Discoidal Phospholipid Bilayer Nanoparticles with Membrane Scaffold Proteins. *Nano Lett.* **2**, *853–856* (2002).

18. Bayburt, T. H. and Sligar, S. G. Membrane Protein Assembly into Nanodiscs. *FEBS Lett.* **584**, *1721–1727* (2010).

19. Mineev, K.S. *et al*. NMR Dynamics of Transmembrane and Intracellular Domains of p75NTR in Lipid-Protein Nanodiscs. *Biophys. J.* **109**, *772–782* (2015).

20. Gregersen, J. L.; Fedosova, N. U.; Nissen, P; Boesen, T. P-Type ATPases. *Springer New York, 403–409* (2016).

21. Duan, H.; Civjan, N. R.; Sligar; S. G.; Schuler, M. A.. Co-incubation of heterologously expressed *Arabidopsis* cytochrome P450 and P450 reductase into soluble nanoscale lipid bilayers. *Arch. Biochem. Biophys.* **424**, *141–153* (2004).

22. Denisov, I. G. and Sligar, S. G. Nanodiscs for structural and functional studies of membrane proteins. *Nat. Struct. Mol. Biol.* **23**, *481–486* (2016).

23. Shi, L. *et al*. Preparation and characterization of SNARE-containing nanodiscs and direct study of cargo release through fusion pores. *Nat. Protoc.* **8**, *935–948* (2013).

24. Ritchie, T.K. *et al*. Reconstitution of membrane proteins in phospholipid bilayer nanodiscs. *Methods Enzymol.* **464**, *211–231* (2009).

25. Grisshammer, R. Understanding recombinant expression of membrane proteins. *Curr. Opin. Biotechnol.* **17**, *337–340* (2006).

26. Duong-Ly, K. C. and Gabelli, S. B. Laboratory Methods in Enzymology: Protein Part C, *Elsevier*. **541**, *209–229* (2014).

27. Hansen, C. and Quake, S. R. Microfluidics in structural biology: smaller, faster…better. *Curr. Opin. Struct. Biol.* **13**, *538–544* (2003).

28. Whitesides, G. M. The origins and the future of microfluidics. *Nature*. **442**, *368–373* (2006).

29. Duncombe, T. A.; Tentori; A. M.; Herr, A. E. Microfluidics: Reframing biological enquiry. *Nat. Rev. Mol. Cell Biol.* **16**, *554–567* (2015).

30. Funakoshi, K.; Suzuki, H.; Takeuchi, S. Lipid Bilayer Formation by Contacting Monolayers in a Microfluidic Device for Membrane Protein Analysis. *Anal. Chem.* **78**, *8169–8174* (2006).

31. He, M and Herr, A. E. Automated microfluidic protein immunoblotting. *Nat. Protoc.* **5**, *1844–1856* (2010).

32. Hu, R. *et al.* Rapid, highly efficient extraction and purification of membrane proteins using

a microfluidic continuous-flow based aqueous two-phase system. *J. Chromatogr. A.* **1218**, *171–177* (2011).

33. Hughes, A. J. and Herr, A. E. Microfluidic Western blotting. *Proc. Natl. Acad. Sci. U. S. A.* **109**, *21450–21455* (2012).

34. Millet, L. J. *et al.* Modular microfluidics for point-of-care protein purifications. *Lab Chip.* **15**, *1799–1811* (2015).

35. Gillam, E.M. *et al.* Expression of Modified Human Cytochrome P450 3A4 in Escherichia coli and Purification and Reconstitution of the Enzyme. *Arch. Biochem. Biophys.* **305**, *123–131* (1993).

36. Hosea, N. A.; Miller, G. P.; Guengerich, F. P. Elucidation of Distinct Ligand Binding Sites for Cytochrome P450 3A4. *Biochemistry*. **39**, *5929–5939* (2000).

37. Domanski, T. L. *et al*. Phenylalanine and tryptophan scanning mutagenesis of CYP3A4 substrate recognition site residues and effect on substrate oxidation and cooperativity. *Biochemistry*. **40**, 10150–10160 (2001).

38. Denisov, I. G.; Baas, B. J.; Grinkova Y. V.; Sligar, S. G. Cooperativity in Cytochrome P450 3A4: Linkages in Substrate Binding, Spin State, Uncoupling, and Product Formation. *J. Biol. Chem.* **282**, *7066–7076* (2007).

39. Levario, T. J. *et al*. Microfluidic trap array for massively parallel imaging of Drosophila embryos. *Nat. Protoc.* **8**, *721–736* (2013).

40. Antharavally, B. S. *et al*. Efficient removal of detergents from proteins and peptides in a spin column format, *Anal. Biochem.* **416**, *39–44* (2011).

41. Urbani, A and Warne, T. A colorimetric determination for glycosidic and bile salt-based detergents: applications in membrane protein research. *Anal. Biochem.* **336**, *117–124* (2005).

42. Schindelin, J. *et al.* Fiji: an open-source platform for biological-image analysis. *Nat. Methods*. **9**, *676–682* (2012).

43. Morrissey, J. H.; Tajkhorshid, E.; Sligar, S. G.; Rienstra, C.M. Tissue Factor/Factor VIIa Complex: Role of the Membrane Surface. *Thromb. Res.* **129 Suppl 2**, *S8–10* (2012).

44. Sloan, C. D. K.; Marty, M. T.; Sligar, S. G.; Bailey, R. C. Interfacing lipid bilayer nanodiscs and silicon photonic sensor arrays for multiplexed protein-lipid and protein-membrane protein interaction screening. *Anal. Chem.* **85**, *2970–2976* (2013).

45. Gajsiewicz, J. M. and Morrissey, J. H. Seminars in thrombosis and hemostasis, *Thieme Medical Publishers*, **41**, *682–690* (2015).

46. Danielson, P. B. The cytochrome P450 superfamily: biochemistry, evolution and drug

metabolism in humans. *Curr. Drug Metab.* **3**, *561–597* (2002).

47. Guengerich, F. P. Cytochrome P-450 3A4: Regulation and Role in Drug Metabolism. *Annual Review of Pharmacology and Toxicology*. **39**, *1–17* (1999).

48. Baas, B. J.; Denisov, I. G.; Sligar, S. G. Homotropic cooperativity of monomeric cytochrome P450 3A4 in a nanoscale native bilayer environment. *Arch. Biochem. Biophys.* **430**, *218–228* (2004).

49. Nath, A; Grinkova, Y. V.; Sligar, S. G.; Atkins, W. M. Ligand Binding to Cytochrome P450 3A4 in Phospholipid Bilayer Nanodiscs. *J. Biol. Chem.* **282**, *28309–28320* (2007).

50. Kijac, A. Z.; Li, Y.; Sligar, S. G; Rienstra, C.M. Magic-Angle Spinning Solid-State NMR Spectroscopy of Nanodisc-Embedded Human CYP3A4. *Biochemistry*. **46**, *13696–13703* (2007).

51. Das, A et al. Screening of Type I and II Drug Binding to Human Cytochrome P450-3A44 in Nanodiscs by Localized Surface Plasmon Resonance Spectroscopy. *Anal. Chem.* **81**, *3754–3759* (2009).

52. Baylon, J. L.; Lenov, I. L.; Sligar, S. G.; Tajkhorshid, E. Characterizing the Membrane-Bound State of Cytochrome P450 3A4: Structure, Depth of Insertion, and Orientation. *J. Am. Chem. Soc.***135**, *8542–8551* (2013).

53. Segall, M.D. An ab Initio Study of Biological Systems. *Cambridge*, (1997).

Chapter 4: Microfluidic Platform for Library Nanodisc Assembly from Whole Cell Lysate to Measure Activity of the Epidermal Growth Factor Receptor

I would like to acknowledge the assistance of Professor Mukesh Nyati of the Radiation Oncology Department at the University of Michigan for providing the Ba/F3 cell lines used in this chapter, as well as for multiple conversations and sharing of EGFR knowledge. Along with Prof. Nyati, I would like to thank his lab members, Ranjit Mehta and Sanjima Pal, for directly providing the Ba/F3 cells. Initial cells utilized in this chapter (GBM PDX cells) were provided by the Mayo Clinic, specifically Brett Carlson and Mark Schroeder. Finally, I would like to thank the undergraduate students that worked with me on this chapter, Jenny Choi and Briana Bowen.

Introduction

Oncogenic tyrosine kinases have emerged as critical targets for therapeutics,[1] and inhibition of their enzymatic activity using small molecules has become a mainstay of anticancer therapy. Receptor tyrosine kinases (RTKs) are an important class of kinases that are integral within the cellular membrane. Epidermal growth factor receptor (EGFR) is one such RTK that has been implicated in a wide range of cancers including glioblastoma (GBM) and non-small cell lung cancer (NSCLC).[2,3] About 15 percent of NSCLC (314,000 new patients/year) contain mutations within the EGFR kinase domain. There are multiple EGFR mutations that have been implicated in NSCLC, which has made EGFR a high-profile target for treatment through the development of Tyrosine Kinase Inhibitors (TKI).[4] First- and second-generation EGFR TKIs

have been developed and approved for treatment in NSCLC patients with the two most common EGFR mutations- L858R mutation or exon 19 deletion (Δex19).[5] However, within 9-15 months of treatment, almost all patients acquire resistance, often in the form of a secondary mutation in EGFR (T790M).[6,7] Patients initially respond well to osimertinib, which is a 3rd generation TKI; but again, they eventually acquire resistance to this treatment. A substantial fraction of these patients acquire a tertiary mutation in EGFR at the osimertinib binding site (C797S), which inhibits drug binding[8] and currently has no approved TKI treatment.[9,10]

Membrane proteins, including RTKs, are notoriously difficult to assay in vitro due to their inherent instability outside of the plasma membrane. Nanodiscs are soluble, protein stabilized discoidal lipid bilayers that offer many advantages for studying membrane protein structure and activity.[11] Nanodiscs provide access to both sides of the bilayer, and precise control of bilayer composition, stoichiometry, and size.[12–14] For these reasons, Nanodiscs have emerged as a preferred lipid bilayer mimetic system for many applications in membrane protein biology.[11,15]

In conventional formation, Nanodiscs are created by slowly removing the detergent solubilizing a solution of phospholipids, membrane proteins, and an amphipathic membrane scaffold protein (MSP). Depending on the lipid content and membrane protein of interest, this detergent removal process takes between 2 hours and 18 hours.[16] During this process, Nanodiscs self-assemble with MSP wrapping around a discoidal phospholipid bilayer with an integrated membrane protein.[12] A wide variety of membrane proteins have been loaded into Nanodiscs, including libraries of membrane proteins incorporated from crude cell membrane preparations.[17–20] Importantly, the Nanodisc construct has previously been demonstrated to impart tremendous structural and functional stability to EGFR.[21]

While effective, traditional "bulk" methods of Nanodisc assembly are laborious, time-consuming, and require large amounts of input membrane protein. To circumvent these drawbacks, we recently developed an integrated microfluidic platform that supports rapid Nanodisc assembly at greatly reduced membrane protein consumption.[22] Illustrated in **Figure 4.1**, this device, which comfortably fits on a standard 25 x 75 mm microscope slide, features a fluidic bed packed with detergent removal resin. Taking advantage of efficient on-chip mixing and a high surface-to-volume ratio, the device rapidly removes surfactant to facilitate Nanodisc self-assembly in ~5 minutes, as opposed to the standard "bulk" overnight incubation. Additionally, the basic device design can be used for downstream purification processes. We were able to demonstrate that fully competent membrane proteins (Cytochrome P450 CYP3A4) are efficiently incorporated into Nanodisc constructs with minimal reagent consumption using this simple microfluidic module.

Most previous Nanodisc research has been performed using a single membrane protein of interest which first must be isolated and purified at sufficiently high concentration, usually using a recombinant protein expression system.[17,23] To avoid this, soluble membrane protein libraries instead use isolated cell membranes or whole cell lysate to incorporate membrane proteins directly from the native cell membrane into Nanodiscs.[24–26] Using whole cell lysate allows the membrane proteins to remain in a more native environment throughout the process, preventing loss of structure and function. Native lipids may still be associated with the membrane proteins as the Nanodiscs are formed, which is important as certain membrane proteins require specific lipid compositions for activity.[27] The membrane proteins incorporate at full length and have all post-translational modifications, both of which can be difficult to obtain in recombinant systems.[28]

Library Nanodiscs can be used both for studies of all membrane proteins in a cell or for the successful incorporation and purification of a specific membrane protein of interest that is difficult to obtain using recombinant expression. A specific membrane protein might be of interest if it is suspected to be implicated in a disease or if the protein is a common pharmaceutical target. Incorporating the membrane protein into Nanodiscs can allow for further studies that might be impossible in the cell itself or in the cell lysate.

The ability to determine the activity of the membrane proteins in a cancer patient's cells and how these proteins will respond to specific drugs provides practical information for patient treatment. The potential to take patient cancer cells, form Library Nanodiscs using the microfluidic device and perform activity assays on these Nanodiscs to test the viability of various inhibitors could lead to interesting patient treatment decisions. Using a Ba/F3 IL-3-dependent mouse leukemia cell line that does not natively express EGFR, specific EGFR mutations have been engineered into these cells.[29]

We will use these EGFR mutants expressed in Ba/F3 cells as a well-controlled test system of the ability to form Library Nanodiscs incorporating active EGFR, as the cells should be very similar other than the EGFR protein expressed. After ensuring successful EGFR incorporation in the Nanodiscs formed with our microfluidic device, we will determine if drug-screening assays can be performed on these Nanodiscs to determine the mutant-specific response to each inhibitor. The long-term goals would be to being with cells from a patient, in order to perform drug screening before patient treatment.

Experimental Methods

Materials: The membrane scaffold protein MSP1E3D1, Amberlite XAD-2 hydrophobic beads and other chemicals were purchased from Sigma Aldrich (St. Louis, MO, USA) unless otherwise

noted. Phospholipids 1,2-dimyristoyl-snglycero-3-phosphocholine (DMPC) and 1-palmitoyl-2-oleoyl-snglycero-3-phosphocholine (POPC) were purchased from Avanti Polar Lipids (Alabaster, AL, USA). Pierce Detergent Removal Resin and HisPur Ni-NTA resin were purchased from ThermoFisher Scientific (Waltham, MA, USA).

Microfluidic device fabrication: Microfluidic devices will be fabricated as previously reported using standard soft lithography and PDMS (Monomentive)[22]. After fabrication, the detergent removal bed was filled with Pierce Detergent Removal Resin beads, which have a high surfactant removal capacity that we previously verified and the packed bead bed is washed with methanol and deionized water to prime the beads and remove any potential contaminants from the resin.

Cell culture and lysis: The initial experiments were performed with glioblastoma patient-derived xenograft cells (GBM-PDX) provided by Brett Carlson and Mark Schroeder from the Department of Radiation Oncology at the Mayo Clinic (Rochester, Minnesota).[30] These cells were cultured in Dulbecco's Modification of Eagel's media (DMEM) with 10% by volume Fetal Bovine Serum (FBS) and 1% by volume Penicillin/Streptomycin/Glutamine. The cells were lysed by washing with cold Phosphate-Buffered Saline (PBS) followed by the addition of Cell Lysis Buffer with 1 mM PMSF (Cell Signaling Technologies). The cells were lysed on ice with mixing for five minutes, followed by vortexing and centrifuged at 13k rpm for 10 minutes at 4 °C to remove debris.

Ba/F3 cells were obtained from the Nyati lab: WT Ba/F3 cells do not express EGFR and therefore serve as an important negative control. Other versions of the Ba/F3 line grown in the Nyati lab express wild-type EGFR, as well as clinically-relevant mutations, including L858R, Δex19, T790M, C797S, and mutation combinations (i.e. the triple mutant of L858R, T790M, and C797S—abbreviated LTC) that are clinically-observed combinations in NSCLC patients. WT Ba/F3 is IL-3

dependent so cell survival and proliferation requires addition of IL-3 (From mouse; Sigma) into the cell media (RPMI 1640 with 10% by volume FBS and 1% by volume Penicillin/Streptomycin/Glutamine; all from Fisher). Ba/F3 L858R and LTC are grown in the same cell media but without IL-3. All Ba/F3 cells were lysed by centrifuging the cells in the media at 300k xg for 5 minutes (at 4 °C), followed by washing the cell pellet in DPBS (Fisher) and the addition of approximately 1 mL per 10^8 cells of cell lysis buffer (Cell Lysis Buffer as described for GBM cells or NP40 cell lysis buffer (Fisher) supplemented with 1 mM PMSF (Cell Signaling), protease inhibitor cocktail (Sigma) and phosphatase inhibitor (Fisher). The cells are lysed on ice for 30 minutes with vortexing every 10 minutes, centrifuged at 13k rpm for 10 minutes (at 4 °C) and a BCA assay (Fisher) is performed for total protein content before storage at -80 °C. As only the total protein concentration (in μg/mL) is determined, we use 100 kDa as an average protein molecular weight to convert to μM for the Nanodisc preparation calculations. **(Table 4.1)**

Nanodisc assembly and purification: Following the general microfluidic Nanodisc assembly procedure previously described[22], Nanodisc assembly procedure involves combining a commercially-available MSP (MSP1E3D1; from Sigma) with lipids at a 1:110 molar ratio (MSP:lipid) with cell lysate added at a 1:5 molar ratio (lysate total protein content:MSP). **(Table 4.1)** 1-palmitoyl-2-oleoyl-sn-glycero-3-phosphocholine (POPC), the most abundant lipid in the extracellular membrane was the lipid used. This mixture of components was dissolved in Standard Disc Buffer (20 mM Tris, 100 mM NaCl, 0.5 mM EDTA, 0.01% NaN3) and solubilized by the addition of 20 mM sodium cholate. This solution was incubated for ten minutes on ice then flowed through the microfluidic device, also on ice, at a constant flow rate.

The eluent, containing library Nanodiscs, is collected over a total of five minutes for further analysis to confirm Nanodisc assembly.

After Nanodisc formation, purification can also be performed in microfluidic devices. The MSP1E3D1 used for the Nanodisc formation has a 6-Histadine tag engineered on the N-terminal end so Nickel-nitriloacetic acid (Ni-NTA) resin can be used to purify Nanodiscs. We have demonstrated that purification of Nanodiscs containing CYP3A4 can occur by loading Ni-NTA resin into the microfluidic device.[22] Components not containing the His-tag will be eluted in wash steps while Nanodiscs will remain bound until imidazole-containing buffer is used for collection. The microfluidic purification method can also be used on Library Nanodiscs formed using whole cell lysate. Following purification, SDS-PAGE can be used to confirm the successful Library Nanodisc formation and purification **(Figure 4.3).** As the membrane proteins from the whole cell lysate do not have His-tags, these proteins flow directly through the purification device. The membrane proteins that are collected in the elution fractions will be those incorporated in the Nanodiscs.

Size-exclusion chromatography: Nanodiscs were characterized using size-exclusion chromatography (SEC) after Bulk or microfluidic Nanodisc preparation to confirm Nanodisc formation. Samples were injected onto a Superdex 200 Increase 3.2/300 column (GE Healthcare, Pittsburgh, PA, USA) at a flow rate of 50 μL/min and absorbance was monitored at 280 nm. A mixture of Thyroglobulin, γ-globulin, Ovalbumin, Myoglobin and Vitamin B_{12} (BioRad, Hercules, CA, USA) were used as chromatographic standards. The running buffer used was standard disc buffer (SDB – 20 mM Tris, 100 mM NaCl, 0.5 mM EDTA, 0.01% sodium azide).

Table 4.1: Nanodisc Component Preparation Calculations.

Library Nanodiscs with POPC, MSP1E3D1, BaF3 L858R	
Inputs	
Total Sample Volume (mL)	1.20
[MSP1E3D1] (µM) (from NanoDrop measurement)	153.3743272
Library Stock Concentration (µM)	13.2
Library Stock Concentration (µg/mL)	1323
Desired MSP:Library Ratio	5
Desired POPC:MSP1E3D1 Ratio	110
[POPC] stock (mM) (what's the concentration from vendor?)	33.0
Stock POPC (µL) (how much did you add to test tube?)	200.0
Desired [POPC] (mM) (within the test tube)	50.0
Desired final [cholate] (mM)	20
Desired [Library] (µM)	3.0
Filled Nandodisc Prep	**Volume (µL)**
0: 100 mM cholate into Lipid Film	132.0
1: Library Stock	272.1
1: MSP1E3D1 stock	117.4
1: 50 mM POPC Stock	39.6
1: SDB(-) Buffer	611.3
1: 100 mM cholate Stock	159.6
Fraction Collection	
Instructions	**Flow Rate (µL/min)**
Fraction Volume (µL)	60
Fraction Time (s)	120
Discarded Volume (µL)	45
Total # Fractions	2

SDS-PAGE and Western Blotting: To determine success of Nanodisc formation and purification sodium dodecyl sulfate polyacrylamide gel electrophoreses (SDS-PAGE) was used. Two 4-12% gradient gels were run identically under reducing conditions and one was stained with Coomassie Blue following standard recommended protocols (Bio-Rad). To verify electrotransfer and molecular weights, prestained molecular weight markers (Bio-Rad) and biotinylated protein ladders (Cell Signaling) were used. To determine specific protein identities through Western Blot, the second gel was transferred to a Nitrocellulose Membrane (Cell Signaling, Danvers, MA, USA) following manufacturer suggested protocols. After transfer, the membrane was washed with Tris-Buffered Saline with 20% Tween (Cell Signaling), blocked with 5% nonfat dry milk (Cell Signaling) in TBST, washed in TBST and incubated overnight with the primary antibody of interest in 5% bovine serum albumin in TBST. The following day the membrane was washed in TBST and incubated for one hour in the matching secondary antibody(s) in the 5% nonfat dry milk in TBST solution. The membrane was finally stained with Signal Fire Reagents (Cell Signaling) and imaged (BioRad Chemidoc).

EGFR Activity Assay: The sample of lysate or library Nanodisc is incubated with either 200 nM of Osimertinib (obtained from Nyati lab) or DMSO for 10 minutes followed by the addition of a 200 ng/mL EGFR-specific substrate (Anaspec), 200 nM ATP and 2 ng/μL coupling phosphatase supplied by the Universal Kinase Activity Kit (R&D Systems). Active EGFR in the lysate or Nanodiscs will phosphorylate the EGFR specific substrate by converting ATP to ADP and the coupling phosphatase will convert all ADP formed into AMP and inorganic phosphate. The inorganic phosphate can be measured using Malachite Green (Universal Kinase Activity Kit) and the absorbance intensity at 620 nm after 20 minutes is directly related to the activity of the EGFR in the sample. The inhibition for each sample is compared by subtracting the absorbance of the

sample with DMSO from the absorbance of the sample with Osimertinib and that difference is divided by the absorbance of the sample with the DMSO control. The assay is performed in a phosphatase buffer: 25 mM HEPES, 150 mM NaCl, 10 mM $MgCl_2$ and 10 mM $CaCl_2$. The total volume of the phosphate buffer in the well is at least 1x the sample volume, which is either lysis buffer or SDB.

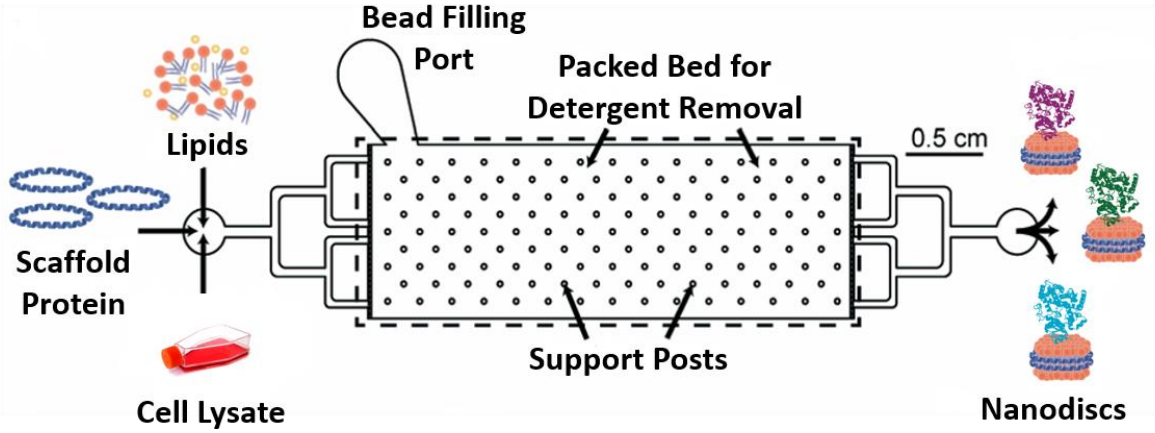

Figure 4.1: Microfluidic device designed for rapid and efficient formation of Nanodiscs with integrated membrane proteins. The fluidic bed packed with detergent removal resin enables rapid Nanodisc assembly in 5 minutes, as compared to overnight in bulk preparation, and requires less input material.

Results and Discussion:

We have demonstrated the ability to create robust Nanodisc libraries from the whole cell lysate. **Figure 4.2A** shows representative size-exclusion chromatography (SEC) traces for library Nanodiscs prepared using the GBM-PDX lysate. Importantly, the peak centered at ~0.79 mL of elution volume for both microfluidically- and bulk-prepared Nanodiscs confirms high quality constructs of appropriate size by comparison with protein standards. Furthermore, with equal SEC injection volumes for both separations, the higher absorbance signal for the

microfluidically-prepared sample supports the fact that there is less sample loss using the microfluidic device and overall more efficient Nanodisc assembly. This attribute of our microfluidic device is important as lower sample inputs can be utilized for Nanodisc formation and activity profiling—an essential quality for future clinical translation of this technology to sample-limited specimens.

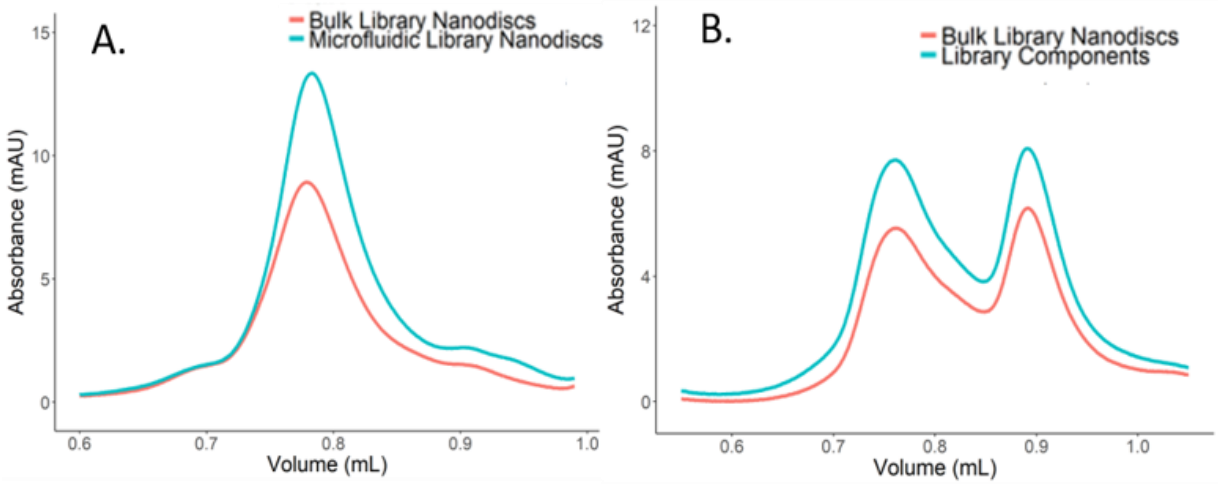

Figure 4.2: Formation of Library Nanodiscs using microfluidic device compared to bulk preparations as detected by SEC. A). Both microfluidic and conventional bulk Nanodiscs are well-formed. B). Bulk Nanodiscs using microfluidic time scales (5 minutes) show no Nanodisc formation as compared to components before detergent removal.

To confirm that the microfluidic device is essential for forming Nanodiscs on this time scale, Bulk Nanodiscs were formed from the same components mixture as that used in **Figure 2A** but were only mixed with the detergent removal beads for five minutes instead of the standard overnight bulk preparation. The SEC traces determined that this was not a sufficient amount of time for Bulk Nanodisc formation, as the microfluidic-scale Bulk Nanodiscs form two aggregate peaks instead of the single Nanodisc peak **(Figure 4.2B).** The components mixture

with no detergent removal has the same two aggregate peaks, indicating that Nanodiscs cannot be formed in Bulk on a microfluidic time scale, the microfluidic device is necessary.

SDS-PAGE followed by Western blotting was utilized to confirm the incorporation of EGFR into Ni-NTA purified Library Nanodiscs **(Figure 4.3).** The gel **(Figure 4.3A)** demonstrates that a number of unidentified proteins from the lysate, especially those of lower molecular weight, end up in the purified Nanodiscs, though at lower intensities than the MSP1E3D1 band (~32 kDa), as expected. The inclusion of EGFR was verified from WT Ba/F3 cells expressing either the L858R or LTC mutants of EGFR and WT Ba/F3 cells (EGFR-). **Figure 3B** shows a Western blot confirming EGFR in the raw cell lysate and incorporated into purified Nanodiscs for both the L858R and LTC cell lines (denatured SDS-PAGE gel; blot with anti-EGFR mAb clone D38B1 from Cell Signaling), and a clear absence of EGFR in the WT specimen. The confirmation of EGFR bands in the Nanodisc lanes suggests successful incorporation into Nanodiscs as otherwise the EGFR would be washed away during the Ni-NTA purification process.

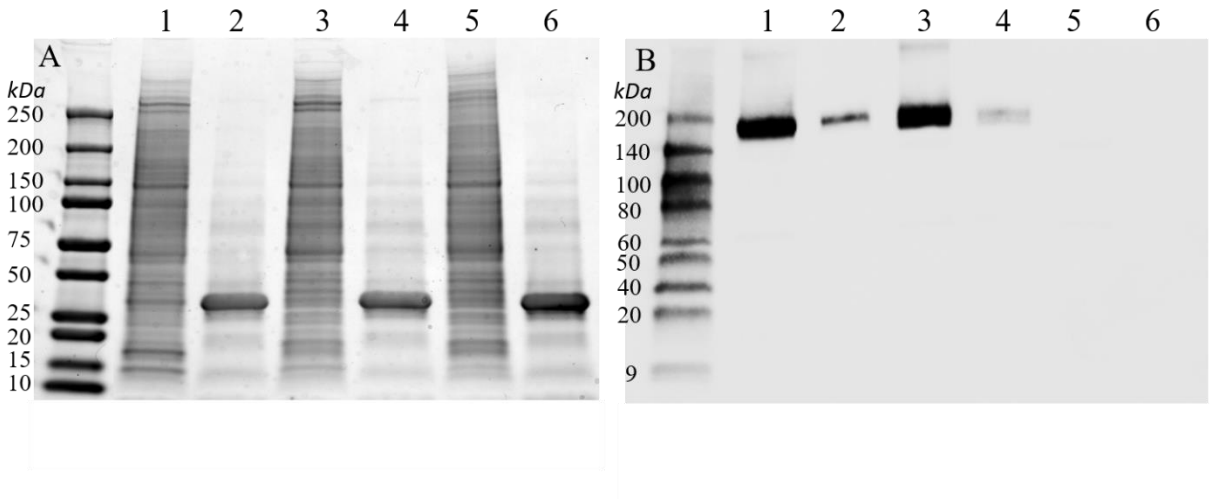

Figure 4.3: SDS-PAGE and Western Blot of Purified Nanodiscs to confirm EGFR incorporation. *Lane 1:* L858R Lysate; *Lane 2*: L858R Nanodiscs after purification; *Lane 3*: L858R/T790M/C797S (LTC) lysate; *Lane 4*: LTC Nanodiscs after purification; *Lane 5*: WT lysate; *Lane 6*: WT Nanodiscs after purification. A) SDS-PAGE to visualize all proteins in the samples. MSP1E3D1 is the band present ~32 kDa in all the Nanodisc lanes (even numbered lanes). B) Western Blot for EGFR shows that EGFR is successfully incorporated into the L858R and LTC Nanodiscs. The WT lysate does not contain EGFR, as expected. Since the membrane protein bands are present after Ni-NTA purification, the membrane proteins must be incorporating into Nanodiscs, as any free membrane protein will be eluted during the purification process.

EGFR activities in Nanodiscs were assessed *in vitro* using commercially available colorimetric assays that utilize enzyme-specific substrates to obtain specificity using the Universal Kinase Activity kit (R&D Systems) in conjunction with an EGFR-specific peptide substrate (ADEYLIPQQ; Anaspec). **Figure 4.4** is a representation of the assay, modified from the R&D systems methods. In this assay, a sample of library Nanodiscs (or raw cell lysate) is combined with the peptide substrate (200 ng/mL), a coupling phosphatase (2 ng/μL), and 200 nM ATP, and incubated for 10 minutes. Active EGFR will phosphorylate the peptide EGFR-specific substrate, derived from a known phosphorylation target of EGFR, converting ATP to ADP. The coupling phosphatase then converts the ADP into AMP and inorganic phosphate, with

the inorganic phosphate quantified by absorbance spectrophotometry (λ=620 nm) using a Malachite Green reagent. In order to probe relative EGFR inhibition, activity assays for each of the EGFR mutants (formed from the previously described Ba/F3 and A431 cell lines) were be performed both in the presence and absence of osimertinib, an EGFR inhibitor. By comparing activities with and without inhibitors, the EGFR inhibition can be determined.

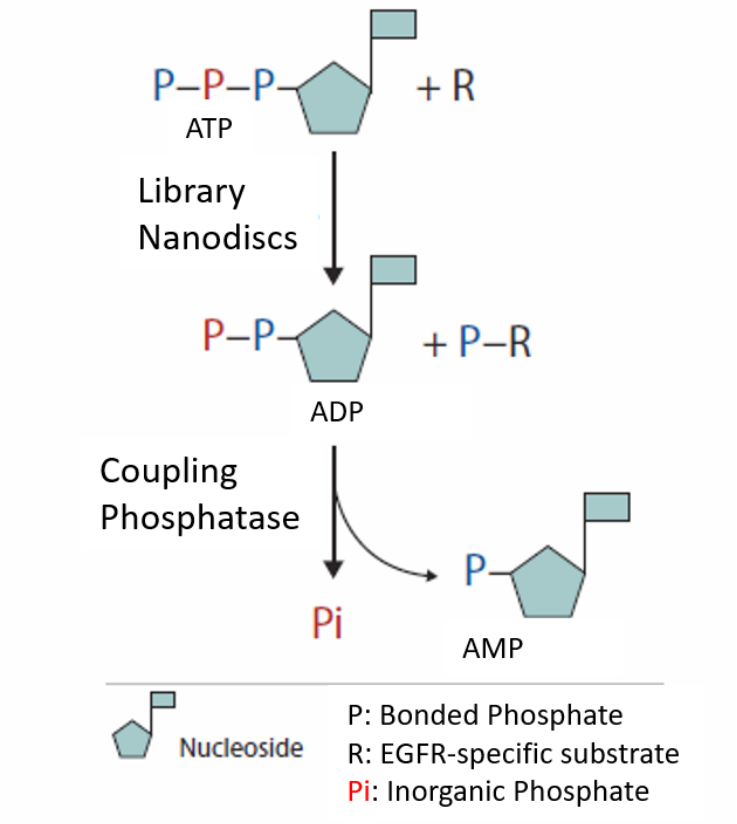

Figure 4.4: The Universal Kinase Activity Assay schematic. ATP, an EGFR specific substrate, and the sample of interest (in this case Library Nanodiscs) are incubated together. If the sample contains active EGFR, the protein will phosphorylate the substrate using the tertiary phosphate of the ATP, leaving ADP. Then, coupling phosphatase is added to convert ADP to AMP and a free phosphate. Malachite Green reagents are added to colorimetrically measure the concentration of free phosphate, which corresponds to the activity of the EGFR in the sample. Modified from the Universal Kinase Assay Directions.

Osimertinib inhibitor was used to assay both purified library Nanodiscs and cell lysate from the L858R, LTC, and WT (no EGFR) Ba/F3 cell lines. Osimertinib is a third-generation

tyrosine kinase inhibitor that covalently binds to EGFR. This inhibitor was developed to treat the mutation T790M which often occurs after 7-13 months of treatment of non-small cell lung cancer by first and second generation non-covalent TKIs such as dacomitinib or erlotinib. However, treatment with osimertinib has led to a tertiary mutation, C797S which no longer responds to osimertinib treatment as this is the amino acid osimertinib binds.[2] This initial inhibition assay used cells containing a L858R mutation that should respond to osimertinib and a L858R/T790M/C797S mutation that should not respond to osimertinib, as well as the WT Ba/F3 cells without EGFR that should have no activity and thus no inhibition. These were initial experiments with the goal of adding additional cell lines expressing various mutations, including the L858R/T790M mutation that should respond to osimertinib but not dacomitinib, once the activity assays were optimized.

The results, shown in **Figure 4.5,** reveal two very important observations. First, all three of the cell lysate samples show small percent activity change inhibition responses compared to Nanodisc-incorporated EGFR, about equal to the inhibition seen in the buffer control sample, indicating the changes measured were more an assay issue than a real inhibition. This is as expected because EGFR is not in its proper confirmation in crude cell lysate and therefore minimally responsive to inhibition. This strongly supports the need for the Nanodisc environment to effectively probe in vitro RTK activity. Second, for the Nanodisc samples, the L858R Nanodiscs show the largest relative inhibition to osimertinib after a ten minute exposure to 200 nM drug (~2.5x greater inhibition than LTC Nanodiscs). This is consistent with the known specificities of these mutations to this treatment (IC_{50} for osimertinib of ~6 nM for L858R and ~1000 nM for LTC).[2] It should be noted that while the inhibition of the L858R Nanodiscs is greater than the inhibition seen in any other samples, a t-test as compared to the

buffer control resulted in a p-value of 0.082, indicating a significant change at an alpha value of 0.1. All other samples did not show significant differences from the control. Importantly, this differential inhibition not only portends well for mutation-based therapeutic identification, but also suggests that this in vitro profiling method can be used to establish dose-response relationships that correlate with whole cell and in vivo-based IC_{50}s.

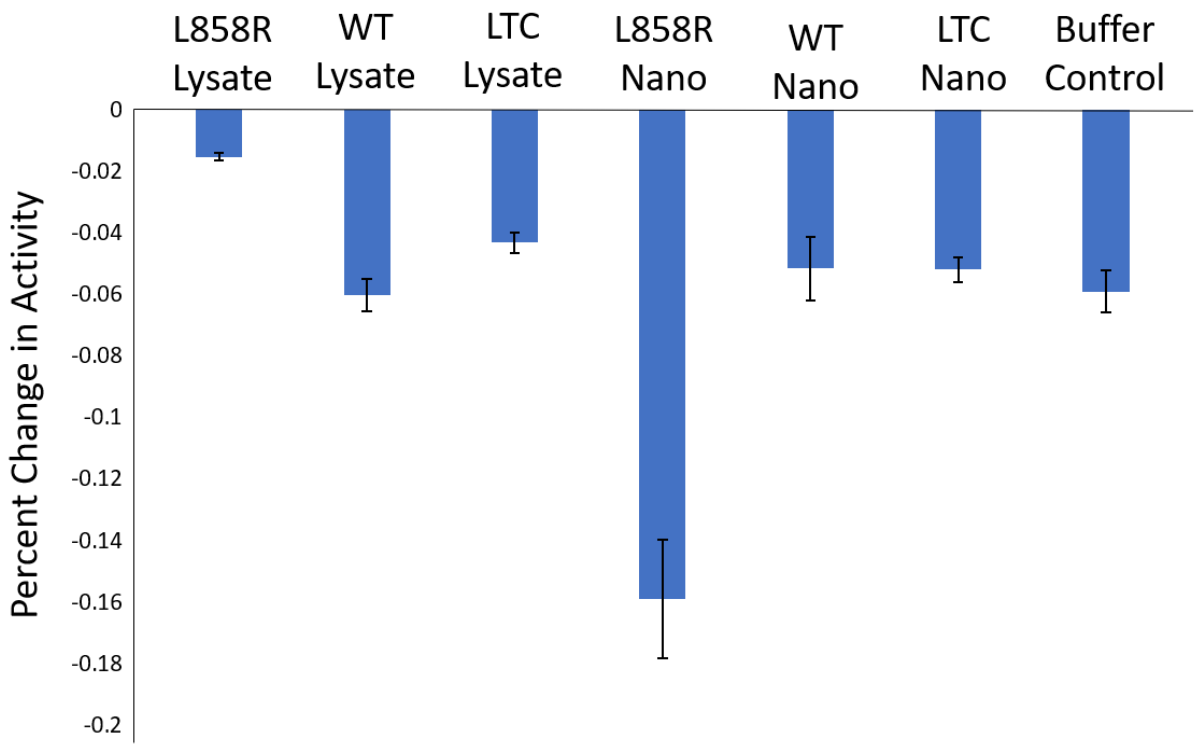

Figure 4.5: EGFR Activity Assay. The samples were each incubated with either 200 nM Osimertinib or DMSO as a control, with three wells for each condition. The average of the sample with inhibitor was subtracted from the average of the sample with DMSO and this number was divided by the average of the sample with DMSO, resulting in the change in activity. This value was calculated for the lysate samples and purified Nanodiscs as well as a SDB buffer control. The assay was repeated three times with three separate Nanodisc preparations and the relative changes in activity were averaged. One-tailed t-tests were performed for all the samples as compared to the buffer control, with resulting p-values of 0.189 for L858R Lysate, 0.494 for WT Lysate, 0.402 for LTC Lysate, 0.082 for L858R Nanodiscs, 0.423 for WT Nanodiscs, and 0.452 for LTC Nanodiscs. There are no samples that have a significant difference from the control at a α-value of 0.05 but the L858R Nanodiscs do have a significant difference from the control at a α-value of 0.1. This suggests that only the L858R Nanodiscs might show significant inhibition after Osimertinib addition.

Conclusion and Future Work

Considerable effort has been dedicated to the discovery of RTK inhibitors (TKIs) with many FDA-approved anti-cancer therapies of this kind. It is well established that RTK inhibitors can have differential efficacy and that underlying RTK mutation status is an important predictor of patient response. Therefore, the ability to rapidly determine the responsiveness of an individual's tumor to different RTK inhibitors represents an opportunity and currently unmet clinical need in the domain of personalized medicine. Adding to the significance of this work is the generality of the approach to any RTK. We envisage high throughput screening of tumor samples against large panels of potential therapeutic inhibitors. This would include the various generations of TKIs, including dacomitinib and erlotinib which can inhibit the most common initial EGFR mutations (L858R or exon 19 deletion) and osimertinib which can inhibit both the initial EGFR mutations and the secondary T790M mutations. We could also include various inhibitors that are currently being studied to inhibit the tertiary C797S mutation, which does not respond to the mentioned TKI inhibitors, such as monoclonal antibodies that prevent ligand binding to EGFR and inhibitors that would break down the EGFR to prevent further activity.[31]

The overexpression and/or mutational status of RTKs can be assessed through a combination of RNA analysis and massively parallel sequencing. However, these approaches have yet to find widespread adoption in clinical oncology. The rapid assessment of RTK therapeutic inhibition can be more directly determined through functional protein activity measurements. We have developed a microfluidic platform that enables rapid functional activity profiling, thereby providing the potential to quickly reveal the most efficacious TKI therapy at the level of individual patients, as in practice providing the correct therapy is not as simple as simply preforming testing for known EGFR mutations.[32]

In contrast to sequencing, which often reveals inconsequential mutations that are not drivers of disease, functional, activity-based inhibition profiling will quickly provide clinically-actionable information in a format consistent with conventional immunodiagnostics in terms of time and cost.

Though the initial activity assay results suggested that this method could be very successful in determining the impact of EGFR mutation status on the change in activity after inhibitors are added, further assay issues prevented us from publishing the initial data. We were concerned that the actual measured absorbances and error were significantly higher for the lysate samples than the Nanodisc samples **(Figure 4.6).** It seems clear that there is an issue with the lysate samples, most likely because of native ADP or free phosphate in the lysate and the presence of proteins other than EGFR that can convert ATP to ADP. We attempted a number of strategies to remove this background issue.

The first approach was to subtract out background controls, including running the assay without the EGFR specific substrate or ATP added **(Figure 4.7).** The L858R lysate samples overall have a significantly higher absorbance, both with and without EGFR substrate and ATP added **(Figure 4.7A).** This indicates that the majority of the "activity" measured in the lysate is not actually EGFR activity but just background noise. This is not seen in the Nanodiscs to the same extent, as there is a big drop in the absorbance measured when all the components are present versus the Nanodisc samples without the EGFR substrate and/or ATP **(Figure 4.7B).** These Nanodisc controls without ATP are approximately equal in absorbance to buffer controls, indicating minimal activity in Nanodiscs if there is no ATP added. Though these experiments helped confirm that background activity is causing the high lysate absorbances, subtracting these

controls has been problematic as the two large absorbances lead to very high error in the final value.

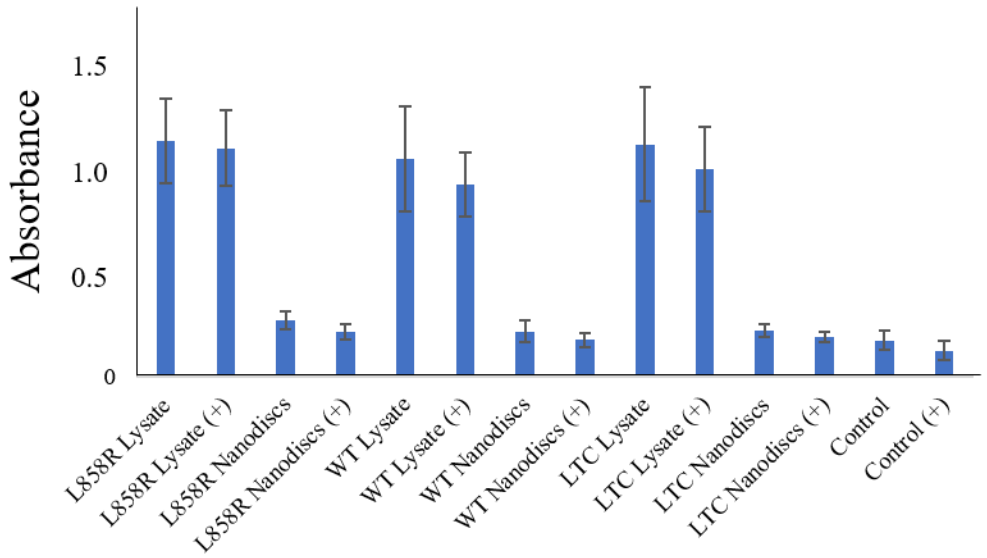

Figure 4.6: Absorbances of the various samples in the Universal Kinase Assay. (+) indicates that 200 nM Osimertinib inhibitor was added to the sample. The samples without the (+) have DMSO added as the control. The absorbances are n=3 replicates of different Nanodisc samples, each with n=3 wells averaged.

Along with this background subtraction, we also tested the impact of each of the buffers used throughout the formation and purification processes to determine if the buffers were adding to the background. We found the background were potentially problematic for buffers containing detergent or imidazole and buffers at a low pH. (data not shown).

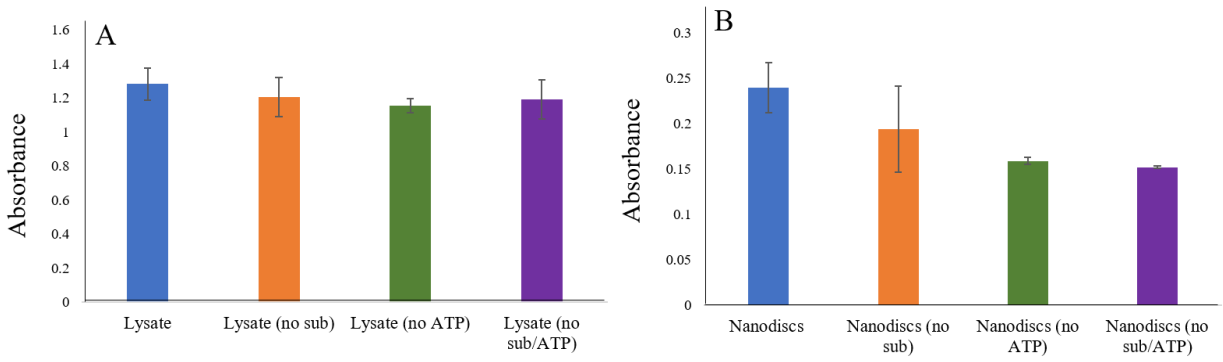

Figure 4.7: Absorbance values for the samples and controls for both Ba/F3 lysate (A) and Library Nanodiscs (B). The samples with the full activity assay are blue, the controls without the EGFR specific substrate are orange, the controls without ATP are green, and the controls without both EGFR substrate and ATP are purple. Note the differences in the absorbance axis for the lysate (0-1.6 absorbance units) and the Nanodiscs (0-0.3 absorbance units).

The second method we have been using to improve the activity assays is a secondary purification step for EGFR. By adding an EGFR-specific purification to the initial Ni-NTA purification for MSP we will end up with just Nanodiscs containing EGFR in our final sample. Not only will this remove most of the background activity issues, it will also make the activity assays more controlled between samples, as currently we only have total protein concentrations, not specific EGFR concentrations. I have tested multiple methods for EGFR purification, all using different types of anti-EGFR antibody conjugated or absorbed to a bead, so that the method would be viable with our current microfluidic device design.

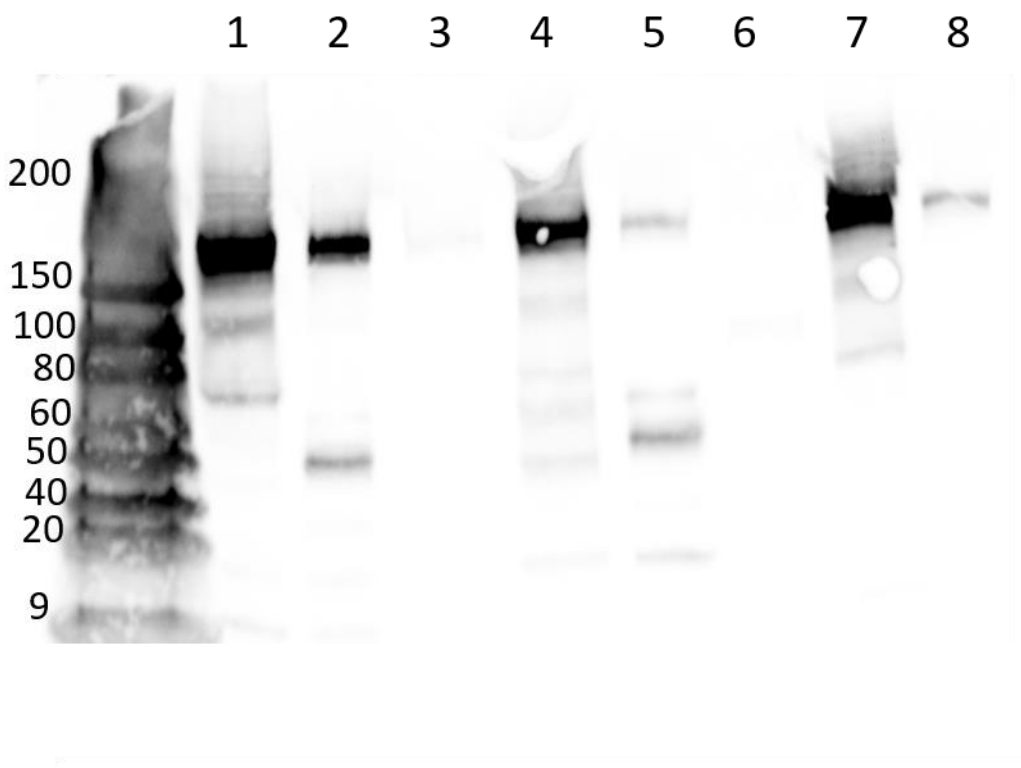

Figure 4.8: Western Blot for EGFR of the EGFR-specific purification of L858R lysate and Nanodiscs using Protein A beads. *Lane 1*: L858R Lysate; *Lane 2*: Pure Lysate Fraction 1; *Lane 3*: Pure Lysate Fraction 2; *Lane 4*: L858R Nanodiscs; *Lane 5*: Pure Nanodiscs Fraction 1; *Lane 6*: Pure Nanodiscs Fraction 2; *Lane 7*: Lysate Wash Step; *Lane 8*: Nanodisc Wash Step.

I found that Pierce Protein A Agarose (ThermoFisher) can be loaded into our basic microfluidic device and then anti-EGFR monoclonal antibodies (Cell Signaling Technology) can be flowed across the device and bind to the Protein A. The samples can then be loaded to the device, washed with PBS to remove any non-specific binding **(Figure 4.8**, Lanes 7-8) and then EGFR can be eluted using a low pH glycine buffer (0.2 M glycine, pH 2.2). These elution steps (**Figure 4.8**, Lanes 2-3 (lysate) and Lanes 5-6 (Nanodiscs)) were able to purify EGFR in lysate or in Nanodiscs, though a significant amount of EGFR is lost in the wash steps. There is also a concern that the need to use the low pH buffer to elute the EGFR might impact the stability of the EGFR, causing issues with the downstream activity assays planned.

To avoid the necessity to elute the EGFR with low pH buffers, I decided to switch the bead used to a Pierce Avidin agarose (ThermoFisher). Usually, Avidin beads are used to strongly bind biotinylated antibodies; however, this binding is so strong that low pH is needed to release the EGFR. Instead, desthiobiotinylated (DTB) antibodies have been used in similar applications,[33] as this allows for the EGFR to be released by flowing 20 mM biotin through the device, which should have less impact on the stability and activity of the EGFR. Significant amounts of EGFR do not bind to the Avidin beads (**Figure 4.9**, Lane 2) or are washed off with the PBS rinses (**Figure 4.9**, Lane 3), even with multiple optimization attempts. Initially, a small amount of EGFR was believed to be purified (**Figure 4.9**, Lane 8) at a low concentration, with the band only detected after a 10 kDa spin column (ThermoFisher) for protein concentration. An equal intensity band at the same molecular weight is also seen when Laemelli buffer (BioRad, with 5% β-mercaptoethanol, **Figure 4.9**, Lane 9) is added. However, further tests determined that these protein bands are at a higher molecular weight than EGFR and is seen in control samples without lysate added to the beads, indicating these bands in **Figure 4.9**, Lanes 8-9 are not EGFR, but a component from the Avidin beads or the antibody.

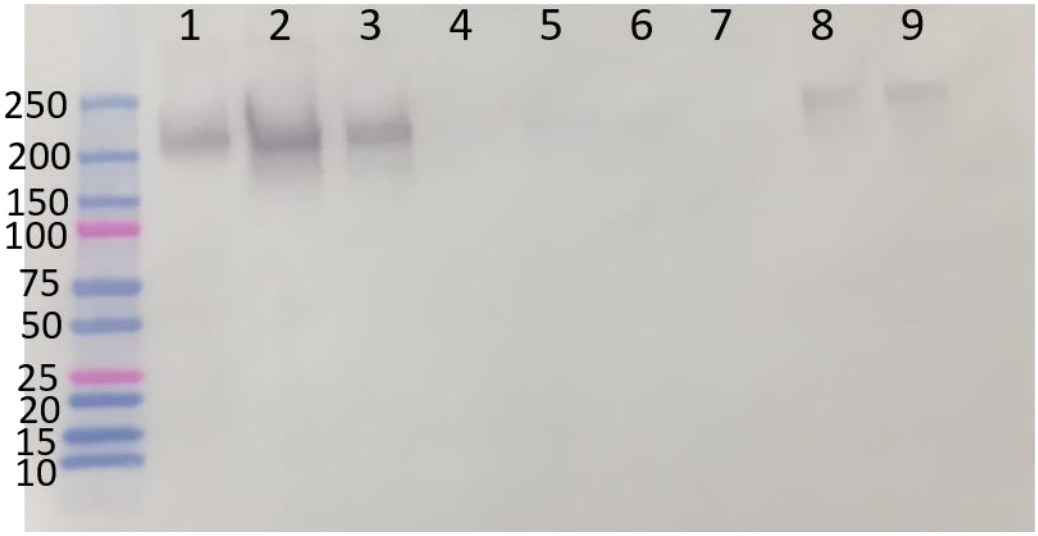

Figure 4.9: Western Blot for EGFR of the EGFR-specific purification of L858R lysate using Avidin beads and desthiobiotinylated antibodies. *Lane 1*: L858R lysate; *Lane 2*: Loading lysate to beads (material that does not bind to beads); *Lane 3*: Wash step 1; *Lane 4:* Wash step 5; *Lane 5*: Biotin Elution 1; *Lane 6*: Biotin Elution 2; *Lane 7*: Biotin Elution 3; *Lane 8*: Combined & Concentrated Biotin Elutions; *Lane 9*: Laemelli Buffer Elution. The Laemelli buffer is used to completely denature the beads and release any EGFR not released by the biotin. The EGFR band is just above the 200 kDa band in the ladder, and the unknown band in Lanes 8-9 is approximately 250 kDa.

These antibody-based purification methods have had a number of issues, including significant loss of sample, potential for protein destabilization and problems with inconsistencies between purifications. There is potential that in the future this antibody purification could still be optimized, by testing other beaded resins or antibodies for better binding affinities. Recent data has determined that, for both GBM (not shown) and Ba/F3 lysate with various EGFR mutations **(Figure 4.10),** a Sepharose bead pre-conjugated with anti-EGFR from Cell Signaling Technologies is the most successful at binding EGFR from lysate with minimal loss of sample. However, there is no way to remove the protein without destroying the protein by adding Laemelli Buffer with 5% β-mercaptoethanol. The ability to purify EGFR in Nanodiscs or perform activity assays while the EGFR is bound to the beads, as well as the applicability of

these beads to our microfluidic devices, all remain to be tested. For membrane proteins that are not recombinantly expressed with a purification tag, antibody purification of some kind seems to still be the best way to obtain just the membrane protein of interest in the Nanodiscs.

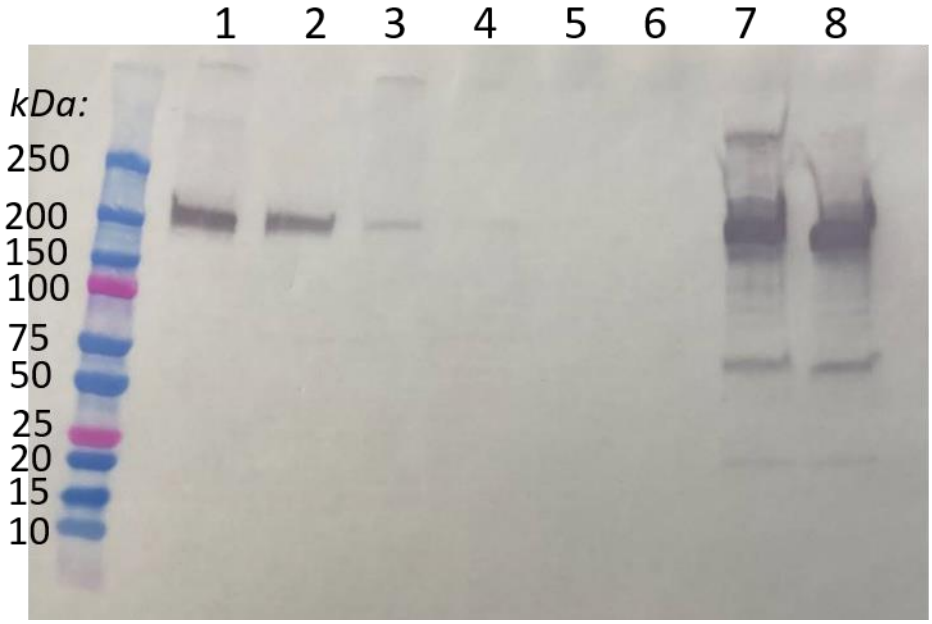

Figure 4.10: Western Blot for EGFR of the EGFR-specific purification of L858R and WT EGFR lysate using Sepharose beads pre-conjugated with anti-EGFR. *Lane 1*: L858R lysate; *Lane 2*: WT EGFR Lysate; *Lane 3*: Loading L858R lysate to beads (material that does not bind to beads); *Lane 4:* Loading WT EGFR lysate to beads; *Lane 5*: Wash L858R-loaded beads; *Lane 6*: Wash WT EGFR-loaded beads; *Lane 7*: Laemelli Buffer Elution of L858R; *Lane 8*: Laemelli Buffer Elution of WT EGFR. The Laemelli buffer is used to completely denature the beads and release all EGFR. The EGFR band is just above the 200 kDa band in the ladder.

There are other methods that could potentially lead to cleaner Nanodisc samples, though not completely purified Nanodiscs. The current Library Nanodisc preparations have been performed using whole cell lysate, however, the initial Library Nanodiscs described by the Sligar lab utilized isolated cell membranes instead.[24] Membrane isolation requires specialized centrifuges which were not immediately available over the past year, but moving forward, performing this membrane isolation will remove any soluble proteins and internal cell materials

that could be contributing to the high background in the cell lysate in particular. This change will probably require re-optimizing the ratio of MSP to the total protein concentration in the lysate, as there will be more membrane proteins present, which will probably require a higher MSP ratio as there will be more proteins that can insert into the Nanodiscs. We initially had hoped to not need this membrane isolation step, which has been possible in Bulk,[26] because of the time and equipment requirements. For a project with a long-term goal of applicability to patient samples for quickly determining treatment options, the more unnecessary steps we could avoid seemed optimal. However, if this membrane isolation can significantly improve the Nanodisc formation with EGFR incorporated, it might be worth the extra steps.

The other possibility is to change the way that the activity is measured. We have already tested a different general kinase assay, the ADPGlo Kinase assay (Promega), which involves the same basic methodology of incubating the sample, ATP, and a specific substrate to be phosphorylated. The detection method is the main difference, with ADPGlo measuring the activity using reagents that stop the reaction and deplete the remaining ATP, convert the ADP that was formed by the EGFR back into ATP, and then convert the ATP to light using luciferase. We have been able to measure EGFR activity using this assay, however this assay has many of the same issues as the Universal Kinase Assay described above, with significant background, as well as more well-to-well variability in the same samples. It is also more difficult to measure the luciferase, as the plate reader used for the colorimetric detection cannot measure luciferase activity.

One possibility is to use a radiolabeled [γ-^{32}P] ATP and calculate the amount of labeled phosphate that is incorporated into the kinase-specific substrate.[34,35] This would prevent background signal from any ATP or free phosphate present in the samples, though there will still

be issues with other proteins in the sample phosphorylating other proteins or peptides present. The remaining radiolabeled ATP and newly radiolabeled substrate are usually detected via SDS-PAGE followed by autoradiogram (for qualitative visualization) or scintillation counting (for accurate quantitation). If there are other peptides in the same size range as the kinase-specific substrate used, this could cause false higher activity. The requirement of running gels before quantitation also significantly lower-throughput than the current use of 96 well plates, which could prevent widespread use of these activity assays even if successful to measure the EGFR mutation-specific response to TKIs.

Another method that could be implemented to measure kinase activity is mass spectrometry (MS). Quantitation of the amount of the kinase-specific substrate that remains in the native state versus substrate that is phosphorylated (by the active kinase) can be determined.[36] Standards do need to be introduced in order to quantitate the samples, and it is possible to combine the radiolabeled [γ-^{32}P] ATP test with MS detection, to avoid the impact of native ATP on driving up activity. Again, there could be potential issues if there are native peptides that are very similar in molecular weight and charge to the kinase-specific substrate, so that would need to be tested for and potentially controlled for as well. Ion mobility-mass spectrometry could be used to confirm if the inhibitors are binding the EGFR if that is a potential concern for why inhibition is not successfully measured.[37] Accessibility of the eventual goal of applying this project to a simple patient-treatment development methodology is a major reason to avoid the necessity of more involved processes, such as radiolabeled assays or MS.

There are a few possibilities that remain to be tested to remove background noise via either purification methods or different activity assays that are potentially more selective. Though each of these has drawbacks, these possibilities remain as future experiments that can be

done to complete this EGFR Library Nanodisc project. Once the activity assays are optimized, there are a few experiments that remain. These include testing the different EGFR mutations against a range of TKIs, including osimertinib and dacomitinib, and obtaining inhibition measurements at a range of drug concentrations. There are other important considerations when measuring EGFR activity, including the lipid composition of the Nanodiscs and the buffers and detergents used, which I have spent some time optimizing for Nanodisc formation, but not yet for activity, which could also be interesting.

Though this project has not yet been completed, there has been a number of advancements and an encouraging outlook. We have successfully demonstrated EGFR incorporation from both GBM and Ba/F3 cell lysate into Library Nanodiscs using our microfluidic device. The EGFR-specific purification remains to be optimized, as each of the three types of antibody-bead-based purification had advantages and disadvantages. Similarly, the high background on the EGFR activity assays remains an issue that we are yet to fully resolve, though potentially the EGFR-purifications will improve this problem. We have many ideas of future improvements to the purifications and activity assays that will hopefully continue to move this project forwards.

References:

1. Engelman, D. M. Membranes are more mosaic than fluid. *Nature* **438**, 578–580 (2005).

2. Chakraborty, S. *et al.* Constitutive and ligand-induced EGFR signalling triggers distinct and mutually exclusive downstream signalling networks. *Nat. Commun.* **5**, 5811 (2014).

3. da Cunha Santos, G., Shepherd, F. A. & Tsao, M. S. EGFR Mutations and Lung Cancer. *Annu. Rev. Pathol. Mech. Dis.* **6**, 49–69 (2011).

4. Jackman, D. *et al.* Clinical definition of acquired resistance to epidermal growth factor receptor tyrosine kinase inhibitors in non-small-cell lung cancer. *J. Clin. Oncol.* **28**, 357–360 (2010).

5. Okimoto, R. A. *et al.* Activating Mutations in the Epidermal Growth Factor Receptor Underlying Responsiveness of Non-Small-Cell Lung Cancer to Gefitinib. *New England Journal of Medicine*. **350**, *2129–2139* (2004).

6. Pao, W. *et al.* Acquired resistance of lung adenocarcinomas to gefitinib or erlotinib is associated with a second mutation in the EGFR kinase domain. *PLoS Med.* **2**, 0225–0235 (2005).

7. Yu, H. A. *et al.* Analysis of tumor specimens at the time of acquired resistance to EGFR-TKI therapy in 155 patients with EGFR-mutant lung cancers. *Clin. Cancer Res.* **19**, 2240–2247 (2013).

8. Cournia, Z. *et al.* Membrane Protein Structure, Function, and Dynamics: a Perspective from Experiments and Theory. *J. Membr. Biol.* **248**, 611–640 (2015).

9. Cross, D. A. E. *et al.* AZD9291, an irreversible EGFR TKI, overcomes T790M-mediated resistance to EGFR inhibitors in lung cancer. *Cancer Discov.* **4**, 1046–1061 (2014).

10. Wang, S., Tsui, S. T., Liu, C., Song, Y. & Liu, D. EGFR C797S mutation mediates resistance to third-generation inhibitors in T790M-positive non-small cell lung cancer. *J. Hematol. Oncol.* **9**, 1–5 (2016).

11. Cross, T. A., Sharma, M., Yi, M. & Zhou, H. X. Influence of solubilizing environments on membrane protein structures. *Trends Biochem. Sci.* **36**, 117–125 (2011).

12. Stagljar, I. & Fields, S. Analysis of membrane protein interactions using yeast-based technologies. *Trends Biochem. Sci.* **27**, 559–563 (2002).

13. Garavito, R. M. & Ferguson-Miller, S. Detergents as Tools in Membrane Biochemistry. *J. Biol. Chem.* **276**, 32403–32406 (2001).

14. Akbarzadeh, A., Rezaei-sadabady, R., Davaran, S., Joo, S. W. & Zarghami, N. Liposome : classification , preparation , and applications. *Nano Review.* **8**, *1–9* (2013).

15. Zhou, H. X. & Cross, T. Influences of Membrane Mimetic Environments on Membrane Protein Structure. *Annu. Rev. Biophys*. **42**, *361–392* (2013).

16. Ritchie, T. K. *et al. Chapter 11 Reconstitution of Membrane Proteins in Phospholipid Bilayer Nanodiscs*. *Methods in Enzymology* **464**, (Elsevier Masson SAS, 2009).

17. Denisov, I. G. & Sligar, S. G. Nanodiscs in Membrane Biochemistry and Biophysics. *Chem. Rev.* **117**, 4669–4713 (2017).

18. Bayburt, T. H., Grinkova, Y. V. & Sligar, S. G. Self-Assembly of Discoidal Phospholipid Bilayer Nanoparticles with Membrane Scaffold Proteins. *Nano Lett.* **2**, 853–856 (2002).

19. Denisov, I. G., Grinkova, Y. V., Lazarides, A. A. & Sligar, S. G. Directed Self-Assembly of Monodisperse Phospholipid Bilayer Nanodiscs with Controlled Size. *J. Am. Chem. Soc.* **126**, 3477–3487 (2004).

20. Grinkova, Y. V., Denisov, I. G. & Sligar, S. G. Engineering extended membrane scaffold proteins for self-assembly of soluble nanoscale lipid bilayers. *Protein Eng. Des. Sel.* **23**, 843–848 (2010).

21. Bayburt, T. H. & Sligar, S. G. Membrane protein assembly into Nanodiscs. *FEBS Lett.* **584**, 1721–1727 (2010).

22. Wade, J. H. *et al.* Microfluidic platform for efficient Nanodisc assembly, membrane protein incorporation, and purification. *Lab Chip* **17**, 2951–2959 (2017).

23. Duong-Ly, K. C. & Gabelli, S. B. Gel filtration chromatography (size exclusion chromatography) of proteins. *Methods in Enzymology* **541**, (2014).

24. Marty, M. T., Wilcox, K. C., Klein, W. L. & Sligar, S. G. Nanodisc-solubilized membrane protein library reflects the membrane proteome. *Anal. Bioanal. Chem.* **405**, 4009–4016 (2013).

25. Roy, J., Pondenis, H., Fan, T. M. & Das, A. Direct Capture of Functional Proteins from Mammalian Plasma Membranes into Nanodiscs. *Biochemistry* **54**, 6299–6302 (2015).

26. Mak, S., Sun, R., Schmalenberg, M., Peters, C. & Luppa, P. B. Express incorporation of membrane proteins from various human cell types into phospholipid bilayer nanodiscs. *Biochem. J.* **474**, 1361–1371 (2017).

27. Morrissey, J. H. *et al.* Protein-membrane interactions: Blood clotting on nanoscale bilayers. *J. Thromb. Haemost.* **7**, 169–172 (2009).

28. Duong-Ly, K. C. & Gabelli, S. B. Explanatory chapter: Troubleshooting recombinant protein expression. *General*. *Methods in Enzymology* **541**, (2014).

29. Warmuth, M., Kim, S., Gu, X., Xia, G. & Adria, F. Ba/F3 cells and their use in kinase drug discovery. *Current Opinion in Oncology*. **19,** 55–60 (2007).

30. Carlson, B. L., Pokorny, J. L., Schroeder, M. A. & Sarkaria, J. N. Establishment, Maintenance, and In Vitro and In Vivo Applications of Primary Human Glioblastoma Multiforme (GBM) Xenograft Models for Translational Biology Studies and Drug Discovery. *Curr. Protoc. Pharmacol.* **14**, 1–23 (2011).

31. Gerber, D.E. EGFR Inhibition in the Treatment of Non-Small Cell Lung Cancer. *Drug Dev. Res.* **69**, 359-372 (2008).

32. Gainor, J. F. & Shaw, A. T. Emerging paradigms in the development of resistance to tyrosine kinase inhibitors in lung cancer. *J. Clin. Oncol.* **31**, 3987–3996 (2013).

33. Lo, T. W. *et al.* Microfluidic device for high-throughput affinity-based isolation of extracellular vesicles. *Lab Chip* **20**, 1762–1770 (2020).

34. Karra, A. S., Stippec, S. & Cobb, M. H. Assaying protein kinase activity with radiolabeled ATP. *J. Vis. Exp.* **2017**, 1–8 (2017).

35. Hastie, C. J., McLauchlan, H. J. & Cohen, P. Assay of protein kinases using radiolabeled ATP: A protocol. *Nat. Protoc.* **1**, 968–971 (2006).

36. Beltran, L *et al.* Global profiling of protein kinase activities in cancer cells by mass spectrometry. *Journal of Proteomics*. **27**, 482-503 (2012).

37. Rabuck, J.N. *et al.* Activation state-selective kinase inhibitor assay based on ion-mobility mass spectrometry. *Anal Chem.* **85**, 6885-7002 (2013).

Chapter 5: Incorporation of Viperin into Library Nanodiscs

This chapter was performed in collaboration with Professor Neil Marsh and his lab members, Dr. Timothy Grunkemeyer and Ayesha Patel. I appreciate their viperin knowledge and our conversations on how to push this project forwards in interesting directions.

Introduction:

The *v*irus *i*nhibitory *p*rotein, *e*ndoplasmic *r*eticulum-associated, *in*terferon-inducible protein, or viperin, was first identified 20 years ago when searching for the mechanism that interferons (IFNs) use to inhibit human cytomegalovirus (HCMV) replication.[1] Since then, viperin has also been associated with the inhibition of many other viruses including flaviviruses such as hepatitis C virus (HCV) and West Nile virus.[2–4] Interestingly, it has been determined that viperin can be expressed in infected cells in both an IFN-dependent and independent manner.[5]

Viperin interacts with a variety of lipid membranes within the cell, including the endoplasmic reticulum (ER), mitochondria, and lipid vesicles.[6–8] Each of these has a unique lipid composition and a variety of other membrane proteins present, which could play an interesting role in the function of viperin under different conditions.[9] The ability to learn more about how full-length viperin interacts with distinct lipid bilayers, with or without the presence of other membrane proteins, and how this impacts viperin activity, could lead to interesting information about the role of these different membrane locations on viperin's various modes of action.

The Nanodisc is a type of model membrane system that has been widely utilized to study a variety of membrane proteins, including both integral and membrane-associated proteins.[10–12] The soluble lipid bilayer is held together with a membrane scaffold protein (MSP), which can be tailored to different diameters to study larger membrane proteins or even protein complexes. Another advantage of using Nanodiscs is that the lipid composition can be precisely tuned when interested in studying interactions between a membrane protein of interest and specific lipids. The Bailey lab has developed a gradient microfluidic device that allows us to screen the lipid composition over the course of a single five minute experiment in order to determine the optimal conditions for specific membrane protein incorporation.[13]

We plan to incorporate viperin into Nanodiscs of various lipid compositions to determine if the lipid environment plays a role in viperin structure and function. The N-terminal domain of viperin is an amphipathic α-helix which can insert into lipid membranes to associate with both the lipids and nearby membrane proteins.[14] Library Nanodiscs will be formed from lysed HEK cells overexpressing viperin. The Marsh lab has developed activity assays for viperin activity in solution. The enzyme catalyzes the dehydration of CTP to form the antiviral nucleotide 3'-deoxy-3',4'-didehydro-CTP (ddhCTP). This occurs through a radical mechanism concomitant with the reductive cleavage of SAH to form 5'deoxyadenosine which is detected by LC-MS. These viperin activity measurements have occurred both alone and in the presence of other proteins of interest in immune signaling.[15,16] We will determine if the incorporation of viperin into Nanodiscs changes the activity of viperin as compared to viperin in solution.

Experimental Methods:

Nanodisc formation: Nanodisc formation was tested using both standard bulk preparation methods and the microfluidic device previously described by the Bailey lab.[13] Briefly, for either

method the components (lipids, membrane scaffold protein, HEK lysate) were combined in 20 mM sodium cholate and a 50 mM HEPES pH 7.4, 150 mM sodium chloride buffer. For the standard bulk preparation, the components were incubated at 4 °C for 2 hours with mixing, followed by the addition of Amberlite detergent removal beads (1/2 the components volume) and incubated overnight at 4 °C with mixing. The beads were removed the following morning using a 0.22 μm filter (Millipore) and 3 mL syringe.

For microfluidic preparation, the devices were formed as previously described.[13] Briefly, devices were designed using AutoCAD and the mask design printed by CAD/Art Services. Masters were fabricated using SU8-2100 (Microchem), a negative photoresist that is spin coated to the appropriate height (200 μm) on a silicon wafer. After master fabrication, devices were formed of poly(dimethylsiloxane) (PDMS) (Momentive), combined at a 1:10 ratio of initiator to monomer and degassed under vacuum before pouring on the master for curing at 70 °C. The devices were then peeled off the master mold, holes punched for inlets and outlets, and the devices sealed to a glass slide using an oxygen plasma. The devices were filled with Pierce detergent removal resin (Thermo) and washed with methanol and water at 30 μL/min for at least 15 minutes. The microfluidic devices and components mixture were incubated for 20 minutes on ice prior to Nanodisc formation, and then the components mix was followed through the device at 30 μL/min for up to 5 minutes.

Nanodisc purification: To ensure the sample contained only Nanodiscs containing viperin, multiple steps of purification were used. First, Ni-NTA purification was performed against the histidine tag on the membrane scaffold protein, to remove anything except Nanodiscs and remaining MSP. Again, this purification was performed both in bulk and microfluidics. In bulk, 0.2 mL Ni-NTA spin columns (ThermoFisher) were used. The resin was equilibrated by washing

with 400 µL purification buffer (50 mM HEPES pH 7.4, 150 mM sodium chloride) followed by centrifugation at 700 xg for 2 minutes to remove the buffer. Samples were loaded to the resin via incubation at 4 °C for 30 minutes, followed by centrifugation to remove unbound sample. The resin was washed three times with 400 µL wash buffer, the purification buffer with 30 mM imidazole. Nanodiscs were eluted using 200 µL elution buffer, the purification buffer with 300 mM imidazole. For microfluidic purification, the same basic devices were used, but were filled with Ni-NTA resin (ThermoFisher) instead of the detergent removal resin. The same buffers were used, with a preparation step of 12 minutes of flowing the purification buffer at 30 µL/min, loading the sample at 10 uL/min and washing for 12 minutes with the wash buffer at 30 µL/min. The sample was eluted using the elution buffer at 10 µL/min for up to 30 minutes.

Size-exclusion Chromatography: SEC was used for both Nanodisc purification (for a homogenous sample) and to confirm successful Nanodisc formation. The column used was the Superdex 200 Increase 3.2/200 at a flow rate of 75 µL/min. Nanodisc elution was monitored at 280 nm and fractions were collected of the Nanodisc peak and the aggregate peak.

Anti-FLAG purification: To get a homogenous sample of viperin incorporated Nanodisc, another purification step was added. Anti-FLAG magnetic beads were used against FLAG tag on the viperin gene. The Nanodisc elution peak fractions from SEC were incubated with equilibrated anti-FLAG magnetic beads for 2 hr at room temperature with end-to-end mixing. The resin was then washed three times with 200 uL of purification buffer. Finally, viperin incorporated Nanodiscs were eluted by incubating the resin with 0.5 ug/uL 3x FLAG peptide for 30 min at room temperature with end-to-end mixing. Western blotting was used to probe viperin in the eluted fraction, and silver staining was used to check the purity of the enzyme.

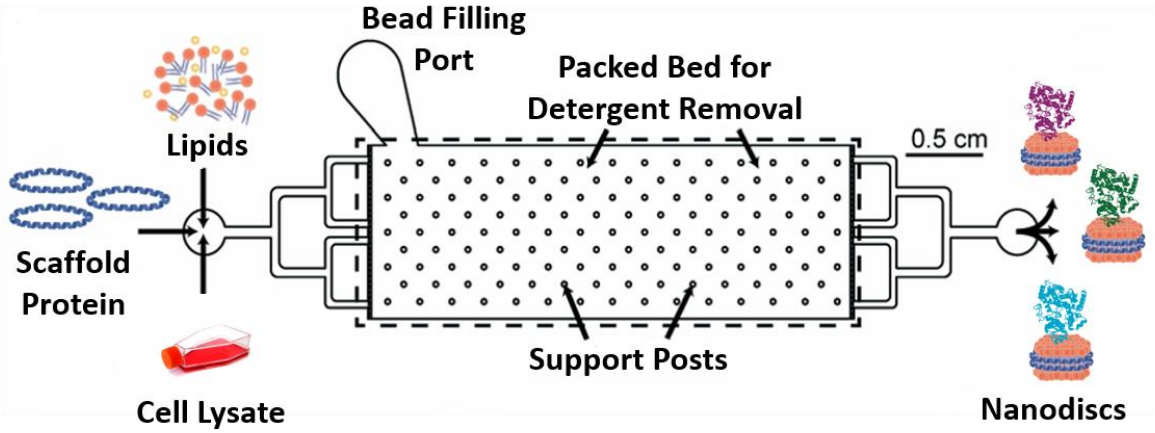

Figure 5.1: The microfluidic device used to form Library Nanodiscs. The components mixture containing MSP, lipids and cell lysate is introduced through the inlet and flows though the packed bead bed filled with detergent removal resin. As the detergent is removed, the Nanodiscs spontaneously self-assemble, incorporating membrane proteins, which can be collected through the outlet.

Results & Discussion

We initially tested incorporation of viperin from HEK cell lysate into 1-palmitoyl-2-oleoyl-sn-glycero-3-phosphocholine (POPC) Nanodiscs using our microfluidic device. **(Figure 5.1)** However, we saw minimal incorporation of the viperin into Nanodiscs, with less than 5% of the viperin (as calculated using quantitative immunoblotting, data not shown) incorporating into the Nanodiscs. The remaining viperin was found to be forming aggregates that elute earlier in the size-exclusion chromatography used to confirm Nanodisc formation. **(Figure 5.2)** We think that the low viperin incorporation percentage is because viperin is a membrane-associated protein and is thus more stable in solution than the previously incorporated integral membrane proteins. The concentration of viperin incorporated into these initial Nanodiscs was too low for activity assay measurements to be performed.

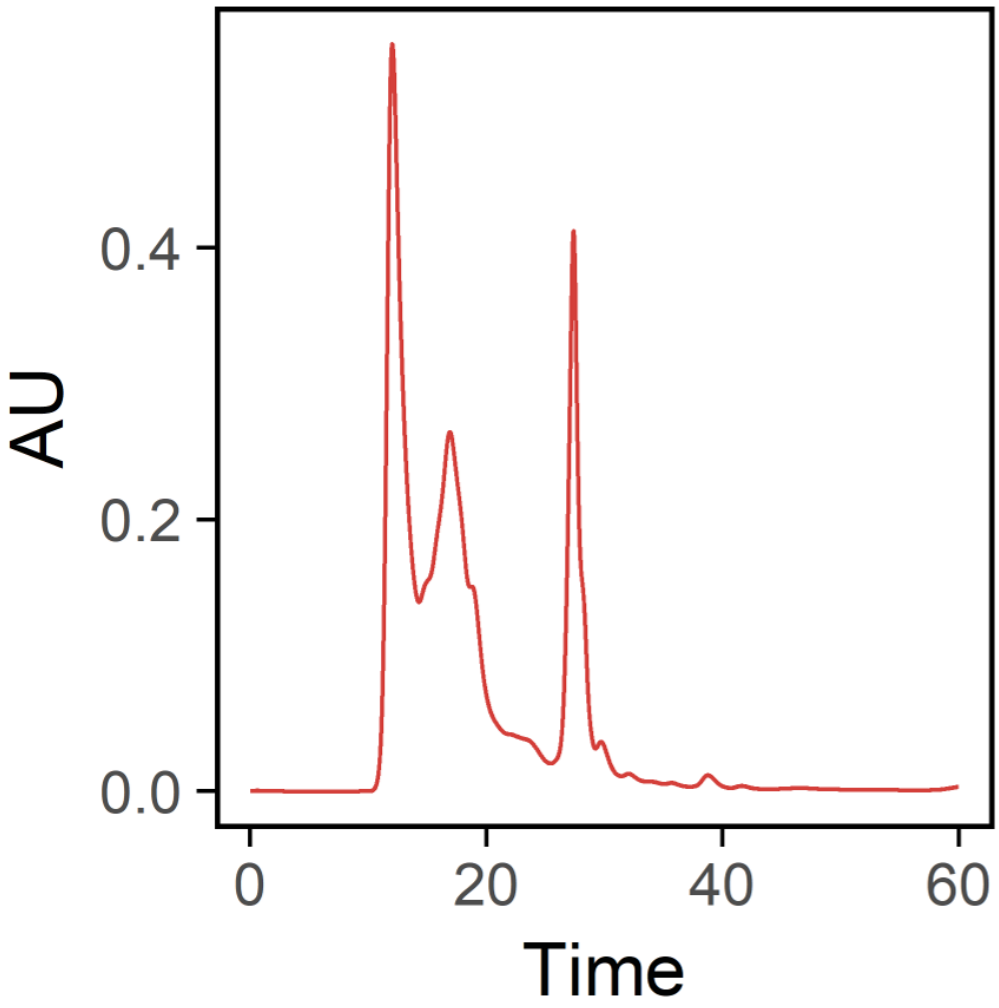

Figure 5.2: Size-Exclusion Chromatograph of the Nanodiscs containing viperin. The first peak around 12 minutes is the aggregate peak, composed of lipids, MSP and cell lysate components that have not incorporated into the Nanodisc. The second peak at ~18 minutes is the Nanodisc peak. There is another smaller peak around 28 minutes of any buffer and lysate components that are exceptionally small. As no purification was performed after Library Nanodisc formation, the SEC trace contains contaminants from the lysate components.

To improve the percentage of viperin incorporated to allow for high enough protein incorporation for downstream analysis, we decided to test other lipid compositions in the Nanodisc. Though there is no literature indicating that viperin preferentially interacts with certain lipids, there are other membrane-associated proteins that are known to only interact with

specific lipids, such as proteins in the blood clotting pathway.[17] To improve viperin lipid incorporation, we formed Nanodiscs that contained the main two lipid components common between all three membranes that viperin has been known to associate with, the ER, mitochondria, and lipid droplets.[6,8,18] These three membranes contain 20-40% 1-palmitoyl-2-oleoyl-sn-glycero-3-phosphoethanolamine (POPE) and at least 40% POPC.[19]

We tested three mixtures of these lipids, 20% POPE, 30% POPE and 40% POPE, with the remaining lipid percentage POPC for each Nanodisc. **(Figure 5.3)** The Nanodiscs were separated from free viperin that did not incorporate using size-exclusion chromatography (SEC), with both the aggregate of unincorporated lipids and proteins and the Nanodisc peak being collected. Both of these fractions (labeled as A for aggregate and N for Nanodisc) and the initial Nanodiscs before purification (labeled as B) were tested using Western Blotting to determine if viperin incorporation was successful. Significantly more viperin ends up in the aggregate peak than in the Nanodiscs, but the best incorporation appears to occur in the Nanodiscs containing 20% POPE and 80% POPC.

Adding POPE to the Nanodisc did increase viperin incorporation slightly but the incorporation rate is still very low. Both POPC and POPE lipid headgroups have a net neutral charge, so we decided to test if a charged Nanodisc would increase the viperin incorporation. 1-palmitoyl-2-oleoyl-sn-glycero-3-phosphate (POPA) and 1-palmitoyl-2-oleoyl-sn-glycero-3-phospho-L-serine (POPS) were both tested in ratios of 10, 30, and 50%, again with the remaining lipid composition POPC. The lipid structures and charges can be seen in **Figure 5.4**.

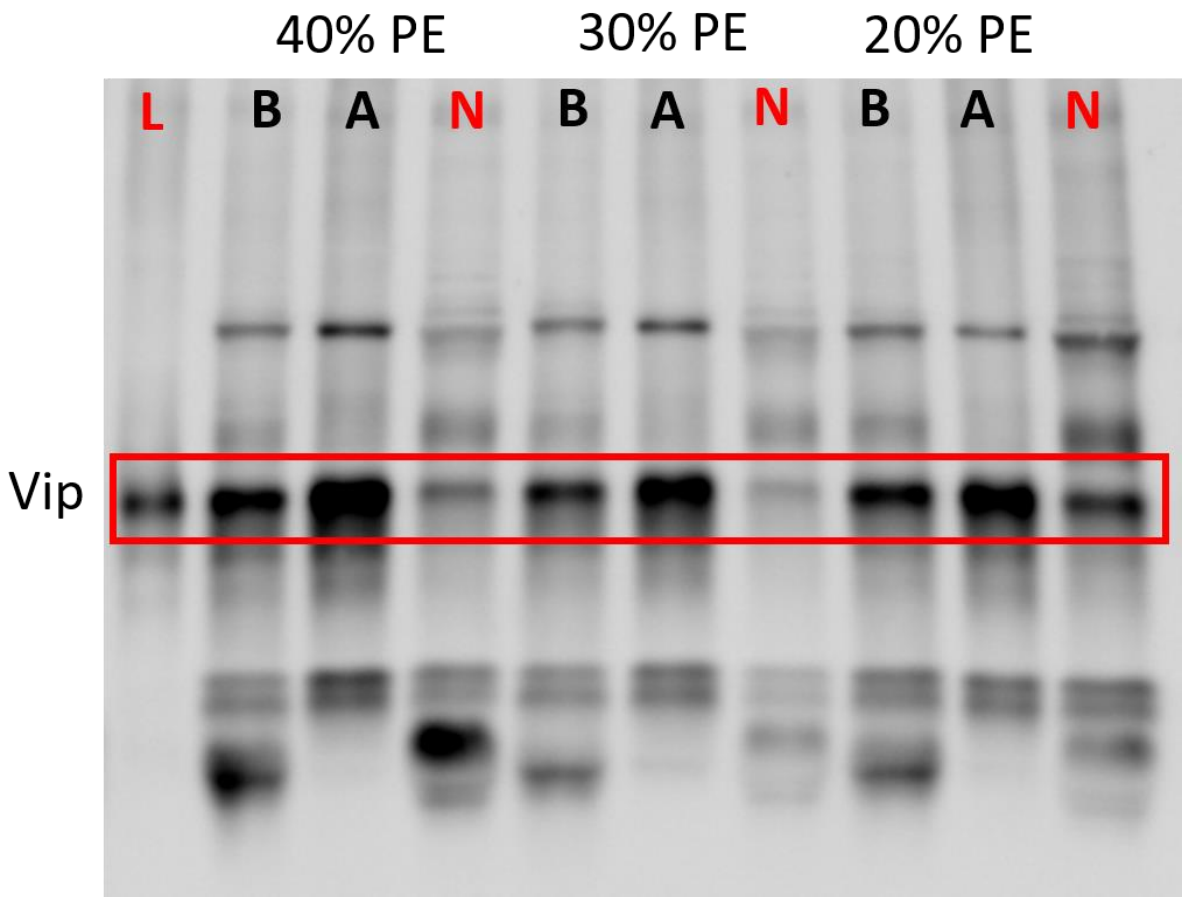

Figure 5.3: Western blot for anti-viperin of the Nanodiscs using different percentages of POPE, with the remaining lipid composition POPC. The lanes are labeled as follows: **B**: Before purification Nanodiscs; **A**: SEC Aggregate Peak; **N**: SEC Nanodisc peak; **L**: HEK cell lysate. The viperin band is noted by the red box across all lanes. Based on relative intensities of the viperin band in the SEC Nanodisc peaks, the 20% POPE 80% POPC Nanodisc lipid composition was determined to be optimal.

Incorporating either POPS or POPA into the Nanodiscs did not improve viperin incorporation as compared to a POPC control Library Nanodisc. **(Figure 5.5)** The percentage of incorporation was calculated in ImageJ by dividing the intensity of the SEC-fraction collected Nanodisc band by the intensity of the HEK cell lysate band. The 100% POPC Nanodiscs had about a 4.5% incorporation, which is about average for what has been seen previously for these control Nanodiscs. Using 10-50% POPA led to percentages of between 4.7 and 5.1%, all

reasonably within error of each other and the control POPC Nanodiscs when considering the method used for quantitation. The 10-50% POPS Nanodiscs had slightly lower incorporation percentages, from 2.5-3.7% incorporation. This seems to suggest that the viperin does not preferentially incorporate into Nanodiscs with charged lipids, though it does not necessarily prevent incorporation when POPA lipids are used.

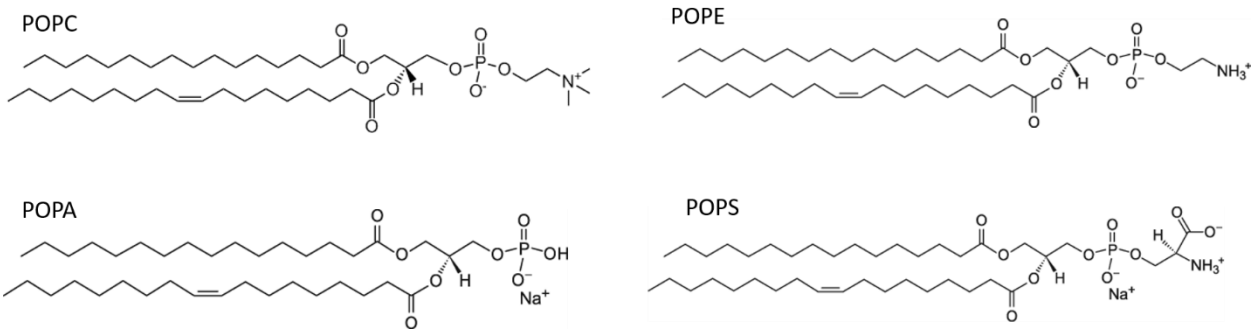

Figure 5.4: The structures and charges of the four lipids used throughout this chapter. Each lipid has the same tails but distinct lipid head groups. Top left: POPC; Top right: POPE. Both of these lipids are zwitterionic, with a net neutral charge. Bottom left: POPA, which has a negative charge. Bottom right: POPS, which contains 2 negative and 1 positive charge, leading to a net negative charge.

We decided to move forward with the 20% POPE 80% POPC Nanodiscs that have consistently showed the best viperin incorporation. To obtain higher concentration of viperin as needed for downstream applications, we switched from using the microfluidic devices for Nanodisc formation to using Bulk formation methods. Our current microfluidic devices are limited to forming approximately 90 µL of Nanodiscs each, based on the volume of 20 mM sodium cholate able to be removed by the beads in the 60 µL bead bed. The number of microfluidic devices required to form 5 mL of Nanodiscs is unreasonable. Bulk methods do require the overnight step for detergent removal, but the ability to do a single Bulk preparation

for this large volume is advantageous. We have also been able to preform this Bulk preparation step in an oxygen-free environment, which is important for the viperin activity.[20]

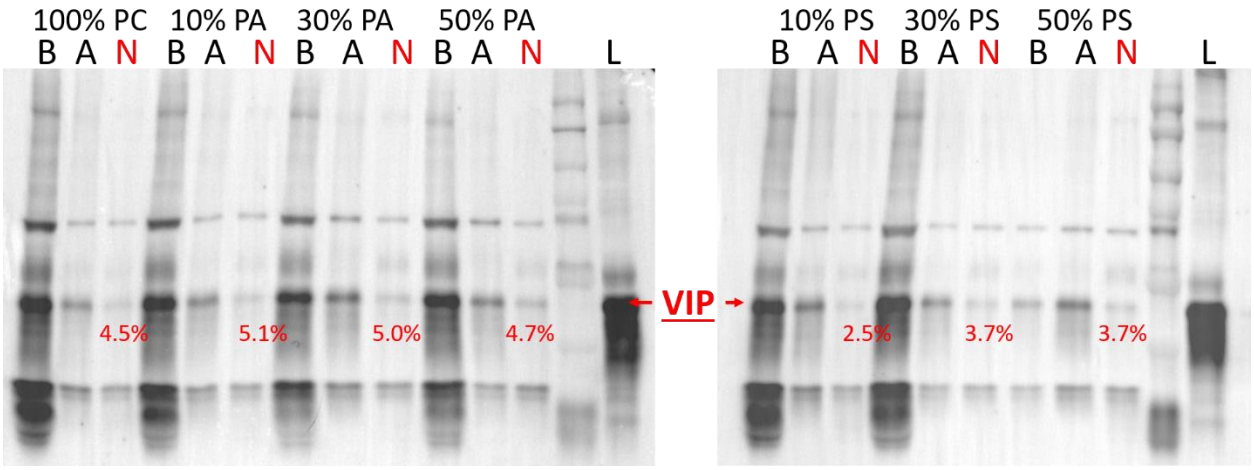

Figure 5.5: Western Blot using anti-viperin of the Nanodiscs formed with POPA (left) and POPS (right). The key labeling the lanes is as follows: B: Before purification Nanodiscs; A: SEC Aggregate Peak; N: SEC Nanodisc peak; L: HEK cell lysate. The viperin band is noted by the red VIP for both blots. The red numbers indicate the percent incorporation, calculated by dividing the viperin band intensity in that lane by that of the lysate lane.

After Nanodisc formation, there are two steps of purification that we have implemented to ensure the final solution contains just Nanodiscs containing viperin. We begin with a Ni-NTA purification for the His-tag on the MSP, followed by an anti-FLAG purification for the FLAG-tag engineered on the viperin. **(Figure 5.6)** SDS-PAGE and Western blotting after the two-step purification confirm that viperin is strongly associating with the Nanodiscs, as both viperin and MSP1E3D1 are present after the two purifications. These purifications are also now performed in Bulk in an oxygen-free environment. If necessary, we have also performed a final step of size-exclusion chromatography (SEC) followed by fractionation to ensure the Nanodiscs are all equal in size.

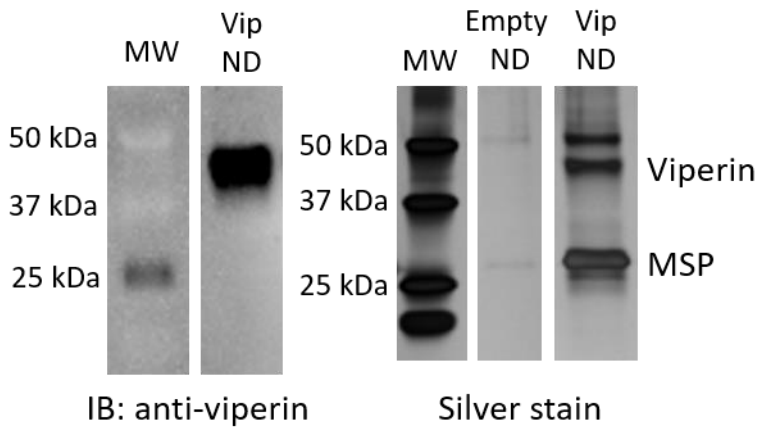

Figure 5.6: Western Blot (left) and SDS-PAGE (right) after the two-step viperin Nanodisc purification process. On the left, the blot probed with anti-viperin. The viperin band is present at approximately 42 kDa. On the right, the SDS-PAGE gel stained with silver stain, in which both the 42 kDa viperin band and the ~32 kDa MSP1E3D1 bands are visible. Lower-concentration Empty Nanodiscs were also run, and the MSP band is present while the viperin band is not. There is a band slightly higher than 50 kDa that appears to be a contaminant in the MSP, as it is seen in both the Empty and Viperin Nanodiscs, though further confirmation should be performed.

Conclusions and Future Work:

We have successfully incorporated viperin into Nanodiscs directly from HEK cells, as confirmed using SDS-PAGE and Western Blotting. An advantage of using the viperin recombinantly expressed in HEK cells is that a FLAG-tag was engineered on the viperin, which made purification after Nanodisc formation significantly easier. Purification for MSP using the His-tag followed by viperin using the FLAG-tag led to a sample containing only Nanodiscs with viperin incorporated. This is advantageous for our planned downstream assays, including transmission electron microscopy (TEM) and viperin activity assays.

We have performed initial viperin activity assays using 80% POPC 20% POPE Nanodiscs containing viperin. The Marsh lab has developed an activity assay that measures the ability of viperin to form ddhCTP, with MS assistance from the Kennedy lab. Initial activity

assays indicate that we are able to measure viperin activity in Nanodiscs (data not shown), though we still have to replicate the Nanodisc measurements and compare to viperin in solution. We are interested in the impact the lipid bilayer has on viperin activity, as previous activity experiments have used a concentrated form of viperin in solution. Beyond these comparisons, we are also interested in further determining if different Nanodisc lipid compositions might cause differences in viperin activity, as we have previously determined that viperin will incorporate, with low efficiency, into Nanodiscs containing a variety of lipids, including the negatively charged lipids POPA and POPS. The Marsh lab has also previously determined that other membrane proteins, including the E3 ubiquitin ligase tumor necrosis factor receptor-associated factor 6 (TRAF6), can impact viperin activity.[15] We plan to test if these protein-protein interactions change when incorporated into Nanodiscs, and if this changes the viperin activity as compared to interactions in solution.

There has not yet been an example of obtaining structural information about full-length viperin, as most previous viperin structural studies have used viperin expressed with a truncated N-terminus.[21] The N-terminus is the section of the protein that interacts with the lipid bilayer and could have interesting impacts on the overall viperin structure, especially if structural information is obtained with the N-terminus within a lipid bilayer. We plan to obtain structural information about full-length viperin in Nanodiscs, starting with TEM and eventually moving to Cryo-EM. These microscopy techniques do require large concentrations of viperin in Nanodiscs, which will require large Bulk preparations, but we hope will lend significant knowledge to the impact of the Nanodisc lipid bilayer on full-length viperin.

References:

1. Chin, K. C. & Cresswell, P. Viperin (cig5), an IFN-inducible antiviral protein directly induced by human cytomegalovirus. *Proc. Natl. Acad. Sci. U. S. A.* **98**, 15125–15130 (2001).

2. Vonderstein, K. *et al.* Viperin Targets Flavivirus Virulence by Inducing Assembly of Noninfectious Capsid Particles. *J. Virol.* **92**, 1–15 (2017).

3. Helbig, K. J. *et al.* The antiviral protein viperin inhibits hepatitis C virus replication via interaction with nonstructural protein 5A. *Hepatology* **54**, 1506–1517 (2011).

4. Hee, J. S. & Cresswell, P. Viperin interaction with mitochondrial antiviral signaling protein (MAVS) limits viperin-mediated inhibition of the interferon response in macrophages. *PLoS One* **12**, 1–19 (2017).

5. Zhu, H., Cong, J. P. & Shenk, T. Use of differential display analysis to assess the effect of human cytomegalovirus infection on the accumulation of cellular RNAs: Induction of interferon-responsive RNAs. *Proc. Natl. Acad. Sci. U. S. A.* **94**, 13985–13990 (1997).

6. Seo, J. Y., Yaneva, R. & Cresswell, P. Viperin: A multifunctional, interferon-inducible protein that regulates virus replication. *Cell Host Microbe* **10**, 534–539 (2011).

7. Hinson, E. R. & Cresswell, P. The N-terminal amphipathic α-helix of viperin mediates localization to the cytosolic face of the endoplasmic reticulum and inhibits protein secretion. *J. Biol. Chem.* **284**, 4705–4712 (2009).

8. Fujimoto, T. & Parton, R. G. Not just fat: The structure and function of the lipid droplet. *Cold Spring Harb. Perspect. Biol.* **3**, 1–17 (2011).

9. Harayama, T. & Riezman, H. Understanding the diversity of membrane lipid composition. *Nat. Rev. Mol. Cell Biol.* **19**, 281–296 (2018).

10. Denisov, I. G. & Sligar, S. G. Nanodiscs in Membrane Biochemistry and Biophysics. *Chem. Rev.* **117**, 4669–4713 (2017).

11. Denisov, I. G., Grinkova, Y. V., Lazarides, A. A. & Sligar, S. G. Directed Self-Assembly of Monodisperse Phospholipid Bilayer Nanodiscs with Controlled Size. *J. Am. Chem. Soc.* **126**, 3477–3487 (2004).

12. Bayburt, T. H. & Sligar, S. G. Membrane protein assembly into Nanodiscs. *FEBS Lett.* **584**, 1721–1727 (2010).

13. Wade, J. H. *et al.* Microfluidic platform for efficient Nanodisc assembly, membrane protein incorporation, and purification. *Lab Chip* **17**, 2951–2959 (2017).

14. Jiang, D. *et al.* Identification of Five Interferon-Induced Cellular Proteins That Inhibit West Nile Virus and Dengue Virus Infections. *J. Virol.* **84**, 8332–8341 (2010).

15. Dumbrepatil, A. B. *et al.* Viperin interacts with the kinase IRAK1 and the E3 ubiquitin ligase TRAF6, coupling innate immune signaling to antiviral ribonucleotide synthesis. *J. Biol. Chem.* **294**, 6888–6898 (2019).

16. Ghosh, S. *et al.* Interactions between Viperin, Vesicle-Associated Membrane Protein A, and Hepatitis C Virus Protein NS5A Modulate Viperin Activity and NS5A Degradation. *Biochemistry* **59**, 780–789 (2020).

17. Morrissey, J. H. *et al.* Protein-membrane interactions: Blood clotting on nanoscale bilayers. *J. Thromb. Haemost.* **7**, 169–172 (2009).

18. Hinson, E. R. & Cresswell, P. The antiviral protein, viperin, localizes to lipid droplets via its N-terminal amphipathic α-helix. *Proc. Natl. Acad. Sci. U. S. A.* **106**, 20452–20457 (2009).

19. van Meer, G. & de Kroon, A. I. P. M. Lipid map of the mammalian cell. *J. Cell Sci.* **124**, 5–8 (2011).

20. Makins, C. *et al.* Does viperin function as a radical S-adenosyl-L-methioninedependent enzyme in regulating farnesylpyrophosphate synthase expression and activity? *J. Biol. Chem.* **291**, 26806–26815 (2016).

21. Fenwick, M. K., Li, Y., Cresswell, P., Modis, Y. & Ealick, S. E. Structural studies of viperin, an antiviral radical SAM enzyme. *Proc. Natl. Acad. Sci. U. S. A.* **114**, 6806–6811 (2017).

Chapter 6: Mass Spectrometry to Study Membrane Proteins in Nanodiscs

The research in this chapter was performed in collaboration with the labs of Professor Brandon Ruotolo (Department of Chemistry, University of Michigan) and Professor Philip Andrews (Department of Biochemistry, University of Michigan). I would like to thank Marina Sarcinella, Kristine Parson and Lolita Piersimoni for their contributions to this research in this chapter, as well as providing figures, methods, and editing.

Introduction:

The importance of membrane proteins in a variety of biological functions, such as downstream signal transduction and energy production, is known but not well understood.[1,2] Though membrane proteins represent approximately 60% of all drug targets, the study of membrane proteins has lagged significantly behind that of soluble proteins.[2–4] Less than 3% of protein structures in the protein data bank (PDB) represent membrane proteins, even though membrane proteins comprise about 30% of the human proteome.[5,6] This disparity has occurred because of the higher difficulty in studying membrane proteins as once removed from the native cell bilayer, these proteins tend to misfold and aggregate, making it difficult to study the native protein structure and function.[7,8]

One major area of interest in expanding membrane protein knowledge is determining the impact of the complex, global membrane environment on the membrane protein structure and function. There have been a number of model membrane systems developed to allow for the study of membrane proteins in a more native-like lipid bilayer without the intricacies of the

entire cell membrane.[9,10] Utilizing a lipid bilayer allows for stabilizing the membrane protein structure and activity in a more native state as opposed to in detergent or solution. It also allows for studying the impact on specific lipids on the membrane protein by varying the model membrane system composition.

Lipid Nanodiscs are a type of model membrane system that have been gaining traction as a simple, tunable and soluble lipid bilayer that have been used to study a number of different classes of membrane proteins.[11,12] The ability to control Nanodisc size and lipid composition is essential to study the impact of the specific membrane environment on a membrane protein of interest. Though traditional methods of optimizing Nanodisc formation are tedious and slow, we have recently demonstrated a microfluidic device that allows for rapid Nanodisc formation with less reagents required.[13]

There are a number of analytical methods that have been used to determine high-resolution MP structures in Nanodiscs, including using X-ray crystallography,[14] NMR[15] and Cryo-EM.[16] However, each of these methods are low-throughput, requiring large amounts of highly purified membrane proteins, which can be very challenging to obtain. These approaches also often cannot identify specific binding locations of lipids or other ligands to the membrane protein, which is an area of significant interest. To allow for the study of membrane protein structure as impacted by the surrounding membrane environment a variety of mass spectrometry (MS) tools have been developed.[17–19]

Ion-Mobility MS (IM-MS) has recently been employed to study membrane protein structure and function.[20–22] IM-MS is a form of 2D separation that separates ions based on both size, shape, and charge. With the use of membrane mimetics such as Nanodiscs, the native conformation of the membrane proteins is retained and can be studied using a gas phase

technique such as IM-MS. Briefly, in IM-MS nano electrospray ionization (nESI) is used to ionize and desolvate intact protein complexes. The ions then travel through a quadrupole and into a T-wave ion guide that functions as an ion trap, where collision-induced unfolding (CIU) and collision-induced dissociation (CID) experiments can be performed by accelerating the ions into the neutral gas present in the collision cell. Following activation, ions are separated in the ion mobility chamber. In an IM experiment, ions traverse through a drift cell, which is filled with an inert buffer gas, under the influence of a weak electric field

Unfolding of gas phase ions can be traced by monitoring the increase in arrival time from IM measurements. The Ruotolo lab has pioneered the technology of CIU which utilizes collisional heating to rapidly monitor the gas-phase unfolding and stability of protein-protein complexes, and protein-ligand complexes. This approach is analogous to differential scanning calorimetry (DSC) experiments carried out in solution, but can more rapidly measure protein stabilities, without the need to purify or label the proteins of interest.[23–25] IM-MS with CIU has been used to determine information about lipid and ligand binding to proteins. Comparing the unfolding fingerprints of membrane proteins in the presence of different lipids or ligands can provide information about the impact these interactions have on the protein of interest.

To study all the membrane proteins in a sample, a different type of MS can be used, often called peptide fingerprinting.[26,27] The membrane proteins are enzymatically digested into shorter peptides using trypsin prior to LC-MS. The peptides are identified by molecular weight and then the sequences are compared to databases to determine the membrane proteins present in the initial sample. This method has previously been used to determine which membrane proteins were successfully incorporated into Library Nanodiscs from isolated cell membranes.[28]

By combining the membrane environment of the Nanodisc with MS as a downstream analytical tool, we hope to delve deeply into the impact of a specific membrane environment on membrane protein structure and function. Utilizing microfluidic devices will allow for high throughput and rapid formation and optimization of Nanodiscs, with potential to eventually couple these microfluidic devices directly in-line with the various MS techniques. We will focus on two types of membrane protein studies using MS, with one project focused on native MS of one specific protein of interest while the second project focuses broadly on incorporating all membrane proteins from lysate into Nanodiscs. Both projects rely on forming Nanodiscs of specific lipid compositions and testing the impact of these lipids on the membrane protein structure and function through MS.

Experimental Methods:

Materials: Membrane scaffold proteins MSP1D1 and MSP1E3D1 were purchased from Sigma Aldrich while the modified MSP1D1(-) was created by removing the His-tag using a Tobacco Etch Virus protease to completely and specifically cleave the tag. Cytochrome P450 3A4 (CYP3A4) was expressed by a collaborator at UIUC from the NF-14 construct in the pCWOri+ vector with a histidine affinity tag. Isolated mitochondria were provided by a collaborator to the Andrews lab. Lipids 1,2-dimyristoyl-snglycero-3-phosphocholine (DMPC) and 1-palmitoyl-2-oleoyl-snglycero-3-phosphocholine (POPC) were purchased from Avanti Polar Lipids. Other chemicals, including the Pierce detergent removal resin and sodium cholate, were purchased from Sigma Aldrich.

Microfluidic Device Preparations: Microfluidic devices were prepared as previously described.[13] Briefly, the devices are designed using AutoCad and the photomasks were printed by CAD/Art Services Inc. The masters are formed on silicon wafers using SU-8 2100, a negative photoresist,

which is spin coated to 200 μm high followed by standard photolithography. After master fabrication, polydimethylsiloxane (PDMS) from Momentive at a 10:1 monomer:initiator ratio is degassed under vacuum, poured over the master mold, and cured at 70 °C for at least 1 hour. The PDMS is then peeled off, holes are punched for inlets and outlets, and the PDMS is bonded to a glass microscope slide using an oxygen plasma. After device formation, Pierce detergent removal beads were introduced through the bead-filling port in a slurry with DI water until the bead-bed is fully packed. The beads are cleaned with water, methanol, water for 10-20 minutes each at 30 μL/min prior to Nanodisc assembly.

Mitochondrial isolation and lysis: Mitochondria were isolated from Wistar rat heart cells (removed from a living rat under anesthesia) by a collaborator to the Andrews lab using differential centrifugation as follows. The heart was homogenized in cardioplegia buffer and centrifuged for 10 minutes at 8000 rcf. The pellet was washed twice with isolation buffer (IB) and resuspended in IB. The sample was then centrifuged for 10 minutes at 700 rcf to separate the mitochondria from the debris, which ends up in the pellet. The supernatant, which contains the mitochondria, is then centrifuged for a final time for 10 minutes at 8000 rcf, with the mitochondria ending up in the pellet. The pellet was then frozen until use. Before forming Nanodiscs, the mitochondria were thawed and lysed with detergent, a few of which were tested, including Triton X-100 and dodecyl maltoside. The mitochondria and detergent were vortexed, incubated for 10 minutes at 4 °C, and centrifuged to remove debris. The total protein concentration was then determined via Bicinchoninic Acid (BCA) assay.

Nanodisc preparations: Lipids were purchased solubilized in chloroform and were dried down at specific concentrations in test tubes under nitrogen before storage for at least 4 hours under vacuum. 100 mM sodium cholate was added to the dried lipids to resolubilize, and then mixed

with the membrane scaffold protein and the CYP3A4 membrane protein or mitochondrial lysate in buffer at the appropriate ratios of lipid:MSP and MSP:MP **(Table 6.1)**. The buffer used was Standard Disc Buffer (SDB): 20 mM Tris pH 7.4, 100 mM NaCl, 0.5 mM EDTA, and 0.01% sodium azide. This components mixture was then introduced into the microfluidic device at 30 μL/min using Pump 11 Pico Plus Elite Dual Syringe Pump from Harvard Apparatus and collected for 5 minutes.

Nanodisc purification: Library Nanodiscs were purified after microfluidic Nanodisc formation to remove any mitochondrial lysate components not incorporated into the Nanodiscs. The MSP1E3D1 used to make the Nanodiscs contained a N-terminal 6-Histidine tag that was used for the purification using Ni-NTA. Purification was performed on microfluidic devices of the same design as the Nanodisc formation device but filled with Ni-NTA resin instead of the detergent removal beads. Samples were loaded onto the beads using the syringe pumps at a rate of 10 μL/min. Any non-specifically bound proteins are removed by flowing the Wash buffer (20 mM Tris HCL pH 7.4, 100 mM sodium chloride, 50 mM imidazole) at 30 μL/min for 12 minutes. The Nanodiscs were then eluted with Elution Buffer (20 mM Tris HCL pH 7.4, 100 mM sodium chloride, 500 mM imidazole).

Nanodisc characterization via SEC: Nanodiscs were characterized using Size-Exclusion Chromatography to test for optimal Nanodisc formation, as well as a purification step by collecting fractions of the Nanodisc peak. The columns used were the Superdex 200 Increase 3.2/300 or 10/300 column, depending on the sample size. Both columns were operated at a flow rate of 75 μL/min. Absorbances were measured at 280 nm to monitor Nanodisc formation using the overall protein absorbance and 417 nm to follow CYP3A4 incorporation, using the heme

cofactor absorbance.[29] The hydrodynamic radius of the Nanodiscs was compared to a set of five protein standards obtained from BioRad.

Nanodisc preparation for MS: The concentrations of the purified Nanodiscs were determined using the Qubit assay and 2 aliquots of 20 μg of each Nanodisc were dried down. The samples were resuspended in 20 μL of 8 M urea, 20 mM HEPES, pH 8 and then 0.8 μL of 100 mM 1,4-Dithiothreitol (DTT) was added and was left to mix at 54 °C for 30 minutes. After this incubation, 4 μL of 100 mM iodacetamide (IAA) was added to each sample and incubated for another 30 minutes in the dark. The reaction was quenched with 3.2 μL of 100 mM DTT, and 1 aliquot of each Nanodiscs had 132 μL of 20 mM HEPES added while the other aliquot had 80 μL of 2% LDS in 20 mM HEPES. Both aliquots were vortexed, sonicated and incubated at 4 °C for 30 minutes and vortexed again. Then the protein precipitation was performed by adding 400 μL methanol, 200 μL chloroform and 300 μL water. The mixture was centrifuged and then the upper phase was removed. Another 400 μL of methanol was added, the sample was centrifuged again, and the supernatant was removed. The protein pellet was re-suspended in 160 μL of 10 mM HEPES. Then 0.4 μg of Trypsin and 0.4 μg of GluC were added to each sample and incubated overnight at 37 °C for protein digestion. The next morning the digestion was stopped by adding 1% FA and the samples were sent through 100 μL C18 zipTip cleanUp columns. The samples were eluted with 50 μL 50% acetonitrile (ACN) followed by 50 μL 70% ACN in 0.1% FA. The samples were dried down and then resuspended in 45 μL.

Peptide Mass Spectrometry: 9 μL of each sample were injected into the mass spectrometer (Thermo Orbitrap Fusion Lumos). The raw files were analyzed with Proteome Discoverer 2.3.

Table 6.1: Example of the tables used to prepare the components for the Nanodisc formation. Information such as the concentrations and ratios can be modified and the necessary volumes needed to be combined will update.

Filled Nanodisc Formation with POPC and MSP1D1	
Inputs	
Total Sample Volume (mL)	0.80
[MSP1D1] (uM) (from NanoDrop measurement)	175.0
CYP 3A4 Stock Concentration (μM)	26.4
Desired MSP:CYP3A4 Ratio	10
Desired POPC:MSP1D1 Ratio	65
[POPC] stock (mM) (what's the concentration from vendor?)	33.0
Stock POPC (μL) (how much did you add to test tube?)	200.0
Desired [POPC] (mM) (within the test tube)	50.0
Desired final [Cholate] (mM)	20
Desired [CYP 3A4] (μM)	3.0
Filled Nandodisc Prep	**Volume (μL)**
0: 100 mM Cholate into Lipid Film	132.0
1: CYP 3A4 Stock	90.9
1: MSP1D1 stock	137.1
1: 50 mM POPC Stock	31.2
1: SDB(-) Buffer	411.9
1: 100 mM Cholate Stock	128.8

Results & Discussion:

Cytochrome P450 Microfluidic Nanodisc Formation and Purification:

Nanodiscs were prepared using the smaller MSP1D1 (~9.7 nm diameter) and POPC lipids with the cytochrome P450 CYP3A4 using a 65:1 POPC:MSP and 10:1 MSP:CYP ratio **(Table 6.1).** The components were mixed together in 20 mM sodium cholate and SDB buffer and incubated for about 15 minutes on ice, as the lipid transition temperature for POPC is 4 °C. The microfluidic devices were also incubated in ice for 15 minutes before and throughout the Nanodisc formation. Multiple microfluidic devices were used on the same components mixture, and the samples were combined after, as each device is only able to remove a certain detergent

concentration (~90 µL of 20 mM sodium cholate), so if a higher volume sample is desired multiple devices are utilized.

The Nanodiscs were both characterized and purified using size-exclusion chromatography **(Figure 6.1).** Successful Nanodisc formation is often confirmed using SEC with a single, sharp peak at the appropriate elution time as compared to known protein standards. These initial Nanodiscs do not show perfect formation, as there is some aggregation of excess lipids and unincorporated CYP. For this reason, fractions were collected from the main Nanodisc peak to use for the ion-mobility mass spectrometry measurements, to ensure only properly-formed Nanodiscs incorporating CYP3A4 are used for these downstream analyses.

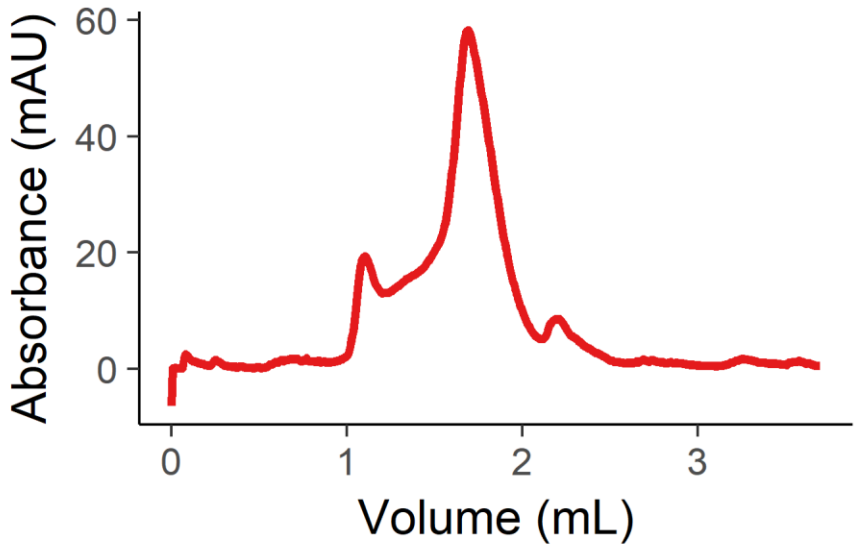

Figure 6.1: Size-exclusion chromatogram of the Filled Nanodiscs using MSP1D1, POPC and CYP3A4. The Nanodiscs elute around 1.8 mL and there is a clear aggregate peak that elutes just after 1 mL. Fractions were collected every minute to separate the aggregate from the Nanodiscs. The highest concentration fractions from the main Nanodisc peak were used for IM-MS.

Ion-Mobility Mass Spectrometry Lipid Comparisons

Nanodiscs were formed with either 100% DMPC or 100% POPC lipids, which have the same headgroup but different lipid tails, as the DMPC tails are fully saturated while POPC tails are unsaturated, with one double bond. This impacts the ability of the lipids to pack within the Nanodisc, so a higher DMPC:MSP1D1 (80:1) ratio than POPC:MSP1D1 (65:1) is used. The Nanodiscs were formed in microfluidic devices and purified via fraction collection on the SEC.

CIU analysis was used to detect structural stability changes due to lipid environment when CYP 3A4 was liberated from POPC and DMPC Nanodiscs. CIU fingerprints **(Figure 6.2)** show differences in unfolding trajectory between CYP3A4 15^{+} species when liberated from POPC and DMPC Nanodiscs. The main difference between the two fingerprints is the drift time of the last feature and the shape in transitions out of the DMPC ND **(Figure 6.2).** To quantify these differences, we computed the difference in CIU fingerprints and calculated root mean square deviation (RMSD), as shown in **Figure 6.3**. This comparison plot illustrates structural dissimilarities in the last feature with CYP 3A4 unfolding housed in either POPC Nanodiscs (red trace) or DMPC Nanodiscs (blue trace).

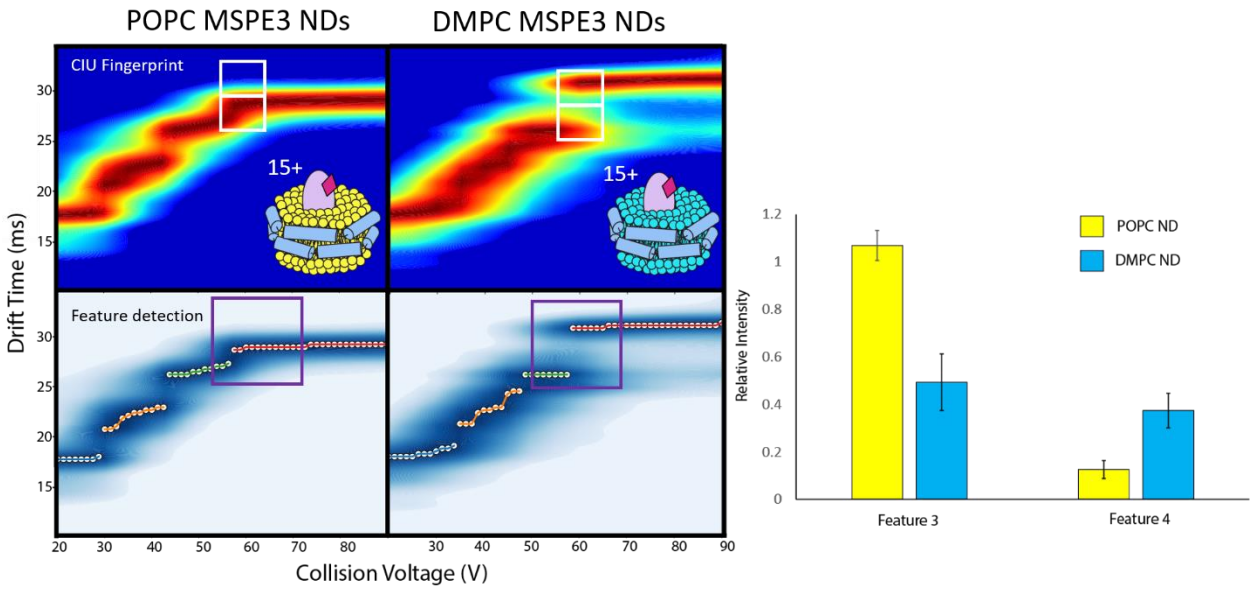

Figure 6.2: Ion-Mobility Mass Spectrometry of POPC and DMPC Nanodiscs. Top: Collision-Induced Unfolding (CIU) Fingerprints for the 15+ CYP3A4 liberated from POPC ND (left) and DMPC NDs (right) Bottom: Feature detection analysis performed using CIUSuite2 illustrates discrete features, unfolding, resulting from various lipid composition the CYP3A4 is liberated from POPC (left) and DMPC (right). Bar graph: Intensity values extracted from the CIU fingerprints (indicated by white boxes) for the third feature and fourth feature to visualize differences in the 55-65V region. POPC NDs yellow bars, DMPC NDs blue bars.

The CIU fingerprints for the POPC and DMPC Nanodiscs **(Figure 6.2)** show differences in gas phase unfolding. These differences can be quantified by comparing the relative intensity differences of two features between the two lipid compositions. Directly comparing the CIU fingerprints **(Figure 6.3)** of the two distinct Nanodiscs is another way to visualize the differences in the protein unfolding patterns. The CYP3A4 in the DMPC Nanodiscs appears to begin unfolding at lower collisions voltages than the CYP3A4 in the POPC Nanodiscs, indicating that the stability of the protein is distinct between the two lipid compositions.

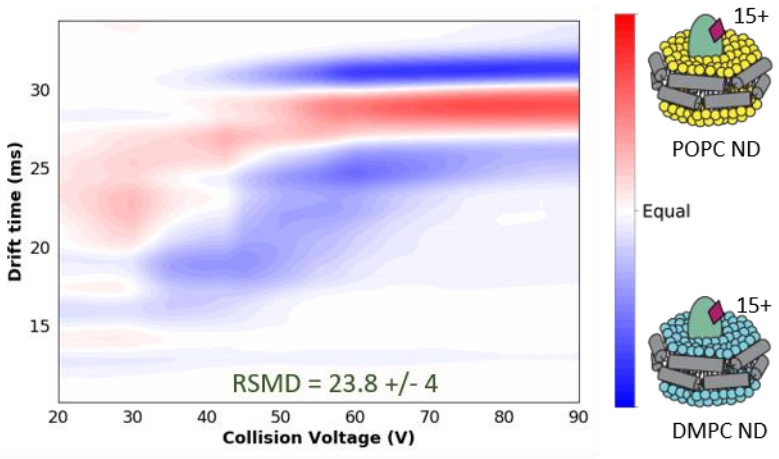

Figure 6.3: The Root Mean Square Deviation plot. This indicates structural dissimilarities between the CYP liberated from its lipid environment (RMSD baseline values Holo DMPC: 10.3 and Holo POPC: 6.9.

Mitochondrial Library Nanodisc Formation and Purification

Library Nanodiscs of three distinct lipid compositions were formed from isolated mitochondria. The mitochondria is a fascinating organelle as it is composed of two lipid bilayers of distinct lipid and protein composition, with about 25% of the mitochondria-resident proteins either associated with or embedded in one of the membranes.[30] The outer membrane contains both α-helical and β-barrel transmembrane proteins, with the largest lipid compositions being 54% POPC and 29% POPE. The inner membrane has mostly α-helical proteins, and though POPC (40%) and POPE (34%) are still the largest two lipid compositions, cardiolipin is also at a high percentage, around 18%. The cardiolipin percentage is the biggest difference in the lipid composition of the inner and outer membranes of the mitochondria. We were interested to determine if membrane proteins preferentially incorporate into only Nanodiscs of specific lipid compositions utilizing MS.

Mitochondrial Library Nanodiscs were formed with three different lipid compositions: a 100% POPC Nanodisc as a control, a 50% POPC and 50% POPE Nanodisc as a model of the outer membrane, and a 40% POPC, 40% POPE and 20% cardiolipin (CL) Nanodisc as a model of the inner membrane. The same mitochondrial lysate was used for each Nanodisc and the Nanodiscs were formed with a 130 lipid: 1 MSP1E3D1 molar ratio. After microfluidic Nanodisc formation, Ni-NTA purification was performed to remove any proteins, lipids, and other lysate material not incorporated in the Nanodiscs. These purified Nanodiscs were then broken apart and exposed to a trypsin digestion before MS peptide analysis.

All peptides detected were run through the database and the membrane proteins were identified. In total, 168 peptides were incorporated into the 100% POPC Nanodiscs, 96 peptides were incorporated into the 50% POPC and 50% POPE Nanodiscs, and 161 peptides were identified in the 40% POPC, 40% POPE, 20% CL Nanodiscs. The protein distribution into each Nanodisc was plotted in a Venn Diagram to show the breakdown of the number of proteins identified only in one specific lipid compositions, in two lipid compositions, or in all three lipid compositions. **(Figure 6.4).** Around 28% of the identified peptides were found in all the Nanodiscs, suggesting that these proteins will incorporate into a lipid bilayer for stability regardless of the lipid composition. In total, about 42% of the identified peptides were found in only one of the three lipid compositions, which suggests that these proteins might have a preference for specific lipids, such as cardiolipin.

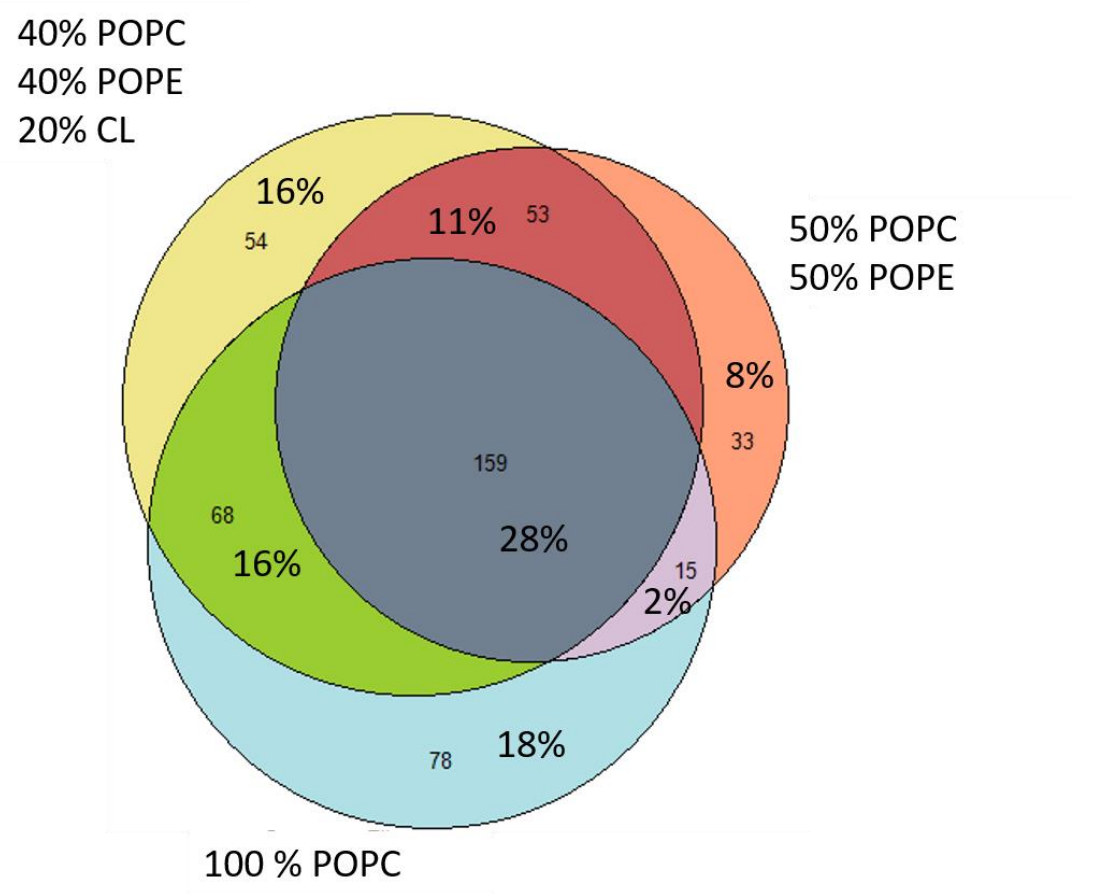

Figure 6.4: Venn diagram indicating the number of identified peptide sequences for each of the three lipid compositions. The smaller number is the total number of unique sequences identified while the larger number indicates the percentage of the total that falls within that section. The lipid identities at 40% POPC, 40% POPE and 20% cardiolipin (CL) on the top left; 50% POPC and 50% POPE on the top right; and 100% POPC on the bottom.

The identified proteins in each Nanodisc were classed as inner membrane, outer membrane, intramembrane, or matrix proteins. **(Figure 6.5).** The 50% POPC and 50% POPE Nanodiscs should be the best representation of the outer membrane and the 40% POPC, 40% POPE, 20% CL Nanodiscs should be the best representation of the inner membrane. The 100% POPC Nanodiscs were a control, for membrane proteins that will incorporate into a membrane of a basic lipid composition, as opposed to a more specific composition that mirrors one of the mitochondrial membranes. Interestingly, there is not a clear indication that a specific lipid

composition leads to more of that particular protein class in the Nanodisc. There are more inner membrane proteins in the 100% POPC Nanodiscs than in the Nanodiscs containing cardiolipin that should be a better model of the inner membrane. There are overall less outer membrane proteins than inner membrane proteins detected, though it is not clear why this occurred. There does not seem to be any indication that the outer membrane proteins prefer the 50% POPC and 50% POPE Nanodiscs that model the outer membrane. There are a number of matrix proteins as well that interact with the Nanodisc but are not integral membrane proteins, and these seem to have a relatively equal interaction with all three lipid compositions, with slightly more interaction with the inner membrane models. There were the least intramembrane proteins detected, and these did not incorporate often into the 100% POPC Nanodiscs but had about equal incorporation into the inner and outer membranes.

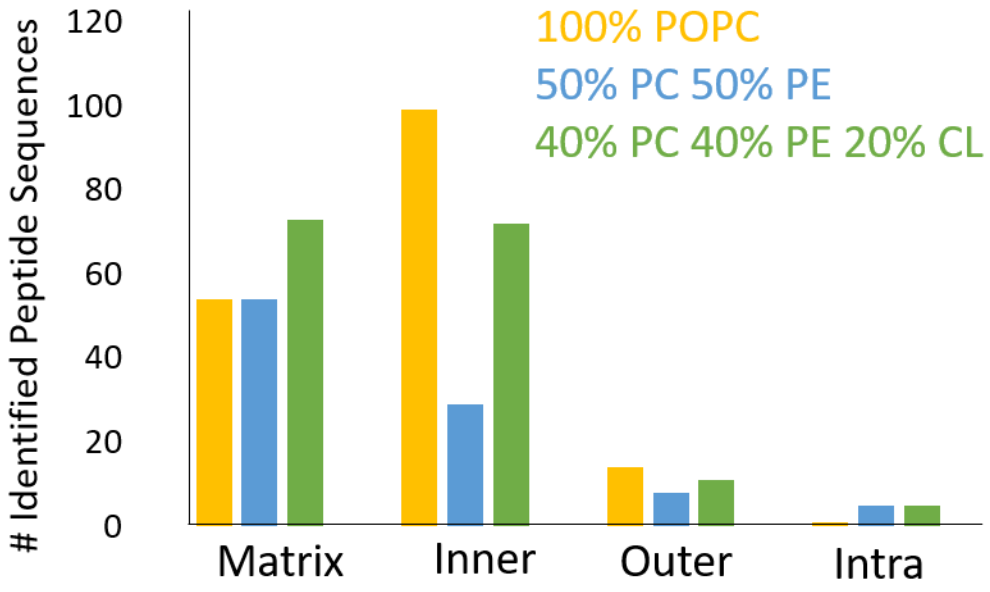

Figure 6.5: Graph showing the classification of the identified proteins in each of the Nanodisc lipid compositions. The 100% POPC Nanodiscs are in yellow, the 50% POPC and 50% POPE Nanodiscs are in blue, and the 40% POPC, 40% POPE and 20% CL Nanodiscs are in green.

It is important to note that all of the mitochondrial Library Nanodisc data has no replicates, it is a single experiment. This data is interesting as it shows that there are clearly differences in the membrane proteins identified in each lipid composition, however conclusions about how significant this information is cannot be drawn until more biological replicates are obtained. Even if all the membrane proteins do not incorporate into the same Nanodiscs in each replicate, this information could be interesting knowledge about membrane protein-lipid interactions.

Conclusions and Future Work:

Our initial experiments were very promising as we were able to demonstrate that Nanodisc formed with different lipid compositions led to distinct mass spectra results. Altering the lipid composition of Nanodiscs containing CYP3A4 caused changes in the drift time and unfolding of the protein, indicating that the identity of the lipids interacting with the protein has an impact on the protein structure. The lipid identity also might influence the incorporation of certain mitochondrial membrane proteins into Nanodiscs. Interestingly, the preliminary experiments indicate that some membrane proteins will incorporate into a lipid bilayer regardless of the lipid composition while other membrane proteins will only incorporate into specific lipid bilayers. Though significant work still needs to be done to confirm and expand upon these results, these initial results have demonstrated interesting applications of mass spectrometry to membrane protein research in Nanodiscs.

Kristine and Marina have continued to push this project forwards in exciting and interesting directions. They have significantly expanded the lipid identities and ratios tested for Nanodiscs containing both CYP3A4 and CYP2B4, the human and rabbit homologs of the cytochrome. Our initial experiments used simple, one-component lipid Nanodiscs as a proof-of-

concept. However, the various membranes within the cell are complex lipid mixtures each with distinct lipid compositions and ratios. Forming Nanodiscs with lipid compositions more similar to that of the Endoplasmic Reticulum, where cytochromes are located, will theoretically give us a better idea of the native structure of the cytochrome as it interacts with local lipids. As the lipid composition of the ER is very complicated **(Table 6.2),** in addition to testing this full mixture, testing each lipid in simpler mixtures of one to three lipids will allow for a better understanding of the impact of each individual lipid identity on the protein structure.

In addition to our interest in the impact of lipids on cytochrome proteins, we are also interested in how the biding of various ligands changes the protein unfolding. Cytochromes are involved in the breakdown of a wide range of pharmaceuticals and cytotoxic compounds, so furthering our understanding of how the binding of these various ligands to the cytochrome impacts the protein structure is important.[31–33] Knowledge about the binding of these different ligands to the cytochromes could lend information to how the structure of the protein impacts the function.

Table 6.2: Lipid Mixture to Emulate Endoplasmic Reticulum in Nanodiscs.

Lipid	**Percentage**
POPC	58
POPE	20
POPI	7
POPS	7
Sphingomyelin	4
Cholesterol	4

Further optimization of the microfluidic devices is another key to the future of the project. The devices currently are run at a flow rate of 30 μL/min, which is a higher volume than can be directly coupled to the MS. Marina has been developing microfluidic devices that are on a

smaller scale, to allow for a better match between the microfluidic formation and analysis. The bigger problem is that we are currently doing a SEC separation before the IM-MS and a Ni-NTA purification and trypsin digestion before the peptide fingerprinting MS. The Ni-NTA purification can be performed on a microfluidic scale, though on a separate device. We could implement a different type of microfluidics employed in the Bailey lab, termed droplet microfluidics, to perform on-chip trypsin digestion.[34,35] These droplet microfluidic devices have delay channels needed for the enzyme to have time for protein digestion, as well as picoinjectors that can be used to inject the stop material. There have been examples of size-based separation on a microfluidic device, but usually for separation of larger molecules such as cells or liposomes.[36,37] However, these basic designs could be optimized for the separation of the Nanodiscs of interest from the aggregates.

The mitochondrial membrane protein project requires replication to determine if the membrane proteins incorporate into the same lipid compositions each time. Regardless of the results, it could be interesting, as it would be informational to understand how important the lipid composition is for each membrane protein. Determining how many membrane proteins consistently incorporate into Nanodiscs only of a certain lipid composition versus how many membrane proteins will incorporate into any Nanodiscs might be a good indication of how important any lipid bilayer is to a membrane protein.

Beyond this interesting knowledge we could gain about membrane protein – lipid interactions, we are also interested in utilizing Nanodiscs of specific lipid compositions to differentially extract membrane proteins of interest for structural proteomic assays. The Andrews lab has significant experience in developing chemical cross linking (CXL) tools that we could utilize to study membrane protein complexes, which play an essential role in the mitochondria,

especially within the electron transport chain (ETC). We have written a proposal on uniting the three labs within this project to utilize CXL and microfluidic Nanodiscs with IM-MS to determine information about the membrane proteins interactions within the mitochondria. This includes the ETC proteins Complexes I, II, II and IV and the CYP-associated complexes with cytochrome P450 reductase (CRP) and Adrenodoxin (Adx), which are believed to play a role in CYP phosphorylation and confirmation in the lipid membrane. The goals of this project are to develop the technology, including the microfluidics, MS, and CXL improvements needed, to allow for structural information of novel MPs that have previously not been successfully studied. These developments could then be applied to a wider range of membrane proteins of interest to improve our general ability to determine membrane protein structural information within a lipid bilayer.

References:

1. Fagerberg, L., Jonasson, K., Von Heijne, G., Uhlén, M. & Berglund, L. Prediction of the human membrane proteome. *Proteomics* **10**, 1141–1149 (2010).

2. Overington, J. P., Al-Lazikani, B. & Hopkins, A. L. How many drug targets are there? *Nat. Rev. Drug Discov.* **5**, 993–996 (2006).

3. Wallin, E. & Von Heijne, G. Genome-wide analysis of integral membrane proteins from eubacterial, archaean, and eukaryotic organisms. *Protein Sci.* **7**, 1029–1038 (1998).

4. Yildirim, M. A., Goh, K. Il, Cusick, M. E., Barabási, A. L. & Vidal, M. Drug-target network. *Nat. Biotechnol.* **25**, 1119–1126 (2007).

5. Hendrickson, W. A. Atomic-level analysis of membrane-protein structure. *Nat. Struct. Mol. Biol.* **23**, 464–467 (2016).

6. Konijnenberg, A., Van Dyck, J. F., Kailing, L. L. & Sobott, F. Extending native mass spectrometry approaches to integral membrane proteins. *Biol. Chem.* **396**, 991–1002 (2015).

7. Cross, T. A., Sharma, M., Yi, M. & Zhou, H. X. Influence of solubilizing environments on membrane protein structures. *Trends Biochem. Sci.* **36**, 117–125 (2011).

8. Goehring, A. *et al.* Screening and large-scale expression of membrane proteins in mammalian cells for structural studies. *Nat. Protoc.* **9**, 2574–2585 (2014).

9. Garavito, R. M. & Ferguson-Miller, S. Detergents as Tools in Membrane Biochemistry. *J. Biol. Chem.* **276**, 32403–32406 (2001).

10. Akbarzadeh, A., Rezaei-sadabady, R., Davaran, S., Joo, S. W. & Zarghami, N. Liposome : classification , preparation , and applications. *Nano Review.* **8**, 1–9 (2013).

11. Denisov, I. G., Grinkova, Y. V., Lazarides, A. A. & Sligar, S. G. Directed Self-Assembly of Monodisperse Phospholipid Bilayer Nanodiscs with Controlled Size. *J. Am. Chem. Soc.* **126**, 3477–3487 (2004).

12. Denisov, I. G. & Sligar, S. G. Nanodiscs in Membrane Biochemistry and Biophysics. *Chem. Rev.* **117**, 4669–4713 (2017).

13. Wade, J. H. *et al.* Microfluidic platform for efficient Nanodisc assembly, membrane protein incorporation, and purification. *Lab Chip* **17**, 2951–2959 (2017).

14. Kermani, A. A. A guide to membrane protein X-ray crystallography. *FEBS J.* 1–17 (2020).

15. Liang, B., Tamm, L. K. & Struct Mol Biol Author manuscript, N. NMR as a Tool to Investigate Membrane Protein Structure, Dynamics and Function. *Nat Struct Mol Biol* **23**,

468–474 (2016).

16. Yao, X., Fan, X. & Yan, N. Cryo-EM analysis of a membrane protein embedded in the liposome. *Proc. Natl. Acad. Sci. U. S. A.* **117**, 18497–18503 (2020).

17. Eschweiler, J. D., Kerr, R., Rabuck-Gibbons, J. & Ruotolo, B. T. Sizing up protein-ligand complexes: The rise of structural mass spectrometry approaches in the pharmaceutical sciences. *Annu. Rev. Anal. Chem.* **10**, 25–44 (2017).

18. Benesch, J. L. P. & Ruotolo, B. T. Mass spectrometry: Come of age for structural and dynamical biology. *Curr. Opin. Struct. Biol.* **21**, 641–649 (2011).

19. Hilton, G. R. & Benesch, J. L. P. Two decades of studying non-covalent biomolecular assemblies by means of electrospray ionization mass spectrometry. *J. R. Soc. Interface* **9**, 801–816 (2012).

20. Clemmer, D. E., Russell, D. H. & Williams, E. R. Characterizing the conformationome: Toward a structural understanding of the proteome. *Acc. Chem. Res.* **50**, 556–560 (2017).

21. Eschweiler, J. D., Frank, A. T. & Ruotolo, B. T. Coming to Grips with Ambiguity: Ion Mobility-Mass Spectrometry for Protein Quaternary Structure Assignment. *J. Am. Soc. Mass Spectrom.* **28**, 1991–2000 (2017).

22. May, J. C. & McLean, J. A. Ion mobility-mass spectrometry: Time-dispersive instrumentation. *Anal. Chem.* **87**, 1422–1436 (2015).

23. Graves, D. B. Transport properties of ions in gases by Edward A. Mason and Earl W. McDaniel, John Wiley and Sons, New York, 1988, 560+ xvi pp. *AIChE J.* **35**, 701–701 (1989).

24. Revercomb, H. E. & Mason, E. A. Theory of plasma chromatography/gaseous electrophoresis. Review. *Anal. Chem.* **47**, 970–983 (1975).

25. Dwivedi, P., Wu, C. & Hill, H. H. Gas Phase Chiral Separations By Ion Mobility Spectrometry. *Anal. Chem.* **78**, 8020-8206 (2006).

26. Thiede, B. *et al.* Peptide mass fingerprinting. *Methods* **35**, 237–247 (2005).

27. Gonnet, F., Lemaître, G., Waksman, G. & Tortajada, J. MALDI/MS peptide mass fingerprinting for proteome analysis: Identification of hydrophobic proteins attached to eucaryote keratinocyte cytoplasmic membrane using different matrices in concert. *Proteome Sci.* **1**, 1–7 (2003).

28. Roy, J., Pondenis, H., Fan, T. M. & Das, A. Direct Capture of Functional Proteins from Mammalian Plasma Membranes into Nanodiscs. *Biochemistry* **54**, 6299–6302 (2015).

29. Fernando, H., Halpert, J. R. & Davydov, D. R. Resolution of multiple substrate binding sites in cytochrome P450 3A4: The stoichiometry of the enzyme-substrate complexes

probed by FRET and Job's titration. *Biochemistry* **45**, 4199–4209 (2006).

30. Tatsuta, T., Scharwey, M. & Langer, T. Mitochondrial lipid trafficking. *Trends Cell Biol.* **24**, 44–52 (2014).

31. Šrejber, M. *et al.* Membrane-attached mammalian cytochromes P450: An overview of the membrane's effects on structure, drug binding, and interactions with redox partners. *J. Inorg. Biochem.* **183**, 117–136 (2018).

32. Denisov, I. G., Makris, T. M., Sligar, S. G. & Schlichting, I. Structure and chemistry of cytochrome P450. *Chem. Rev.* **105**, 2253–2277 (2005).

33. Gay, S. C., Roberts, A. G. & Halpert, J. R. Structural features of cytochromes P450 and ligands that affect drug metabolism as revealed by X-ray crystallography and NMR. *Future Med. Chem.* **2**, 1451–1468 (2010).

34. Doonan, S. R. & Bailey, R. C. K-Channel: A Multifunctional Architecture for Dynamically Reconfigurable Sample Processing in Droplet Microfluidics. *Anal. Chem.* **89**, 4091–4099 (2017).

35. Xu, Y. *et al.* A droplet microfluidic platform for efficient enzymatic chromatin digestion enables robust determination of nucleosome positioning. *Lab Chip* **18**, 2583–2592 (2018).

36. Dalili, A., Samiei, E. & Hoorfar, M. A review of sorting, separation and isolation of cells and microbeads for biomedical applications: microfluidic approaches. *Analyst* **144**, 87–113 (2019).

37. Wyatt Shields Iv, C., Reyes, C. D. & López, G. P. Microfluidic cell sorting: A review of the advances in the separation of cells from debulking to rare cell isolation. *Lab Chip* **15**, 1230–1249 (2015).

Chapter 7: Conclusions and Future Work

I would like to thank Dr. Vishal Sahore and Robert Moeller for their contributions to the thermoplastic microfluidic device development described in this chapter. I also appreciate the contributions of Marina Sarcinella and Matt Sorensen for their work on the lipid identification using HPLC-MS. Finally, I thank Nicolas Mesyngier for our discussions about applying Nanodisc formation and purification to droplet microfluidics.

Conclusions:

In this thesis, I have described my efforts to increase knowledge of membrane proteins by developing and implementing microfluidic devices to form Nanodiscs. Chapter 1 provided a background into Nanodiscs, including the standard formation process and the various advantages and disadvantages. In chapter 2, I reviewed how microfluidic devices have been utilized to study membrane proteins thus far, both to form membrane mimetics containing proteins and to study membrane protein structure and function.

In chapter 3, I described the microfluidic devices that we developed to incorporate membrane proteins into Nanodiscs on a faster time scale and using less material. Initially we tested detergent removal and optimized the flow rate of the device. We then formed empty Nanodiscs, containing just lipids and the scaffold protein, and tested formation using size-exclusion chromatography, atomic force microscopy and dynamic light scattering. We incorporated the cytochrome P450 CYP3A4 into Nanodiscs using the microfluidic device, which

I confirmed via SDS-PAGE. The CYP3A4 retained functionality, as tested with binding assays. The success of these initial experiments encouraged us to continue utilizing the microfluidic device to form Nanodiscs with other membrane proteins of interest.

Chapter 4 details another type of Nanodisc that we can form using our device, the Library Nanodisc, which is formed with whole cell lysate or isolated membranes instead of a recombinantly expressed and isolated membrane protein. I was able to incorporate the epidermal growth factor receptor (EGFR) from glioblastoma patient-derived xenograft cell lines and from Ba/F3 mouse leukemia cell lines that had specific EGFR mutations expressed. EGFR incorporation into Nanodiscs was confirmed with size-exclusion chromatography and Western Blots. The activity of the EGFR in Nanodiscs was also measured, and I found that the various EGFR mutants responded as expected to inhibitors. However, there were problems with high background in the activity assays that led to a decision to implement an EGFR-specific purification before the assay. I was able to purify EGFR, in lysate or in Nanodiscs, but there was significant loss of EGFR during the purification process, leading to too low EGFR for measuring activity. There are potentially other methods that can be applied to increase the concentration of EGFR in the final sample, including further optimization of the purification and starting with a higher percentage of EGFR in the lysate with initial membrane isolation.

The next two chapters covered two collaborations that use the microfluidic device to form interesting Nanodiscs and work with collaborators for unique downstream analyses. Chapter 5 describes a collaboration with the Marsh lab focused on the impact of a Nanodisc lipid bilayer on viperin, a membrane-associated protein. We optimized viperin incorporation by varying the lipid content and confirmed viperin incorporation with SDS-PAGE and Western Blot and transmission electron microscopy. We also tested the impact of the Nanodisc on viperin

activity, as compared to viperin in solution. Chapter 6 details the start of a collaboration with the Ruotolo and Andrews labs applying mass spectrometry to Nanodiscs. With the Ruotolo lab, we formed Nanodiscs with CYP3A4 and used ion-mobility MS to test for the impact of different lipid compositions on the protein structure. With the Andrews lab, we formed Library Nanodiscs using lysed mitochondria and performed trypsin digest followed by peptide library sequencing to identify which membrane proteins incorporated into Nanodiscs of different lipid compositions.

There are a number of areas in which we can further implement microfluidics to form Nanodiscs for studying more membrane proteins of interest. We have plans on ways to improve the microfluidic aspect of the project, by changing the device materials to make the device more accessible, and ways to make the Nanodisc formation more consistent. There are also interesting questions on the biological side, with incorporating different membrane proteins and focusing more on the impact of lipids.

Future Work:

Microfluidic Device Improvements for Nanodisc Formation

One area in which this project can be improved is by continuing to modify the microfluidic devices to improve the accessibility of the device or allow for more detergent removal without necessitating multiple devices. The devices are difficult to produce without a cleanroom and sufficient training, which limits the applicability to certain settings. The current device design is also limited by the size of the bead bed, which sets the volume of beads that can be added and thus the amount of detergent that can be retained by the beads. This translates to a maximum volume of 90 μL of the Nanodisc components mixture containing 20 mM sodium

cholate. Often times a higher concentration of Nanodiscs is required, which means that multiple microfluidic devices need to be used to obtain a sufficient concentration of Nanodiscs.

To enable the formation of microfluidic devices without a cleanroom and specialized training, we have done some preliminary research into using different materials to make the devices. The current microfluidic devices are made using polydimethylsiloxane (PDMS) on a glass slide, which is advantageous while optimizing a new microfluidic device because changing the device design is relatively fast. There are potential issues with using PDMS, including that PDMS absorbs small hydrophobic molecules and solvents, the PDMS surface is hydrophobic, and water can evaporate from within a PDMS device.[1] A cleanroom is also necessary for device formation and there is no way to mass produce PDMS device.

The majority of this work was performed by Dr. Vishal Sahore and Robert Moeller. We have formed similar devices in rigid thermoplastic devices. Because the devices are rigid, there is no need for the support posts used to keep the PDMS devices from collapsing before filling with beads, which is advantageous because these are small features that are more likely to cause issues in fabrication. Thermoplastics are also known to have better biocompatibility, cost-effectiveness, and mass production capacity using either injection molding or hot embossing.[2–4] The Bailey lab has previous experience converting more complex microfluidic devices from PDMS to thermoplastics, specifically using cyclic olefin polymer materials prepared by hot embossing.[5]

Another advantage of switching to thermoplastics is that they have previously been used for *in situ* monolith polymerization for applications such as chromatography.[6] We currently remove the detergent using a packed bead bed, but there are difficulties properly filling the device with beads. For an untrained user, an average 2/3 of devices will fail to be filled, usually

because of the PDMS unsealing from the glass slide during the filling process. Even a trained user has an average failure rate of ¼. For every device that fails, more time must be spent in the cleanroom and more materials are consumed. There can also be issues with replicability, as in the exact amount of detergent each device can remove, based on slight differences in bead packing. This needs to be tested before each device is used for Nanodisc formation, as any detergent remaining in the sample prevents proper Nanodiscs forming. To decrease the failure rate and to increase the wider applicability to untrained users, we decided to try to grow monoliths in the bed of the microfluidic device to remove the detergent without the need for beads.

Methacrylate-based organic porous polymers have previously been formed in microfluidic devices and used for sample preparation.[7] We used these materials as they are easy to prepare, can be anchored to the channel walls, and it is possible to add functional groups if necessary to help bind specific detergents for removal.[7] These monoliths can also be formed using photopolymerization, to crosslink the polymer materials only in the specific area of interest, the bed of the device, using a photomask to control the area of UV illumination.[8] The porosity (an important factor for ensuring fluid flow through the device at reasonable backpressures) and surface chemistry (important for removing the detergent) are both able to be well controlled by optimizing porogen composition[8] and monomer chemistry.[9]

Figure 7.1: Photograph of a Nanodisc formation device fabricated using hot embossing in cyclic olefin copolymer. A C_{18} acrylate monolith was then directly photopolymerized within the device.

We have performed some initial device fabrication and monolith formation experiments. **(Figure 7.1).** The device design is very similar to the initial PDMS design, though a few changes have been made. There is no longer a bead filling port to the side or posts on the inlet and outlet sides of the bed, as these are not required as there are no beads to prevent from leaving the bed. There are also no support posts, as the polymer is rigid enough not to collapse when the bed is empty. These devices were formed using hot embossing of the device design into a 1 mm thick cyclic olefin copolymer (COC) using silicon masters.[5]

The initial monolith was formed using a stearyl methacrylate monomer with a C_{18} moiety and an ethylene glycol dimethacrylate cross-linker for biocompatibility. The goal for the pore diameter was ~100 nm, using a 70% porogen solution (7:3 1,4-butanediol:1-propanol). An example of a successful formation of the monolith within the microfluidic device can be seen in **Figure 7.1**. However, there were some issues with inconsistency of forming the monolith equally across the entire microfluidic device. Additionally, tests for the removal of sodium cholate showed minimal success at removing the detergent, with the best results indicating less than 50% of the detergent removed and over a smaller volume, only 10-20 μL. (results not shown)

Further optimization of the monolith identity and porogen percentages will be necessary to completely remove the detergent from the Nanodisc components mixture as is needed for

Nanodisc self-assembly. These included attempting both C_8 and C_{18} frameworks for the monoliths, as well as considering the possibility of needing to find specific monoliths for the removal of each detergent of interest, starting with sodium cholate, a commonly used detergent for Nanodisc formation. The ability of the devices to remove cholate will be tested using a standard colormetric assay, in which sulfuric acid is added to the elutent from the device, resulting in a color change based on the concentration of sodium cholate present.[10] This will both confirm the complete removal of the detergent and determine the detergent removal capacity of the device. We will then attempt to form lipid-only empty Nanodiscs to ensure the devices can be used for Nanodisc formation.

There still exists a problem with this new detergent removal plan using monoliths, which is that there will once again be a limited amount of detergent that can be removed by one device. The current device design is limited to a discrete volume of detergent removal, but continuous operation would be optimal. This means that for the current device, downstream applications requiring larger volumes, requires either multiple microfluidic devices be used or the same device needs to be washed and re-used, a process which takes about 40 minutes. The Bailey lab has previous experience with developing droplet microfluidic devices for continuous processing of samples, independent of input volume, instead of having to optimize the device to the sample size.[11]

Droplet microfluidics uses inert oil to segment aqueous samples, creating femtoliter to nanoliter sized independent microreactors.[12] This segmentation using immiscible phases allows for separate and precise control of each droplet, including adding or removing fluid and coalescing droplets.[13,14] Rapid mixing occurs within droplets, causing more efficient chemical and biological reactions, and thus shortening the reaction time.[12] For all these reasons, a number

of biochemical assays have been converted to droplet microfluidics, including drug screening, DNA sequencing, and single-cell analysis.[15–18]

The potential to form Nanodiscs in droplets has a number of advantages, even over the current microfluidic device. The first is removing the requirement to fill the bead bed, which as discussed earlier causes a significant amount of device failure, wasting time and materials. The second is that the volume of Nanodiscs formed is no longer limited by the bead bed volume, as there is not a limit to the number of droplets that can be formed, it just requires running the device longer. Finally, having the Nanodiscs in droplets will allow for direct coupling to interesting downstream applications requiring droplet microfluidics, some of which are mentioned below.

There are a few different ways that we have considered removing the detergent in droplets, most of which still rely on the detergent removal beads. There are a number of already-developed microfluidic technologies for adding and removing material from droplets, such as the K-channel described by the Bailey lab.[19] We could use these technologies to form aqueous droplets containing the Nanodisc components mixture and the detergent removal beads segmented by the inert oil. Then, we would have a number of delay channels, which will allow for sufficient mixing within the droplet and enough time to remove the detergent. The beads will then be removed, and there are a few potential ways to do this, including splitting the droplet, with the beads going to waste and the formed Nanodiscs continuing on the device, either to collect for off-chip applications or for further downstream analysis on-chip. **(Figure 7.2)**

Very minimal work has been done so far in determining if these ideas are possible. I have tested some of the impacts of the inert oil on the resin and detergent in bulk, by combining the oil, sodium cholate, and the detergent removal resin. Neither the beads nor the cholate partition

into the oil. We have considered that other detergents that have more nonionic characteristics might partition into the oil or form a layer between the oil and aqueous phases. Detergents are sometimes used to stabilize the oil-aqueous interface in droplet microfluidics,[20] and we think there is the possibility of using these natural characteristics to remove detergent from the Nanodisc mixture. This is potentially something that we could further research, but we are concerned that it would limit the ability for downstream analysis, as any perturbations to the droplet surface might cause the detergent to be re-introduced to the interior of the droplet, causing the Nanodiscs to break apart. For now, it appears that this does not occur for sodium cholate, so using the detergent removal beads seems necessary.

After developing a microfluidic device that contains the needed inlets, delay chambers, and a method to separate the droplets **(Figure 7.2)**, a large amount of optimization will be needed. The first step will be determining the bead concentration to be added to each droplet, as there needs to be sufficient beads to completely remove the detergent in each droplet while making sure the beads do not cause clogging in the small channels before being integrated into droplets. This ties in closely with the second issue, which is the number of delay channels needed to give enough time to completely remove the detergent. Adding more delay channels will mean a longer droplet occupancy time on-chip, allowing for longer detergent removal. There might end up being a balance between bead concentration and the needed time for removal, where adding more beads will allow for a shorter time frame, but that needs to be tested.

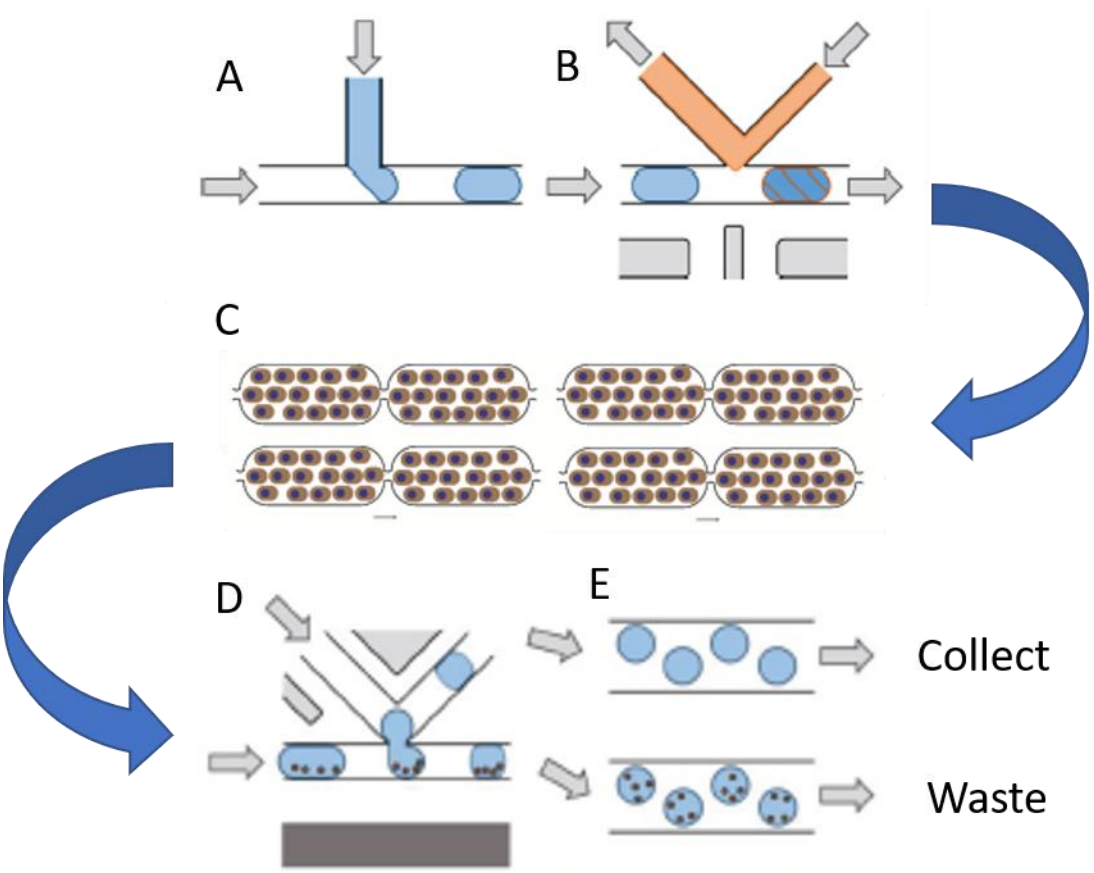

Figure 7.2: An illustration of the types of modules that could be used to develop droplet microfluidic Nanodisc formation devices. These images were modified from Doonan *et. al.*[19] and Xu *et. al.*[11] and are not to scale. (A) A T-junction demonstrates one method of droplet formation, with the oil phase in white and the aqueous phase in blue. The arrows indicate the direction of flow. (B) A K-channel which can be used to add material to droplets (in orange). The solution is added to the blue droplet, as shown by the diagonal orange lines in the droplet to the right. The gray lines underneath the channel are an electrode channel which might be necessary to destabilize the droplet to add solution. (C) Delay channels used to add time on device to allow for the detergent removal reaction to take place. The number and size of these delay channels can be optimized as necessary. (D) Using a K-channel design to split droplets by flowing oil through the K-channel (white). (E) The beads remain in the main channel while the solution-only droplets are pulled up into another channel, which can then be collected for downstream analysis.

The final aspect of this initial device design will be to determine the best way to remove the detergent removal beads from the formed Nanodiscs. Our initial idea is to test splitting the droplet, removing the beads in one droplet while the Nanodiscs remain in the other droplet. There are some concerns with this plan, as there could be issues completely removing the beads

without losing significant amounts of Nanodiscs. One potential way around that issue is to combine the detergent bead removal step with a downstream purification step that will be discussed in the next section, thus removing both the used beads and any Nanodisc component waste. The beads are large enough to be visible in a droplet using a microscope, so we can visually check the success of our removal technique. There are many existing approaches for bead manipulation that have previously been developed in droplet microfluidics, including using acoustic, hydrodynamic and magnetic manipulations, so there are a wide range of potential methods we can implement if necessary.[21]

New Microfluidic Devices for Downstream Analysis

Beyond using droplet microfluidics to form Nanodiscs of flexible volumes, we think droplet microfluidics could also be used for multiple downstream analysis as well, including Nanodisc purification and membrane protein activity assays. Though we already have purification devices, these have the same limitations as the standard detergent removal device, in that they require the difficult bead bed filling step and have a limit in terms of the amount of sample that can be purified on one device. Converting the EGFR activity assay from 96 well plates to droplet microfluidics could lower the protein concentration needed, which has been a significant problem as the number of purifications required has increased. There is also precedence for directly coupling droplet microfluidics to mass spectrometry, which is something that would require large adaptations to our current microfluidic devices because of the mismatch of flow rates.

Developing new purification methods in droplet microfluidics would have a few advantages, especially if transitioning to forming the Nanodiscs in droplets as well. As mentioned for the detergent removal device, removing the packed bead bed is important for

preventing device failure and increasing device replicability and the usable time of each device. One of the benefits of droplet microfluidics is that it is possible to transfer droplets from one device to another, so we can begin with separate formation and purification devices, or even forming the Nanodiscs in bulk or with the old microfluidic device, and then put the Nanodiscs in droplets to test the new purification devices. This will allow us to optimize the Nanodisc formation and purification devices separately without each depending on the success of the other. Then, once both devices are working, they can be combined into a single device for simplicity. It is important to note that droplet microfluidics can also be transferred to thermoplastics as discussed above for the current device design, which could be useful for applications for people who do not have access to a cleanroom or to mass produce the devices.[5]

My initial idea for Nanodisc purification in droplets is based on the previously published Coalesce-Attract-Resegment (CAR)-Wash device developed in the Bailey lab **(Figure 7.3).**[22] This device requires the use of magnetic beads that have a tag specific to the desired purification target, which are added to the droplet containing the sample and allowed to mix and bind in delay channels. Then the droplet aqueous-oil interface is disrupted by a destabilizing electric field, causing the aqueous interior of the droplet to coalesce with a parallel-flowing wash buffer. The unwanted material is washed away to waste with the buffer while the magnetic beads bound to the target of interest is attracted to a magnet placed below the wash channel. Just above the magnet at the bottom of the channel there is a co-flowing oil that is used to resegment the beads into aqueous droplets containing wash buffer and the beads. The Bailey lab has previously used this device to purify a green fluorescent protein-histone H2B (GFP-H2B) from HeLa cells using 10 μm streptavidin microparticle magnetic beads tagged with a polyclonal anti-GFP antibody.[22]

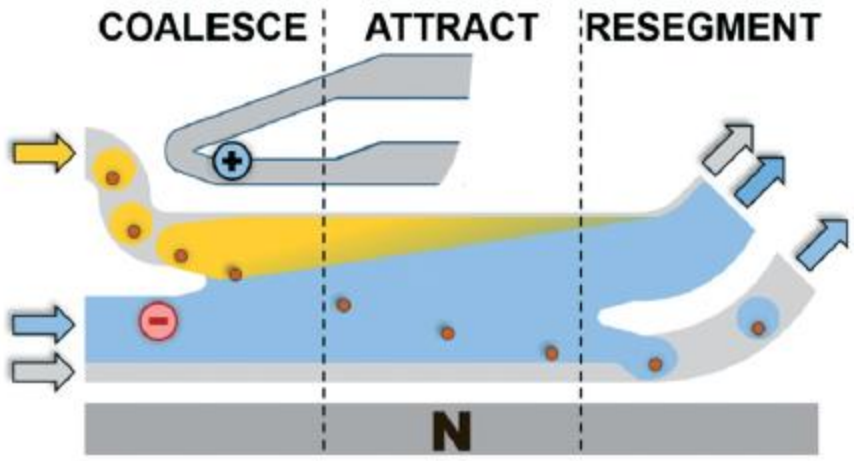

Figure 7.3: The CAR-Wash Technique. This device involves electrocoalescence of input droplets using an electric field applied across the washing buffer stream (in blue) and a nearby ground electrode. Next, a channel-adjacent permanent magnet attracts sample-enriched magnetic beads (brown circles) across the buffer stream while flow forces confine waste material (in yellow) to the original streamline. An oil co-flow (in grey) prevents bead trapping at the bottom channel walls and, at the end of the module, resegments droplets in washing buffer for further manipulations. Arrows indicate flow directions. Reprinted from Doonan *et. al*.[22]

To purify for the MSP on Nanodiscs, we currently use His-Pure Ni-NTA beads in the packed bead bed. There are magnetic versions of this bead available, which could be used with the flowing wash buffer containing a small amount of imidazole to remove non-specific binding. However, the mean diameter of these beads is listed as 1 μm, which might cause problems as they are significantly smaller than the streptavidin beads used in the previous experiments. A concern would be that smaller particles are not attracted to the magnet as quickly as the larger particles, which would cause the particles and samples to be lost to waste instead of being resegmented into droplets. It is possible that changes to the device, such as increasing the length of the wash channel or optimizing the magnet strength and location, would allow for success in attracting these smaller particles, which Claire Cook in the Bailey Lab has been optimizing for a different project. The other solution would be to use the same 10 μm streptavidin microparticles

with a biotinylated anti-Histidine tag antibody instead, as those beads have already been optimized for the device, so all that would need to be optimized is the binding of this new antibody to the beads, not any microfluidic changes.

We hope to also use the CAR-Wash device for membrane protein specific purification. The streptavidin magnetic beads can be used to bind any biotinylated antibodies, allowing for wide application. Though I have had problems with successfully purifying high concentrations of EGFR, either from lysate or in Nanodiscs, with other bead-based antibody purification systems, it is possible that this method will work better for other proteins of interest. There is the issue that to end up with just Nanodiscs containing the membrane protein of interest two runs through the CAR-Wash device will be needed, one for purifying the MSP and one for the membrane protein, but that is true with the current purification methods as well.

Beyond purification, I think we can use droplet microfluidics to expand Nanodisc applications. One application that has a significant amount of previous research, including by the Kennedy lab, is coupling of droplets directly to mass spectrometry using nanoelectrospray ionization.[23–25] For the mass spectrometry applications discussed in Chapter 6 and some potential new applications discussed later, direct coupling both saves time and prevents loss of sample. The current microfluidic device design operates at too fast a flow rate for direct coupling to nanoESI and the device does not allow for any modifications that might be needed between formation or purification and MS. The droplet microfluidic devices allow for the introduction of different modules that would allow for any materials that need to be introduced before MS or removing part of the sample volume if less material can be sprayed.[19]

Finally, there is potential to transition the EGFR activity assays discussed in Chapter 4 from 96 well plates to droplet microfluidics. The current assay requires 10 μL of sample for each

replicate, but since droplets are on the scale of femtoliters-nanoliters, we could drop that sample volume significantly. Though initially I did not have issues with measuring activity in the standard well-based assay, further investigation indicated that a significant amount of this activity was from the lysate background. After EGFR-specific purifications, no activity was measured, potentially because of very low concentrations, below measurable by a BCA assay. If purification cannot be improved to increase the end concentration, converting these assays to smaller volumes with very concentrated pure sample might be an option to measure EGFR activity.

For the current Universal Kinase Assay, a relatively simple droplet microfluidic device could be developed. The samples would be introduced and segmented by the inert oil into droplets. Then we could use a sample introduction method such as the K channel to add the remaining necessary components for the assay (ATP, EGFR-specific substrate and the coupling phosphatase) followed by delay channels to allow for the phosphorylation to occur. A second K channel could be used to introduce the Malachite Green reagents to measure the amount of free phosphate form by the active EGFR. The colormetric response can be measured by the VEO 640L high speed camera (vision Research Inc) camera the Bailey lab has on a DMi8 light microscope (Leica Microsystems). Each sample can be introduced separately into the device consecutively and there is no sample crossover because of the consistently moving inert oil phase. This is one of many possibilities to improve the EGFR activity assays, with a few other ideas presented in Chapter 4.

Lipid Identity

I have previously discussed the importance of the synthetic lipids added to the Nanodiscs and how these impact the membrane protein incorporation or structure. However, we have also

been interested in the potential of lipids from the native cell membrane that might be also incorporating into Library Nanodiscs. When using cell lysate or isolated membranes as the starting material, the lipids from the cell will be in the Nanodisc components mixture with the added synthetic lipids, allowing these native lipids to incorporate into Nanodiscs the same as the synthetic lipids. There are a few reasons that we are interested in these native lipids. It is possible that important lipids to the membrane protein structure and function will remain close to the protein and co-incorporate into the Nanodiscs with these proteins, which would lend both interesting biological information and could be good knowledge for adding that lipid synthetically to improve Nanodisc incorporation.[26]

To identify the lipid in Nanodiscs, liquid chromatography separation followed by mass spectrometry can be used. To do this it is necessary to break apart the Nanodiscs and isolate only the lipids to identify all the lipids present via HPLC-MS. To the best of my best knowledge, this method has not been used to identify the native lipids in Library Nanodiscs but has been used to identify hundreds of lipids in a complex biological sample.[27,28] This method relies on a library of lipid mass spectra based on lipid standards, which could potentially be problematic if the lipids of interest have not been previously added to the library for comparison. The other issue is that this method combines a large number of Nanodiscs each containing potentially distinct lipid compositions, providing an average lipid composition of the Nanodiscs instead of the exact lipid composition for each Nanodisc. The Bailey Lab has begun working with the Kennedy lab to use HPLC-MS to confirm the synthetic lipids used to form empty Nanodiscs are of the expected lipid composition (data not shown), with the goal of eventually reaching a point where Library Nanodiscs could be probed to identify unique lipids not synthetically added.

Other Membrane Proteins of Interest

Part of the goal of the microfluidic device is to allow for the optimization of Nanodisc formation across a wide range of membrane protein identities. Over the course of this thesis, I have covered many different membrane proteins that have been incorporated into Nanodiscs, including integral membrane proteins and membrane associated proteins. Though I do not have sufficient data to present, some membrane proteins that we have already and continue to probe in our lab include Anaplastic Lymphoma Kinase (ALK, a key membrane protein that experiences a fusion in certain forms of lymphoma[29]) and Receptor tyrosine-protein kinase erbB-2 (also known as HER2, a family member of EGFR implicated in aggressive breast cancer[30]). There are thousands more membrane proteins that could be very interesting to study in the future, both within the lab and in collaboration, to determine either structural or functional information.

References:

1. Halldorsson, S., Lucumi, E., Gómez-Sjöberg, R. & Fleming, R. M. T. Advantages and challenges of microfluidic cell culture in polydimethylsiloxane devices. *Biosens. Bioelectron.* **63**, 218–231 (2015).

2. Van Midwoud, P. M., Janse, A., Merema, M. T., Groothuis, G. M. M. & Verpoorte, E. Comparison of biocompatibility and adsorption properties of different plastics for advanced microfluidic cell and tissue culture models. *Anal. Chem.* **84**, 3938–3944 (2012).

3. Matellan, C. & Del Río Hernández, A. E. Cost-effective rapid prototyping and assembly of poly(methyl methacrylate) microfluidic devices. *Sci. Rep.* **8**, 1–13 (2018).

4. Gencturk, E., Mutlu, S. & Ulgen, K. O. Advances in microfluidic devices made from thermoplastics used in cell biology and analyses. *Biomicrofluidics* **11**, (2017).

5. Sahore, V., Doonan, S. R. & Bailey, R. C. Droplet microfluidics in thermoplastics: device fabrication, droplet generation, and content manipulation using integrated electric and magnetic fields. *Anal. Methods* **10**, 4264–4274 (2018).

6. Sonker, M., Knob, R., Sahore, V. & Woolley, A. T. Integrated electrokinetically driven microfluidic devices with pH-mediated solid-phase extraction coupled to microchip electrophoresis for preterm birth biomarkers. *Electrophoresis* **38**, 1743–1754 (2017).

7. Knob, R., Sahore, V., Sonker, M. & Woolley, A. T. Advances in monoliths and related porous materials for microfluidics. *Biomicrofluidics* **10**, (2016).

8. Svec, F. Porous polymer monoliths: Amazingly wide variety of techniques enabling their preparation. *J. Chromatogr. A* **1217**, 902–924 (2010).

9. Yu, C., Xu, M., Svec, F. & Fréchet, J. M. J. Preparation of monolithic polymers with controlled porous properties for microfluidic chip applications using photoinitiated free-radical polymerization. *J. Polym. Sci. Part A Polym. Chem.* **40**, 755–769 (2002).

10. Urbani, A. & Warne, T. A colorimetric determination for glycosidic and bile salt-based detergents: Applications in membrane protein research. *Anal. Biochem.* **336**, 117–124 (2005).

11. Xu, Y. *et al.* A droplet microfluidic platform for efficient enzymatic chromatin digestion enables robust determination of nucleosome positioning. *Lab Chip* **18**, 2583–2592 (2018).

12. Baroud, C. N., Gallaire, F. & Dangla, R. Dynamics of microfluidic droplets. *Lab Chip* **10**, 2032–2045 (2010).

13. Mazutis, L. & Griffiths, A. D. Selective droplet coalescence using microfluidic systems. *Lab Chip* **12**, 1800–1806 (2012).

14. Chokkalingam, V. *et al.* An electro-coalescence chip for effective emulsion breaking in

droplet microfluidics. *Lab Chip* **14**, 2398–2402 (2014).

15. Teh, S. Y., Lin, R., Hung, L. H. & Lee, A. P. Droplet microfluidics. *Lab Chip* **8**, 198–220 (2008).

16. Seemann, R., Brinkmann, M., Pfohl, T. & Herminghaus, S. Droplet based microfluidics. *Reports Prog. Phys.* **75**, (2012).

17. Huebner, A. *et al.* Microdroplets: A sea of applications? *Lab Chip* **8**, 1244–1254 (2008).

18. Dressler, O. J., Maceiczyk, R. M., Chang, S. I. & Demello, A. J. Droplet-based microfluidics: Enabling impact on drug discovery. *J. Biomol. Screen.* **19**, 483–496 (2014).

19. Doonan, S. R. & Bailey, R. C. K-Channel: A Multifunctional Architecture for Dynamically Reconfigurable Sample Processing in Droplet Microfluidics. *Anal. Chem.* **89**, 4091–4099 (2017).

20. Baret, J. C. Surfactants in droplet-based microfluidics. *Lab Chip* **12**, 422–433 (2012).

21. Tenje, M., Fornell, A., Ohlin, M. & Nilsson, J. Particle Manipulation Methods in Droplet Microfluidics. *Anal. Chem.* **90**, 1434–1443 (2018).

22. Doonan, S. R., Lin, M. & Bailey, R. C. Droplet CAR-Wash: Continuous picoliter-scale immunocapture and washing. *Lab Chip* **19**, 1589–1598 (2019).

23. Steyer, D. J. & Kennedy, R. T. High-Throughput Nanoelectrospray Ionization-Mass Spectrometry Analysis of Microfluidic Droplet Samples. *Anal. Chem.* (2019).

24. Diefenbach, X. W. *et al.* Enabling Biocatalysis by High-Throughput Protein Engineering Using Droplet Microfluidics Coupled to Mass Spectrometry. *ACS Omega* **3**, 1498–1508 (2018).

25. Ngernsutivorakul, T., Steyer, D. J., Valenta, A. C. & Kennedy, R. T. In Vivo Chemical Monitoring at High Spatiotemporal Resolution Using Microfabricated Sampling Probes and Droplet-Based Microfluidics Coupled to Mass Spectrometry. *Anal. Chem.* **90**, 10943–10950 (2018).

26. Cebecauer, M. *et al.* Membrane Lipid Nanodomains. *Chem. Rev.* **118**, 11259–11297 (2018).

27. Danne-Rasche, N., Coman, C. & Ahrends, R. Nano-LC/NSI MS Refines Lipidomics by Enhancing Lipid Coverage, Measurement Sensitivity, and Linear Dynamic Range. *Anal. Chem.* **90**, 8093–8101 (2018).

28. Drotleff, B. & Lämmerhofer, M. Guidelines for selection of internal standard-based normalization strategies in untargeted lipidomic profiling by LC-HR-MS/MS. *Anal. Chem.* **91**, 9836–9843 (2019).

29. Tort, F. *et al.* Molecular characterization of a new ALK translocation involving moesin (MSN-ALK) in anaplastic large cell lymphoma. *Lab. Investig.* **81**, 419–426 (2001).

30. Gutierrez, C. & Schiff, R. HER2: Biology, detection, and clinical implications. *Arch. Pathol. Lab. Med.* **135**, 55–62 (2011).